

Available online at [www.sciencedirect.com](http://www.sciencedirect.com)

SCIENCE @ DIRECT®

Prog. Polym. Sci. xx (2003) xxx–xxx

PROGRESS IN  
POLYMER SCIENCE[www.elsevier.com/locate/ppolysci](http://www.elsevier.com/locate/ppolysci)

## Polymer/layered silicate nanocomposites: a review from preparation to processing

Suprakas Sinha Ray\*, Masami Okamoto

*Advanced Polymeric Materials Engineering, Graduate School of Engineering, Toyota Technological Institute, 2-12-1 Hisakata, Tempaku, Nagoya 468 8511, Japan*

Received 22 May 2003; revised 18 August 2003; accepted 22 August 2003

### Abstract

A review is given of the academic and industrial aspects of the preparation, characterization, materials properties, crystallization behavior, melt rheology, and processing of polymer/layered silicate nanocomposites. These materials are attracting considerable interest in polymer science research. Hectorite and montmorillonite are among the most commonly used smectite-type layered silicates for the preparation of nanocomposites. Smectites are a valuable mineral class for industrial applications because of their high cation exchange capacities, surface area, surface reactivity, adsorptive properties, and, in the case of hectorite, high viscosity and transparency in solution. In their pristine form they are hydrophilic in nature, and this property makes them very difficult to disperse into a polymer matrix. The most common way to remove this difficulty is to replace interlayer cations with quaternized ammonium or phosphonium cations, preferably with long alkyl chains.

*Abbreviations:* AA, acrylamide; AEA, *N,N*-dimethylaminoethyl acrylate; AFM, atomic force microscopy; AIBN, *N*-azobis(isobutyronitrile); AN, acrylonitrile; ANI, aniline; APES, aliphatic polyester; ATRP, atom transfer radical polymerization; BDMA, benzyltrimethylammonium; BPO, dibenzoyl peroxide; CEC, cation exchange capacity; CL,  $\epsilon$ -caprolactone; CSA, camphorsulphonic acid; DBSA, dodecylbenzenesulfonic acid; DETDA, diethyltoluene diamine; DGEBA, diglycidylether of bisphenol A; DMA, dynamic mechanical analysis; DMF, dimethylformamide; DSC, differential scanning calorimetry; EG, ethylene glycol; EPDM, ethylene propylene diene methylene linkage rubber; EPR, epoxy polymer resin; EVA, poly(ethylene-co-vinyl acetate); FTIR, Fourier transformed infrared; HBP, hyperbranched polymer; HDPE, high-density polyethylene; [(HE)<sub>2</sub>M<sub>1</sub>R<sub>1</sub>], bis(hydroxyethyl)(methyl)-rapeseedquaternary ammonium; HHMPA, hexahydro-4-methylphthalic anhydride; IC, isophthaloyl chloride; MAO, methylaluminoxane; MMA, methyl methacrylate; M-MDI, 4,4'-di-phenylmethane diisocyanate; MMT, montmorillonite; MPP, modified polyether polyol; N6, nylon-6; NMR, nuclear magnetic resonance; NVC, *N*-vinylcarbazole; OMLS, organically modified layered silicate; PAA, *N,N*-dimethylaminopropyl acrylamide; PANI, polyaniline; PBO, polybenzoxazole; PBS, poly(butylene succinate); PBT, poly(butylene terephthalate); PC, polycarbonate; PCL, poly( $\epsilon$ -caprolactone); PDS, poly(dimethyl siloxane); PDT, polymer delamination temperature; PE, polyethylene; PEG, poly(ethylene glycol); PEI, poly(etherimide); PEO, polyethylene oxide; P2Epy, poly(2-ethanypyridin); PET, poly(ethylene terephthalate); PEVA, poly(ethylene vinyl alcohol); PHA, polyhydroxyamide; PHB, polyhydroxy butyrate; PI, polyimide; PLA, polylactide; PLS, polymer/layered silicate; PMMA, poly(methyl methacrylate); PMT, poly(trimethylene terephthalate); PNVC, poly(*N*-vinyl carbazole); PP, polypropylene; PP-MA, maleic anhydride grafted polypropylene; PPV, poly(*p*-phenylene vinylene); PPY, polypyrrole; PSF, polysulfone; PSPI, polystyrene-polyisoprene; PS, polystyrene; PVA, poly(vinyl alcohol); PVP, poly(*N*-vinyl pyrrolidone); PU, polyurethane; PUU, polyurethane urea; QA<sup>+</sup>, quaternaryammonium cation; S, styrene; SAN, poly(styrene-co-acrylonitrile); sap, saponite; SAXS, small angle X-ray scattering; SFM, synthetic fluorine mica; SPN, diethylmethylammonium modified smectite; sPP, syndiotactic polypropylene; STN, methyltrioctylammonium modified smectite; TEM, transmission electron microscopy; TGA, thermogravimetric analysis; TGAP, trifunctional triglycidyl *p*-amino phenol; TGDDM, tetrafunctional tetraglycidyl diamino diphenylmethane; THF, tetrahydrofuran; WAXD, wide angle X-ray diffraction.

\* Corresponding author. Tel.: +81-52-809-1863; fax: +81-52-809-1864.

E-mail addresses: [sinharays@toyota-ti.ac.jp](mailto:sinharays@toyota-ti.ac.jp) (S. Sinha Ray); [okamoto@toyota-ti.ac.jp](mailto:okamoto@toyota-ti.ac.jp) (M. Okamoto).

A wide range of polymer matrices is covered in this review, with special emphasis on biodegradable polymers. In general, polymer/layered silicate nanocomposites are of three different types, namely (1) *intercalated nanocomposites*, for which insertion of polymer chains into a layered silicate structure occurs in a crystallographically regular fashion, with a repeat distance of few nanometers, regardless of polymer to clay ratio, (2) *flocculated nanocomposites*, for which intercalated and stacked silicate layers flocculated to some extent due to the hydroxylated edge–edge interactions of the silicate layers, and (3) *exfoliated nanocomposites*, for which the individual silicate layers are separated in the polymer matrix by average distances that depend only on the clay loading. This new family of composite materials frequently exhibits remarkable improvements of material properties when compared with the matrix polymers alone or conventional micro- and macro-composite materials. Improvements can include a high storage modulus, both in solid and melt states, increased tensile and flexural properties, a decrease in gas permeability and flammability, increased heat distortion temperature, an increase in the biodegradability rate of biodegradable polymers, and so forth.

© 2003 Elsevier Ltd. All rights reserved.

**Keywords:** Polymers; Layered silicates; Nanocomposites; Preparation and characterizations; Materials properties; Crystallization behavior; Rheology; Processing; Applications; Review

## Contents

|   |     |
|---|-----|
| 1. Introduction . . . . .   | 000 |
| 1.1. Structure and properties of layered silicates . . . . .                                | 000 |
| 1.2. Structure and properties of organically modified layered silicate (OMLS) . . . . .     | 000 |
| 1.3. Types of nanocomposites . . . . .  | 000 |
| 1.4. Types of polymers used for nanocomposites preparation with layered silicates . . . . . | 000 |
| 1.4.1. Vinyl polymers . . . . .   | 000 |
| 1.4.2. Condensation (step) polymers . . . . .   | 000 |
| 1.4.3. Polyolefins . . . . .  | 000 |
| 1.4.4. Specialty polymers . . . . .   | 000 |
| 1.4.5. Biodegradable polymers . . . . .   | 000 |
| 2. Techniques used for the characterization of nanocomposites . . . . .                     | 000 |
| 3. Preparative methods and morphological study . . . . .                                    | 000 |
| 3.1. Intercalation of polymer or pre-polymer from solution . . . . .                        | 000 |
| 3.2. In situ intercalative polymerization method . . . . .                                  | 000 |
| 3.3. Melt intercalation . . . . .   | 000 |
| 4. Nanocomposite properties . . . . .   | 000 |
| 4.1. Mechanical properties . . . . .  | 000 |
| 4.1.1. Dynamic mechanical analysis . . . . .  | 000 |
| 4.1.2. Tensile properties . . . . .   | 000 |
| 4.1.3. Flexural properties . . . . .  | 000 |
| 4.2. Heat distortion temperature . . . . .  | 000 |
| 4.3. Thermal stability . . . . .  | 000 |
| 4.4. Fire retardant properties . . . . .  | 000 |
| 4.5. Gas barrier properties . . . . .   | 000 |
| 4.6. Ionic conductivity . . . . .   | 000 |
| 4.7. Optical transparency . . . . .   | 000 |
| 4.8. Biodegradability of biodegradable polymers-based nanocomposites . . . . .              | 000 |
| 4.9. Other properties . . . . .   | 000 |
| 5. Crystallization behavior and morphology of nanocomposites . . . . .                      | 000 |
| 6. Rheology . . . . .   | 000 |
| 6.1. Melt rheology and structure–property relationship . . . . .                            | 000 |
| 6.1.1. Dynamic oscillatory shear measurements . . . . .                                     | 000 |
| 6.1.2. Steady shear measurements . . . . .  | 000 |
| 6.1.3. Elongation flow rheology . . . . .   | 000 |
| 6.2. Electrorheology . . . . .  | 000 |

|   |     |
|---|-----|
| 7. Processing of nanocomposites . . . . .   | 000 |
| 7.1. Foam processing . . . . .  | 000 |
| 7.2. Shear processing . . . . .   | 000 |
| 8. Conclusions: status and prospects of polymer/layered silicate nanocomposites . . . . . | 000 |
| Acknowledgements . . . . .  | 000 |
| References . . . . .  | 000 |

## 1. Introduction

In recent years polymer/layered silicate (PLS) nanocomposites have attracted great interest, both in industry and in academia, because they often exhibit remarkable improvement in materials properties when compared with virgin polymer or conventional micro- and macro-composites. These improvements can include high moduli [1–6], increased strength and heat resistance [7], decreased gas permeability [8–12] and flammability [13–17], and increased biodegradability of biodegradable polymers [18]. On the other hand, there has been considerable interest in theory and simulations addressing the preparation and properties of these materials [19–34], and they are also considered to be unique model systems to study the structure and dynamics of polymers in confined environments [35–41].

Although the intercalation chemistry of polymers when mixed with appropriately modified layered silicate and synthetic layered silicates has long been known [42,43], the field of PLS nanocomposites has gained momentum recently. Two major findings have stimulated the revival of interest in these materials: first, the report from the Toyota research group of a Nylon-6 (N6)/montmorillonite (MMT) nanocomposite [1], for which very small amounts of layered silicate loadings resulted in pronounced improvements of thermal and mechanical properties; and second, the observation by Vaia et al. [44] that it is possible to melt-mix polymers with layered silicates, without the use of organic solvents. Today, efforts are being conducted globally, using almost all types of polymer matrices.

This review highlights the major developments in this area during the last decade. The different techniques used to prepare PLS nanocomposites, their physicochemical characterization, and the improved materials properties that those

materials can display; their processing and probable application of PLS nanocomposites will be discussed.

### 1.1. Structure and properties of layered silicates

The commonly used layered silicates for the preparation of PLS nanocomposites belong to the same general family of 2:1 layered or phyllosilicates. Their crystal structure consists of layers made up of two tetrahedrally coordinated silicon atoms fused to an edge-shared octahedral sheet of either aluminum or magnesium hydroxide. The layer thickness is around 1 nm, and the lateral dimensions of these layers may vary from 30 nm to several microns or larger, depending on the particular layered silicate. Stacking of the layers leads to a regular van der Waals gap between the layers called the *interlayer* or *gallery*. Isomorphic substitution within the layers (for example,  $\text{Al}^{3+}$  replaced by  $\text{Mg}^{2+}$  or  $\text{Fe}^{2+}$ , or  $\text{Mg}^{2+}$  replaced by  $\text{Li}^{1+}$ ) generates negative charges that are counterbalanced by alkali and alkaline earth cations situated inside the galleries. This type of layered silicate is characterized by a moderate surface charge known as the cation exchange capacity (CEC), and generally expressed as mequiv/100 gm. This charge is not locally constant, but varies from layer to layer, and must be considered as an average value over the whole crystal.

MMT, hectorite, and saponite are the most commonly used layered silicates. Layered silicates have two types of structure: tetrahedral-substituted and octahedral substituted. In the case of tetrahedrally substituted layered silicates the negative charge is located on the surface of silicate layers, and hence, the polymer matrices can react interact more readily with these than with octahedrally-substituted material. Details regarding the structure and chemistry for

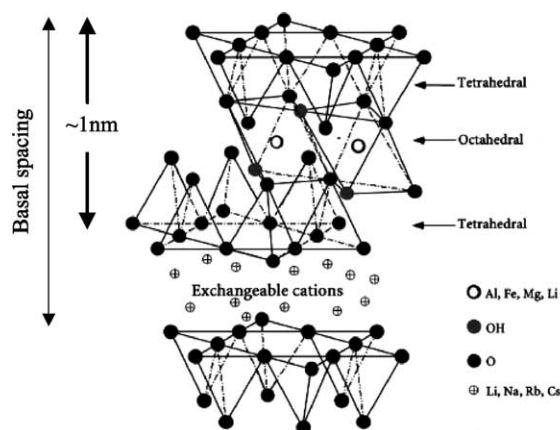


Fig. 1. Structure of 2:1 phyllosilicates.

these layered silicates are provided in Fig. 1 and Table 1, respectively.

Two particular characteristics of layered silicates that are generally considered for PLS nanocomposites. The first is the ability of the silicate particles to disperse into individual layers. The second characteristic is the ability to fine-tune their surface chemistry through ion exchange reactions with organic and inorganic cations. These two characteristics are, of course, interrelated since the degree of dispersion of layered silicate in a particular polymer matrix depends on the interlayer cation.

### 1.2. Structure and properties of organically modified layered silicate (OMLS)

The physical mixture of a polymer and layered silicate may not form a nanocomposite. This situation is analogous to polymer blends, and in most cases separation into discrete phases takes place. In immiscible systems, which typically correspond to the more conventionally filled polymers, the poor physical interaction between

the organic and the inorganic components leads to poor mechanical and thermal properties. In contrast, strong interactions between the polymer and the layered silicate in PLS nanocomposites lead to the organic and inorganic phases being dispersed at the nanometer level. As a result, nanocomposites exhibit unique properties not shared by their micro counterparts or conventionally filled polymers [1–6].

Pristine layered silicates usually contain hydrated  $\text{Na}^+$  or  $\text{K}^+$  ions [45]. Obviously, in this pristine state, layered silicates are only miscible with hydrophilic polymers, such as poly(ethylene oxide) (PEO) [46], or poly(vinyl alcohol) (PVA) [47]. To render layered silicates miscible with other polymer matrices, one must convert the normally hydrophilic silicate surface to an organophilic one, making the intercalation of many engineering polymers possible. Generally, this can be done by ion-exchange reactions with cationic surfactants including primary, secondary, tertiary, and quaternary alkylammonium or alkylphosphonium cations. Alkylammonium or alkylphosphonium cations in the organosilicates lower the surface energy of the inorganic host and improve the wetting characteristics of the polymer matrix, and result in a larger interlayer spacing. Additionally, the alkylammonium or alkylphosphonium cations can provide functional groups that can react with the polymer matrix, or in some cases initiate the polymerization of monomers to improve the strength of the interface between the inorganic and the polymer matrix [42,48].

Traditional structural characterization to determine the orientation and arrangement of the alkyl chain was performed using wide angle X-ray diffraction (WAXD). Depending on the packing density, temperature and alkyl chain length, the chains were thought to lie either parallel to the silicate layers forming mono or bilayers, or radiate away from the silicate layers forming mono or

Table 1  
Chemical formula and characteristic parameter of commonly used 2:1 phyllosilicates

| 2:1 phyllosilicates | Chemical formula   | CEC (mequiv/100 g) | Particle length (nm) |
|---------------------|--|--------------------|----------------------|
| Montmorillonite     | $\text{M}_x(\text{Al}_{4-x}\text{Mg}_x)\text{Si}_8\text{O}_{20}(\text{OH})_4$            | 110                | 100–150              |
| Hectorite           | $\text{M}_x(\text{Mg}_{6-x}\text{Li}_x)\text{Si}_8\text{O}_{20}(\text{OH})_4$            | 120                | 200–300              |
| Saponite            | $\text{M}_x\text{Mg}_6(\text{Si}_{8-x}\text{Al}_x)\text{Si}_8\text{O}_{20}(\text{OH})_4$ | 86.6               | 50–60                |

M, monovalent cation; x, degree of isomorphous substitution (between 0.5 and 1.3).

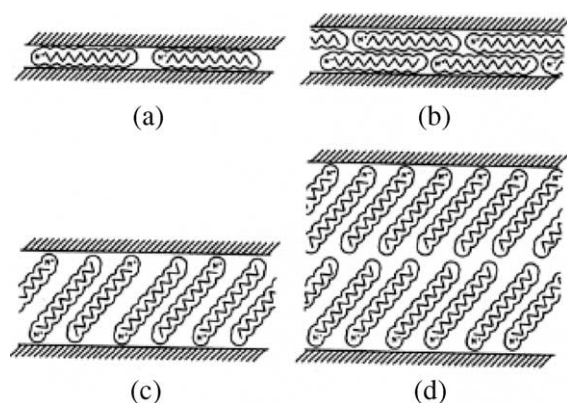


Fig. 2. Arrangements of alkylammonium ions in mica-type layered silicates with different layer charges. Hatch areas are silicate layers [50]. Reproduced from Vaia, Teukolsky and Giannelis by permission of American Chemical Society, USA.

bimolecular arrangements (see Fig. 2) [49]. However, these idealized structures have been shown to be unrealistic by Vaia et al. [50] using FTIR experiments. They showed that alkyl chains can vary from liquid-like to solid-like, with the liquid-like structure dominating as the interlayer density or chain length decreases (see Fig. 3), or as the temperature increases. This occurs because of the relatively small energy differences between the *trans* and *gauche* conformers; the idealized models described earlier assume all *trans* conformations. In addition, for longer chain length surfactants, the surfactants in the layered silicate can show thermal transition akin to melting or liquid-crystalline to liquid-like transitions upon heating.

### 1.3. Types of nanocomposites

In general, layered silicates have layer thickness on the order of 1 nm and a very high aspect ratio

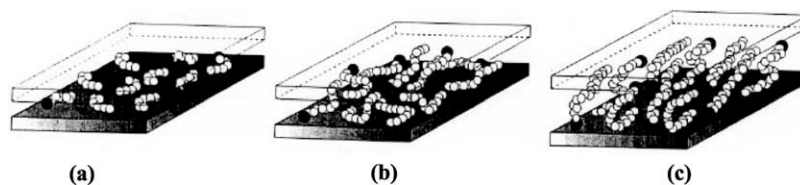


Fig. 3. Alkyl chain aggregation models: (a) short chain lengths, the molecules are effectively isolated from each other, (b) medium lengths, quasi-discrete layers form with various degree of in plane disorder and interdigitation between the layers and (c) long lengths, interlayer order increases leading to a liquid-crystalline polymer environment. Open circles represent the  $\text{CH}_2$  segments while cationic head groups are represented by filled circles [50]. Reproduced from Vaia, Teukolsky and Giannelis by permission of American Chemical Society, USA.

(e.g. 10–1000). A few weight percent of layered silicates that are properly dispersed throughout the polymer matrix thus create much higher surface area for polymer/filler interaction as compared to conventional composites. Depending on the strength of interfacial interactions between the polymer matrix and layered silicate (modified or not), three different types of PLS nanocomposites are thermodynamically achievable (see Fig. 4):

- Intercalated nanocomposites*: in intercalated nanocomposites, the insertion of a polymer matrix into the layered silicate structure occurs in a crystallographically regular fashion, regardless of the clay to polymer ratio. Intercalated nanocomposites are normally interlayer by a few molecular layers of polymer. Properties of the composites typically resemble those of ceramic materials.
- Flocculated nanocomposites*: conceptually this is same as intercalated nanocomposites. However, silicate layers are some times flocculated due to hydroxylated edge–edge interaction of the silicate layers.
- Exfoliated nanocomposites*: in an exfoliated nanocomposite, the individual clay layers are separated in a continuous polymer matrix by an average distances that depends on clay loading. Usually, the clay content of an exfoliated nanocomposite is much lower than that of an intercalated nanocomposite.

### 1.4. Types of polymers used for nanocomposites preparation with layered silicates

The large variety of polymer systems used in nanocomposites preparation with layered silicate can be conventionally classified as below.

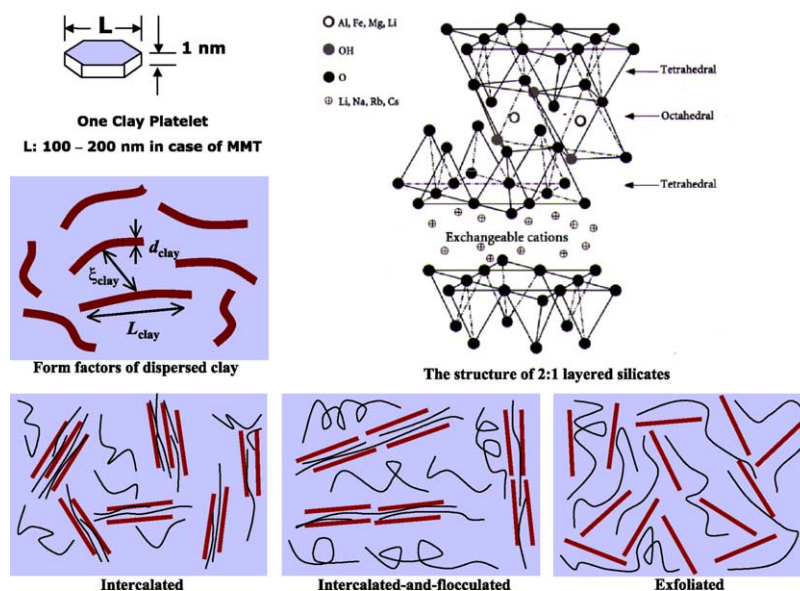


Fig. 4. Schematically illustration of three different types of thermodynamically achievable polymer/layered silicate nanocomposites [391]. Reproduced from Sinha Ray, Okamoto and Okamoto by permission of American Chemical Society, USA.

#### 1.4.1. Vinyl polymers

These include the vinyl addition polymers derived from common monomers like methyl methacrylate [42,51–64], methyl methacrylate copolymers [65–68], other acrylates [69–71], acrylic acid [72, 73], acrylonitrile [74–77], styrene (S) [38,44, 78–103], 4-vinylpyridine [104], acrylamide [105, 106], poly(*N*-isopropylacrylamide) [107] and tetrafluoro ethylene [108]. In addition, selective polymers like PVA [47,109–112], poly(*N*-vinyl pyrrolidone) [113–117], poly(vinyl pyrrolidinone) [118,119], poly(vinyl pyridine) [120], poly(ethylene glycol) [121], poly(ethylene vinyl alcohol) [122], poly(vinylidene fluoride) [123], poly(*p*-phenylenevinylene) [124], polybenzoxazole [125], poly(styrene-*co*-acrylonitrile) [126], ethyl vinyl alcohol copolymer [127], polystyrene–polyisoprene diblock copolymer [128, 129] and others [130] have been used.

#### 1.4.2. Condensation (step) polymers

Several technologically important polycondensates have been used in nanocomposites preparation with layered silicate. These include N6 [1,12,131–155], several other polyamides [15,16,19,156–162], poly( $\epsilon$ -caprolactone) (PCL) [10,163–175], poly(ethylene terephthalate) [176–182], poly(trimethylene

terephthalate) [183,184], poly(butylene terephthalate) [185], polycarbonate (PC) [186,187], PEO [36,40,46, 188–208], ethylene oxide copolymers [209,210], poly(ethylene imine) [211], poly(dimethyl siloxane) [212–217], polybutadiene [218], butadiene copolymers [219–221], epoxidized natural rubber [222, 223], epoxy polymer resins (EPR) [224–247], phenolic resins [248,249], polyurethanes (PU) [250–254], polyurethane urea [8], polyimides [255–272], poly(amic acid) [273,274], polysulfone [275], polyetherimide [276,277], and fluoropoly(ether-imide) [278].

#### 1.4.3. Polyolefins

Polyolefins such as polypropylene (PP) [279–319], polyethylene (PE) [320–329], polyethylene oligomers [330], copolymers such as poly(ethylene-*co*-vinyl acetate) (EVA) [331], ethylene propylene diene methylene linkage rubber (EPDM) [332] and poly(1-butene) [333] have been used.

#### 1.4.4. Specialty polymers

In addition to the above mentioned conventional polymers, several interesting developments occurred in the preparation of nanocomposites of layered silicates with specialty polymers including

the *N*-heterocyclic polymers like polypyrrole (PPY) [334–339], poly(*N*-vinylcarbazole) (PNVC) [340, 341], and polyaromatics such as polyaniline (PANI) [342–356], poly(*p*-phenylene vinylene) [357] and related polymers [358]. PPY and PANI are known to display electric conductivity [359], and PNVC is well known for its high thermal stability and characteristic optoelectronic properties [360–363]. Research has also been initiated with liquid crystalline polymer (LCP)-based nanocomposites [364–368], hyperbranched polymers [369], cyanate ester [370], Nafion<sup>®</sup> [371], and aryl-ethanyl-terminated coPoss imide oligomers [372].

#### 1.4.5. Biodegradable polymers

Today, tremendous amounts and varieties of plastics, notably polyolefins, polystyrene and poly(vinyl chloride) produced mostly from fossil fuels, are consumed and discarded into the environment, ending up as wastes that do not degrade spontaneously. Their disposal by incineration produces large amounts of carbon dioxide, and contributes to global warming, some even releasing toxic gases. For these reasons, there is an urgent need for the development of *green polymeric materials* that would not involve the use of toxic or noxious components in their manufacture, and could allow degradation via a natural composting process. Accordingly, polylactide (PLA) is of increasing commercial interest because it is made from renewable resources and readily biodegradable.

Recently, our group has started the preparation, characterization, and materials properties of various kinds of biodegradable polymers/layered silicate nanocomposites having properties suitable for a wide range of applications. So far reported biodegradable polymers for the preparation of nanocomposites are PLA [18,373–388], poly(butylene succinate) (PBS) [389–393], PCL [163–175], unsaturated polyester [394], polyhydroxy butyrate [395–397], aliphatic polyester [398–401], etc.

## 2. Techniques used for the characterization of nanocomposites

Generally, the structure of nanocomposites has typically been established using WAXD analysis and transmission electron micrographic (TEM)

observation. Due to its easiness and availability WAXD is most commonly used to probe the nanocomposite structure [2–6] and occasionally to study the kinetics of the polymer melt intercalation [80]. By monitoring the position, shape, and intensity of the basal reflections from the distributed silicate layers, the nanocomposite structure (*intercalated* or *exfoliated*) may be identified. For example, in an *exfoliated* nanocomposite, the extensive layer separation associated with the delamination of the original silicate layers in the polymer matrix results in the eventual disappearance of any coherent X-ray diffraction from the distributed silicate layers. On the other hand, for *intercalated* nanocomposites, the finite layer expansion associated with the polymer intercalation results in the appearance of a new basal reflection corresponding to the larger gallery height.

Although WAXD offers a convenient method to determine the interlayer spacing of the silicate layers in the original layered silicates and in the intercalated nanocomposites (within 1–4 nm), little can be said about the spatial distribution of the silicate layers or any structural non-homogeneities in nanocomposites. Additionally, some layered silicates initially do not exhibit well-defined basal reflections. Thus, peak broadening and intensity decreases are very difficult to study systematically. Therefore, conclusions concerning the mechanism of nanocomposites formation and their structure based solely on WAXD patterns are only tentative. On the other hand, TEM allows a qualitative understanding of the internal structure, spatial distribution of the various phases, and views of the defect structure through direct visualization. However, special care must be exercised to guarantee a representative cross-section of the sample. The WAXD patterns and corresponding TEM images of three different types of nanocomposites are presented in Fig. 5.

Both TEM and WAXD are essential tools [402] for evaluating nanocomposite structure. However, TEM is time-intensive, and only gives qualitative information on the sample as a whole, while low-angle peaks in WAXD allow quantification of changes in layer spacing. Typically, when layer spacing exceed 6–7 nm in intercalated nanocomposites or when the layers become relatively disordered in exfoliated nanocomposites, associated WAXD features weaken to the point of not being useful. However, recent

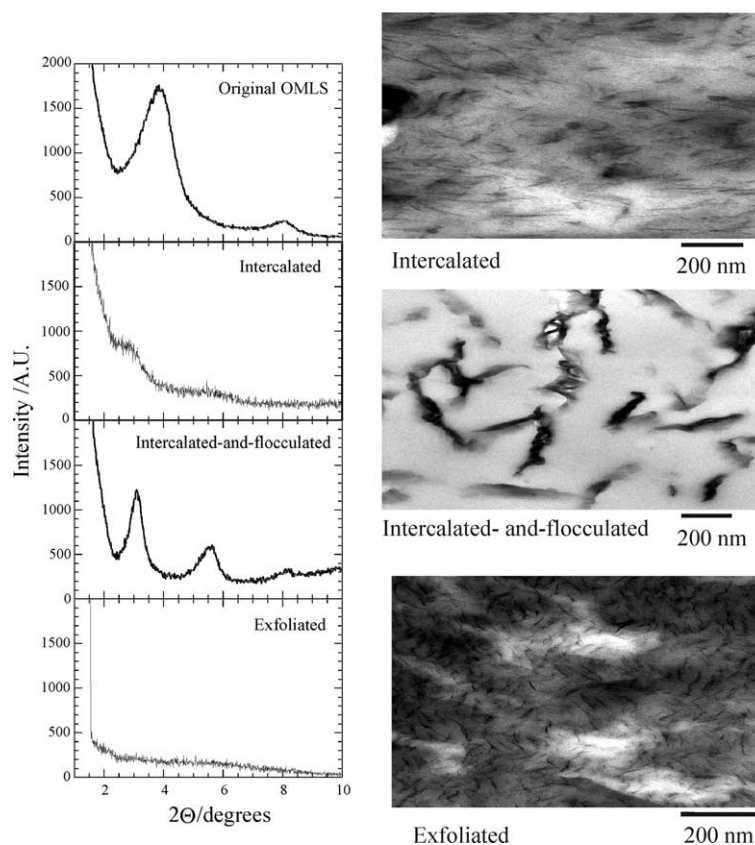


Fig. 5. (a) WAXD patterns and (b) TEM images of three different types of nanocomposites.

simultaneous small angle X-ray scattering (SAXS) and WAXD studies yielded quantitative characterization of nanostructure and crystallite structure in N6 based nanocomposites [403].

Very recently, Bafna et al. [329] developed a technique to determine the three-dimensional (3D) orientation of various hierarchical organic and inorganic structures in a PLS nanocomposite. They studied the effect of compatibilizer concentration on the orientation of various structures in PLS nanocomposites using 2D SAXS and 2D WAXD in three sample/camera orientations. Reflections and orientation of six different structural features were easily identified: (a) clay clusters/tactoids ( $0.12\ \mu\text{m}$ ), (b) modified/intercalated clay stacking period (002) ( $24\text{--}31\ \text{\AA}$ ), (c) stacking period of unmodified clay platelets (002) ( $13\ \text{\AA}$ ), (d) clay (110) and (020) planes, normal to (b) and (c), (e) polymer crystalline lamellae (001) ( $190\text{--}260\ \text{\AA}$ ), long period ((001) is an average

crystallographic direction), and (f) polymer unit cell (110) and (200) planes.

The corresponding identified reflections are presented in Fig. 6. A 3D study of the relative orientation of the above-mentioned structures was carried out by measuring three projections of each sample. Quantitative data on the orientation of these structural units in the nanocomposite film was determined through calculations of the major axis direction cosines and through a ternary, direction-cosine plot called a 'Wilchinsky triangle' [404–407], previously proposed in lamellar orientation studies [405]. It allows a direct comparison of average preferred orientations for different structural features. In this way it is conceptually more useful than stereographic projections involving orientation density maps for a single WAXD reflection.

VanderHart et al. [408] first used solid-state nuclear magnetic resonance (NMR) ( $^1\text{H}$  and  $^{13}\text{C}$ )



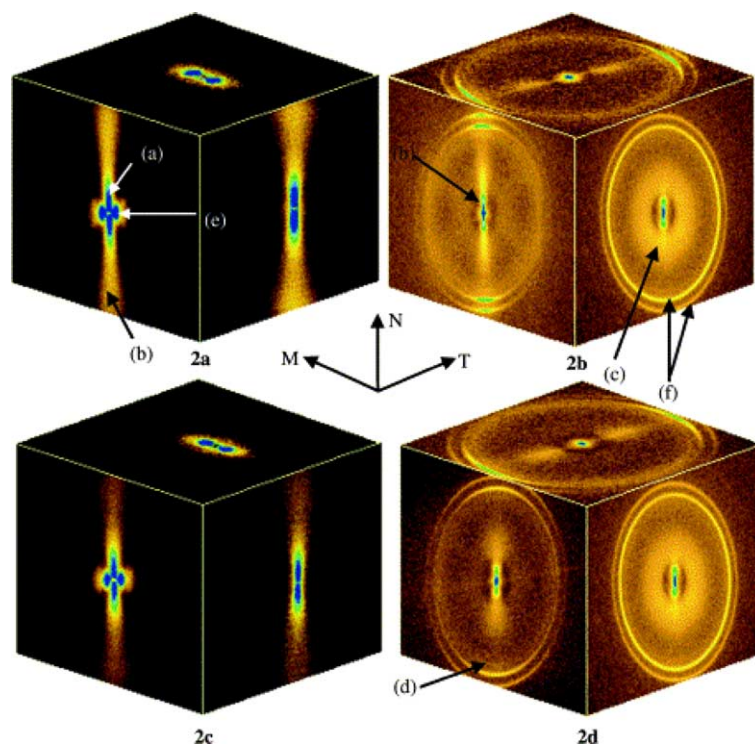


Fig. 6. 2D SAXS (a and c) and WAXS (b and d) patterns for orientation MN (left face), NT (right face) and MT (top face) of films HD603 (a and b) and HD612 (c and d). The numbers in the parenthesis represent the reflections from the following: (a) clay tactoids, (b) modified/intercalated clay (002) plane, (c) unmodified clay (002) plane, (d) clay (110) and (020) plane, (e) polymer crystalline lamellar, (f) polymer unit cell (110) plane (inner ring) and (200) plane (outer ring) [329]. Reproduced from Bafna, Beaucage, Mirabella and Mehta by permission of Elsevier Science Ltd, UK.

as a tool for gaining greater insight about the morphology, surface chemistry, and to a very limited extent, the dynamics of exfoliated polymer clay nanocomposites. They were especially interested in developing NMR methods to quantify the level of clay exfoliation, a very important facet of nanocomposite characterization.

The main objective in solid-state NMR measurement is to connect the measured longitudinal relaxations,  $T_1^H$ s, of proton (and  $^{13}\text{C}$  nuclei) with the quality of clay dispersion. Because the extent of and the homogeneity of the dispersion of the silicate layers within the polymer matrix are very important for determining physical properties.

The surfaces of naturally occurring layered silicates such as MMT are mainly made of silica tetrahedral while the central plane of the layers contains octahedrally coordinated  $\text{Al}^{3+}$  (see Fig. 1 and Table 1) with frequent non-stoichiometric

substitutions, where an  $\text{Al}^{3+}$  is replaced by  $\text{Mg}^{2+}$  and, somewhat less frequently, by  $\text{Fe}^{3+}$ . The concentration of the later ion is very important because  $\text{Fe}^{3+}$  is strongly paramagnetic (spin = 5/2 in this distorted octahedral environment [409]). Typical concentrations of  $\text{Fe}^{3+}$  in naturally occurring clays produce nearest-neighbor Fe–Fe distances of about 1.0–1.4 nm [410], and at such distances, the spin-exchange interaction between the unpaired electrons on different Fe atoms is expected to produce magnetic fluctuations in the vicinity of the Larmor frequencies for protons or  $^{13}\text{C}$  nuclei [410]. The spectral density of these fluctuations is important because the  $T_1^H$ , of protons (and  $^{13}\text{C}$  nuclei) within about 1 nm of the clay surface can be directly shortened. For protons, if that mechanism [411] is efficient, relaxation will also propagate into the bulk of the polymer by spin diffusion [412]. Thus, this paramagnetically induced relaxation will influence the overall measured  $T_1^H$  to

an extent that will depend both on the Fe concentration in the clay layer and, more importantly, on the average distances between clay layers. The later dependence suggests a potential relationship between measured  $T_1^H$  values and the quality of the clay dispersion. If the clay particles are stacked and poorly dispersed in the polymer matrix, the average distances between polymer/clay interfaces are greater, and the average paramagnetic contribution to  $T_1^H$  is weaker. VanderHart et al. [147,413] also employed the same arguments in order to understand the stability of a particular OMLS under different processing conditions.

Yang and Zax [410] also used NMR in order to determine the relative mobility of bulk and interphase polymers in intercalated PEO nanocomposites, and Mathias et al. [403] used NMR to determine the phase structure of polyamide-6/clay nanocomposites. In a very recent report, Sahoo et al. [414] studied the structure and dynamics of the polymer chains inserted between the MMT lamellae. The  $^{13}\text{C}$  NMR chemical shifts of the polymer component of the nanocomposite that was prepared by in situ intercalative polymerization were assigned by analyzing the difference between the chemical shift values of the bulk and bulk-intercalated poly(2-ethanypyridin) (P2EPy) nanocomposite material. The results of solid-state NMR and X-ray diffraction studies clearly demonstrate a spontaneous polymerization of 2EPy within the galleries of MMT. The polymer thus formed is mostly bound to the surface of MMT at either the Brønsted or Lewis acid sites. IR analysis suggests the existence of positive charge on the nitrogen atom of the polymer inside the lamellar gallery. Bulk synthesized P2EPy-bulk in both protonated and deprotonated forms was also intercalated and studied by solid-state NMR. The intercalation of poly(styrene-ethylene oxide) block copolymers into a smectite clay, hectorite, has also been studied by multinuclear solid-state NMR [415].

In another report, Forte et al. [65] used  $^{13}\text{C}$  solid-state NMR for the determination of the structure of clay/methyl methacrylate copolymer nanocomposites. They prepared interlayer complexes of several MMA/2-(*N*-methyl-*N,N*-diethylammonium iodide) ethyl acrylate (MDEA) copolymers with two different clays (bentonite and hectorite) using two different preparations, and then complexes were studied by

means of solid-state  $^{13}\text{C}$  NMR. Given the relatively high content of paramagnetic centers in bentonite, which is approximately 50 times more paramagnetic than hectorite, the SPE/MAS and CP/MAS spectra of the different nanocomposites with bentonite show differences according to the proximity of the different copolymer moieties to the clay surface. The dynamics of the organic molecules in the inorganic interlayers were investigated by measuring relaxation times. The paramagnetic force of the clay, where relevant, strongly influences the relaxation time measured, whereas in the other cases the different relaxation times allow one to discern differences in the structural organization and mobility of the organic molecules depending on the nanocomposite preparation. Finally, the structure of the nanocomposite was determined by combining both the NMR results and WAXD pattern.

Some authors [95,416] also used FTIR spectroscopy to understand the structure of the nanocomposites. Very recently, Nascimento et al. [356] presented for the first time the resonance Raman characterization of a polymer/clay nanocomposite formed by aniline polymerization in the presence of MMT.

### 3. Preparative methods and morphological study

Intercalation of polymers in layered hosts, such as layered silicates, has proven to be a successful approach to synthesize PLS nanocomposites. The preparative methods are divided into three main groups according to the starting materials and processing techniques:

*Intercalation of polymer or pre-polymer from solution.* This is based on a solvent system in which the polymer or pre-polymer is soluble and the silicate layers are swellable. The layered silicate is first swollen in a solvent, such as water, chloroform, or toluene. When the polymer and layered silicate solutions are mixed, the polymer chains intercalate and displace the solvent within the interlayer of the silicate. Upon solvent removal, the intercalated structure remains, resulting in PLS nanocomposite.

*In situ intercalative polymerization method.* In this method, the layered silicate is swollen within the liquid monomer or a monomer solution so the polymer

formation can occur between the intercalated sheets. Polymerization can be initiated either by heat or radiation, by the diffusion of a suitable initiator, or by an organic initiator or catalyst fixed through cation exchange inside the interlayer before the swelling step.

*Melt intercalation method.* This method involves annealing, statically or under shear, a mixture of the polymer and OMLS above the softening point of the polymer. This method has great advantages over either in situ intercalative polymerization or polymer solution intercalation. First, this method is environmentally benign due to the absence of organic solvents. Second, it is compatible with current industrial process, such as extrusion and injection molding. The melt intercalation method allows the use of polymers which were previously not suitable for in situ polymerization or solution intercalation.

### 3.1. Intercalation of polymer or pre-polymer from solution

Water-soluble polymers, such as PEO [46], PVA [47], PVP [113], and PEVA [122], have been intercalated into the clay galleries using this method. Examples from non-aqueous solvents are nanocomposites of PCL/clay [164] and PLA/clay [373] in chloroform as a co-solvent, and high-density polyethylene (HDPE) with xylene and benzonitrile [320]. Nematic liquid crystal PLS nanocomposites have also been prepared using this method in various organic solvents, such as toluene and DMF [365].

The thermodynamics involved in this method are described in the following. For the overall process, in which polymer is exchanged with the previously intercalated solvent in the gallery, a negative variation in the Gibbs free energy is required. The driving force for the polymer intercalation into layered silicate from solution is the entropy gained by desorption of solvent molecules, which compensates for the decreased entropy of the confined, intercalated chains [21]. Using this method, intercalation only occurs for certain polymer/solvent pairs. This method is good for the intercalation of polymers with little or no polarity into layered structures, and facilitates production of thin films with polymer-oriented clay intercalated layers. However, from commercial point of view, this method involves the copious use of

organic solvents, which is usually environmentally unfriendly and economically prohibitive.

In 1992, Aranda and Ruiz-Hitzky [46] reported the first preparation of PEO/MMT nanocomposites by this method. They performed a series of experiments to intercalate PEO ( $M_w = 105$  g/mol) into  $\text{Na}^+$ -MMT using different polar solvents: water, methanol, acetonitrile, and mixtures (1:1) of water/methanol and methanol/acetonitrile. In this method the nature of solvents is critical in facilitating the insertion of polymers between the silicate layers, polarity of the medium being a determining factor for intercalations [43,417]. The high polarity of water causes swelling of  $\text{Na}^+$ -MMT, provoking cracking of the films. Methanol is not suitable as a solvent for high molecular weight (HMW) PEO, whereas water/methanol mixtures appear to be useful for intercalations, although cracking of the resulting materials is frequently observed. PEO intercalated compounds derived from the homoionic  $\text{M}^{+n}$ -MMT and  $\text{M}^{+n}$ -hectorite, can satisfactorily be obtained using anhydrous acetonitrile or a methanol/acetonitrile mixture as solvents.

The resulting PEO/silicate materials show good stability toward treatment with different solvents (e.g. acetonitrile, methanol, ethanol, water, etc.) in experiments carried out at room temperature for long time periods (> 24 h). In addition, the lack of PEO replacement by organic compounds having high affinity toward the parent silicate, such as dimethyl sulfoxide and crown ethers, indicates again the high stability of PEO-intercalated compounds. On the other hand, treatment with salt solutions provokes the replacement of the interlayer cations without disturbing the PEO. For example,  $\text{Na}^+$  ions in PEO/ $\text{Na}^+$ -MMT are easily replaced by  $\text{NH}_4^+$  or  $\text{CH}_3(\text{CH}_2)_2\text{NH}_3^+$  ions, after treatment (2 h) at room temperature with an aqueous solution of their chloride, perchlorate and thiocyanate salts (1N solutions), in a reversible process.

Wu et al. [188] reported the intercalation of PEO in  $\text{Na}^+$ -MMT and  $\text{Na}^+$ -hectorite using this method in acetonitrile, allowing the stoichiometric incorporation of one or two polymer chains in between the silicate layers and increasing the inter sheet spacing from 0.98 to 1.36 and 1.71 nm, respectively. Study of the chain conformation using 2D double-quantum NMR on  $^{13}\text{C}$  enriched PEO intercalated in  $\text{Na}^+$ -hectorite reveals

that the conformation of the ‘–OC–CO–’ bonds of PEO is  $(90 \pm 5)\%$  *gauche*, inducing constraints on the chain conformation in the interlayer [195].

Recently, Choi et al. [200] prepared PEO/MMT nanocomposites by a solvent casting method using chloroform as a co-solvent. WAXD analyses and TEM observations established the intercalated structure of these nanocomposites. Other authors [201,206] have also used the same method and same solvent for the preparation of PEO/clay nanocomposites.

Poly(dimethylsiloxane)/MMT nanocomposites were synthesized by sonicating a mixture of silanol-terminated poly(dimethylsiloxane) (PDMS) and a commercial organosilicate at room temperature for 2 min [212]. A schematic illustration of nanocomposite synthesis is shown in Fig. 7. Delamination of the silicate particles in the PDMS matrix was accomplished by suspending and sonicating the organosilicate in PDMS at room temperature. WAXD analyses of various nanocomposites revealed no distinct features at low scattering angles, indicating the formation of exfoliated nanocomposites.

This technique was successfully used by Yano et al. [11,255] for the preparation of polyimide/MMT nanocomposites from a dimethylacetamide (DMAC) solution of poly(amic acid) and a DMAC dispersion of MMT modified with dodecylammonium cations. A flow chart for the synthesis of polyimide/MMT nanocomposite is presented in Fig. 8. Table 2 shows the dispersibility of various kinds of organically modified MMT(s) in DMAC and the average diameter of organophilic MMT(s), obtained from a dynamic light scattering experiment. In the case of 12CH<sub>3</sub>-MMT, the MMT appeared to disperse in DMAC homogeneously, and the average diameter of the dispersed MMT particles was the smallest of all. Another interesting aspect is that as the carbon number of the surfactant increases, the hydrophilicity of the organophilic MMT decreases. Table 2 also

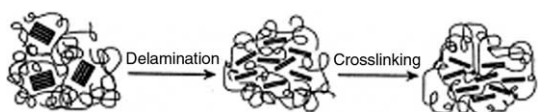


Fig. 7. Schematic illustration of nanocomposite synthesis [212]. Reproduced from Burnside and Giannelis by permission of American Chemical Society, USA.

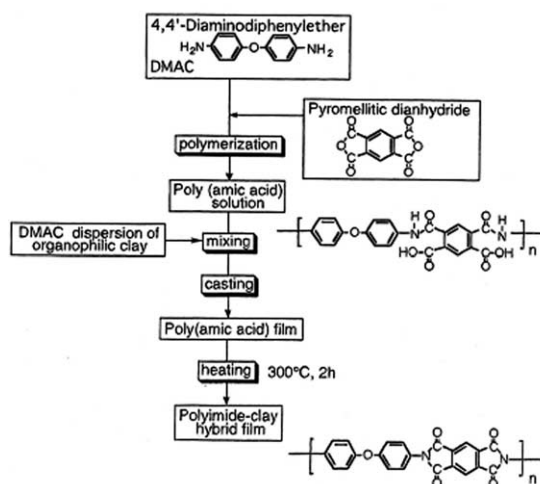


Fig. 8. Synthesis of polyimide/clay nanocomposite film [11]. Reproduced from Yano, Usuki, Okada, Kurauchi and Kamigaito by permission of John Wiley and Sons, Inc., USA.

indicates that 10–12 carbon atoms are appropriate for organophilic MMT to be dispersed in DMAC.

Fig. 9 shows the WAXD patterns of C10A-MMT, 12COOH-MMT, and 12CH<sub>3</sub>-MMT in the region of  $2\theta = 2-10^\circ$ . Each pattern has one peak, at  $2\theta = 7.2, 5.8,$  and  $5.9^\circ$ , respectively. These peaks are assigned to the (001) lattice spacing of MMT. WAXD patterns of various polyimide/MMT nanocomposites are presented in Fig. 10. The WAXD pattern of the nanocomposite prepared using 12CH<sub>3</sub>-MMT shows almost exfoliated structure, while WAXD patterns of the nanocomposites prepared with 12COOH-MMT or C10A-MMT revealed that a part of MMT was not homogeneously dispersed in the polyimide matrix.

In further work, they used four different types of OMLS in order to investigate the effect of OMLS on the structure and properties of the nanocomposites [257]. Hectorite, saponite, MMT, and synthetic mica were used as pristine layered silicates. The CEC of hectorite, saponite, MMT and synthetic mica are 55, 100, 110, and 119 mequiv/100 gm, respectively, and all of them were modified with dodecylammonium cations using a cation exchange reaction.

Parts a and b of Fig. 11, respectively, represents the WAXD patterns of various OMLS and corresponding nanocomposites of polyimide in the range of  $2\theta = 2-10^\circ$ . WAXD patterns (see Fig. 11b) revealed that

Table 2  
Dispersibility and average diameter of organically modified montmorillonite in DMAC [11]

| Intercalated salts                                     | Dispersibility of organophilic MMT in DMAC | Average diameter <sup>a</sup> (μm) |
|--|--|------------------------------------|
| <i>n</i> -Octyltrimethylammonium chloride              | Not dispersible                            | –                                  |
| Ammonium salt of dodecylamine (12CH <sub>3</sub> -MMT) | Dispersible                                | 0.44                               |
| Ammonium salt of 12-aminododecanoic acid (12COOH-MMT)  | Partly dispersible                         | 3.75                               |
| <i>n</i> -Decyltrimethylammonium chloride (C10A-MMT)   | Partly dispersible                         | 0.61                               |
| <i>n</i> -Dodecyltrimethylammonium chloride            | Not dispersible                            | –                                  |
| <i>n</i> -Hexadecyltrimethylammonium chloride          | Not dispersible                            | –                                  |
| <i>n</i> -Dioctadecyldimethylammonium chloride         | Not dispersible                            | –                                  |
| <i>n</i> -Trioctylmethylammonium chloride              | Not dispersible                            | –                                  |
| <i>n</i> -Benzyltrimethylammonium chloride             | Not dispersible                            | –                                  |

Reproduced from Yano, Usuki, Okada, Kurauchi and Kamigaito by permission of John Wiley and Sons, Inc, USA.

<sup>a</sup> Values of average diameter are much bigger than 2000 Å, because an average diameter from light scattering measurement includes solvent around a substance.

the nanocomposites prepared with MMT or mica clay did not show any clear peaks corresponding to the exfoliated structure, while nanocomposites prepared with hectorite or saponite clay show small peaks, indicating that some portions of OMLS were stacked. The reason why MMT or mica dispersed homogeneously in the polyimide matrix was not explained properly by the authors, but there may be a greater interaction between the polyimide matrix and

the organically modified MMT or synthetic mica compared to that of the polyimide matrix and organically modified hectorite or saponite clay. This behavior is more clearly observed in TEM images. From the TEM images it is established that OMLS particles are dispersed homogeneously into the polyimide matrix and oriented parallel to the film surface when MMT or mica-based OMLS is used for nanocomposites preparation, whereas most of the OMLS are dispersed homogeneously with small stacking in the saponite-based nanocomposite. On

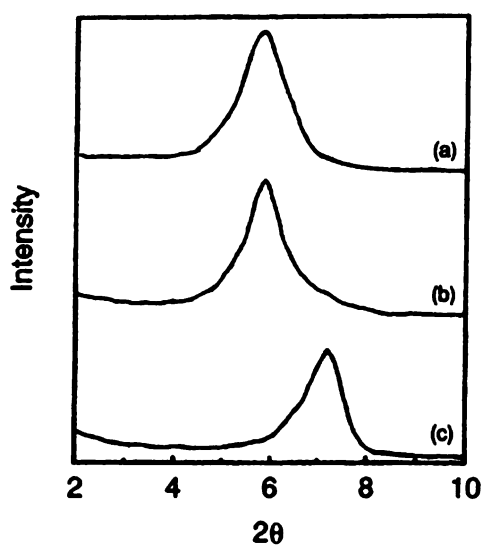


Fig. 9. WAXD patterns of: (a) 12CH<sub>3</sub>-MMT, (b) 12COOH-MMT, and (c) C10A-MMT [11]. Reproduced from Yano, Usuki, Okada, Kurauchi and Kamigaito by permission of John Wiley and Sons, Inc., USA.

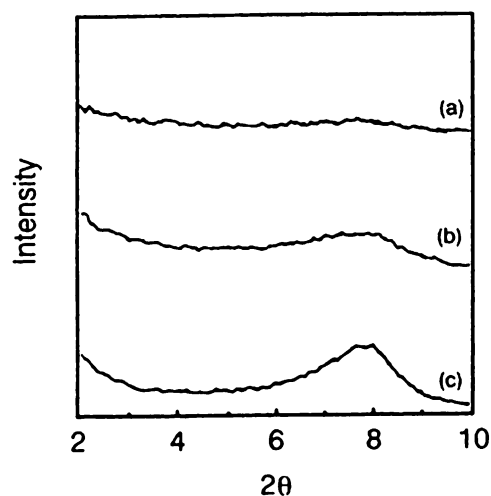


Fig. 10. WAXD patterns of polyimide/clay nanocomposites prepared with: (a) 12CH<sub>3</sub>-MMT, (b) 12COOH-MMT, and (c) C10A-MMT [11]. Reproduced from Yano, Usuki, Okada, Kurauchi and Kamigaito by permission of John Wiley and Sons, Inc., USA.

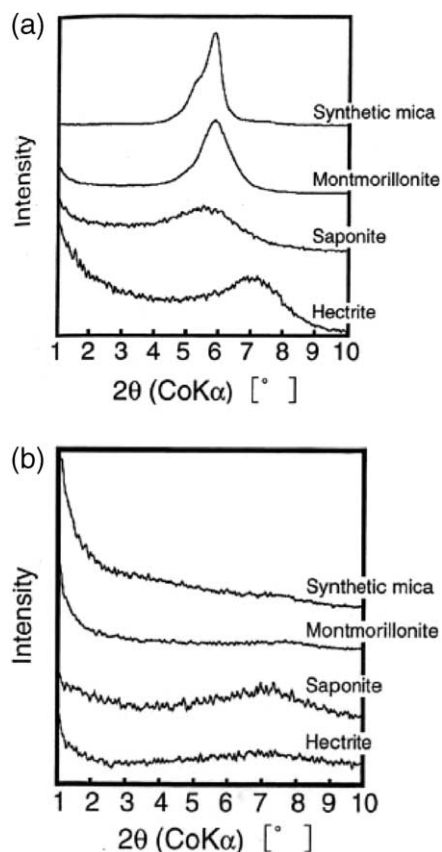


Fig. 11. WAXD patterns of: (a) various organoclays and (b) corresponding nanocomposites with polyimide [257]. Reproduced from Yano, Usuki and Okada by permission of John Wiley and Sons, Inc., USA.

the other hand, OMLS are dispersed as aggregates in the nanocomposite when hectorite was used. These results are nicely correlated with the WAXD patterns, as observed in Fig. 11b.

In another report [270] polyimide/MMT nanocomposites were prepared using the solvent cast method from solutions of poly(amic acid) precursors and dodecyl-MMT using *N*-methyl-2-pyrrolidone as a solvent. The cured films of the rigid-rod polyimide/MMT nanocomposites were characterized by FTIR, TEM and WAXD to be exfoliated nanocomposites at low MMT content and partially exfoliated structures at high MMT content.

PLA or PCL-based nanocomposites have also been produced by dissolving the polymers in hot chloroform in the presence of distearyldimethylammonium-modified MMT (2C18-MMT). In the case of

PLA/MMT nanocomposites [373], WAXD and SAXS results showed that the silicate layers forming the clay could not be intercalated in the PLA–MMT blends prepared by the solvent-cast method. In other words, the clay existed in the form of tactoids, consisting of several stacked silicate monolayers. These tactoids are responsible for the formation of remarkable geometrical structures in the blends, which leads to the formation of superstructures in the thickness of the blended film, and that may lead to such a structural feature increases Young's modulus of the blend. Similar behavior was observed for a PCL/2C18-MMT blend [164]. Recently, Lim et al. [401] used the same solvent and method for the preparation of aliphatic polyester/organically modified MMT nanocomposites.

Nanocomposites of nitrile-based copolymer and polyethylene-based polymer have also been prepared with organically modified MMT using this technique MMT [320]. WAXD analysis reveals a broad diffraction peak that has been shifted towards a higher interlayer spacing. The large broadening of the peak may indicate that partial exfoliation has occurred, as opposed to TEM analysis where both stacked intercalated and exfoliated silicate layers coexist.

HDPE-based nanocomposites have been prepared by dissolving HDPE in a mixture of xylene and benzonitrile with dispersed OMLS [320]. The nanocomposite material was then recovered by precipitation from THF followed by several washings with THF. Syndiotactic polystyrene (s-PS) organically modified clay nanocomposites have also been prepared by the solution intercalation technique by mixing pure s-PS and organophilic clay with adsorbed cetyl pyridium chloride [97]. The WAXD analyses and TEM observations clearly established a nearly exfoliated structure of the prepared nanocomposites.

This technique was also applied to the preparation of polysulfone (PSF)/organoclay nanocomposites [275]. PSF/organoclay nanocomposites were obtained by mixing the desired amount of the organoclay with PSF in DMAC at 80 °C for 24 h. WAXD analyses and TEM observations established exfoliation of the organoclay in the nanocomposites.

More recently, Strawhecker and Manias [111] used this method in attempts to produce PVA/MMT nanocomposites films. PVA/MMT nanocomposite films were cast from a MMT/water suspension

containing dissolved PVA. Room temperature distilled water was used to form a suspension of  $\text{Na}^+$ -MMT. The suspension was first stirred for 1 h and then sonicated for 30 min. Low viscosity, fully hydrolyzed atactic PVA was then added to the stirring suspension such that the total solid (silicate plus polymer) was  $\leq 5$  wt%. The mixtures were then heated to  $90^\circ\text{C}$  to dissolve the PVA, again sonicated for 30 min, and finally films were cast in a closed oven at  $40^\circ\text{C}$  for 2 days. The recovered cast films were then characterized by both WAXD and TEM. Fig. 12 shows WAXD scans of 20, 40, 60, 80 and 100 wt% MMT concentration; the inset shows the corresponding  $d$ -spacing distributions for the same concentrations. Both the  $d$ -spacing and their distribution decrease systematically with increasing MMT wt% in the nanocomposites. The TEM photograph of 20 wt% clay containing nanocomposite reveals the co-existence of silicate layers in the intercalated and exfoliated states.

At first glance, this dependence of the intercalated structure and  $d$ -spacing on the polymer/silicate mass ratio seems to be at odds with the theoretical expectations [21,24]. The equilibrium nanocomposite structure predicted from the thermodynamics corresponds to an intercalated periodic nanocomposite with  $d$ -spacing around 1.8 nm, which is expected to be independent of the polymer-to-silicate composition [21]. However, thermodynamics can only predict the equilibrium structure. In this case, the nanocomposite structure that they found is actually kinetically

dictated; in the water solution of PVA and MMT the layers remain in colloidal suspension. Where this suspension is slowly dried, the silicate layers remain distributed and embedded in the polymer gel. Further drying removes all of the water, and although the thermodynamics would predict the MMT layers to re-aggregate in an intercalated fashion, the slow polymer dynamics trap some of the layers apart and therefore remain dispersed in the polymer matrix. Obviously, the kinetic constraints imposed by the polymer become less important as the polymer-to-silicate fraction decreases, and consequently, for higher amounts of MMT, intercalated structures are formed. For these periodic structures, the variation of the  $d$ -spacing with wt% of MMT reflects the different polymer-silicate weight ratios, and upon increasing the amount of MMT the intercalated  $d$ -spacing converges to the equilibrium separation of 1.8 nm. Greenland et al. [47,108] and Ogata et al. [109] also used the same method to fabricate PVA/layered silicate nanocomposites.

Disordered polystyrene–polyisoprene block copolymer/layered silicate nanocomposites were prepared by Krishnamoorti et al. [128,129] by solution mixing of appropriate quantities of finely ground dimethyldioctadecylammonium cation modified MMT (2C18-MMT) and an anionically synthesized monodisperse polystyrene-1,4-polyisoprene (7 mol% 3, 4 and 93 mol% 1, 4) diblock copolymer (PSPI18) in toluene at room temperature. The homogeneous solution was dried extensively at room temperature and subsequently annealed at  $100^\circ\text{C}$  in a vacuum oven for  $\sim 12$  h to remove any remaining solvent and to facilitate complete polymer intercalation between the silicate layers.

The WAXD patterns of PSPI18/2C18-MMT and PS/2C18-MMT clearly indicates the formation of intercalated structures, whereas the composite prepared with 1,4-polyisoprene (PI) showed no change in gallery height (see Fig. 13a). The intercalation of 2C18-MMT by PS and not by PI is consistent with the results of previous experimental work and theories of Vaia et al. [20–22] and of Balazs et al. [24,27]. The intercalation of PS into the silicate layers may be due to the slight Lewis base character imparted by the phenyl ring in PS, leading to the favorable interactions with the 2C18-MMT layers.

Further, the interlayer gallery spacing for the PSPI18/2C18-MMT composites is independent of

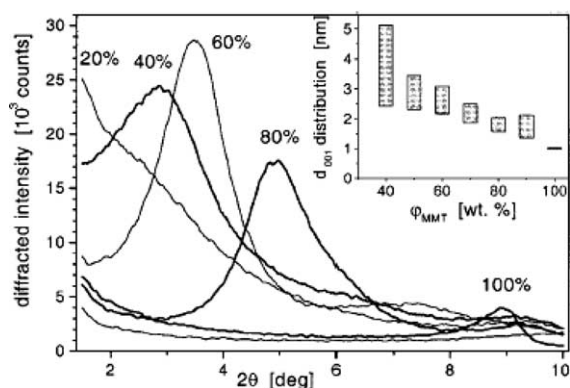


Fig. 12. WAXD patterns of the PVA/MMT nanocomposites as a function of  $\phi_{\text{MMT}}$ . The inset shows the distribution of the MMT intercalated  $d$ -spacing for the respective nanocomposites [111]. Reproduced from Strawhecker and Manias by permission of American Chemical Society, USA.

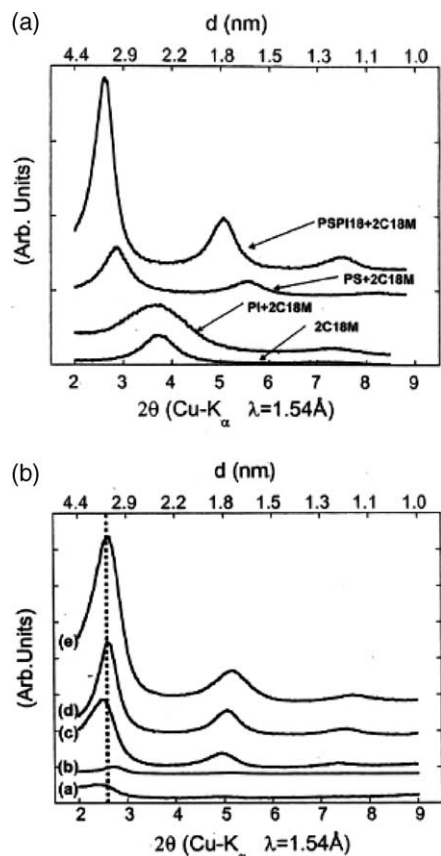


Fig. 13. WAXD spectra for: (left side) pure 2C18M, PI + 2C18M, PS + 2C18M and PSPI18 + 2C18M hybrids, (right side) for PSPI18 + 2C18M intercalated hybrids with silicate loadings (a) 0.7, (b) 2.1, (c) 3.5, (d) 6.7, and (e) 9.5 wt% [128]. Reproduced from Ren, Silva and Krishnamoorti by permission of American Chemical Society, USA.

the silicate loading, as evidenced from Fig. 13b. All of the hybrids exhibit clear regular layered structures, demonstrated by the presence of the  $d_{001}$  and higher-order diffraction peaks. This independence in gallery height on the silicate loading is consistent with the results obtained by Vaia and coworkers on model PS-based nanocomposite systems [20–22]. A simple space filling calculation assuming the polymer density to be unaffected by confinement of the layers suggests that for hybrids with more than 30 wt% polymer, excess polymer exists that is not intercalated.

Biomedical polyurethane urea (PUU)/MMT (MMT modified with dimethyldialuminum ammonium cation) nanocomposites were prepared by adding OMLS suspended in toluene drop-wise to the solution

of PUU in *N,N*-dimethylacetamide (DMAC) [8]. The mixture was then stirred overnight at room temperature. The solution was degassed, and films were cast on round glass Petri dishes. The films were air-dried for 24 h, and subsequently dried under vacuum at 50 °C for 24 h. WAXD analyses indicated the formation of intercalated nanocomposites.

Very recently, Plummer et al. [369] used the following method for the preparation of hyperbranched polymer (HBP)/MMT nanocomposites. The chemical structure of HBP is presented in Fig. 14. Nanocomposites were prepared by introducing the required amount of Na<sup>+</sup>-MMT to 10 g of HBP dispersed in 75 ml of boiling deionized water. The mixture was stirred in air at 50 °C. After evaporation of half the water, the resulting gel was transferred to an open silicone rubber mold, and dried in air for 2 days at 50 °C. The remaining solid was then dried for another 2 days at 120 °C under vacuum, ground, and pressed into 25 mm diameter 1 mm thick disks at 60 °C for WAXD analyses. At high Na<sup>+</sup>-MMT contents, WAXD analyses indicated 2.5–2.8,

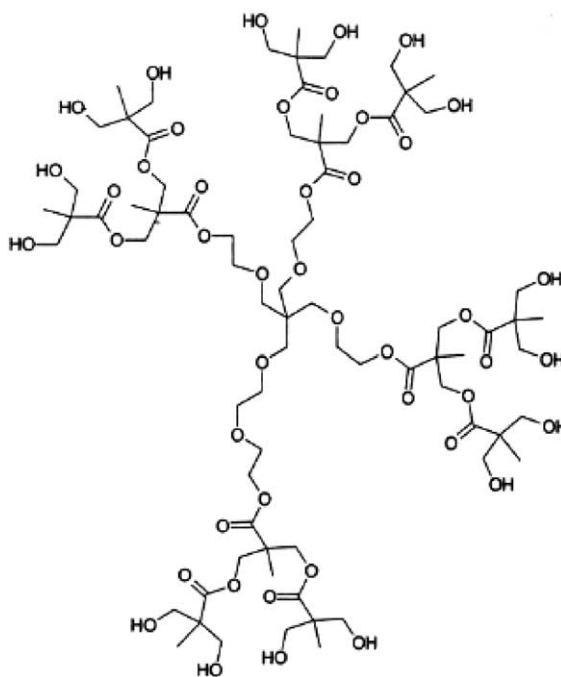


Fig. 14. Chemical structure of the dendrimer analogue of the second pseudo-generation hyperbranched polymer [369]. Reproduced from Plummer, Garamszegi, Leterrier, Rodlert and Manson by permission of American Chemical Society, USA.



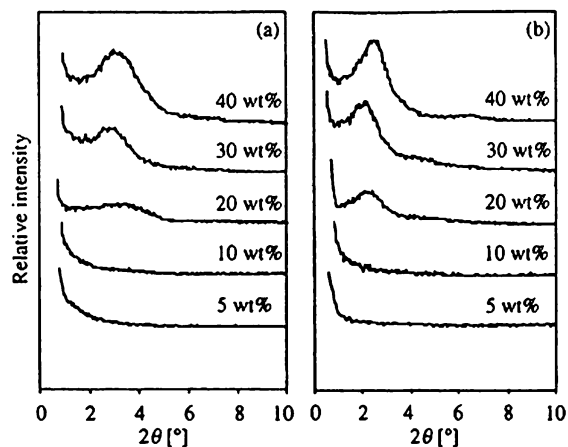


Fig. 15. WAXD patterns for HBP/Na<sup>+</sup>-MMT blends with different compositions: (a) second pseudo-generation HBP; (b) fourth pseudo-generation HBP [369]. Reproduced from Plummer, Garamszegi, Leterrier, Rodlert and Manson by permission of American Chemical Society, USA.

2.8–3, and 3.6–3.9 nm silicate layer basal spacing for the second, third, and fourth pseudo-generation HBPs, respectively, as opposed to 1.06 nm for the as received Na<sup>+</sup>-MMT (see Fig. 15). The corresponding WAXD peaks disappeared as the clay content was reduced to below 20 wt% for all the HBPs (see Fig. 15), consistent with the previous study by Strawhecker et al. [111]. TEM images of nanocomposites containing 20 wt% Na<sup>+</sup>-MMT revealed stacks of 5–10 silicate layers with a relatively well-defined spacing, interspersed with exfoliated silicate layers. At 10 wt% MMT, however, exfoliation was confirmed to dominate.

### 3.2. In situ intercalative polymerization method

Although inter-lamellar polymerization techniques using appropriately modified layered silicate or synthetic layered silicates [42,43] have long been known, the field of PLS nanocomposites gained momentum recently due to the report of a N6/MMT nanocomposite from the Toyota research group [1], where very small amounts of layered silicate loadings resulted in pronounced improvements in thermal and mechanical properties. They first reported the ability of  $\alpha,\omega$ -amino acids ( $\text{COOH}-(\text{CH}_2)_{n-1}-\text{NH}_2^+$ , with  $n = 2, 3, 4, 5, 6, 8, 11, 12, 18$ ) modified Na<sup>+</sup>-MMT to be swollen by the  $\epsilon$ -caprolactam monomer at 100 °C

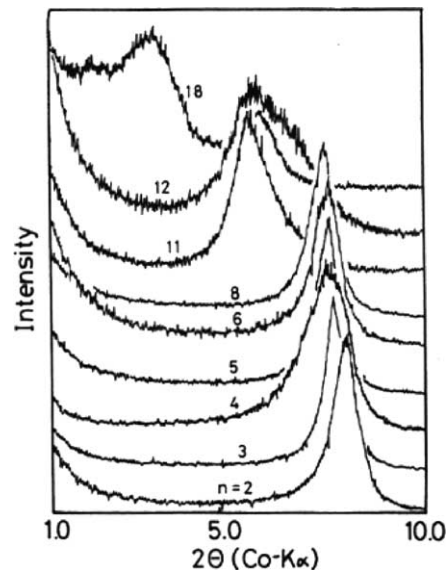


Fig. 16. XRD patterns of  $\omega$ -amino acid [ $\text{NH}_2(\text{CH}_2)_{n-1}\text{COOH}$ ] modified Na<sup>+</sup>-MMT [131]. Reproduced from Usuki, Kawasumi, Kojima, Okada, Kurauchi and Kamigaito by permission of Materials Research Society, USA.

and subsequently initiate its ring opening polymerization to obtain N6/MMT nanocomposites [131]. For the intercalation of  $\epsilon$ -caprolactam, they chose the ammonium cation of  $\omega$ -amino acids because these acids catalyze ring-opening polymerization of  $\epsilon$ -caprolactam. The number of carbon atoms in  $\alpha,\omega$ -amino acids has a strong effect on the swelling behavior as reported in Fig. 16, indicating that the extent of intercalation of  $\epsilon$ -caprolactam monomer is high when the number of carbon atoms in the  $\omega$ -amino acid is high. Fig. 17 represents the conceptual view of

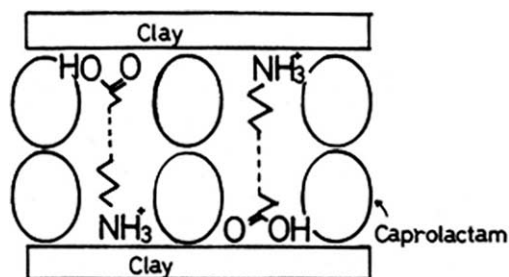


Fig. 17. Swelling behavior of  $\omega$ -amino acid modified mmt by  $\epsilon$ -caprolactam [131]. Reproduced from Usuki, Kawasumi, Kojima, Okada, Kurauchi and Kamigaito by permission of Materials Research Society, USA.

the swelling behavior of  $\alpha,\omega$ -amino acid modified  $\text{Na}^+$ -MMT by  $\epsilon$ -caprolactam.

In a typical synthesis, 12-aminolauric acid modified MMT (12-MMT) and  $\epsilon$ -caprolactam were mixed in a mortar. The content of 12-MMT ranged from 2 to 70 wt%. This was then heated at 250–270 °C for 48 h to polymerize  $\epsilon$ -caprolactam, using 12-MMT as a catalyst. A small amount of 6-aminocaproic acid was added to the mixture to confirm the ring-opening polymerization of  $\epsilon$ -caprolactam, and the 12-MMT content in the mixture became less than 8 wt%. A typical procedure was as follows: A 3 l three-necked separable flask, coupled with a mechanical stirrer, was used as the reaction vessel. In the vessel, 509 g of  $\epsilon$ -caprolactam, 29.7 g of 12-MMT, and 66 g of 6-aminocaproic acid were placed under nitrogen. The mixture was heated at 100 °C in an oil bath while being stirred for 30 min, followed by heating at 250 °C for 6 h. The products were mechanically crushed, washed with 2 l of water at 80 °C for 1 h, and dried at 80 °C overnight. A conceptual scheme for the synthetic method is presented in Fig. 18 [132]. Further work demonstrated that intercalative polymerization of  $\epsilon$ -caprolactam could be realized without the necessity needing to render the MMT surface organophilic. In attempts to carry out the whole synthesis in one pot [135], the system proved to be sensitive to the nature of the acid used to promote the intercalation of  $\epsilon$ -caprolactam. Reichert et al. [157] also used the same method for the preparation of polyamide-12/MMT nanocomposites.

For the preparation of PCL-based nanocomposites, Messersmith and Giannelis [163] modified MMT using protonated aminolauric acid and dispersed the modified MMT in liquid  $\epsilon$ -caprolactone before

polymerizing at high temperature. The nanocomposites were prepared by mixing up to 30 wt% of the modified MMT with dried and freshly distilled  $\epsilon$ -caprolactone for a couple of hours, followed by ring opening polymerization under stirring at 170 °C for 48 h. The same authors [10] also reported a  $\epsilon$ -caprolactone polymerization inside a  $\text{Cr}^{3+}$ -exchanged fluorohectorite at 100 °C for 48 h.

Chen et al. [251] used this PCL-based nanocomposites synthesis technique for the preparation of novel segmented polyurethane/clay nanocomposites articulated on diphenylmethane diisocyanate, butanediol and preformed polycaprolactone diol. Even if the mechanism proposed for the chemical link between the nano-filler surface and the polymer does not appear appropriate, they succeeded in producing a material in which the nano-filler acts as a multifunctional chain extender, inducing the formation of a star-shaped segmented polyurethane. Recently, Wang and Pinnavaia [250] reported the preparation of polyurethane–MMT nanocomposites using a direct in situ intercalative polymerization technique. WAXD analyses of these nanocomposites established the formation of intercalated structure. More recently, Yao et al. [253] reported the preparation of a novel kind of PU/MMT nanocomposite using a mixture of modified 4,4'-di-phenylmethane diisocyanate (M-MDI) modified polyether polyol (MPP) and  $\text{Na}^+$ -MMT. In a typical synthetic route, a known amount of  $\text{Na}^+$ -MMT was first mixed with 100 ml of MPP and then stirred at 50 °C for 72 h. Then, the mixture of MPP and  $\text{Na}^+$ -MMT was blended with a known amount of M-MDI and stirred for 30 s at 20 °C, and finally cured at 78 °C for 168 h.

Pantoustier et al. [167,169] used the in situ intercalative polymerization method for the preparation of PCL-based nanocomposites. They compared the properties of nanocomposites prepared using both pristine MMT, and  $\omega$ -amino dodecanoic acid modified MMT. For nanocomposite synthesis, the desired amount of pristine MMT was first dried under vacuum at 70 °C for 3 h. A given amount of  $\epsilon$ -caprolactone was then added to a polymerization tube under nitrogen and the reaction medium was stirred at room temperature for 1 h. A solution of initiator ( $\text{Sn}(\text{Oct})_2$ ) or  $\text{Bu}_2\text{Sn}(\text{Ome})_2$ ) in dry toluene was added to the mixture in order to reach a [monomer]/[Sn] molar ratio equal to 300. The polymerization was then

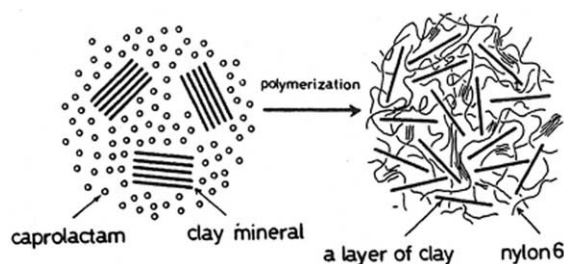


Fig. 18. Schematic illustration for synthesis of Nylon-6/clay nanocomposite [132]. Reproduced from Usuki, Kojima, Kawasumi, Okada, Fukushima, Kurauchi and Kamigaito by permission of Materials Research Society, USA.

allowed to proceed for 24 h at room temperature. The inorganic content of the composite was measured by TGA. After polymerization, a reverse ion-exchange reaction was used to isolate the PCL chains from the inorganic fraction of the nanocomposite. A colloidal suspension was obtained by stirring 2 g of the nanocomposite in 30 ml of THF for 2 h at room temperature. A solution of 1 wt% of LiCl in THF was prepared separately. The nanocomposite suspension was added to 50 ml of the LiCl solution and left to stir at room temperature for 48 h. The resulting solution was centrifuged at 3000 rpm for 30 min. The supernatant was then decanted and the remaining solid washed in 30 ml of THF followed by centrifugation. The combined supernatant was concentrated and precipitated from petroleum ether. The white powder was dried in vacuum at 50 °C.

The polymerization of CL with pristine MMT gives PCL with a molar mass of 4800 g/mol and a narrow distribution. For comparison, the authors also conducted the same experiment without MMT, but found that there is no CL polymerization. These results demonstrate the ability of MMT to catalyze and to control CL polymerization, at least in terms of a molecular weight distribution that remains remarkably narrow. For the polymerization mechanism, the authors assume that the CL is activated through interaction with the acidic site on the clay surface. The polymerization is likely to proceed *via* an activated monomer mechanism using the cooperative functions of the Lewis acidic aluminum and Brønsted acidic silanol functionalities on the initiator walls. On the other hand, the polymerization of CL with the protonated  $\omega$ -amino dodecanoic acid modified MMT yields a molar mass of 7800 g/mol with a monomer conversion of 92% and again a narrow molecular weight distribution. The WAXD patterns of both nanocomposites indicate the formation of intercalated structure. In another very recent publication [170], the same group prepared PCL/MMT nanocomposites using dibutyl tin dimethoxide as an initiator/catalyst in an in situ ring-opening polymerization of CL.

Okamoto et al. [57,67] used organically modified smectite clays for the preparation of PMMA and PS nanocomposites. Organically modified smectite clays (SPN and STN) were prepared by replacing  $\text{Na}^+$ -smectite with  $\text{QA}^+$  (quaternary ammonium salt), oligo (oxypropylene), diethylmethylammonium cation

(SPN) or methyltrioctylammonium cation (STN) by exchange reaction. In a typical synthesis, both lipophilized smectite clays (SPN and STN) were dispersed in methyl methacrylate (MMA) and S *via* ultrasonication at 25 °C for 7 h to obtain suspensions. After that *t*-butyl peroxy-2-ethylhexanate and/or 1,1-bis (*t*-butyl peroxy) cyclohexane as an initiator was added to the suspensions and then free-radical polymerization was carried out in the dark at 80 °C for 5 h (for MMA) and at 100 °C for 16 h (for S) in a silicon oil bath. For comparison, the authors also prepared PMMA and/or PS including  $\text{QA}^+$  under the same conditions. WAXD analyses were performed directly from the suspensions of MMA/SPN, MMA/STN and S/SPN, and corresponding nanocomposites.

From WAXD patterns of the MMA/STN suspension (see Fig. 19a), higher-order peaks corresponding to  $d_{(002)}$  and  $d_{(003)}$  are clearly observed along with a  $d_{(001)}$  peak, suggesting MMA intercalated into the STN gallery without the loss of layer structure, while the corresponding nanocomposite, PMMA/STN, exhibits a rather broad Bragg peaks, indicating the formation of a disordered intercalated structure.

In contrast, for the MMA/SPN suspension (see Fig. 19b), the absence of any Bragg diffraction peaks indicates that the clay has been completely exfoliated or delaminated in the suspension. A similar pattern was observed in the case of the corresponding PMMA/SPN nanocomposite but with a small remnant shoulder as shown in Fig. 19b. At the other extreme, the S/SPN suspension shows a small remnant shoulder that leads to the formation of a disordered intercalated structure, while the corresponding polymer nanocomposite shows strong WAXD diffraction implying the formation PS/SPN of an intercalated structure (Fig. 19c). But for all systems, the  $2\theta$  peaks for nanocomposites are shifted to higher angle. This behavior may be due to the volume shrinkage of monomers ( $\sim 5\%$  in case of MMA and  $\sim 3\%$  in case of S) after polymerization.

Fig. 20 represents the TEM bright field images of various nanocomposites, corresponding to the WAXD patterns as presented in Fig. 19. In the case of the PMMA/STN nanocomposite, individual silicate layers are stacked together and nicely dispersed in the PMMA matrix. Some areas (as indicated by the arrow in Fig. 20a) appear to contain an oriented collection of 10–20 parallel layers with a basal

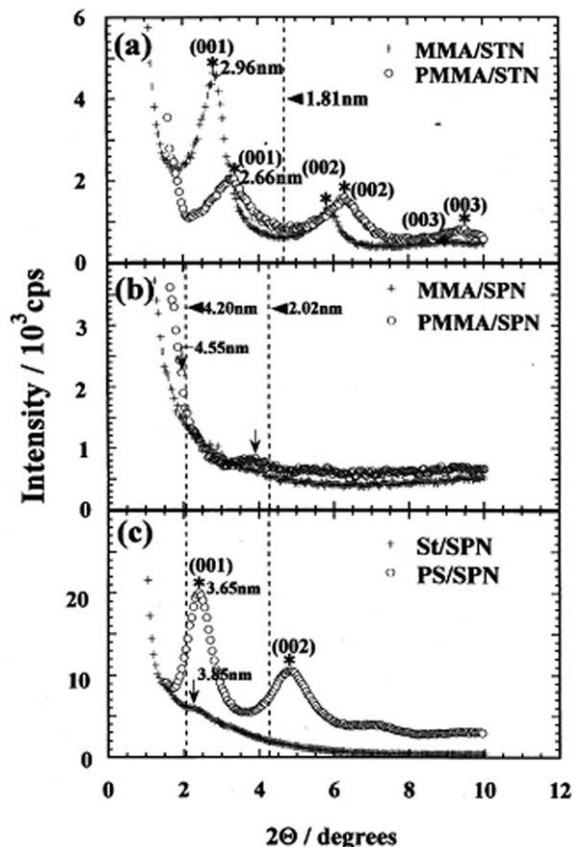


Fig. 19. WAXD patterns of various monomer/OMLS suspensions and corresponding polymer nanocomposites. The dashed lines indicate the location of the silicate (00 $l$ ) reflection of OMLS from suspensions and nanocomposites. The asterisk indicates the position of (00 $l$ ) reflections from suspensions and nanocomposites. The arrows indicate a small shoulder or a weak peak [57]. Reproduced from Okamoto, Morita, Taguchi, Kim, Kotaka and Tateyama by permission of Elsevier Science Ltd, UK.

spacing of about 3 nm, which was consistent with the WAXD data. The PMMA/SPN nanocomposite (see Fig. 20b) shows stacked silicate layers of about 200 nm length and about 40–50 nm thickness that consist of about 10 parallel individual silicate layers, and are randomly distributed in the matrix.

On the other hand, in the case of the PS/SPN nanocomposite system (see Fig. 20c), a stacking of two to three silicate layers, with a distance of 4 nm are dispersed in the PS-matrix. Because of the difference between PS and PMMA matrices towards the compatibility with SPN, the final structure of the nanocomposites is different. As revealed by WAXD pattern, the PS

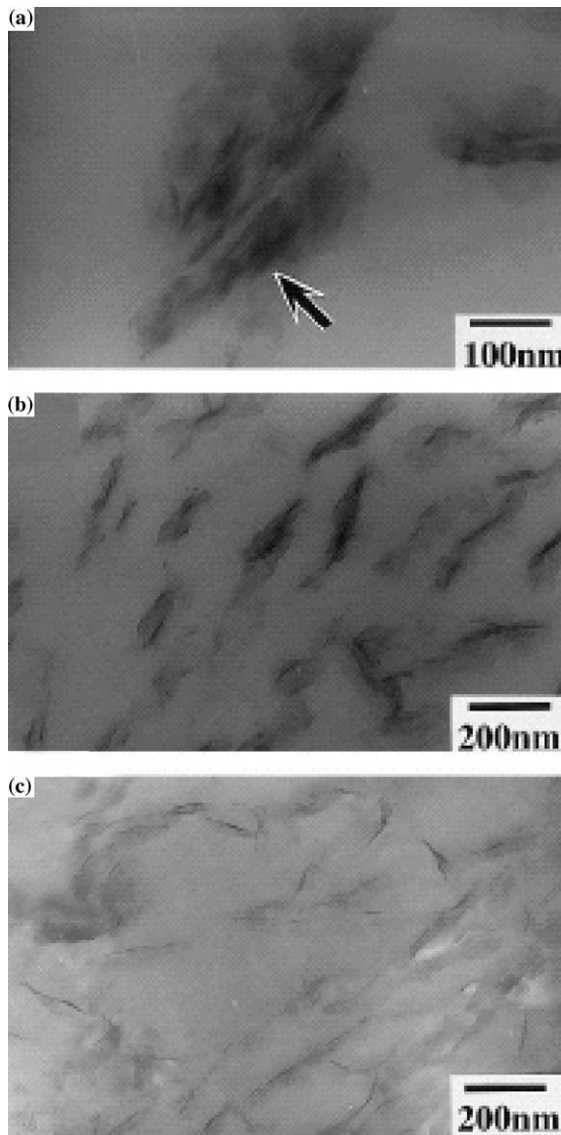


Fig. 20. TEM images of thin section of nanocomposites: (a) PMMA/STN, (b) PMMA/SPN, and (c) PS/SPN. The arrow in panel (a) indicates the oriented collection of STN silicate layers [57]. Reproduced from Okamoto, Morita, Taguchi, Kim, Kotaka and Tateyama by permission of Elsevier Science Ltd, UK.

chains are intercalated in the narrow space of the oriented collections of parallel silicate layers.

Further study by the same group [68] demonstrated the effect of the nature of co-monomers on the structure of PMMA nanocomposites prepared via in situ free-radical co-polymerization of MMA in

the presence of lyophilized smectite clays (each contain 10 wt%). They used three different types of co-monomers (each contain 1 mol%) for the free-radical polymerization of MMA, such as *N,N*-dimethylaminopropyl acrylamide (PAA), *N,N*-dimethylaminoethyl acrylate (AEA) and acrylamide (AA). Fig. 21 represents the results of WAXD patterns of various nanocomposites (each containing 10 wt% of SPN clay) and corresponding TEM images are shown in Fig. 22. For PMMA–AEA(1)/SPN10 (see Fig. 22b), the same behavior is observed, but the thickness of the aggregation slightly decreased compared to that of PMMA/SPN10 (see Fig. 20b). For PMMA–PAA(1)/SPN10 (see Fig. 22c) individual

silicate layers connected through the edge are clearly observed in the PMMA–PAA(1) matrix, and a large anisotropy of the dispersed clay particles is observed. In contrast, the PMMA–AA(1)/SPN10 nanocomposite (see Fig. 22d) exhibited less stacking of 4–5 silicate layers with a distance of about 5 nm as a fine dispersion in the PMMA–AA(1) matrix. The coherent orders of the silicate layers in this system are higher than that in other systems, and are consistent with the WAXD patterns (see Fig. 21). They also prepared a PMMA/SPN10 nanocomposite of AA and AEA co-monomers with high content (3 mol%), and then tried to determine the effect of nanocomposite morphology on the co-monomers amount. Fig. 23 represents TEM bright field images of PMMA–AA(3)/SPN10 and PMMA–AEA(3)/SPN10 nanocomposites containing 3 mol% of respective co-monomers. The length vs. thickness schemes of randomly dispersed silicate layers in the nanocomposites nicely demonstrates the characteristic effects of the polar group in each co-monomer on the morphology (see Fig. 24). Incorporation of 1 mol% of AEA co-monomer possessing a dimethyl amine group appears to lead to a slight edge–edge interaction. On the other hand, the introduction of the AA co-monomer having an amide group appears to play an important role in delaminating the silicate layers. However, incorporation of 3 mol% of AEA and AA led to the stacking of the layers compared to the corresponding 1 mol% copolymer matrix systems. This behavior may be due to the formation of strong hydrogen bonds between the polar groups. For the PAA co-monomer with both polar groups, a much stronger flocculation takes place (see Fig. 22c). Recently, Zeng et al. [99] used this method for the preparation of PS-based nanocomposites. S-monomer was first intercalated into the interlayer space of OMLS. Upon the intercalation, the complex was subsequently polymerized in the confinement environment of the interlayer space with a free radical initiator, 2,2-azobis isobutyronitrile.

Akelah and Moet [79,82] used this in situ intercalative polymerization technique for the preparation of PS-based nanocomposites. They modified  $\text{Na}^+$ -MMT and  $\text{Ca}^{2+}$ -MMT with vinylbenzyltrimethyl ammonium cation using an ion exchange reaction, then used these modified MMT(s) for the preparation of nanocomposites. They first dispersed

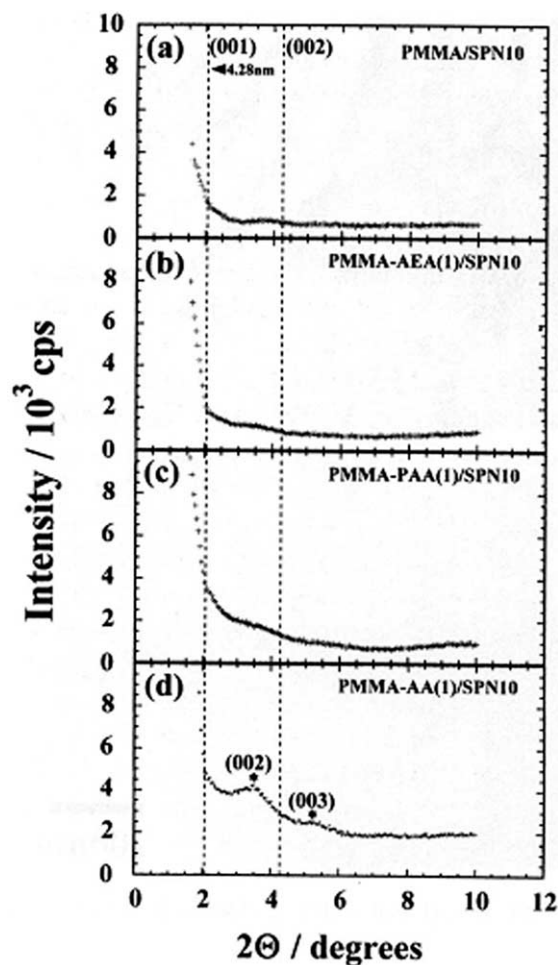


Fig. 21. WAXD patterns of various nanocomposites [68]. Reproduced from Okamoto, Morita, Kim, Kotaka and Tateyama by permission of Elsevier Science Ltd, UK.

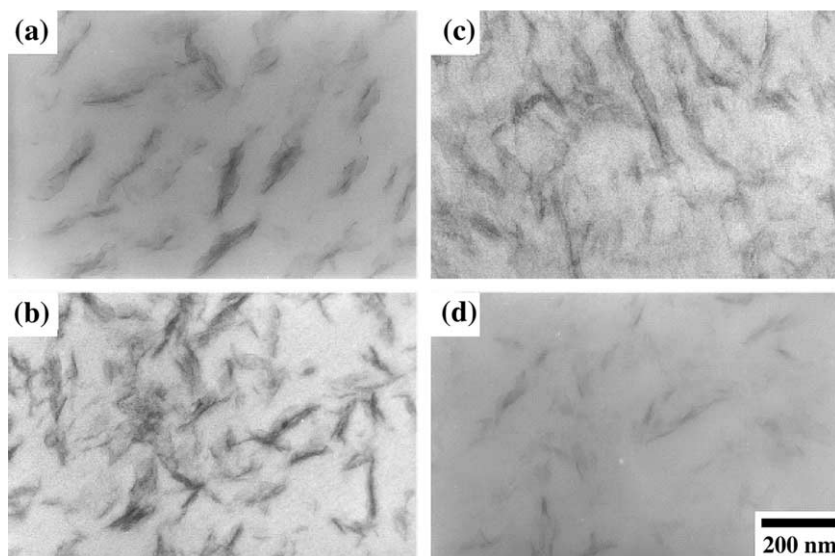


Fig. 22. Bright field TEM images of: (a) PMMA/SPN, (b) PMMA–AEA (1 mol%)/SPN, (c) PMMA–PAA (1 mol%)/SPN, and (d) PMMA–AA (1 mol%)/SPN. Each contain 10 wt% SPN [68]. Reproduced from Okamoto, Morita, Kim, Kotaka and Tateyama by permission of Elsevier Science Ltd, UK.

and swelled the modified clays in various solvent and co-solvent mixtures such as acetonitrile, acetonitrile/toluene and acetonitrile/THF by stirring for 1 h under  $N_2$  atmosphere. To the stirred solution of S and *N-N'*-azobis (isobutyronitrile) (AIBN) was added, and polymerization of S was carried out at  $80^\circ C$  for 5 h. The resulting composites were isolated by precipitation of the colloidal suspension in methanol, filtered off, and dried. In this way, intercalated PS/MMT nanocomposites were produced; the extent of intercalation completely depends upon the nature of solvent used. Although the PS is well intercalated, one drawback in this procedure is that the macromolecule produced is not a pure PS, but rather a copolymer between S and vinylbenzyltrimethylammonium cations. Doh and Cho [85] used MMT for the preparation of PS-based nanocomposites. They compared the ability of several tetra-alkylammonium cations incorporated in  $Na^+$ -MMT through the exchange reaction to promote the intercalation of PS through the free radical polymerization of S initiated by AIBN at  $50^\circ C$ . They found that the structural affinity between the S monomer and the surfactant of modified MMT plays an important role in the final structure and properties of the nanocomposites.

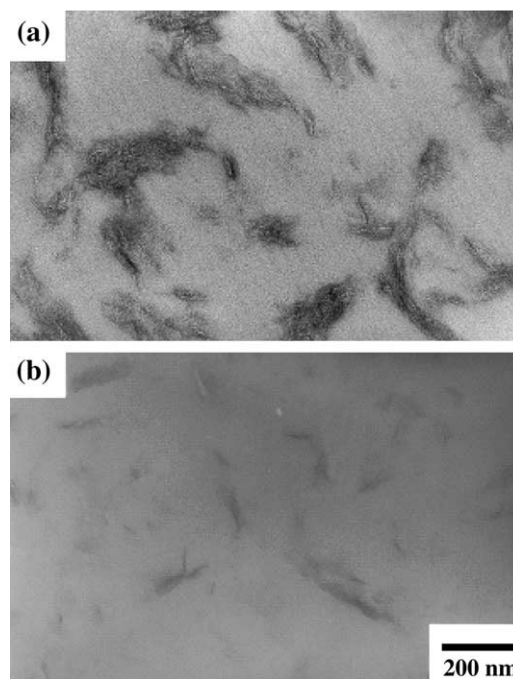


Fig. 23. Bright field TEM images of nanocomposites: (a) PMMA–AEA (3 mol%)/SPN10, and (b) PMMA–AA (3 mol%)/SPN10. SPN content is equal to 10 wt% [68]. Reproduced from Okamoto, Morita, Kim, Kotaka and Tateyama by permission of Elsevier Science Ltd, UK.

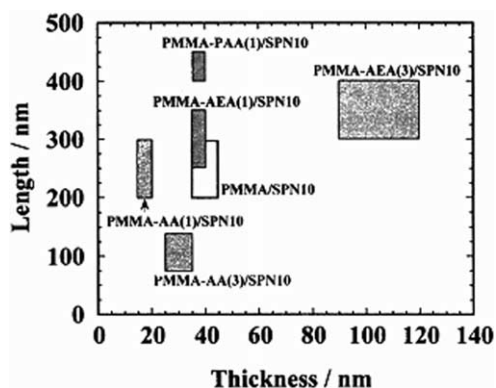


Fig. 24. Plots of length vs. thickness of the dispersed clay particles in various copolymer matrices estimated from TEM images. The estimated values are located within the shaded area [68]. Reproduced from Okamoto, Morita, Kim, Kotaka and Tateyama by permission of Elsevier Science Ltd, UK.

Weimer et al. [89] used this concept in the preparation of PS/MMT nanocomposites. They modified  $\text{Na}^+$ -MMT by anchoring an ammonium cation bearing a nitroxide moiety known for its ability to mediate the controlled/‘living’ free radical polymerization of S in bulk. The absence of WAXD peaks in the low angle area together with the TEM observations of silicate layers randomly dispersed within the PS matrix attest for the complete exfoliation of the layered silicate.

In a recent study, Zhu et al. [98] reported the preparation of PS nanocomposites with three different types of new alkylammonium and alkylphosphonium salt modified MMT(s). Fig. 25 represents the structures of the alkylammonium and phosphonium

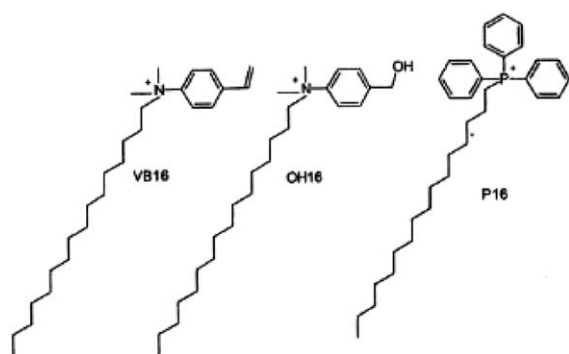


Fig. 25. Structures of alkylammonium and alkylphosphonium salts used for the modification of clays [98]. Reproduced from Zhu, Morgan, Lamelas and Wilkie by permission of American Chemical Society.

salts used for the modification of  $\text{Na}^+$ -MMT. They were attempting to determine differences in thermal stability caused by organo ammonium and phosphonium salt treatments of clay fillers in nanocomposites.

An in situ intercalative polymerization technique was successfully used by Hsu and Chang [125] in order to prepare polybenzoxale (PBO)/clay nanocomposite from a PBO precursor, polyhydroxyamide (PHA) and an OMLS. The PBO precursor, with an inherent viscosity of 0.5 dl/g, was made by a low temperature polycondensation reaction between isophthaloyl chloride (IC) and 2,2-bis(3-amino-4-hydroxyphenyl) hexafluoropropane. For the preparation of the PBO/OMLS nanocomposite, the OMLS was first dispersed in dimethylacetamide in which PHA was dissolved. The PHA/OMLS film was obtained from solution casting and dried at 80 °C under vacuum. Finally, the PBO/clay nanocomposite was obtained by curing the film at 350 °C to form a benzoxazole ring. The WAXD pattern and TEM observation established that silicate layers were delaminated in the PBO/OMLS film. Very recently, Leu et al. [269] showed that this method is also suitable for the preparation of covalently bonded layered silicate/polyimide nanocomposites. Fig. 26 represents the schematic illustration used for the preparation of covalently bonded polyimide/layered silicate nanocomposites. Details regarding the synthetic route are presented in the relevant literature [269].

Polyolefins, which are normally defined as polymers based on alkene-1 monomers or  $\alpha$ -olefins, are the most widely used group of thermoplastic polymers today. Tudor et al. [281] first used the in situ intercalative polymerization method for the preparation of PP/clay nanocomposites (PPCN). They demonstrated the ability of soluble metallocene catalysts to intercalate inside silicate layers, and to promote the coordination polymerization of propylene. Accordingly, a synthetic hectorite (Laponite RD) was first treated with methylaluminoxane (MAO) in order to remove the acidic protons, and to prepare the interlayer spacing to receive the transition metal catalyst. It should be noted that MAO is commonly used in association with metallocenes to produce coordination catalysts active in olefin polymerizations. During this first treatment step, WAXD analysis showed no noticeable increase of the layer spacing,

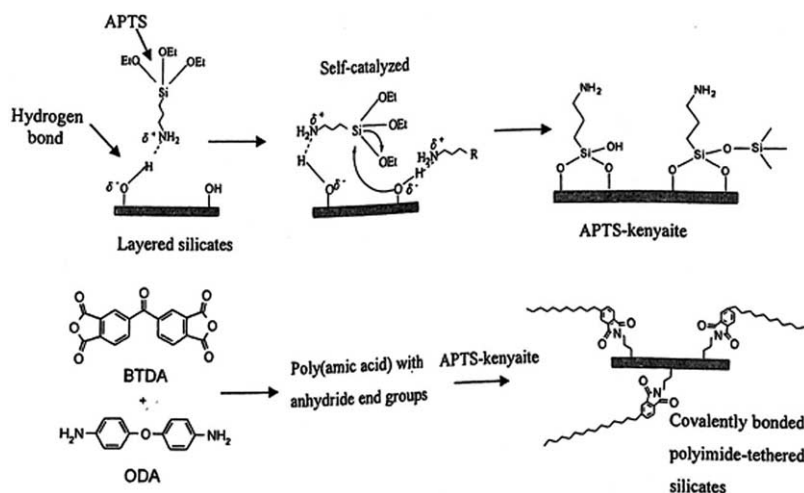


Fig. 26. Schematic drawing of the formation of the process of covalently bonded polyimide tethered layered silicates [269]. Reproduced from Leu, Wu and Wei by permission of American Chemical Society, USA.

although the diffraction peak broadened slightly, but the increase in Al content and complete disappearance of Si–OH signals from IR-spectra agree with MAO reaction/adsorption inside the layered silicate galleries. Upon the addition of the metallocene catalyst ( $[\text{Zr}(\eta\text{-C}_5\text{H}_5)_2\text{Me}(\text{THF})]^+$ ), a cation exchange reaction occurred between the  $\text{Na}^+$  in the MAO-treated hectorite and the metallocene catalyst as demonstrated by an increase of 0.47 nm in the interlayer spacing, consistent with the size of the species. Details can be shown in Fig. 27. Using a synthetic fluorinated mica-type layered silicate deprived from any protons in the galleries; the catalyst was intercalated directly within the silicate layers without the need of MAO

treatment. These two modified layered silicates catalyzed with reasonably high activity with the polymerization of propylene when contacted with an excess of MAO, producing PP oligomers. Unfortunately, the authors did not report any characterization of these composites. In another recent publication, Sun and Garces [310] reported the preparation of PPCNs by in situ intercalative polymerization with metallocene/clay catalysts.

For the synthesis of polyethylene/layered silicate nanocomposites, Bergman et al. [323] used Brookhart's single component palladium-based complex **1**;  $[\{2,6\text{-Pr}_2\text{C}_6\text{H}_3\text{N}=\text{C}(\text{Me})\text{C}(\text{M})=\text{NC}_6\text{H}_3\text{Pr}_2\text{-2,6}\}\text{Pd}(\text{CH}_2)_3\text{CO}_2\text{Me}][\text{B}(\text{C}_6\text{H}_3(\text{CF}_3)_2\text{-3,5})_4]$ , and the

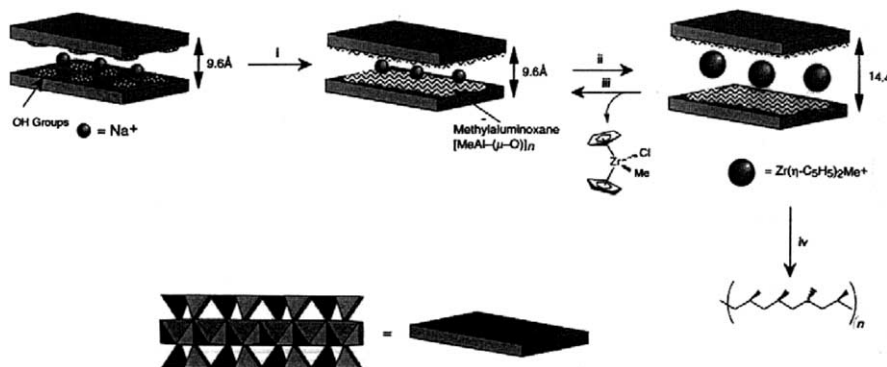


Fig. 27. Schematic illustration of the modification and ion exchange of laponite with  $[\text{Zr}(\eta\text{-C}_5\text{H}_5)_2\text{Me}(\text{thf})]\text{BPh}_4$  and propene polymerization. Details regarding the reagent and conditions are shown in relevant Ref. [281]. Reproduced by Tudor, Willington, O'Hare and Royan by permission of The Royal Society of Chemistry, UK.



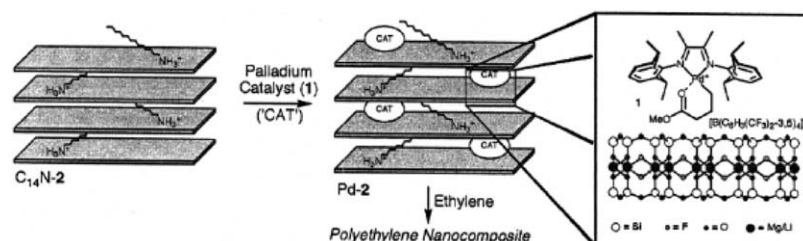


Fig. 28. Schematic representation of the modification of fluorohectorite with palladium catalyst and ethylene polymerization [323]. Reproduced from Bergman, Chen, Giannelis, Thomas and Coates by permission of The Royal Society of Chemistry, UK.

well-studied synthetic silicate fluorohectorite (2) as the polymerization catalyst and inorganic component, respectively. They first tried to intercalate palladium catalyst (1) into the galleries of 1-tetra-decylammonium modified fluorohectorite ( $C_{14}N-2$ ) by suspending the later into the toluene solution of 1. An orange brown powder (Pd-2) was visually distinct from the white, pristine  $C_{14}N-2$ . This reaction is irreversible, as 1 cannot be extracted from Pd-2 with excess toluene. WAXD analysis revealed structural changes of the silicate, as an increase in the basal spacing of  $C_{14}N-2$  from 1.99 to 2.76 nm was measured.

After that, the dry Pd-2 solid was exposed to ethylene gas. Over a 2 h period, they observed monomer consumption and a dramatic increase in the size of the silicate-catalyst composite. After 12 h, the Pd-2 material could not be seen; replacing the small amount of orange, Pd-2 powder was a large mass of colorless, rubbery polymer. Analysis of the toluene-extracted polyethylene by GPC revealed a HMW polymer ( $M_n = 159,000$ ;  $M_w = 262,000$  vs. polystyrene standard). In order to find out the structure of the nanocomposite, the polyethylene composite formed after 24 h was examined by WAXD. The complete absence of diffraction peaks strongly suggests the formation of an exfoliated polymer nanocomposite. Details regarding nanocomposite synthesis are presented in Fig. 28.

Recently, Jin et al. [328] developed an in situ exfoliation method during ethylene polymerization by fixing a Ti-based Ziegler–Natta catalyst at the inner surface of MMT. They used organic salts with hydroxyl groups for the modification of MMT (MMT–OH), because hydroxyl groups in intercalation agents offer facile reactive sites for anchoring catalysts in between silicate layers. Fig. 29 represents the  $TiCl_4$  fixation mechanism between silicate layers

of MMT–OH. The polymerization of ethylene was conducted by injecting ethylene into the catalyst slurry. The polymerization temperature was varied from 30 to 50 °C, and polymerization pressure was fixed at 4 bars in all experiments. After predetermined reaction times, polymerization was quenched with a diluted HCl solution in methanol. The polymer was precipitated in methanol, separated by filtration, and dried in a vacuum. The WAXD pattern of dried powdery reaction products clearly indicates the exfoliation of MMT layers in the matrix. This powder was then used as the master batch and mixed with HDPE by melt extrusion. The WAXD analysis and TEM observation (see Fig. 30) clearly indicates the exfoliation of MMT layers in the HDPE matrix.

Polyethylene/layered silicate nanocomposites have also been prepared by the in situ intercalative polymerization of ethylene using the so-called polymerization filling technique [326]. Pristine MMT and hectorite were first treated with trimethylaluminum-depleted methylaluminoxane before being contacted by a Ti-based constrained geometry catalyst. The nanocomposite was formed by addition and polymerization of ethylene. In the absence of a chain transfer agent, ultra HMW polyethylene was produced. The tensile properties of these nanocomposites were poor and essentially independent on the nature and content of the silicate. Upon hydrogen addition,

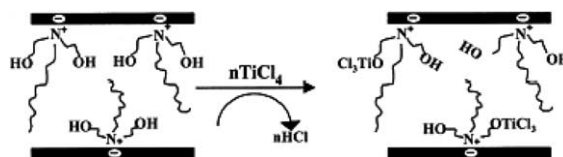


Fig. 29. Mechanistic representation of the fixing of  $TiCl_4$  between the silicate layers of MMT–OH [328]. Reproduced from Jin, Park, Im, Kwak and Kwak by permission of Wiley-VCH, Germany.

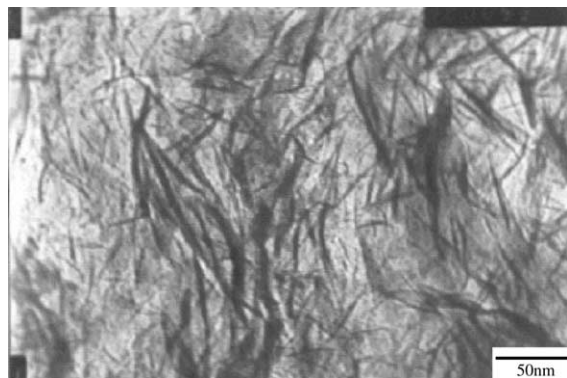


Fig. 30. TEM image of PE/MMT–OH diluted with HDPE (8 wt% of MMT–OH) [328]. Reproduced from Jin, Park, Im, Kwak and Kwak by permission of Wiley-VCH, Germany.

the molecular weight of the polyethylene was decreased with a corresponding improvement of mechanical properties. The formation of exfoliated nanocomposites was confirmed using WAXD and TEM analyses. In another report, Heinemann et al. [321] prepared polyolefin-clay nanocomposites using this method.

There are many literature reports on the preparation and characterization of polyethylene terephthalate (PET)/clay nanocomposites [176–182], however no reports give a detailed description of the preparative method. For example, one report concerns the preparation of a PET nanocomposite by in situ polymerization of a dispersion of organoclay in water; however characterization of the resulting composite was not reported [176]. This report claims that water serves as a dispersing aid for the intercalation of monomers into the galleries of the organoclay, and it discloses that a wide variety of small molecules can serve as dispersing aids in place of, or in combination with, water. Another route that developed by Nanocor, Inc. [180] is based on the novel exfoliation of clays into ethylene glycol, one of the basic monomers for PET. The key to this approach relies on finding a suitable surfactant that allows exfoliation of clay into ethylene glycol and also on finding polymerization conditions that permit polymerization, while maintaining the exfoliation of the clay. Very recently, Imai et al. [182] reported the preparation of higher-modulus PET/expandable fluorine mica nanocomposites with a novel reactive compatibilizer.

Details regarding the synthetic route can be found in the listed reference [182].

Like thermoplastic polymers, this technique has also been widely used for the preparation of thermoset polymers and elastomer/clay nanocomposite systems. The studies of thermoset epoxy systems considered the ring opening polymerization of epoxides to form polyether nanocomposites. Studies of both rubbery and glassy thermoset epoxy/clay nanocomposites formed using different types of amine curing agents were done, and the mechanisms leading to the monolayer exfoliation of clay layers in thermoset epoxy systems were greatly elucidated as a result. In addition, the polymer/clay interfacial properties have been shown to play a dominant role in determining the performance benefits derived from nanolayer exfoliation.

Messersmith and Giannelis [224] first reported the preparation of epoxy resin based nanocomposites of OMLS. They analyzed the effects of different curing agents and curing conditions on the formation of nanocomposites based on the diglycidyl ether of bisphenol A (DGEBA), and MMT modified by bis (2-hydroxyethyl) methyl hydrogenated tallow alkylammonium cation. They found that this modified clay dispersed readily in DGEBA when sonicated for a short time period, as determined by the increase in viscosity at relatively low shear rates and the clarity of the suspension changing from opaque to semitransparent. The increase in viscosity was attributed to the formation of a so-called ‘house-of-cards’ structure in which the edge-to-edge and edge-to-face interactions between dispersed layers form a percolation structure. WAXD patterns of uncured clay-DGEBA samples also indicate that intercalation occurred, and that this intercalation improved in going from room temperature to 90 °C (see Fig. 31).

In a subsequent paper, Wang and Pinnavaia [226] reported the preparation of nanocomposites using the epoxy resin DGEBA, and the concomitant delamination of acidic forms of MMT at elevated temperatures using the self-polymerization technique. They used a series of acidic cations such as  $H^+$ ,  $NH_4^+$ , and acidic onium ions of the type  $[H_3N(CH_2)_{n-1}COOH]^+$ ,  $[H_3N(CH_2)_nNH_2]^+$ ,  $[H_3N(CH_2)_nNH_3]^{2+}$  ( $n = 6$  and 12) for the modification of MMT and carried out the polymerization–delamination process over the temperature range of 198–287 °C, and found that

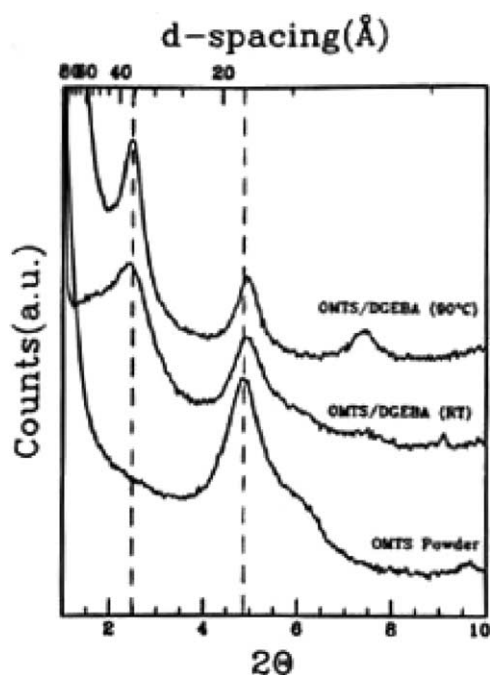


Fig. 31. WAXD patterns of OMTS powder and uncured OMTS/DGEBA mixture. Top scan was obtained at room temperature following heating of OMTS/DGEBA mixture at 90 °C for 1 h [224]. Reproduced from Messersmith and Giannelis by permission of American Chemical Society, USA.

the epoxy-clay delamination temperature (PDT) was dependent on the heating rate and nature of the cation used for the modification of the clay. In general, the PDT increased with decreasing cation acidity and basal spacing of the clay.

The delamination of MMT clay in the polymerized epoxy resin was confirmed by X-ray powder diffraction (XRD) as shown by the powder patterns in parts a and b of Fig. 32, where  $[\text{H}_3\text{N}(\text{CH}_2)_{11}\text{COOH}]^+$ -MMT remains crystalline over the temperature range of 25–229 °C. However, no diffraction peaks were observed for a 5:95 (w/w) clay/polyether nanocomposite formed from  $[\text{H}_3\text{N}(\text{CH}_2)_{11}\text{COOH}]^+$ -MMT at 229 °C (see Fig. 32c). Only very diffuse scattering characteristic of the amorphous polyether appears in the WAXD pattern of the composite. The absence of a 17 Å peak for  $[\text{H}_3\text{N}(\text{CH}_2)_{11}\text{COOH}]^+$ -MMT suggests that the clay particles have been exfoliated and the 9.6 Å-thick clay layers dispersed at the molecular level. TEM provides unambiguous evidence for the delamination of the MMT in the polyether matrix.

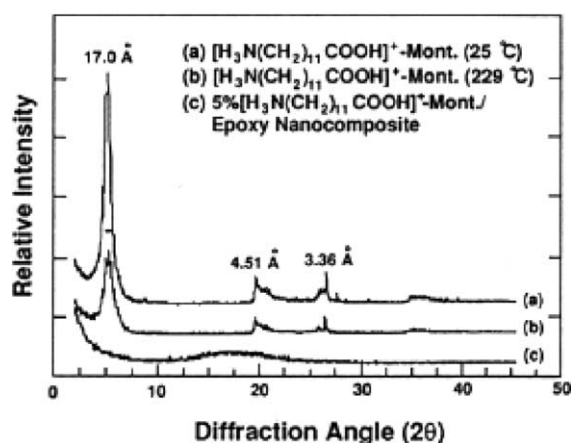


Fig. 32. XRD powder patterns for a freeze-dried  $[\text{H}_3\text{N}(\text{CH}_2)_{11}\text{COOH}]^+$ -MMT, (b)  $[\text{H}_3\text{N}(\text{CH}_2)_{11}\text{COOH}]^+$ -MMT freeze-dried and then heated at 229 °C, and (c) clay-polyether nanocomposite containing 5 wt%  $[\text{H}_3\text{N}(\text{CH}_2)_{11}\text{COOH}]^+$ -MMT [226]. Reproduced from Wang and Pinnavaia by permission of American Chemical Society, USA.

PDT values and thermodynamic data for MMT-polyether nanocomposites formed from bifunctional onium ion MMT and onium ion  $\text{NH}_4^+$ , and  $\text{H}^+$  MMT are, respectively, presented in Tables 3 and 4.

In another study, Pinnavaia and Lan [225] reported the preparation of nanocomposites with a rubber-epoxy matrix obtained from DGEBA derivatives cured with a diamine so as to reach subambient glass transition temperatures. It has been shown that depending on the alkyl chains length of modified MMT, an intercalated and partially exfoliated or a totally exfoliated nanocomposite can be obtained. The same authors [227] also studied other parameters such as the nature of alkyl ammonium cations present in the gallery and the effect of the CEC of the MMT when DGEBA was cured with *m*-phenylene diamine. The same kind of study was also conducted by Zilg et al. [234], who cured DGEBA with hexahydrophthalic acid anhydride in the presence of different types of clays, and also modified with a wide variety of surfactants.

Starting from another type of layered material, magadiite, which is a layered silicic acid, Pinnavaia et al. [228] developed a different kind of exfoliated structure where the layers were still organized, but spaced by approximately 80 Å of elastomeric epoxy matrix arising from the curing of DGEBA derivative

Table 3

PDT values and thermodynamic data for clay–polyether nanocomposites formed from bifunctional onium ion-MMT [226]

| Interlayer cation   | Initial basal spacing (Å) | PDT <sup>a</sup> (°C) | Heat of reaction (J/g) | Heat of polym <sup>b</sup> (kJ/mol) |
|---|---------------------------|-----------------------|------------------------|-------------------------------------|
| [H <sub>3</sub> N(CH <sub>2</sub> ) <sub>11</sub> COOH] <sup>+</sup>              | 17.0 ± 0.1                | 229 ± 1               | 572 ± 16               | 228 ± 6                             |
| [H <sub>3</sub> N(CH <sub>2</sub> ) <sub>5</sub> COOH] <sup>+</sup>               | 13.3 ± 0.0                | 248 ± 1               | 565 ± 06               | 225 ± 2                             |
| [H <sub>3</sub> N(CH <sub>2</sub> ) <sub>12</sub> NH <sub>3</sub> ] <sup>2+</sup> | 13.4 ± 0.1                | 271 ± 1               | 566 ± 08               | 225 ± 3                             |
| [H <sub>3</sub> N(CH <sub>2</sub> ) <sub>6</sub> NH <sub>3</sub> ] <sup>2+</sup>  | 13.1 ± 0.1                | 273 ± 2               | 568 ± 07               | 226 ± 3                             |
| [H <sub>3</sub> N(CH <sub>2</sub> ) <sub>12</sub> NH <sub>2</sub> ] <sup>+</sup>  | 13.5 ± 0.0                | 281 ± 2               | 563 ± 07               | 224 ± 3                             |
| [H <sub>3</sub> N(CH <sub>2</sub> ) <sub>6</sub> NH <sub>2</sub> ] <sup>+</sup>   | 13.2 ± 0.1                | 287 ± 2               | 557 ± 03               | 222 ± 2                             |

The clay:polymer composition was 5:95 (w/w). Reproduced from Wang and Pinnavaia by permission of American Chemical Society, USA.

<sup>a</sup> PDT is the onset temperature for epoxide polymerization–clay delamination at a heating of 20 °C/min.

<sup>b</sup> Heat of reaction for two epoxide equivalents.

by Jeffamine 2000. The same group also synthesized intercalated nanocomposites based on elastomeric polyurethanes [250].

Recently, Kornmann et al. [241] reported the synthesis of epoxy-based nanocomposites using two different types of MMT clays with different CECs, in order to investigate the influence of the CEC of the MMT clay on the synthesis and structure of nanocomposites. The CEC of any clay is a very important factor during nanocomposite synthesis because it determines the amount of surfactants, which can be intercalated between the silicate layers. In this context, the swelling behavior is of critical importance to the final nanocomposite structure. For the preparation of nanocomposites both MMT clays were modified with octadecylammonium cation, with the nanocomposite synthesis used by previous authors. It was found from WAXD patterns that a MMT with a low CEC is already exfoliated during swelling in the epoxy resin prior to curing. A possible mechanism explaining this phenomenon is homopolymerization of the epoxy resin during the swelling phase, causing diffusion of new epoxy

molecules into the clay galleries. The large amount of space available between the layers favors the diffusion. The swelling duration of the clay with high CEC is shown to be critical for the synthesis of an exfoliated nanocomposite. Regarding the structure, TEM observations reveal interlamellar spacing of 90 Å (low CEC) and 110 Å (high CEC). However, multi-platelets of non-exfoliated layers were also observed. In summary, these nanocomposites contain clay/polymer composite particles consisting of heterogeneously distributed silicate layer aggregates with polymer between these layers.

A research group [243] from Australia recently reported the morphology, thermal relaxation and mechanical properties of layered silicate nanocomposites of high-functionality epoxy resins. Three different types of resins were used: bifunctional DGEBA, trifunctional triglycidyl *p*-amino phenol (TGAP), and tetrafunctional tetraglycidyl diamino diphenylmethane (TGDDM). All were cured with diethyltoluene diamine (DETDA); the structure of all resins and curing agent are presented in Table 5. MMT modified

Table 4

PDT values and thermodynamic data for clay–polyether nanocomposites formed from onium ion, NH<sub>4</sub><sup>+</sup>, and H<sup>+</sup> MMT [226]

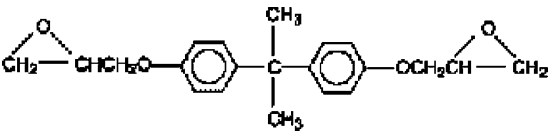
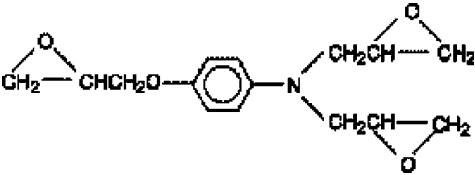
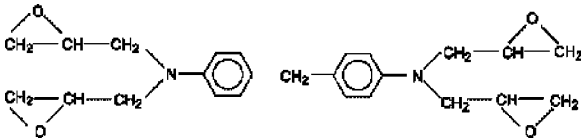
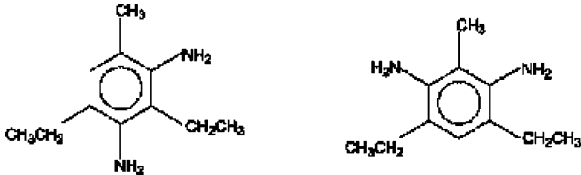
| Interlayer cation  | Initial basal spacing (Å) | PDT <sup>a</sup> (°C) | Heat of reaction (J/g) | Heat of polym <sup>b</sup> (kJ/mol) |
|--|---------------------------|-----------------------|------------------------|-------------------------------------|
| [H <sub>3</sub> N(CH <sub>2</sub> ) <sub>11</sub> CH <sub>3</sub> ] <sup>+</sup> | 15.9 ± 0.2                | 198 ± 1               | 550 ± 3                | 219 ± 2                             |
| [H <sub>3</sub> N(CH <sub>2</sub> ) <sub>5</sub> CH <sub>3</sub> ] <sup>+</sup>  | 14.9 ± 0.1                | 287 ± 1               | 554 ± 6                | 220 ± 3                             |
| NH <sub>4</sub> <sup>+</sup>   | 12.5 ± 0.1                | 247 ± 1               | 554 ± 5                | 220 ± 2                             |
| H <sup>+</sup>   | 13.9 ± 0.1                | 231 ± 1               | 555 ± 12               | 221 ± 5                             |

Reproduced from Wang and Pinnavaia by permission of American Chemical Society, USA.

<sup>a</sup> The PDT is the onset temperature for epoxide polymerization–clay delamination at a heating rate of 20 °C/min and a composite a clay:polymer composition of 5:95 (w/w).

<sup>b</sup> Heat of polymerization for two epoxide equivalents.

Table 5  
Epoxy resins and hardener as used for the nanocomposite synthesis [243]

| Substance | Formula  |
|-----------|--|
| DGEBA     |    |
| TGAP      |   |
| TGDDM     |  |
| DETDA     |  |

Reproduced from Becker, Varley and Simon by permission of Elsevier Science Ltd, UK.

with octadecylammonium cation was used for the preparation of nanocomposites. The nanocomposites were prepared using in situ intercalative polymerization method. In a typical synthesis, OMLS was first dispersed in the resin at 80 °C using a stirrer at 500 rpm. After mixing the resin–OMLS blend for 30 min the curing agent was added and the system kept under vacuum for another 60–90 min at around 70 °C. The blends were then cured for 2 h at 100 °C, 1 h at 130 °C, 12 h at 160 °C followed by a post-cure for 2 h at 200 °C.

The morphology of the cured samples was investigated using WAXD and different microscopy

techniques. Fig. 33a represents the WAXD patterns of the MMT concentration series and shows that the organoclay with an initial *d*-spacing of 2.3 nm is mainly exfoliated in the DGEBA-based system. On the other hand, high content (10 wt%) OMLS shows intercalated structure, while DGEBA-based systems, resins of higher functionality, show distinctive peaks even at low OMLS loading, indicating that these nanocomposites have a lower degree of exfoliated structure. WAXD patterns are shown in Fig. 33b for TGAP and Fig. 33c for TGADDM-based nanocomposites of MMT. In the case of most nanocomposite systems, the peak observed around 2.5 nm correlates

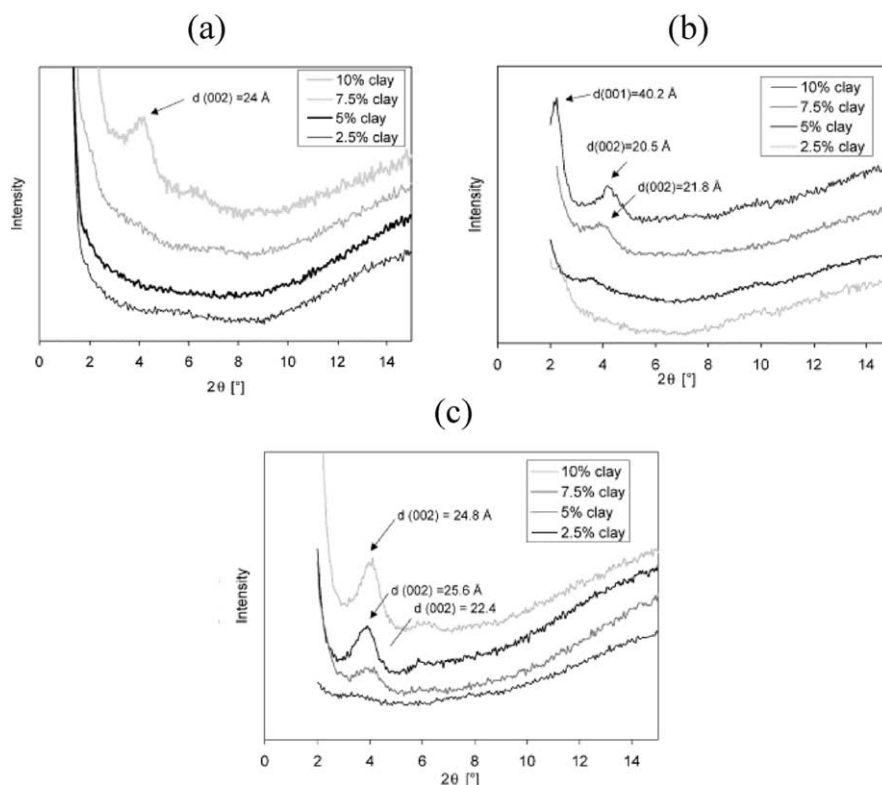


Fig. 33. (a) WAXD patterns of DETDA cured DGEBA nanocomposites containing 0–10 wt% organoclay [243]. Reproduced from Becker, Varley and Simon by permission of Elsevier Science Ltd, UK. (b) WAXD of DETDA cured TGAP nanocomposites containing 0–10 wt% organoclay [243]. Reproduced from Becker, Varley and Simon by permission of Elsevier Science Ltd, UK. (c) WAXD of DETADA cured TGDDM nanocomposites containing 0–10 wt% organoclay [243]. Reproduced from Becker, Varley and Simon by permission of Elsevier Science Ltd, UK.

to the (002) plane and therefore represents only half the distance of the  $d$ -spacing.

Parts a and b of Fig. 34 represent AFM phase contrast images of the DGEBA nanocomposite containing 5 wt% layered silicate. Individual layers cannot be seen by AFM, unlike TEM. A striated structure, however, can be seen with increasing phase intervals at the top of the picture. So from the AFM images it is established that although silicate layers are not homogeneously distributed in the matrix, some stacked layers are present.

Very recently, Chen et al. [244] synthesized an epoxy-MMT nanocomposite using a surface initiated method in order to understand the interlayer expansion mechanism and thermal–mechanical properties of these nanocomposites. MMT modified with bis-2-hydroxyethyl methyl tallow ammonium cation (C30B) was used as the OMLS for nanocomposite

synthesis. 3,4-Epoxy cyclohexylmethyl-3,4-epoxy cyclohexane carboxylate was used as the epoxy monomer, and hexahydro-4-methylphthalic anhydride (HHMPA), ethylene glycol (EG), and benzyldimethylamine (BDMA) were used as curing agent, initiator and catalyst, respectively, during synthesis. In a typical preparative method, the epoxy monomer HHMPA was mixed in a molar ratio of epoxide groups to HHMPA of 1–0.87. The resulting mixture was denoted as the resin by authors. The desired amount of EG, BDMA and C30B were added to the resin, and the materials were then blended using an orbital mixture, until the blend became bubble free and homogeneously mixed. The blended samples were then immediately cured, first isothermally for up to 8 h at temperatures ranging from 70 to 140 °C, followed by 8 h at 180 °C, and finally 12 h at 220 °C under vacuum.

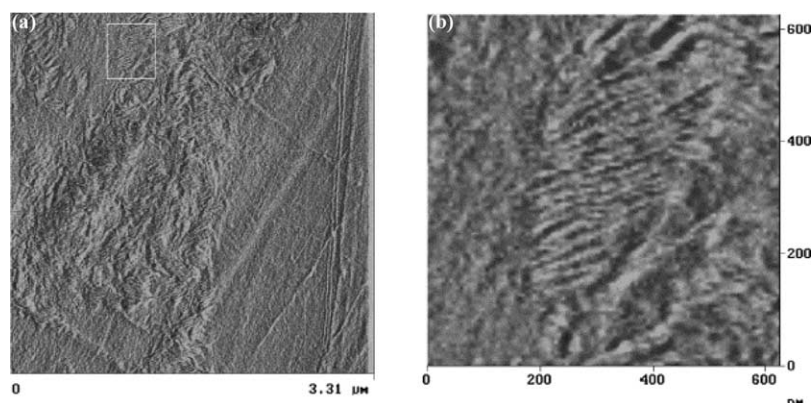


Fig. 34. Phase contrast AFM images of DETDA cured DGEBA containing 5 wt% organoclay [243]. Reproduced from Becker, Varley and Simon by permission of Elsevier Science Ltd, UK.

The curing mechanism for an epoxy–anhydride system with an alcohol initiator is shown in Fig. 35. Amine catalysts like BDMA were added to the mixture to accelerate the reaction by facilitating the ring opening of epoxy groups. Several published papers indicate that intragallery onium ions can catalyze the epoxy curing reaction and thus lead to favorable conditions for obtaining exfoliated nanocomposites. To fully understand this system, Chen et al. [244] verified that the crosslinking reactions in the presence of C30B were due to hydroxy initiation and not due to catalytic reactions. For this reason, the extent of reaction of a resin containing C30B was compared to the extent of reaction for a neat resin and resins containing either EG or BDMA. As seen in Fig. 36, the curing kinetics of the resin–C30B system more closely resembles the curing kinetics of the resin–EG system than that of the resin–BDMA

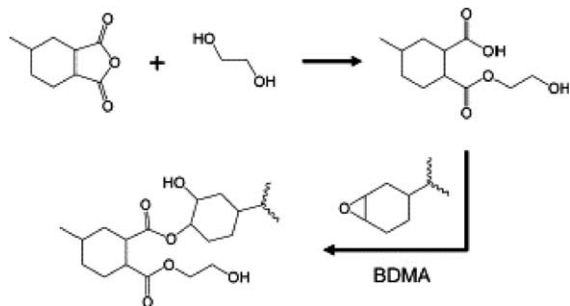


Fig. 35. Schematic illustration of generalized curing reaction involving the epoxy monomer, HHMPA, EG, and BDMA [244]. Reproduced from Chen, Poliks, Ober, Zhang, Wiesner and Giannelis by permission of Elsevier Science Ltd, UK.

system. This is a direct indication that the nanocomposites are predominantly cured via initiation by the surfactant hydroxy groups and not by catalytic means. Fig. 36 also shows that the curing rate of the pristine resin is significantly lower than that of the other mixtures. This highlights an important prerequisite for interlayer expansion, which is that extra-gallery polymerization rates should be slower than intra-gallery polymerization rates.

Time-resolved high-temperature-XRD was used to probe the expansion behavior of the silicate layers during curing of the nanocomposites. Fig. 37 represents the results for a nanocomposite containing 15 wt% C30B held isothermally at 70 °C. In Fig. 38, the changes in *d*-spacing are plotted against

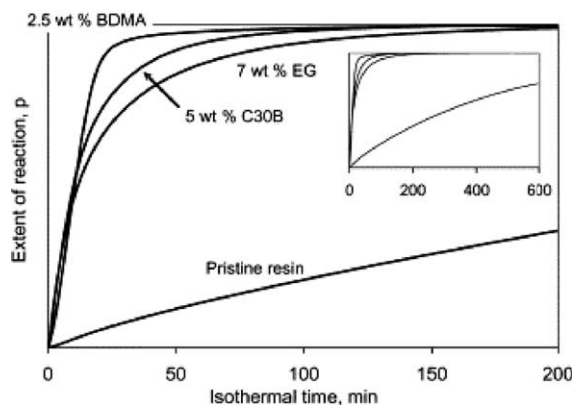


Fig. 36. Extent of reaction of a neat resin and resins containing either C30B, EG, or BDMA. The inset shows the same data but for longer reaction [244]. Reproduced from Chen, Poliks, Ober, Zhang, Wiesner and Giannelis by permission of Elsevier Science Ltd, UK.

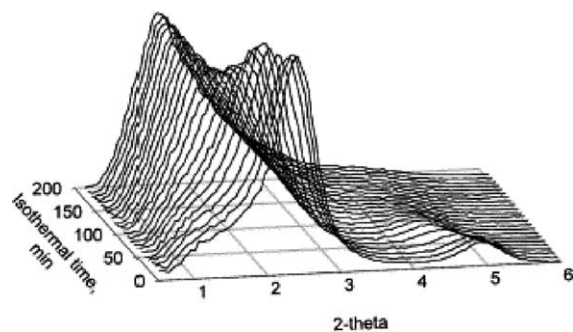


Fig. 37. TT-XRD of a resin containing 15 wt% C30B held isothermally at 70 °C [244]. Reproduced from Chen, Poliks, Ober, Zhang, Wiesner and Giannelis by permission of Elsevier Science Ltd, UK.

the isothermal cure time for various clay loadings and cure temperature. On the basis of various characterization methods, authors proposed a three-stage surface-initiated exfoliation mechanism for epoxy nanocomposites. In the first stage, the interlayer expansion induced by intra-gallery polymerization must overcome any polymer chains that bridge the silicate layers. The interlayer expansion cannot proceed beyond the first stage if the number of bridging units is too great. The second stage was characterized by a steady and linear increase in interlayer spacing, and accounts for the majority of the total expansion realized. During this stage, the silicate layers could be monitored via isothermal DSC experiments. Also, for samples that exhibited large increases in interlayer expansion, it was found that the activation energy associated with the interlayer expansion was less than the activation energy associated with the curing. The reverse was true for samples that showed no increase in interlayer spacing. In the third stage, the interlayer expansion slowed then stopped, and in some cases decreased slightly. This was ascribed to the evolving modulus of the extra-gallery polymer such that the interlayer expansion stopped when the modulus of the extra-gallery polymer became equal to or exceeded the modulus of the intra-gallery polymer.

By using this method specialty polymer-based nanocomposites were successfully prepared by various authors. Sinha Ray and Biswas [340] first reported the preparation of PNVC/MMT nanocomposites by direct polymerization of *N*-vinylcarbazole (NVC) (solid or in solution) in presence of MMT without the use of any free radical initiator. Melt polymerization of NVC in

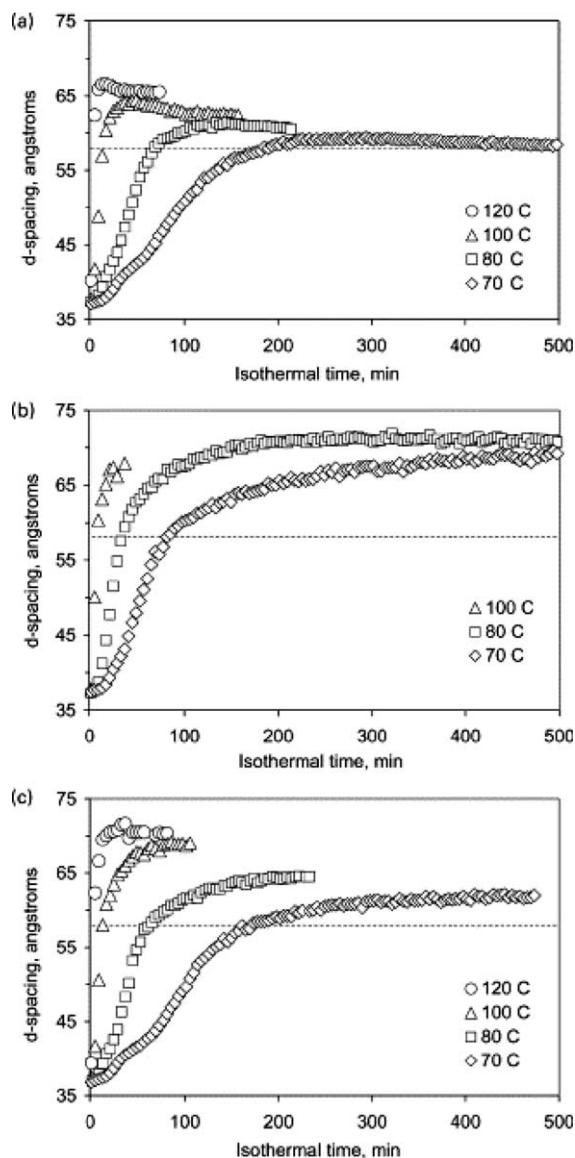


Fig. 38. Changes in  $d_{001}$  as a function of the curing time and temperature: (a) 5, (b) 10, and (c) 15 wt% silicate loading. The dashed lines denote the qualitative detection limit of the TT-XRD setup [244]. Reproduced from Chen, Poliks, Ober, Zhang, Wiesner and Giannelis by permission of Elsevier Science Ltd, UK.

MMT (at 70 °C) as well as in solution (benzene) polymerization of NVC in the presence of MMT at 50 °C resulted in the formation of a PNVC/MMT nanocomposite with an intercalated structure. The surface-adsorbed PNVC was extracted with benzene, but the intercalated PNVC could not be removed by



repeated benzene extraction. WAXD analyses confirmed intercalation of PNVC in MMT interlayer galleries.

The authors suggested that the initiation in the NVC/MMT system was cationic, involving Brønsted acid sites in MMT arising from the dissociation of interlayer water molecules coordinated to the exchangeable cations [6,340]. Yet another possibility, especially with NVC, was cationic initiation of NVC via the transition metal oxides ( $\text{Fe}_2\text{O}_3/\text{TiO}_2$ ) present in MMT [6,340]. The same authors subsequently reported that direct interaction of MMT with pyrrole (PY) gave only a ca. 5% yield of PPY in 3 h, while aniline (ANI) could not be polymerized by MMT [6,337]. According to them, such a trend is not surprising since NVC is more susceptible to cationic polymerization in comparison with the latter monomers.

In a study of the NVC/MMT polymerization/nanocomposite formation system, Sinha Ray and Biswas evaluated the addition of  $\text{FeCl}_3$ . Results of a recent study [341] indicated that in NVC–MMT polymerization/nanocomposites formation system with the addition of  $\text{FeCl}_3$  the percentage loading of PNVC in the composite increased. Polymerization via nanocomposite formation in PY/MMT–water and ANI/MMT–water systems was possible using  $\text{FeCl}_3$  and  $(\text{NH}_4)_2\text{S}_2\text{O}_8$  [337,343] as the oxidants for the two systems. Kim et al. [342] first used this method for the preparation of PANI/MMT nanocomposites using dodecylbenzenesulphonic acid (DBSA) and camphor-sulphonic acid (CSA) as the dopant. In a typical synthetic method, the  $\text{Na}^+$ -MMT clay was first dispersed in an aqueous medium, and then sonicated using an ultrasonic generator. The DBSA or CSA dopants were dissolved in distilled water and mixed with ANI monomer solution at a 1:1 molar ratio, and then the emulsion solutions were mixed in a 4-neck reactor, while the temperature was held constant at 25 °C. The oxidant initiator,  $(\text{NH}_4)_2\text{S}_2\text{O}_8$  was added drop wise into the reactor. The resultant powder was then washed, filtered and dried. WAXD patterns of representative samples are presented in Fig. 39. From the WAXD analysis, the formation of intercalated nanocomposites is clearly observed.

Finally, Kim et al. [339] reported the preparation of intercalated PPY/ $\text{Na}^+$ -MMT nanocomposites via an inverted emulsion pathway method.

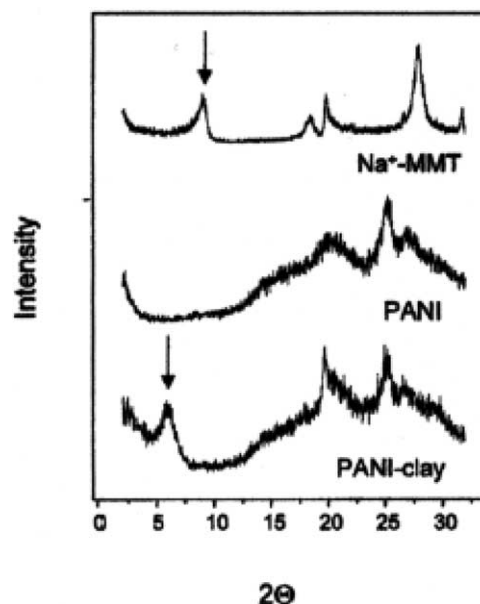


Fig. 39. WAXD patterns of  $\text{Na}^+$ -MMT, PANI and PANI/ $\text{Na}^+$ -MMT [342]. Reproduced from Kim, Kim, Choi and John by permission of Wiley-VCH, Germany.

### 3.3. Melt intercalation

Recently, the melt intercalation technique has become the standard for the preparation of PLS nanocomposites. During polymer intercalation from solution, a relatively large number of solvent molecules have to be desorbed from the host to accommodate the incoming polymer chains. The desorbed solvent molecules gain one translational degree of freedom, and the resulting entropic gain compensates for the decrease in conformational entropy of the confined polymer chains. Therefore, there are many advantages to direct melt intercalation over solution intercalation. For example, direct melt intercalation is highly specific for the polymer, leading to new hybrids that were previously inaccessible. In addition, the absence of a solvent makes direct melt intercalation an environmentally sound and an economically favorable method for industries from a waste perspective.

Fig. 40 represents a schematic illustration of nanocomposite formation by direct melt intercalation in OMLS. This process involves annealing a mixture of the polymer and OMLS above the softening point of the polymer, statically or under shear. While annealing, the polymer chains diffuse from the bulk

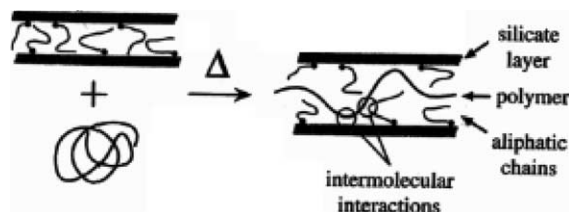


Fig. 40. Schematic depicting the intercalation process between a polymer melt and an OMLS [21]. Reproduced from Vaia and Giannelis by permission of American Chemical Society, USA.

polymer melt into the galleries between the silicate layers. A range of nanocomposites with structures from intercalated to exfoliate can be obtained, depending on the degree of penetration of the polymer chains into the silicate galleries. So far, experimental results indicate that the outcome of polymer intercalation depends critically on silicate functionalization and constituent interactions. The present authors observe that (a) an optimal interlayer structure on the OMLS, with respect to the number per unit area and size of surfactant chains, is most favorable for nanocomposite formation, and (b) polymer intercalation depends on the existence of polar interactions between the OMLS and the polymer matrix.

In order to understand the thermodynamic issue associated with nanocomposite formation, Vaia et al. [21,22] applied a mean-field statistical lattice model, reporting that calculations based on the mean field theory agree well with experimental results. Details regarding this model and explanation are presented in Ref. [21]. Although there is an entropy loss associated with the confinement of a polymer melt with nanocomposite formation, this process is allowed because there is an entropy gain associated with the layer separation, resulting in a net entropy change near to zero. Thus, from the theoretical model, the outcome of nanocomposite formation via polymer melt intercalation depends primarily on energetic factors, which may be determined from the surface energies of the polymer and OMLS.

Based on the Vaia et al. [21] study and the construction of product maps, general guidelines may be established for selecting potentially compatible polymer/OMLS systems. Initially, the interlayer structure of the OMLS should be optimized in order to maximize the configurational freedom of the functionalizing chains upon layer separation, and to

maximize potential interaction sites at the interlayer surface. For these systems, the optimal structures exhibit a slightly more extensive chain arrangement than with a pseudo-bilayer. Polymers containing polar groups capable of associative interactions, such as Lewis-acid/base interactions or hydrogen bonding, lead to intercalation. The greater the polarizability or hydrophilicity of the polymer, the shorter the functional groups in the OMLS should be in order to minimize unfavorable interactions between the aliphatic chains and the polymer.

PS was the first polymer used for the preparation of nanocomposites using the melt intercalation technique with alkylammonium cation modified MMT [44]. In a typical preparative method, PS was first mixed with the host OMLS powder, and the mixture was pressed into a pellet, and then heated under vacuum at 165 °C. This temperature is well above the bulk glass transition temperature of PS, ensuring the presence of a polymer melt. Fig. 41 represents the WAXD patterns of the PS35/OMLS hybrid before,

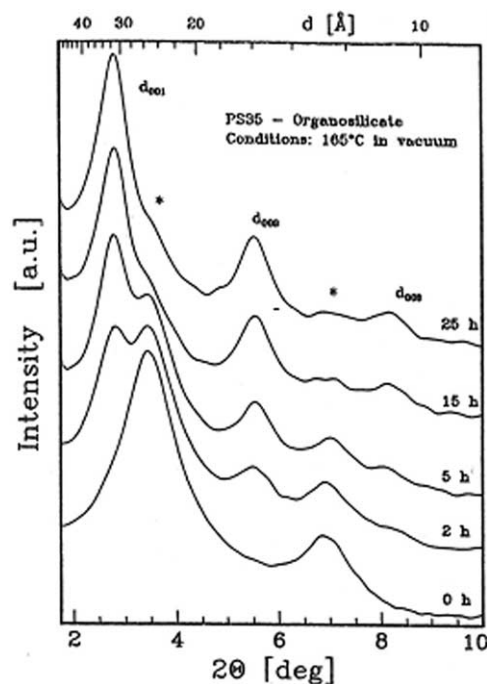


Fig. 41. Representative WAXD of PS35/OMLS hybrid heated to 165 °C for various times. Asterisks indicate the positions of the basal reflections from the pristine OMLS [44]. Reproduced from Vaia, Ishii and Giannelis by permission of American Chemical Society, USA.

and after 2, 5, 15 and 25 h of heating. The WAXD patterns of the hybrid before heating show peaks characteristic of the pure OMLS, and during heating the OMLS peaks were progressively reduced while a new set of peaks corresponding to the PS/OMLS appeared. After 25 h, the hybrid exhibits a WAXD pattern corresponding predominantly to that of the intercalated structure. The same authors also carried out the same experiment under the same experimental conditions using  $\text{Na}^+$ -MMT, but WAXD patterns did not show any intercalation of PS into the silicate galleries, emphasizing the importance of polymer/OMLS interactions. They also attempted to intercalate a solution of PS in toluene with the same OMLS used for melt intercalation, but this resulted in intercalation of the solvent instead of PS. Therefore, direct melt intercalation enhances the specificity for the intercalation of polymer by eliminating the competing host–solvent and polymer–solvent interactions. The schematic illustration of polymer chains intercalated in OMLS is presented in Fig. 42.

Further research by Vaia et al. [22] demonstrated the dispersion of various types of OMLS in a PS matrix. Li-fluorohectorite (F) (CEC = 150 mequiv/100 g), saponite (sap) (100 mequiv/100 g), and  $\text{Na}^+$ -MMT (880 mequiv/100 g) were accordingly modified using various ammonium cations such as dioctadecyldimethylammonium (2C18), octadecyltrimethylammonium (qC18) octadecylammonium (C18), and a series of primary alkylammonium cations with

carbon chains of 6, 9–16 and 18 carbon atoms. The nanocomposites were prepared using procedure as described above. After annealing, they found that FC18, F2C18, MMT2C18 and sap2C18 with PS yielded intercalated nanocomposite systems, however, with MMTC18, and sapC18, it resulted in immiscible, non-intercalated systems. Decreasing the host area per octadecyl chain, as with F2C18, also led to a non-intercalated system. Thus, on the basis of these results, it is established that an intermediate range of interlayer chain conformations are the most favorable for PS melt intercalation.

In order to understand the intermolecular interaction, Vaia et al. [22] also performed melt intercalation of F2C18 and MMT2C18 with various styrene-derivative polymers. Table 6 represents these results. All the polymers are immiscible with F2C18. All polymers except PVCH form intercalated nanocomposite with MMT2C18, indicating that the structure of the pendent group on the polymer chain greatly affects nanocomposite formation.

Fig. 43 represents a temporal series of WAXD patterns for a PS30 ( $M_w = 30,000$ )/FC18 mixture annealed in situ at 160 °C in vacuum. The sample contains excess PS30 to avoid polymer depletion during hybrid formation. Details regarding the data collection and analysis are presented in Ref. [20]. The width of the original non-intercalated peak and the final intercalated peak appear to be similar, suggesting that the PS melt intercalation does not drastically alter the coherence length or disrupt the layer structure of the silicate crystallites.

Recently, a series of experiments has been designed and conducted by Beyer et al. [100] to construct a model for the morphological behavior of PLS nanocomposites, where a PLS nanocomposite is composed of a PS homopolymer, MMT and PS used as surfactant modifiers. The effect of surfactant length on the morphology of PLS nanocomposites was examined using an especially synthesized PS modified MMT as a model surfactant. SAXS data showed the PS homopolymer did not intercalate into the PS modified MMT. This finding is consistent with the results for autophobic dewetting that occurs with densely grafted polymer brushes, based on high surfactant coverage within the layered silicate galleries.

Vaia et al. [189] also applied same method to intercalate PEO in  $\text{Na}^+$ -MMT layers. Intercalation of

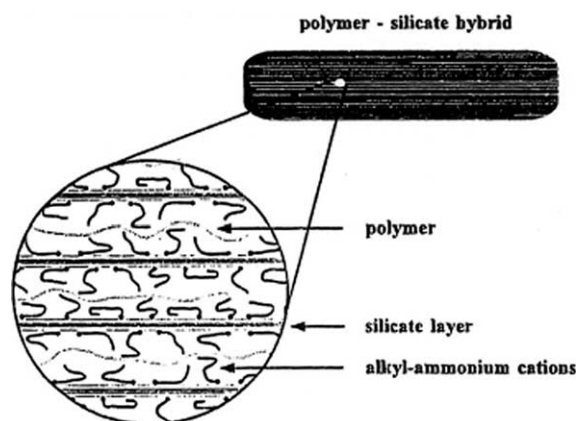
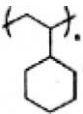
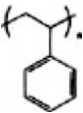
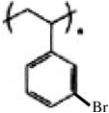
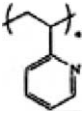


Fig. 42. Schematic illustration of polymer chains intercalated in OMLS [44]. Reproduced from Vaia, Ishii and Giannelis by permission of American Chemical Society, USA.

Table 6  
Summary of melt intercalation of M2C18 and F2C18 with styrene-derivative polymers [22]

| Polymer |   | Net gallery height increase (nm) |       |
|---------|---|----------------------------------|-------|
|         |   | M2C18                            | F2C18 |
| PVCH    |    | 0.00                             | 0.00  |
| PS      |   | 0.82                             | 0.00  |
| PS3Br   |  | 0.96 <sup>a</sup>                | 0.00  |
| PVP     |  | 1.00 <sup>b</sup>                | 0.00  |

Reproduced from Vaia and Giannelis by permission of American Chemical Society, USA.

<sup>a</sup> Intensity decreases observed associated with increased absorption of Br.

<sup>b</sup> Peak broadening and intensity decrease of  $d_{001}$ .

PEO in layered silicate was accomplished by heating the PEO with the  $\text{Na}^+$ -MMT at 80 °C. WAXD patterns of the PEO/ $\text{Na}^+$ -MMT hybrid before and after 2 and 6 h at 80 °C is presented in Fig. 44. The WAXD patterns before any heating occurs contains peaks characteristic of both  $\text{Na}^+$ -MMT and crystalline PEO (see Fig. 44). After heating to 80 °C, the intensity of the peaks corresponding to the non-intercalated silicate and crystalline PEO is progressively reduced, while a set of new peaks appears, corresponding to the PEO-intercalated MMT and signifying the completion of

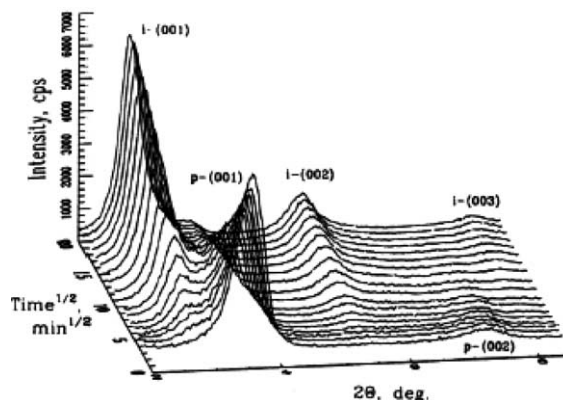


Fig. 43. Temporal series of X-ray diffraction patterns for a PS30/F18 pellet annealed in situ at 160 °C in vacuum [20]. Reproduced from Vaia, Jandt, Kramer and Giannelis by permission of American Chemical Society, USA.

intercalation. Very recently Shen et al. [205] reported the preparation of PEO/OMLS nanocomposites using the melt intercalation technique.

The in situ intercalative polymerization technique is generally used to prepare N6/clay nanocomposites. Liu et al. [142] first applied this technique in the preparation of a commercially available N6 with

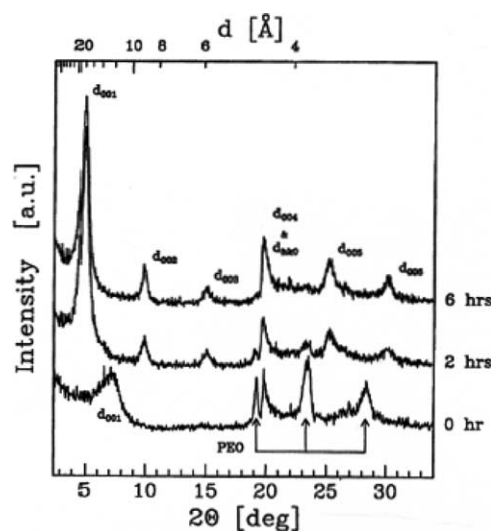


Fig. 44. X-ray diffraction pattern of PEO/ $\text{Na}^+$ -MMT hybrid heated to 80 °C for 0, 2, and 6 h [189]. Reproduced from Vaia, Vasudevan, Krawiec, Scanlon and Giannelis by permission of Wiley-VCH, Germany.

C18-MMT nanocomposites, using a twin-screw extruder. They prepared nanocomposites with MMT content from 1 to 18 wt%. WAXD patterns and TEM observations indicated that nanocomposites prepared with MMT less than 10 wt% led to exfoliated structures, but those with more than 10 wt% MMT led to the formation of intercalated structures. WAXD and DSC analyses also showed that exfoliated structures strongly influenced the nature of the N6 crystallization, favoring the formation of  $\gamma$ -crystals in addition to the crystals of the  $\alpha$ -form observed in the native N6 matrix, and also have strong heterophase nucleation effects. VanderHart et al. [147] prepared N6/OMLS nanocomposites using a melt intercalation method.

Recently, Fornes et al. [149] reported the preparation of N6/OMLS nanocomposites in the molten state, using a twin-screw extruder. They used three different molecular grades of N6 for the preparation of nanocomposites with bis(hydroxyethyl)(methyl)-rape seed quaternary ammonium  $[(HE)_2M_1R_1]$  modified MMT, and attempted to determine the effects of matrix molecular weights on structure, properties, and rheology. Nanocomposites were prepared using a Haake, co-rotating, intermeshing twin-screw extruder, which was operated at 240 °C with a screw speed of 280 rpm, and a feed rate of 980 g/h.

Fig. 45 represents the WAXD patterns of  $(HE)_2M_1R_1$  based MMT and nanocomposites based on the three N6 matrix of low molecular weight (LMW), medium molecular weight (MMW) and HMW, having an approximate MMT concentration of 1.5 wt%. TEM images of various nanocomposites corresponding to the WAXD patterns (see Fig. 45) are presented in Fig. 46. WAXD patterns and TEM observations collectively revealed a mixed structure for the LMW based nanocomposites, while the MMW and HMW based nanocomposites revealed well-exfoliated structures. The average number of platelets per stack was shown to decrease with increasing matrix molecular weight. The mechanical properties of the nanocomposites were consistent with the morphological structure found via WAXD and TEM analyses.

In a later study [151], they examined the effect of OMLS structure on N6 nanocomposite morphology and properties. In order to understand this, a series of organic amine salts were ion exchanged with

$Na^+$ -MMT to form organoclays varying in amine structure or exchange level relative to the MMT. Each organoclay was melt-mixed with a HMW N6 using a twin-screw extruder operated under the same conditions as described above; some organoclays were also mixed with LMW N6. The structure and corresponding nomenclature of various amine compounds for the modification of  $Na^+$ -MMT using ion exchange method are presented in Fig. 47. WAXD patterns and TEM observations of one representative nanocomposite are presented in Fig. 48. On the basis of WAXD analyses the authors concluded that the galleries of the organoclay expand systematically to accommodate the molecular size and the amount of amine surfactant exchanged for the  $Na^+$ -MMT. They also concluded that three distinct surfactant effects were identified that led to greater extents of exfoliation, higher stiffness, and increased yield strengths for nanocomposites based on the HMW N6. These effects are: (a) one long alkyl tail on the ammonium ion rather than two; (b) methyl groups on the amine rather than 2-hydroxy-ethyl groups; and (c) an equivalent rather than excess amount of amine surfactant on the clay.

Recently, Hasegawa et al. [155] reported a novel compounding process for the preparation of N6/MMT nanocomposites, using a  $Na^+$ -MMT water slurry as an

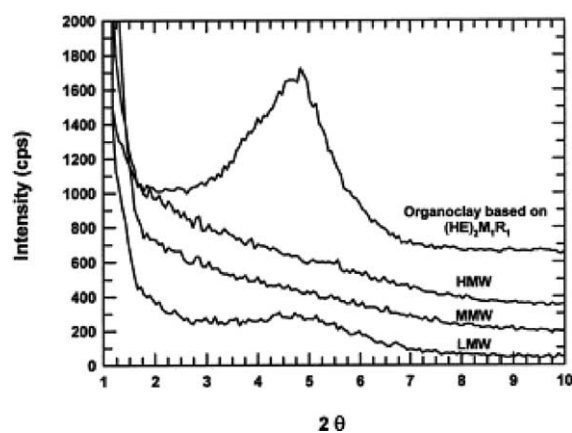


Fig. 45. WAXD patterns for  $(HE)_2M_1R_1$  organoclay and  $(HE)_2M_1R_1$  organoclay nanocomposites based on LMW, MMW, and HMW matrices containing ~1.5 wt% MMT [149]. Reproduced from Fornes, Yoon, Keskkula and Paul by permission of Elsevier Science Ltd, UK.

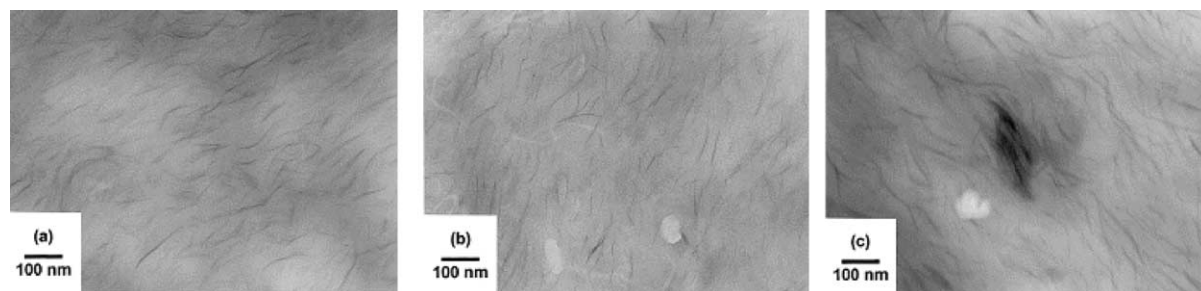


Fig. 46. Bright field TEM images of melt compounded nanocomposites containing ~3 wt% MMT based on (a) HMW, (b) MMW, and (c) LMW N6 [149]. Reproduced from Fomes, Yoon, Keskkula and Paul by permission of Elsevier Science Ltd, UK.

alternate for organically modified MMT. In this process, the  $\text{Na}^+$ -MMT slurry was blended with melting N6 using an extruder, followed by removing the water. WAXD patterns and TEM observations clearly indicates the exfoliation of MMT layers in the N6 matrix but the final properties of N6/ $\text{Na}^+$ -MMT nanocomposites were nearly equal to those of

conventional N6/MMT nanocomposites prepared by dry compounding with MMT.

Fig. 49 shows schematic figures depicting dispersion of the  $\text{Na}^+$ -MMT silicate layers of the clay slurry into the N6 matrix during compounding by an extruder. According to this study, the exfoliation of silicate layers into the N6 matrix occurs as follows:

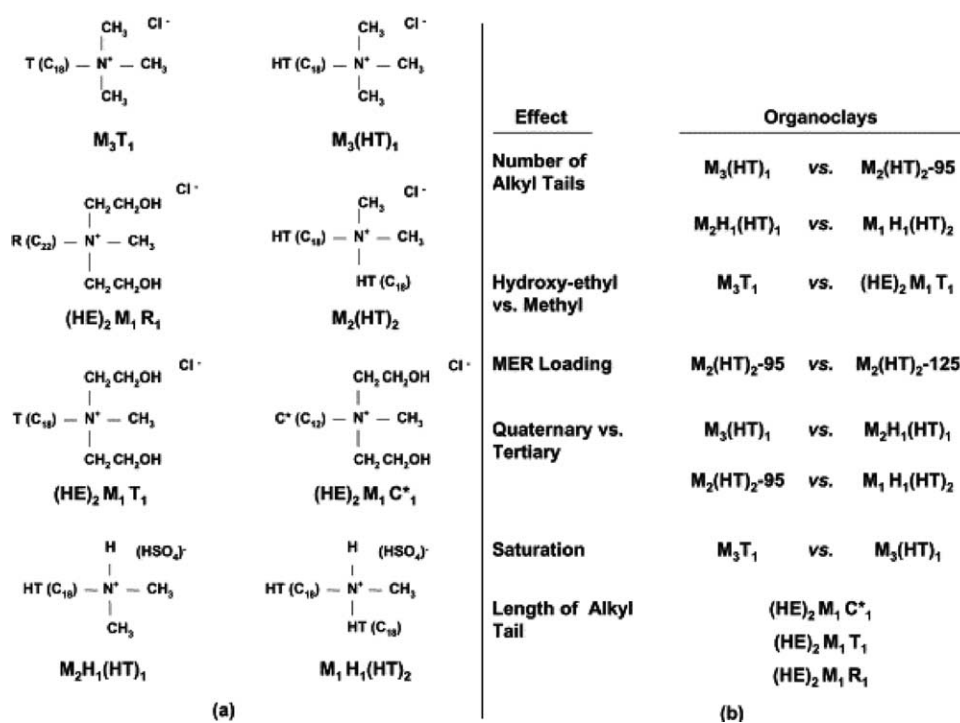


Fig. 47. (a) Molecular structure and nomenclature of amine salts used to organically modify  $\text{Na}^+$ -MMT by ion exchange. The symbols M: Methyl, T: Tallow, HT: hydrogenated tallow, HE: 2-hydroxy-ethyl, R: rapeseed, C: coco, and H: hydrogen designate the substituents on the nitrogen. (b) Organoclays used to evaluate the effect of structural variations of the amine cations on nanocomposite morphology and properties [151]. Reproduced from Fomes, Yoon, Hunter, Keskkula and Paul by permission of Elsevier Science Ltd, UK.

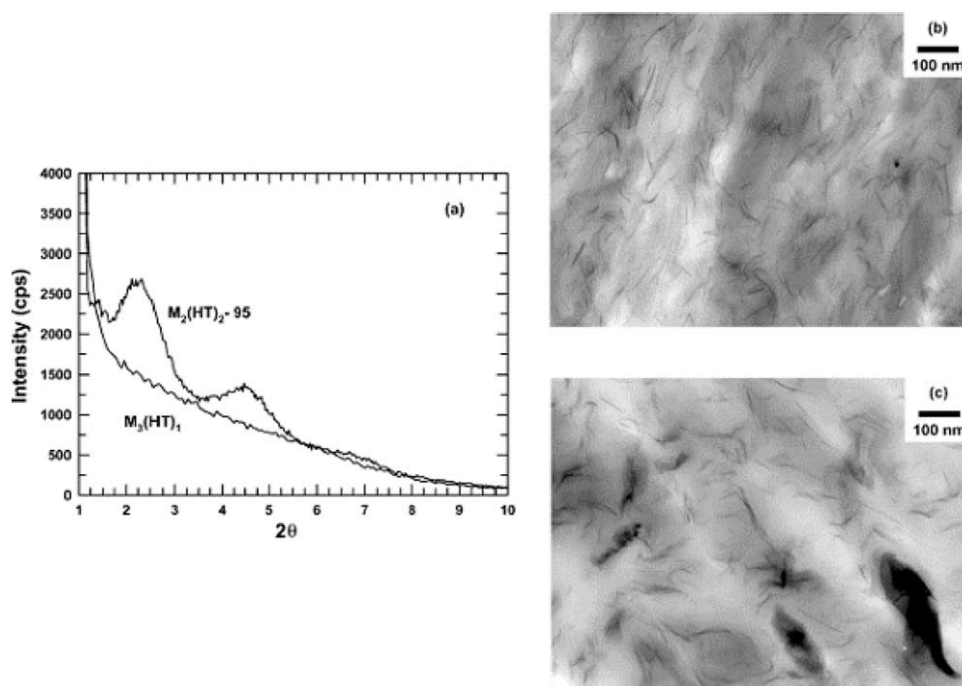


Fig. 48. Morphological analysis of nanocomposites based on HMW Nylon-6 and the organoclays M<sub>3</sub>(HT)<sub>1</sub> and M<sub>2</sub>(HT)<sub>2</sub>-95. (a) WAXD patterns and TEM images of (b) M<sub>3</sub>(HT)<sub>1</sub> and (c) M<sub>2</sub>(HT)<sub>2</sub>-95 based nanocomposites. The concentration of mmt in the M<sub>3</sub>(HT)<sub>1</sub> and M<sub>2</sub>(HT)<sub>2</sub>-95 nanocomposites are 2.9 and 3 wt% [151]. Reproduced from Fornes, Yoon, Hunter, Keskkula and Paul by permission of Elsevier Science Ltd, UK.

(a) the clay slurry is first pumped into the melting matrix under vigorous shear; (b and c) the clay slurry reduces to finer drops during blending and, at the same time, the water of the slurry drops begins to evaporate in contact with the N6 melt; (d) the evaporated water is removed under vacuum, and silicate layers are dispersed into the N6 melt as monolayer or as a few layers. The dispersion of silicate layers in this process is quite different from that of conventional compounding process using organophilic clay, where polymer chains first intercalate into the stacked silicate galleries and then exfoliate into the matrix. In this process, the exfoliated silicate layers directly fixed into the polymer matrix without aggregation of the silicate layers.

Recently, Gilman et al. [101] reported the preparation of polyamide-6 (PA6) and PS-based nanocomposites of MMT modified with trialkylimidazolium cations to obtain high stability of OMLS at high processing temperatures. Fig. 50 represents various kinds of imidazolium salts used for the modification of MMT. For the preparation of nanocomposites they

used a mini-extruder, which was operated at 10 °C above the melting point of the polymer, with a residence time of 3–5 min and a screw speed of 200–300 rpm. WAXD analyses and TEM observations established the formation of an exfoliated structure for a PA6-based nanocomposite, as opposed to an intercalated structure with a PS/MMT system.

Today, propylene (PP) is one of the most widely used polyolefin polymers. Since it has no polar groups in the chain, direct intercalation of PP in the silicate galleries is impossible. Overcoming this difficulty, Usuki et al. [285] first reported a novel approach to prepare PPCNs using a functional oligomer (PP–OH) with polar telechelic OH groups as a compatibilizer. In this approach, PP–OH was intercalated between the layers of 2C18-MMT, and then the PP–OH/2C18-MMT was melt mixed with PP to obtain the nanocomposite with intercalated structure. Further study by the same group [286] reported the preparation of PP/MMT nanocomposites obtained by melt blending of PP, a maleic anhydride grafted PP

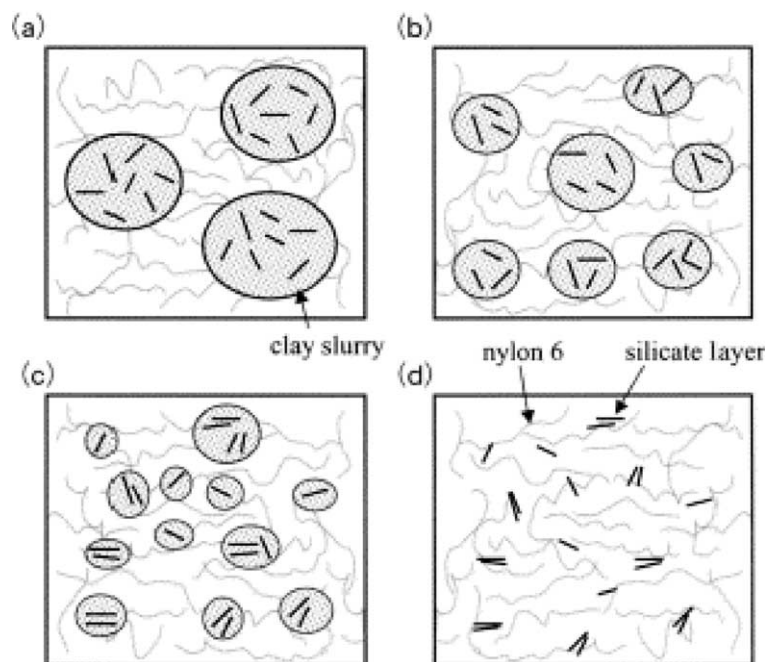


Fig. 49. Schematic figures depicting dispersion of the  $\text{Na}^+$ -MMT slurry into nylon-6 during compounding [155]. Reproduced from Haegawa, Okamoto, Kato, Usuki and Sato by permission of Elsevier Science Ltd, UK.

oligomer (PP-MA), and clays modified with stearylammonium using a twin-screw extruder. In their study, they used two different types of maleic anhydride modified PP oligomer with different amounts of maleic anhydride groups and two types of organically modified clays to understand the miscibility effect of the oligomers on the dispersibility of the OMLS in the PP matrix, and to study the effect of hybridization on their mechanical properties when compared with neat PP and PPCNs without oligomers.

WAXD analyses and TEM observations established the intercalated structure for all nanocomposites. On the basis of WAXD patterns and TEM images, they proposed a possible mechanism for dispersion of intercalated clay layers in the PP matrix. Fig. 51 shows a schematic presentation of the mixing process of the three components i.e. PP, PP-MA, and OMLS into the nanocomposites. The present authors believe that the driving force of the intercalation originates from the maleic anhydride group and the oxygen groups of the silicate through hydrogen bonding.

Hasegawa et al. [287] found that maleic anhydride grafted PP (PP-MA) was able to intercalate into the inter-galleries of OMLS, similar to the functional

oligomer, and described a facile approach for the preparation of PPCN by melt intercalation using a PP-MA and organically modified clay. In a typical preparative method, PPCN pellets were prepared by melt blending pellets of PP-MA and the powder of C18-MMT at 200 °C, using a twin-screw extruder. WAXD patterns and TEM images showed that the silicate layers were exfoliated and uniformly dispersed in the PP-MA matrix. Fig. 52 shows a schematic representation of the clay dispersion process in PP-MA-based

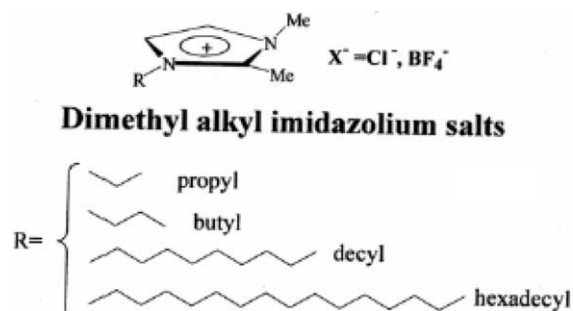


Fig. 50. Structures of various imidazolium salts used to treat  $\text{Na}^+$ -MMT [101]. Reproduced from Gilman, Awad, Davis, Shields, Harris, Davis, Morgan, Sutto, Callahan, Trulove and DeLong by permission of American Chemical Society and NIST, USA.



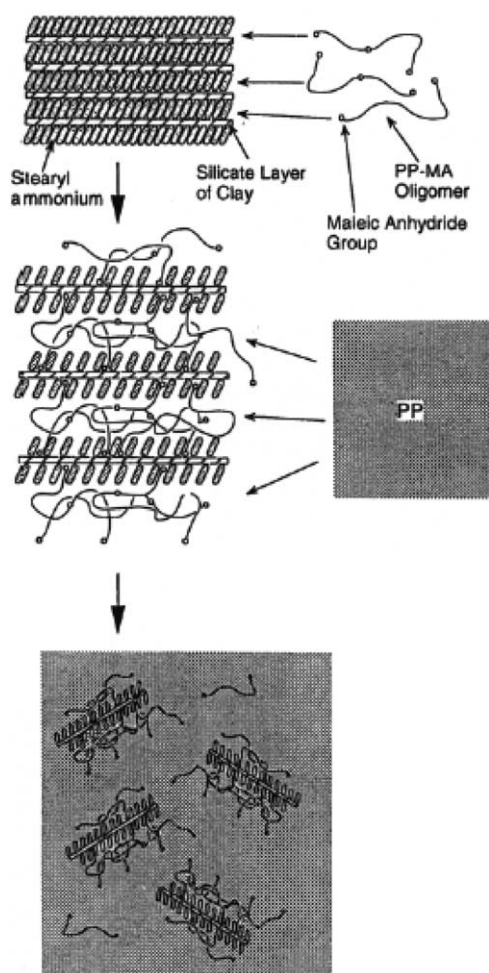


Fig. 51. Schematic representation of the dispersion process of the OMLs in the PP matrix with the aid of PP-MA [286]. Reproduced from Kawasumi, Hasegawa, Kato, Usuki and Okada by permission of American Chemical Society, USA.

nanocomposites. WAXD analysis of PPCN showed no peak representing dispersed C18-MMT in the PP-MA matrix. According to the authors, that means that the driving force of the PP-MA originates from the strong hydrogen bonding between the MA groups and the polar clay surface. The same authors [294] also prepared polyethylene-propylene rubber (EPR)/C18-MMT nanocomposites by melt blending EPR-g-MA and C18-MMT powder using a twin-screw extruder, and then tried to compare the morphology of EPR-based nanocomposites with PPCN.

Recently, Okamoto et al. [303] prepared PP/MMT nanocomposites using method as used described

above. For example, a mixture of PP-MA (0.2 wt% MA) and C18-MMT was melt extruded at 200 °C in a twin-screw extruder. They prepared PPCNs with three different amounts of clay content (2, 4 and 7.5 wt% inorganic part), abbreviated as PPCN2, PPCN4, and PPCN7.5, respectively. The WAXD patterns of C18-MMT, PP-MA and various PPCNs are presented in Fig. 53. WAXD patterns clearly established the formation of nearly exfoliated structures with PPCN2, disordered intercalated nanocomposites with PPCN4, while PPCN7.5 represents ordered intercalated structure. These features are clearly observed with bright field TEM images of various PPCNs as shown in Fig. 54. In order to understand the hierarchical structure of PPCNs, they also used polarizing optical microscopy, light scattering and small angle X-ray diffraction for the characterization of PPCNs. On the basis of these analyses they demonstrated the dispersed clay and inter-fibril structure of PPCNs; the schematic illustration of this structure is presented in Fig. 55.

In another publication [304], Liu and Wu reported the preparation of PPCN via grafting-melt compounding using a new type of co-intercalated organophilic clay which has a larger interlayer spacing than the ordinarily organophilic clay that was modified with alkylammonium cations. One of the co-intercalation monomers is unsaturated so it could tether on the PP backbone through a grafting reaction. The co-intercalated organophilic clay (EM-MMT) was prepared as follows: 130 g hexadecylammonium modified MMT (C<sub>16</sub>-MMT) and 20 g epoxypropyl methacrylate were mixed in a hake Reocorder 40 mixer for 1 h. Before mixing with clay, the initiator for the grafting reaction, dibenzoyl peroxide (BPO) and a donor agent were dissolved in epoxypropyl methacrylate. The nanocomposites were prepared using a twin-screw extruder with a screw speed of 180 rpm and operated at a temperature around 200 °C. WAXD patterns and TEM observations established that the larger interlayer spacing and strong interaction caused by grafting can improve the dispersion effect of silicate layers in the PP-matrix.

Manias et al. [305,418] reported the preparation by melt intercalation technique of PP/organically modified MMT with both intercalated and exfoliated structures. In order to prepare nanocomposites, they (a) introduced functional groups in PP, and (b) used

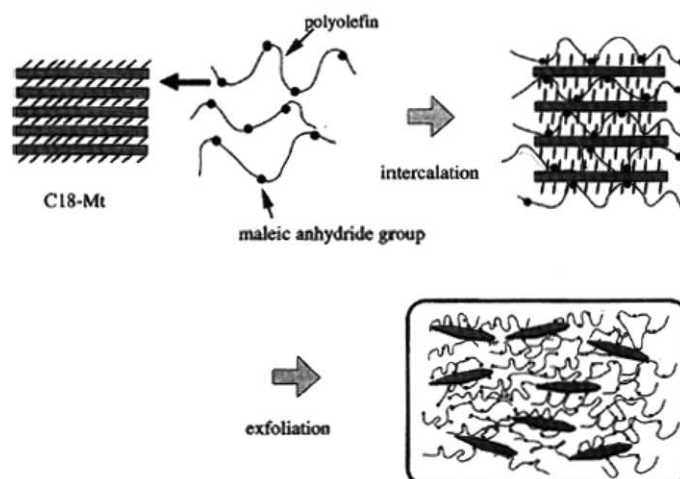


Fig. 52. Schematic illustration of OMLS dispersion process in PP-g-MA matrix [294]. Reproduced from Hasegawa, Okamoto, Kawasumi, Kato, Tsukigase and Usuki by permission of Wiley-VCH, Germany.

common alkylammonium MMT and neat/unmodified PP and a semifluorinated surfactant modification for the MMT (f-MMT). For the first approach, they used random copolymers of PP with 0.5 mol% of functionalized comonomers, or diblock copolymers with 1 mol% of non-PP block copolymers. Details regarding the preparation of functionalized PP copolymers are presented in Ref. [419–422]. Functional groups that promote nanocomposite formation with dimethyldiallammonium-modified MMT include *p*-methylstyrene, maleic anhydride, styrene, and hydroxyl-containing styrene; propylene-*b*-methylmethacrylate diblocks also formed nanocomposites with octadecylammonium-modified MMT. In the second approach, a semifluorinated alkyltrichlorosilane was used to modify octadecylammonium-modified MMT, rendering it miscible with neat PP [423].

Kaempfer et al. [315] reported the preparation of new nanocomposites via melt compounding of syndiotactic polypropylene (sPP) containing OMLS and in situ formed core/shell nanoparticles. Melt compounding of sPP with octadecylammonium modified fluorohectorite in a co-rotating twin-screw extruder, represents an attractive new route to reinforced sPP with considerably greater stiffness. The matrix reinforcement is achieved by in situ formation of silicate nanoparticles through exfoliation combined with simultaneous in situ encapsulation of

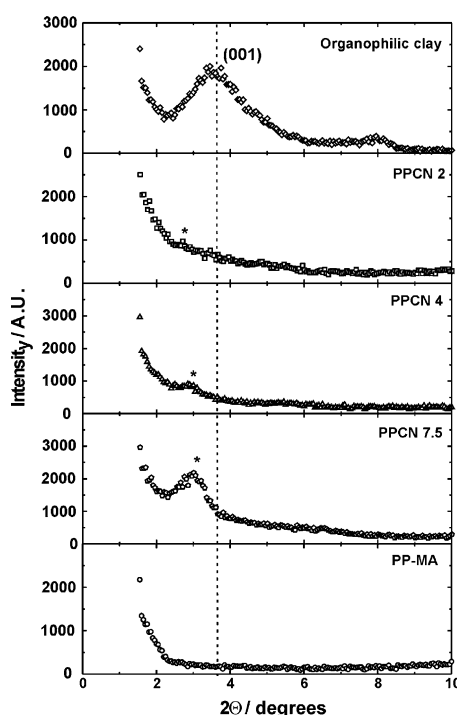


Fig. 53. WAXD patterns for OMLS, PP-g-MA, and various PPCNs. The dashed lines indicate the location of the silicate (001) reflection of OMLS. The asterisks indicate a remnant shoulder for PPCN2 or a small peak for PPCN4 [303]. Reproduced from Nam, Maiti, Okamoto, Kotaka, Hasegawa and Usuki by permission of Elsevier Science Ltd, UK.

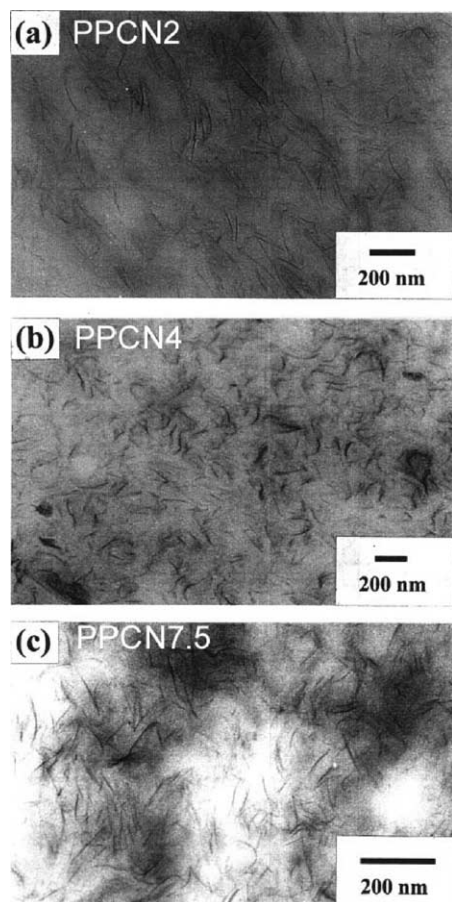


Fig. 54. Bright field TEM images of PPCNs: (a) 2 wt%, (b) 4 wt%, and (c) 7.5 wt% MMT. The dark lines are the cross-sections of silicate layers and the bright areas are the PP-g-MA matrix [303]. Reproduced from Nam, Maiti, Okamoto, Kotaka, Hasegawa and Usuki by permission of Elsevier Science Ltd, UK.

the resulting nanosilicates in a thin shell of iPP-g-MA. The resulting anisotropic core/shell type nanoparticles, containing stacks of organohectorite layers as the core and iPP-g-MA as the shell, represent a very effective class of nucleating agents for sPP crystallization.

Maleic anhydride grafted polyethylene (PE-g-MA)/clay nanocomposites were also prepared using a melt intercalation technique [325]. The extent of exfoliation and intercalation completely depends on the hydrophilicity of the polyethylene grafted with maleic anhydride and the chain length of the organic modifier in the clay. An exfoliated nanocomposite was obtained when the number of methylene groups in the alkylamine (organic modifier) was larger than 16. This nanocomposite, with clay modified with dimethyl dihydrogenated tallow ammonium cations or octadecylammonium cations, had a maleic anhydride grafting level higher than about 0.1 wt%.

Very recently, EPDM/clay nanocomposites were prepared by mixing EPDM with OMLS via a vulcanization process [332]. They used thiuram and dithiocarbamate for the vulcanization accelerator. WAXD analysis and TEM observation revealed that the clay layers were exfoliated and almost dispersed as monolayers. Davis et al. [181] first reported the preparation of PET-based nanocomposite using this method. PET/MMT nanocomposites were compounded via melt blending in a co-rotating mini twin-screw extruder operated at 285 °C using 1,2-dimethyl-3-*N*-alkyl imidazolium salt modified MMT (hexadecyl-MMT) for the nanocomposite preparation. Table 7 summarizes the various conditions and

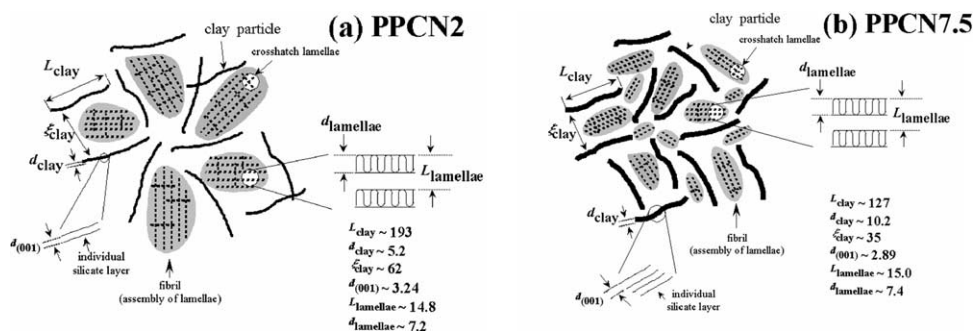


Fig. 55. The schematic illustration for dispersed clay structure and the inter-fibrillar structure for PPCNs with: (a) 2 wt% and (b) 7.5 wt% MMT [303]. Reproduced from Nam, Maiti, Okamoto, Kotaka, Hasegawa and Usuki by permission of Elsevier Science Ltd, UK.

Table 7  
Composition and extrusion condition used during PET-nanocomposites preparation [181]

| Sample | Sample composition (5 wt% clay) | Screw speed (rad/s) | Residence time (min) |
|--------|---------------------------------|---------------------|----------------------|
| CD 12  | PET + hexadecyl-MMT             | 21                  | 2                    |
| CD 5   | PET + hexadecyl-MMT             | 21                  | 5                    |
| CD 9   | PET + hexadecyl-MMT             | 21                  | 7                    |
| CD 13  | PET + hexadecyl-MMT             | 31                  | 5                    |

Reproduced from Davis, Mathias, Gilman, Schiraldi, Shields, Trulove, Sutto and DeLong by permission of John Wiley and Sons, Inc., USA.

samples used during the preparation of PET/MMT nanocomposites. WAXD analyses (see Fig. 56) and TEM (see Fig. 57) observations established that the formation of a mixed delaminated/intercalated structure is achieved in the nanocomposites. Like PET nanocomposites, this method was successfully applied by Chisholm et al. [185] for the preparation of poly(butylene terephthalate) (PBT)/OMLS nanocomposites using sulfonated PBT. Because of the ionic nature of the  $-\text{SO}_3\text{Na}$  groups and the expected insolubility of the  $-\text{SO}_3\text{Na}$  groups in the polyester matrix, it was thought that the presence of the  $-\text{SO}_3\text{Na}$  groups may have provided

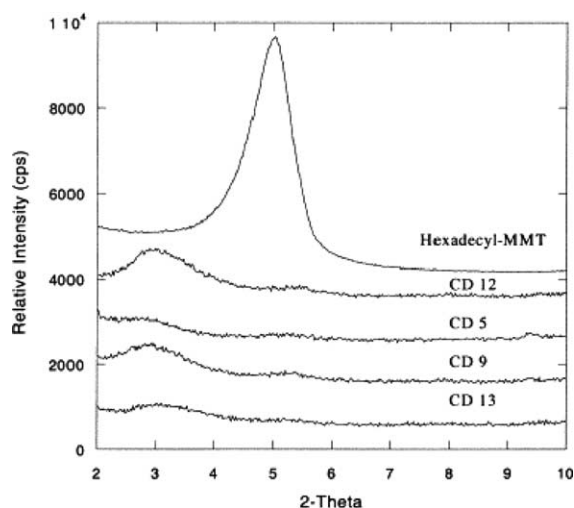


Fig. 56. XRD data of hexadecyl-MMT/PET nanocomposites that were melt-blended at 285 °C for 2, 5 and 7 min at screw speed of 21 and 31 rad/s. Details regarding the figure are shown in Table 8 [181]. Reproduced from Davis, Mathias, Gilman, Schiraldi, Shields, Trulove, Sutto and DeLong by permission of John Wiley and Sons, Inc., USA.

a thermodynamic driving force for the production of nanocomposites derived from MMT. But after preparation and characterization of the nanocomposites, it was found that the degree of intercalation was not strongly dependent on the amount of  $-\text{SO}_3\text{Na}$  groups, yet the mechanical properties increased significantly with increasing  $-\text{SO}_3\text{Na}$  content. This behavior indicates that with high  $-\text{SO}_3\text{Na}$  content the number of interactions increases between the clay particles and the matrix through strong specific interactions involving the  $-\text{SO}_3\text{Na}$  groups.

Recently, Huang et al. [186] reported the synthesis of a partially exfoliated bisphenol PC nanocomposite using carbonate cyclic oligomers and dimethyldiallo-wammonium-exchanged MMT. WAXD patterns indicate that exfoliation of this OMLS occurred after mixing with the cyclic oligomers in a brabender mixer for 1 h at 180 °C. Subsequent ring-opening polymerization of the cyclic oligomers converted the matrix into a linear polymer without disruption of the nanocomposite structure. TEM imaging revealed that partial exfoliation was obtained, although no indication of layer correlation was observed in the WAXD.

PEI/MMT nanocomposites were prepared by melt blending hexadecylamine modified MMT and PEI at 350 °C to prepare thermoplastic poly(etherimide) (PEI) based nanocomposites [276,277]. WAXD patterns of various nanocomposites showed no peaks but TEM observations showed relatively stacked silicate layers heterogeneously dispersed in the polymer matrix. According to the authors, the strong interaction between PEI and OMLS caused a substantial increase at the thermal decomposition temperature, and a drastic decrease in solvent uptake and so forth as compared to the virgin PEI. But they did not check the stability of the intercalated salts in OMLS at this high mixing temperature.

Kim et al. [126] used this method for the preparation of poly(styrene-co-acrylonitrile) (SAN)/OMLS nanocomposites, using PCL as a compatibilizer. They used a two step mixing sequence for the preparation of SAN nanocomposites: PCL/OMLS master batches with different degrees of intercalation were first prepared, and then melt-mixed with SAN, since PCL is miscible with SAN. The intercalation behavior of PCL in the master batches was investigated in terms of the type of OMLS and mixing conditions. Longer mixing times and lower mixing

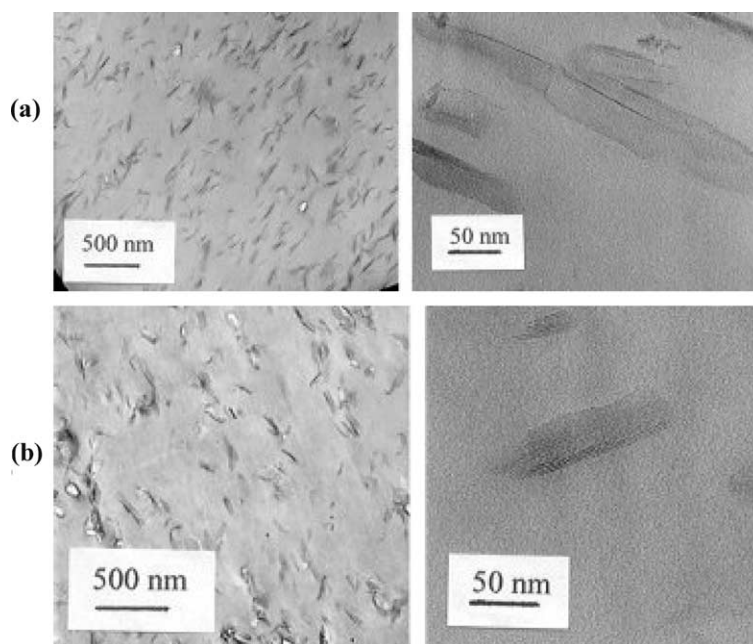


Fig. 57. TEM images of: (a) CD12 showing high levels of dispersion and exfoliation, average tactoids of four sheets per stack and (b) CD13 showing similar levels of dispersion and delamination as compared to CD12 [181]. Reproduced from Davis, Mathias, Gilman, Schiraldi, Shields, Trulove, Sutto and DeLong by permission of John Wiley and Sons, Inc., USA.

temperatures were required for the preparation of PCL master batches with exfoliated structures. As the degree of exfoliation of OMLS increased, the stiffness reinforcement effect of the OMLS increased in both PCL/OMLS master batches and their SAN blends with.

In order to determine the effect of thermal treatment on the amount of PEO and polyethylene–poly(ethylene glycol) (PE–PEG) diblock copolymer intercalated into the layers of  $\text{Na}^+$ -MMT, and on the ionic conductivity of PEO/ $\text{Na}^+$ -MMT, Liao et al. [202] prepared PEO/ $\text{Na}^+$ -MMT and PE–PEG diblock copolymer/ $\text{Na}^+$ -MMT nanocomposites using a melt intercalation technique. It was found that PEO could be intercalated into the layers of  $\text{Na}^+$ -MMT by a simple mechanical blending; part of the PE in PE–PEG diblock copolymers was also intercalated into the layers of  $\text{Na}^+$ -MMT. The intercalated amount increased with thermal treatment time, which ultimately improved the ionic conductivity of the PEO/ $\text{Na}^+$ -MMT nanocomposites. Recently, this method was successfully applied by Artzi et al. [127] for the

preparation of ethylene–vinyl alcohol copolymer/OMLS nanocomposites.

The melt intercalation method is also suitable for the preparation of liquid crystal polymer (DHMS7, 9)-based nanocomposites. Vaia and Giannelis [366] reported the reversible intercalation between OMLS and LCP in the nematic state. Melt intercalation of a model main-chain liquid crystalline co-polymer based on 4,4'-dihydroxy-*a*-methylstilbene and a 50:50 mol ratio mixture of heptyl/nonyl alkyl dibromide (see Fig. 58a) was accomplished by annealing a powder mixture of the polymer and OMLS (see Fig. 58b) within the nematic region of the polymer.

Fig. 59 shows X-ray diffraction patterns at room temperature of the 25 wt% DHMS7, 9/75 wt% dioctadecyldimethylammonium-modified MMT (M2C18) mixture before annealing and after 100, 280, and 620 min annealing at 160 °C. The WAXD pattern before heating contains peaks characteristic of both pristine M2C18 and crystalline DHMS7, 9. After annealing at 160 °C for as little as 100 min, a new series of basal reflections, corresponding to an

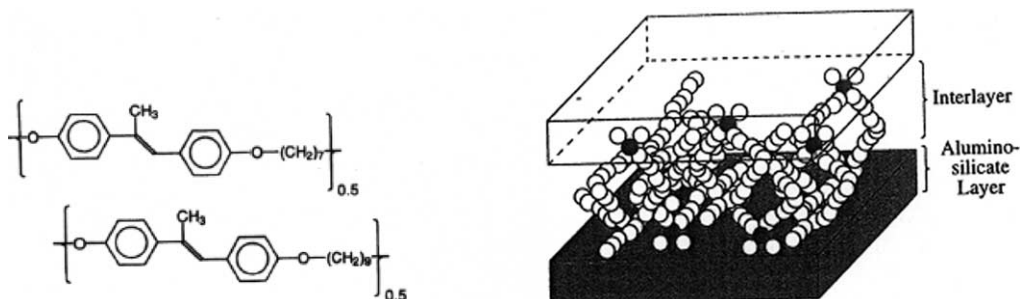


Fig. 58. (a) Chemical structure of liquid crystalline polymer, DHMS7, 9. (b) Schematic structure of OMLS [366]. Reproduced from Vaia and Giannelis by permission of Elsevier Science Ltd, UK.

intercalated structure, dominated the spectrum. The original basal reflections, corresponding to the non-intercalated silicate, are substantially reduced. At the same time, the relative intensity of the crystalline DHMS7, 9 reflections decreased with prolonged annealing time, reflecting the decreased concentration of polymer outside of the OMLS interlayer, and the influence of the OMLS on polymer crystallization. The development of the intercalated phase from the 25 wt% DHMS7, 9/75 wt% M2C18 mixture continues at a substantially reduced rate for annealing times longer than 620 min. This behavior qualitatively agrees with previous kinetic measurements of amorphous polymer melt intercalation, showing that the reaction approaches equilibrium asymptotically [21].

In another report, Chang et al. [368] prepared nanocomposites of thermotropic liquid crystalline

polyester (TLCP) and Cloisite 25A, using a melt intercalation method above the melt transition temperature of the TLCP. The WAXD patterns and TEM observations of nanocomposites containing varying amounts of Cloisite 25A are presented in Fig. 60(a–d). The liquid crystallinity in the nanocomposites was observed when OMLS content was above 6 wt%.

Sinha Ray et al. [374,375] first used this technique for the preparation of intercalated PLA/layered silicate nanocomposites. For nanocomposite (PLACNs) preparation, C18-MMT and PLA were first dry-mixed by shaking them in a bag. The mixture was then melt-extruded using a twin-screw extruder operating at 190 °C to yield light gray strands of PLACNs. Nanocomposites loaded with a very small amount of *o*-PCL as a compatibilizer were also

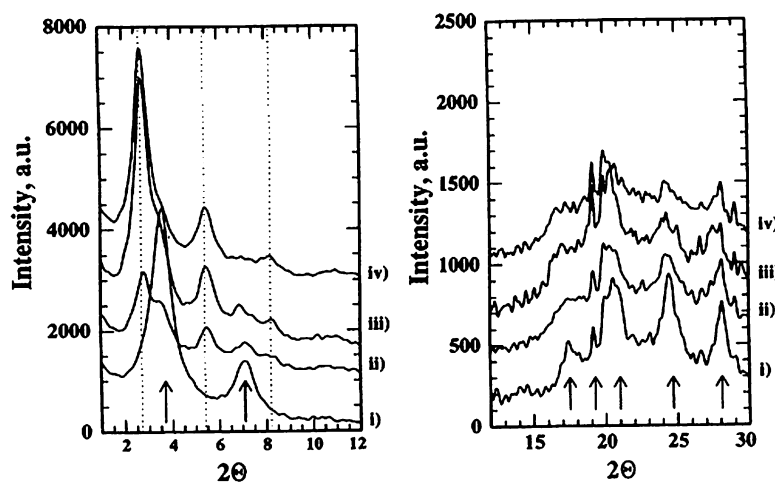


Fig. 59. X-ray diffraction patterns of the 25 wt% DHMS7, 9–75 wt% M2C18 mixture (i) before annealing and (ii) after 100, (iii) 280, and (iv) 620 min anneal at 160 °C. Dotted lines indicate (00 $l$ ) reflections of DHMS7, 9 intercalated M2C18 whereas arrows indicate original reflections of unintercalated M2C18 and DHMS7, 9 [366]. Reproduced from Vaia and Giannelis by permission of Elsevier Science Ltd, UK.

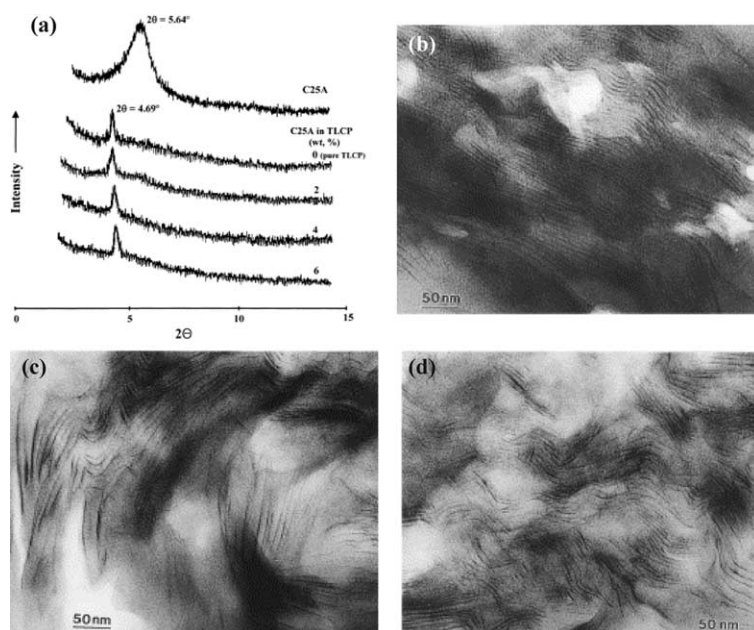


Fig. 60. (a) WAXD patterns of C25A and C25A/TLCP nanocomposites. (b) Bright field TEM images of (a) 2 wt%, (b) 4 wt%, and (c) 6 wt% C25A in TLCP nanocomposites [368]. Reproduced from Chang, Seo and Hwang by permission of Elsevier Science Ltd, UK.

prepared in order to understand the effect of *o*-PCL on the morphology and properties of PLACNs [374]. The compositions of various nanocomposites of PLA with C18-MMT are summarized in Table 8. WAXD patterns of this series of nanocomposites are shown in Fig. 61; Fig. 62 represents the corresponding TEM photographs. Form factors were calculated on the basis of WAXD analyses and TEM observations (see Table 9), i.e. the average length ( $L_{\text{clay}}$ ), thickness of the stacked intercalated silicate layers ( $d_{\text{clay}}$ ), and the correlation length ( $\xi_{\text{clay}}$ ) between them (see Fig. 4). These data clearly established that the silicate layers of the clay were intercalated, and randomly distributed in the PLA matrix. Incorporation of a very small amount of *o*-PCL as a compatibilizer in the nanocomposites led to better parallel stacking of the silicate layers, and also to much stronger flocculation due to the hydroxylated edge–edge interaction of the silicate layers. Owing to the interaction between clay platelets and the PLA matrix in the presence of a very small amount of *o*-PCL, the strength of the disk–disk interaction plays an important role in determining the stability of the clay particles, and hence the enhancement of mechanical properties of such nanocomposites.

In subsequent research [18,376–380,386], Sinha Ray et al. prepared a series of PLACNs with various types of OMLS to investigate the effect of OMLS on the morphology, properties, and biodegradability of PLACNs. Four different types of pristine layered silicates were used, each modified with a different type of surfactant. Details regarding the various types of OMLS used are presented in Table 10. On the basis of WAXD analyses and TEM observations, the authors concluded that four different types of PLACNs were formed. Ordered intercalated-and-flocculated nanocomposites were obtained when ODA was used as the OMLS, disordered intercalated structures were observed in the case of PLA/SBE4 nanocomposites, PLA/SAP4 nanocomposites are nearly exfoliated, while a co-existence of stacked intercalated and exfoliated nanocomposite structures were formed in PLA/MEE4 nanocomposites. Therefore, the nature of the OMLS has a strong effect on the final morphology of PLA-based nanocomposites.

Okamoto et al. [381] prepared a series of PLACNs with three different types of pristine layered silicates, i.e. saponite, MMT, and mica, and each was modified with alkylphosphonium salts having varying chain lengths. In their work, they first tried to determine

Table 8

Composition and characteristic parameters of various PLACNs based on PLA, *o*-PCL and C18-MMT [374]

| Sample           | Composition (wt%) |               |                      | $M_w \times 10^{-3}$ (g/mol) | $M_w/M_n$ | $T_g$ (°C) | $T_m$ (°C) | $\chi_c^a$ /% |
|------------------|-------------------|---------------|----------------------|------------------------------|-----------|------------|------------|---------------|
|                  | PLA               | <i>o</i> -PCL | C18-MMT <sup>b</sup> |                              |           |            |            |               |
| PLACN1           | 97                |               | 3 [2.0]              | 178                          | 1.81      | 60.0       | 169        | 50.65         |
| PLACN2           | 95                |               | 5 [3.0]              | 185                          | 1.86      | 60.0       | 170        | 39.01         |
| PLACN3           | 93                |               | 7 [4.8]              | 177                          | 1.69      | 59.8       | 170        | 43.66         |
| PLACN4           | 94.8              | 0.2           | 5 [3.3]              | 181                          | 1.76      | 58.6       | 170        | 41.47         |
| PLACN5           | 94.5              | 0.5           | 5 [3.3]              | 181                          | 1.76      | 57.6       | 169        | 32.91         |
| PLACN6           | 93                | 2.0           | 5 [2.8]              | 180                          | 1.76      | 54.0       | 168        | –             |
| PLACN7           | 92                | 3.0           | 5 [2.4]              | 181                          | 1.77      | 51.0       | 168        | –             |
| PLA <sup>c</sup> | 100               |               |                      | 187                          | 1.76      | 60.0       | 168        | 36.24         |
| PLA1             | 99.8              | 0.2           |                      | 180                          | 1.76      | 58.0       | 168.5      | 46.21         |
| PLA2             | 99.5              | 0.5           |                      | 180                          | 1.76      | 57.0       | 168.8      | 52.51         |
| PLA3             | 98                | 2.0           |                      | 180                          | 1.76      | 54.7       | 169        | –             |

Reproduced from Sinha Ray, Maiti, Okamoto, Yamada and Ueda by permission of American Chemical Society, USA.

<sup>a</sup> The degree of crystallinity.

<sup>b</sup> Value in the parenthesis indicates the amount of clay (inorganic part) content after burning.

<sup>c</sup>  $M_w$  and PDI of extruded PLA (at 190 °C) are  $180 \times 10^3$  (g/mol) and 1.6, respectively.

the effect of varying the chain length of the alkylphosphonium modifier on the properties of organoclay, and how the various clays behave differently with the same organic modifier. They also studied the effects of dispersion, intercalation, and aspect ratio of the clay on the material properties. Table 11 gives the name,

chemical formula and designation of the various surfactants, and the characteristics of the pristine clay and OMLS used for the preparation of nanocomposites.

Parts a and b of Fig. 63 represent the WAXD patterns of saponite organoclays with different

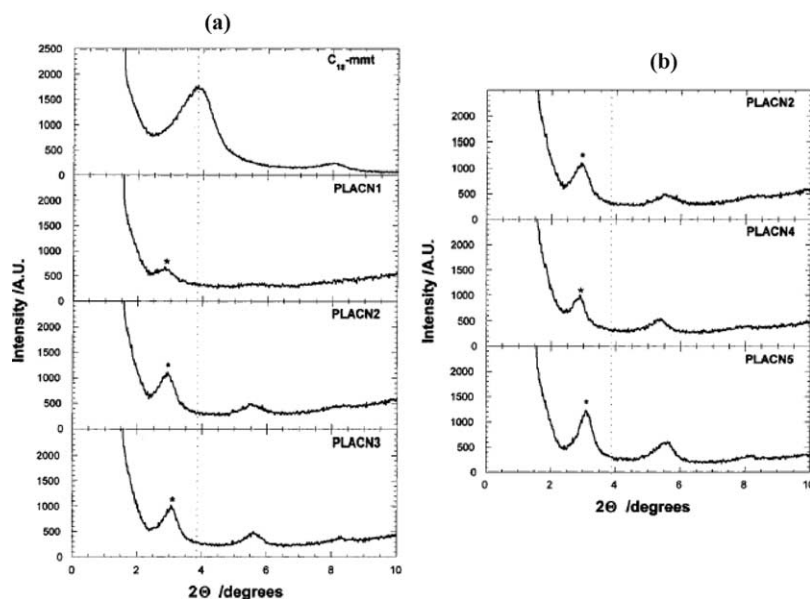


Fig. 61. WAXD patterns for C18-MMT and various PLACNs: (a) without *o*-PCL and (b) with *o*-PCL. The dashed line in each figure indicates the location of the silicate (001) reflection of C18-MMT. The asterisks indicate the (001) peak for C18-MMT dispersed in PLA matrices [374]. Reproduced from Sinha Ray, Maiti, Okamoto, Yamada and Ueda by permission of American Chemical Society, USA.



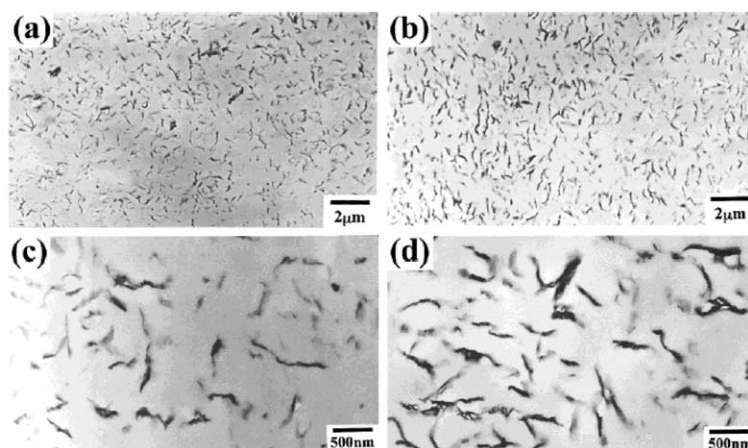


Fig. 62. TEM bright field images: (a) PLACN2 ( $\times 10,000$ ), (b) PLACN4 ( $\times 10,000$ ), (c) PLACN2 ( $\times 400,000$ ), and (d) PLACN4 ( $\times 40,000$ ). The dark entities are the cross-section of intercalated OMLS, and the bright areas are the matrices [374]. Reproduced from Sinha Ray, Maiti, Okamoto, Yamada and Ueda by permission of American Chemical Society, USA.

modifiers, and the same modifier with different pristine clays, respectively. From the WAXD patterns it is clearly observed that the  $d$ -spacing (001) increases with increasing modifier chain length, and for a fixed modifier it increases with increasing lateral dimensions of the clay particle. Two reasons may be offered for the observed spacing behavior: one is the CEC value, and other is the lateral size of various pristine layered silicates. Layered silicates follow the  $d$ -spacing order: mica > MMT > saponite. According to the authors, the CEC value is more important than the lateral size in controlling the  $d$ -spacing/stacking of silicate layers. Since mica has a high lateral size, and also has a higher affinity to surfactant molecules due to its high CEC value, surfactant chains inside the intergallery exhibit a restricted conformation due to physical jamming. This physical jamming is smaller in for saponite due to its lower CEC value and smaller lateral size. The conclusions for OMLS, based on TEM and WAXD analyses, are schematically shown in Fig. 64.

Fig. 65 shows the WAXD patterns of various PLACNs prepared with various types of OMLS. No intercalation of PLA occurs with  $C_{Ph}$ - and  $C_8$ -clay based nanocomposites. It has been suggested that intercalation is prevented because the  $C_{Ph}$ -clay is immiscible with PLA. On the other hand, the space between the silicate galleries in the  $C_8$ -clay is not sufficient for PLA intercalation. The corresponding

bright field TEM images of PLACN2 and PLACN12 are presented in Fig. 66a and b, respectively. The TEM images clearly demonstrate the formation of stacked silicate layers in PLACN12, whereas clay layers are well dispersed in PLACN2. Fig. 67 shows the WAXD patterns of nanocomposites with different clay dimensions having the same clay ( $C_{16}$ -modified) content (3 wt%). For MMT-based nanocomposites, the peaks are sharp, and crystallite sizes are slightly less than those of the corresponding organoclay, indicating a nearly ordered structure of MMT in the nanocomposite. The peaks of the nanocomposites prepared with mica clay are very sharp, similar to those of the corresponding OMLS. The slightly larger

Table 9  
Comparison of form factors between PLACN2 and PLACN4 obtained from WAXD patterns and TEM observations [374]

|                     | PLACN2         | PLACN4        |
|---------------------|----------------|---------------|
| <i>WAXD</i>         |                |               |
| $d_{001}$ (nm)      | 3.03           | 2.98          |
| $d_{clay}$ (nm)     | 13             | 10            |
| <i>TEM</i>          |                |               |
| $d_{clay}$ (nm)     | $38 \pm 17.25$ | $30 \pm 12.5$ |
| $L_{clay}$ (nm)     | $448 \pm 200$  | $659 \pm 145$ |
| $L_{clay}/d_{clay}$ | 12             | 22            |
| $\xi_{clay}$        | $255 \pm 137$  | $206 \pm 92$  |

Reproduced from Sinha Ray, Maiti, Okamoto, Yamada and Ueda by permission of American Chemical Society, USA.

Table 10  
Specifications and designation of OMLS used for the preparation of PLACNs

| OMLS codes | Pristine clay    | Particles length (nm) | CEC (mequiv/100 gm) | Organic salt used for the modification of clay      | Suppliers              |
|------------|------------------|-----------------------|---------------------|---|------------------------|
| ODA        | MMT              | 150–200               | 110                 | Octadecylammonium cation                            | Nanocor Inc., USA      |
| SBE        | MMT              | 100–130               | 90                  | Octadecyltrimethylammonium cation                   | Hojun Yoko Co., Japan  |
| MEE        | Synthetic F-mica | 200–300               | 120                 | Dipolyoxyethylene alkyl(coco) methylammonium cation | CO-OP Chemicals, Japan |
| SAP        | Saponite         | 50–60                 | 86.6                | Tributylhexadecylphosphonium cation                 | CO-OP Chemicals, Japan |

crystallite sizes indicate that the number of stacked silicate layers is the same as that in the original OMLS, but some amount of PLA is intercalated between the galleries, giving rise to a larger crystallite size. The stacking of silicate layers in the organoclays and in various nanocomposites are presented schematically in Fig. 68. More recently, Dubois et al. [382, 384] reported the preparation of plasticized PLA/MMT nanocomposites. The OMLS was MMT modified with bis-(2-hydroxyethyl)methyl (hydrogenated tallow alkyl) ammonium cations. WAXD analyses confirmed the formation of intercalated nanocomposites. Similar to PLA, PBS is an aliphatic thermoplastic polyester with many interesting properties, including biodegradability; melt processability, and thermal and chemical resistance [424]. Although

these properties show potential applications of PBS, some of the other material properties such as softness, gas permeability, flexural properties, etc. are frequently not favorable for a wide range of applications. Sinha Ray et al. [389–393] first reported the preparation of PBS/MMT nanocomposites (PBSCNs) by simple melt extrusion of PBS and OMLS. The resulting nanocomposite exhibited properties suitable for many applications. A sample of MMT modified with octadecylammonium chloride was used as the OMLS for nanocomposite preparation. Fig. 69 represents the WAXD patterns of various PBSCNs. The TEM image of one representative PBSCN is shown in Fig. 70. From the WAXD patterns and TEM observation, it is clearly observed that the silicate layers of C18-MMT were intercalated and randomly

Table 11  
Characteristics of nanocomposites (designation, type of clay, organic modifier, and clay (inorganic part) content) [381]

| Nanocomposite codes | Type of clay | Organic modifier  | Clay content (wt%) |
|---------------------|--------------|---|--------------------|
| PLACN1              | Smectite     | <i>n</i> -Hexadecyl tri- <i>n</i> -butyl phosphonium bromide (C <sub>16</sub> ) | 1.2                |
| PLACN2              | Smectite     | C <sub>16</sub>   | 3                  |
| PLACN3              | Smectite     | C <sub>16</sub>   | 4                  |
| PLACN4              | Smectite     | C <sub>16</sub>   | 5                  |
| PLACN5              | MMT          | C <sub>16</sub>   | 3                  |
| PLACN6              | MMT          | C <sub>16</sub>   | 3.8                |
| PLACN7              | MMT          | C <sub>16</sub>   | 5                  |
| PLACN8              | Mica         | C <sub>16</sub>   | 2.8                |
| PLACN9              | Mica         | C <sub>16</sub>   | 3.8                |
| PLACN10             | Mica         | C <sub>16</sub>   | 5                  |
| PLACN11             | Smectite     | <i>n</i> -Octyl tri- <i>n</i> -butyl phosphonium bromide (C <sub>8</sub> )      | 3.2                |
| PLACN12             | Smectite     | <i>n</i> -Dodecyl tri- <i>n</i> -butyl phosphonium bromide (C <sub>12</sub> )   | 1.7                |
| PLACN13             | Smectite     | Methyl triphenyl phosphonium bromide (C <sub>Ph</sub> )                         | 3.5                |

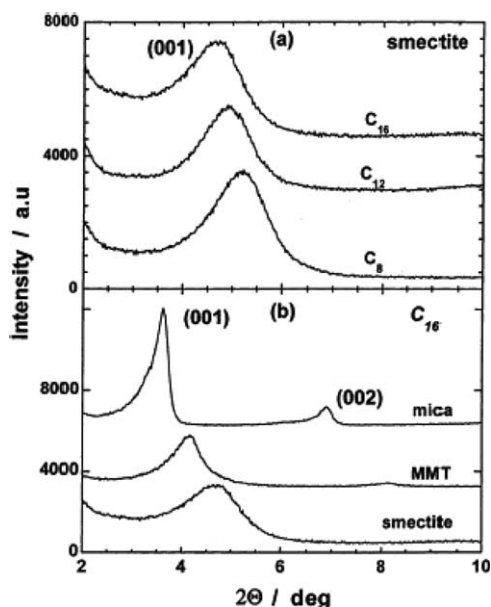


Fig. 63. WAXD patterns of organically modified clay: (a) smectite clay modified with  $C_8$ ,  $C_{12}$ , and  $C_{16}$  phosphonium salt; (b) smectite, MMT, and mica clay modified with  $C_{16}$  phosphonium salt [381]. Reproduced from Maiti, Yamada, Okamoto, Ueda and Okamoto by permission of American Chemical Society, USA.

distributed in the PBS-matrix. In another publication [391], the same authors reported details on structure–property relationships for PBSCNs.

Very recently, Lee et al. [398] reported the preparation of biodegradable aliphatic polyester (APES)/organoclay nanocomposites using a melt intercalation method. Two kinds of organoclays, Cloisite 30B and Cloisite 10A, with different ammonium cations located in the silicate galleries, were chosen for the nanocomposite preparation. The WAXD analyses and TEM observations showed higher degrees of intercalation for APES/Cloisite 30B nanocomposites as compared to that of APES/Cloisite 10A nanocomposites. It was hypothesized that this behavior may be due the stronger

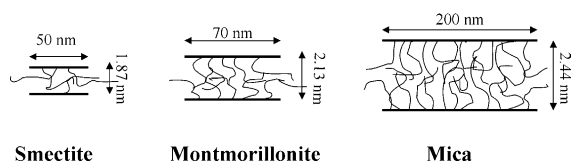


Fig. 64. Schematic representation of organoclays with  $C_{16}$  ion [381]. Reproduced from Maiti, Yamada, Okamoto, Ueda and Okamoto by permission of American Chemical Society, USA.

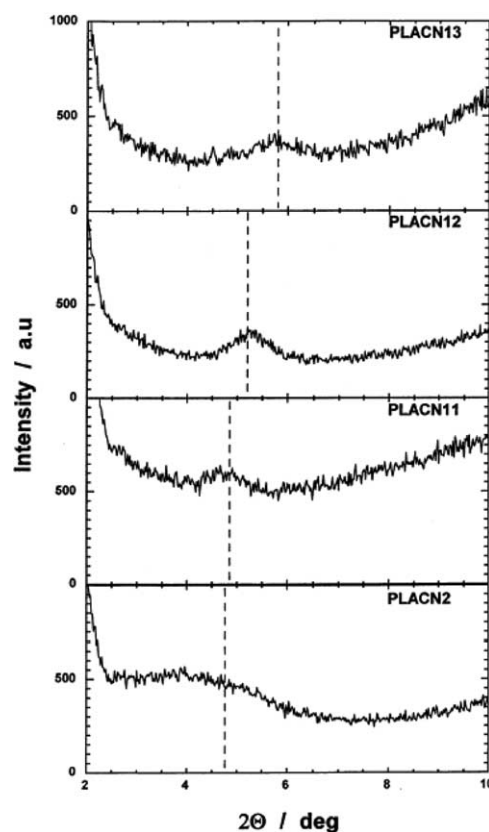


Fig. 65. WAXD patterns of smectite-organoclay nanocomposites having different organic components (chain length dependency on intercalation). The broken lines represent the peak position of the corresponding organoclay [381]. Reproduced from Maiti, Yamada, Okamoto, Ueda and Okamoto by permission of American Chemical Society, USA.

hydrogen-bonding interaction between the APES and the hydroxyl group in the galleries of Cloisite 30B nanocomposites, compared with that of the APES/Cloisite nanocomposites.

#### 4. Nanocomposite properties

Nanocomposites consisting of a polymer and layered silicate (modified or not) frequently exhibit remarkably improved mechanical and materials properties when compared to those of pristine polymers containing a small amount ( $\leq 5$  wt%) of layered silicate. Improvements include a higher modulus, increased strength and heat resistance,

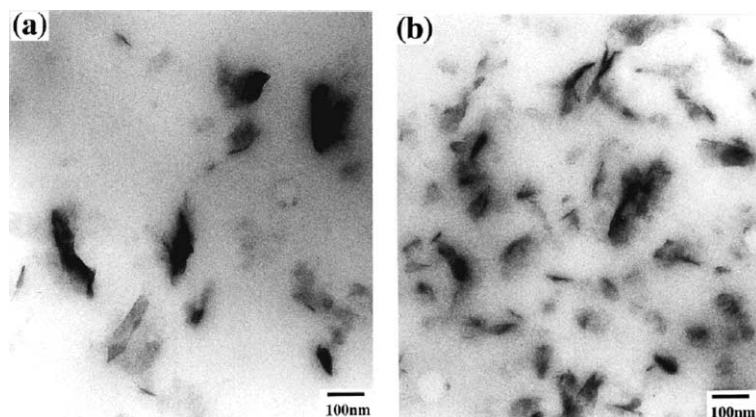


Fig. 66. Bright filed TEM images of (a) PLACN12 ( $C_8$ , 1.7 wt%) and (b) PLACN2 ( $C_{16}$ , 3 wt%) [381]. Reproduced from Maiti, Yamada, Okamoto, Ueda and Okamoto by permission of American Chemical Society, USA.

decreased gas permeability and flammability, and increased biodegradability of biodegradable polymers. The main reason for these improved properties in nanocomposites is the stronger interfacial interaction between the matrix and layered silicate, compared with conventional filler-reinforced systems.

#### 4.1. Mechanical properties

##### 4.1.1. Dynamic mechanical analysis

Dynamic mechanical analysis (DMA) measures the response of a given material to an oscillatory

deformation (here in tension–torsion mode) as a function of temperature. DMA results are composed of three parameters: (a) the storage modulus ( $G'$ ), (b) the loss modulus ( $G''$ ), and (c)  $\tan \delta$ , the ratio ( $G''/G'$ ), useful for determining the occurrence of molecular mobility transitions, such as the glass transition temperature ( $T_g$ ) [391].

DMA has been used to study temperature dependence of the storage modulus of PMMA upon nanocomposite formation under different experimental conditions [141]. Fig. 71 shows the temperature dependence of  $G'$  and  $\tan \delta$  for various

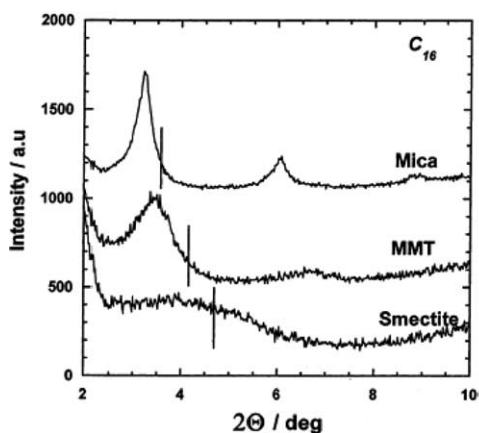


Fig. 67. WAXD patterns of smectite, MMT, and mica nanocomposites with  $C_{16}$  organoclay and same clay content [381]. Reproduced from Maiti, Yamada, Okamoto, Ueda and Okamoto by permission of American Chemical Society, USA.

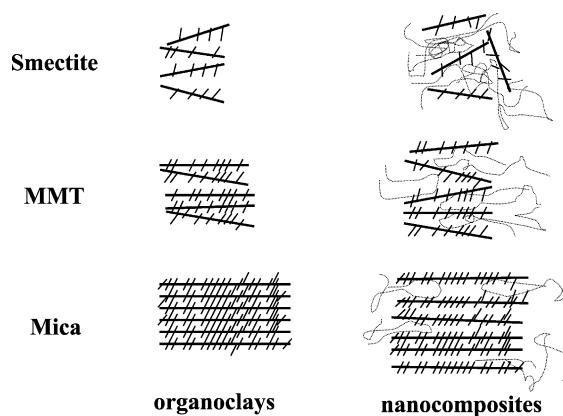


Fig. 68. Schematic presentation of silicate layers in OMLs and in various nanocomposites [381]. Reproduced from Maiti, Yamada, Okamoto, Ueda and Okamoto by permission of American Chemical Society, USA.

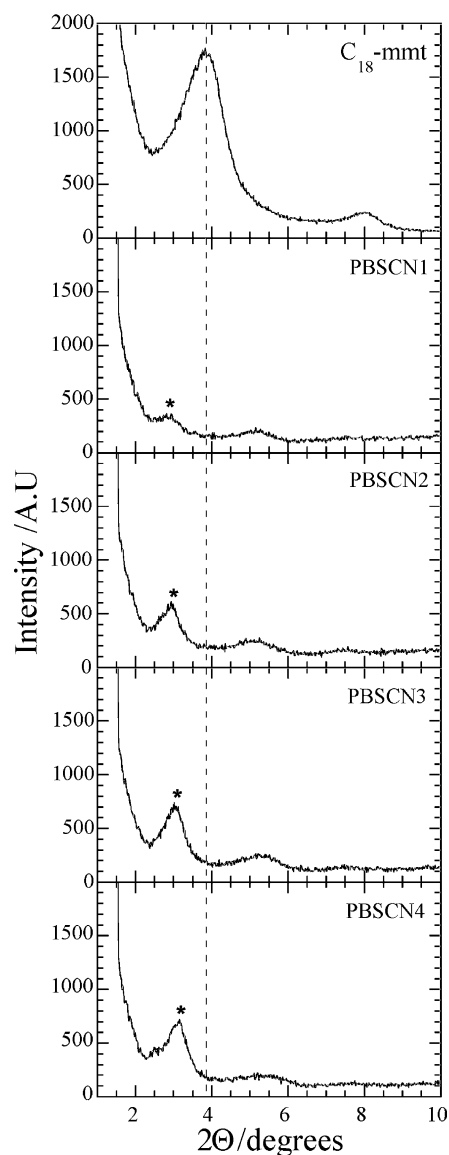


Fig. 69. WAXD patterns of C18-MMT, various PBSCNs and neat PBS. The dashed line indicates the location of the silicate (001) reflection of C18-MMT dispersed in PBS matrix [391]. Reproduced from Sinha Ray, Okamoto and Okamoto by permission of American Chemical Society, USA.

copolymer-based nanocomposites, and the corresponding clay-free copolymer/QA<sup>+</sup> blends. The measurements were carried out using a RDAII instrument with an oscillation frequency of 6.28 rad/s, an amplitude of 0.05%, and a heating rate of 2 °C/min.

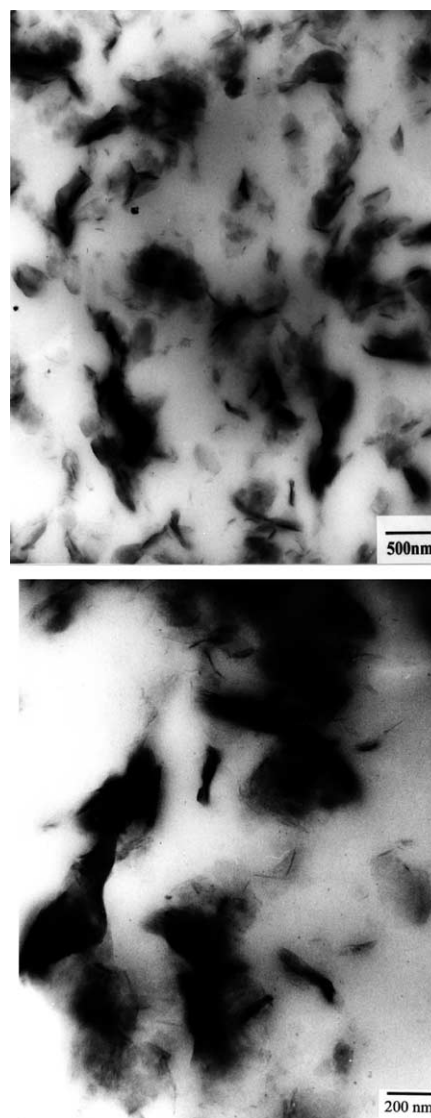


Fig. 70. Bright field TEM images of PBSCN with 2.8 wt% MMT.

For PMMA/SPN10 and PMMA/QA<sup>+</sup> blends, there is no difference in the temperature dependence of  $G'$  or  $\tan \delta$  (see Fig. 71a). Upon incorporation of AEA, PAA, and AA to PMMA, a strong increment in  $G'$  develops at all temperatures as the copolymer matrix appears. This behavior indicates that the addition of copolymer has a strong effect on the elastic properties of the corresponding matrices. On the other hand, the  $\tan \delta$  peaks for the nanocomposites are shifted towards lower temperatures than

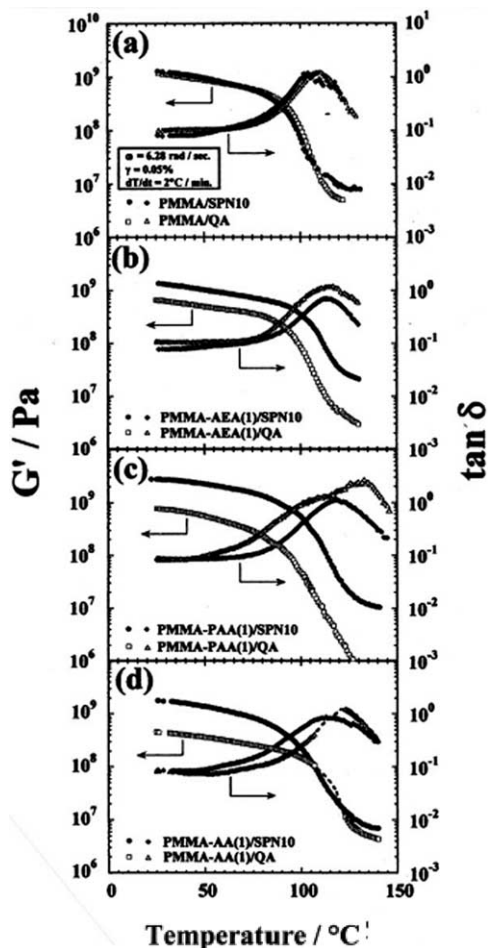


Fig. 71. Temperature dependence of  $G'$  and  $\tan \delta$  for the nanocomposites and corresponding copolymer/QA<sup>+</sup> blends without clay [68]. Reproduced from Okamoto, Morita, Kim, Kotaka and Tateyama by permission of Elsevier Science Ltd, UK.

for the corresponding clay-free blends. Compared with other systems, the behavior of PMMA-AA(1)/SPN10 is somewhat different; above  $T_g$ ,  $G'$  is almost the same for the nanocomposite and corresponding clay-free matrix, although a broadening and a low-temperature shift of  $\tan \delta$  is observed. This behavior may be due to the intercalation of the copolymer chains into the galleries of the clay layers, which leads to the suppression of the mobility of the copolymer segments near the interface. This assumption was supported by the WAXD patterns of these nanocomposites (see Fig. 21d), which exhibit weak

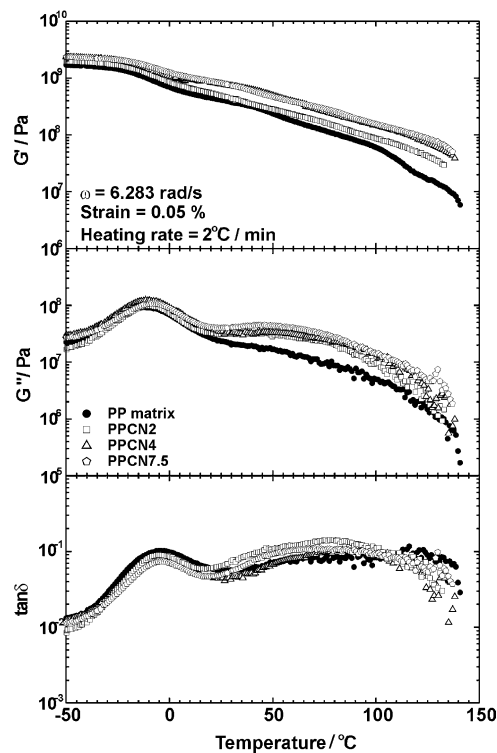


Fig. 72. Temperature dependence of  $G'$ ,  $G''$  and  $\tan \delta$  for for PP-MA matrix and various PPCNs [303]. Reproduced from Nam, Maiti, Okamoto, Kotaka, Hasegawa and Usuki by permission of Elsevier Science Ltd, UK.

but significant peaks from the expanded (002) and (003) planes.

Fig. 72 shows the temperature dependence of  $G'$ ,  $G''$ , and  $\tan \delta$  for the various PPCNs and corresponding PP-MA matrix. For all PPCNs, there is a strong enhancement of the moduli over the investigated temperature range, which indicates the plastic and elastic responses of PP towards deformation are strongly influenced in the presence of OMLS. Below  $T_g$ , the enhancement of  $G'$  is clear in the intercalated PPCNs.

In contrast, the  $\tan \delta$  curves for PPCNs show two peaks: one at  $-5^\circ\text{C}$  and another broad peak between  $50$  and  $90^\circ\text{C}$ . McCrum and colleagues [425] have demonstrated that the  $\tan \delta$  curve of PP exhibits three relaxations localized in the vicinity of  $-80^\circ\text{C}$  ( $\gamma$ ),  $10^\circ\text{C}$  ( $T_g$ ) and  $100^\circ\text{C}$  ( $\alpha$ ). The dominant relaxation at ca.  $10^\circ\text{C}$  is the glass-rubber relaxation of the amorphous portion of PP.

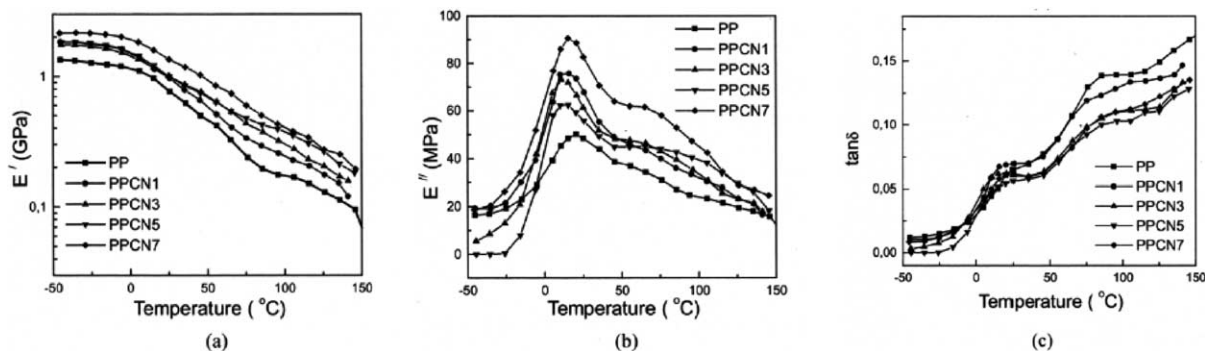


Fig. 73. Dynamic mechanical spectra: (a) storage modulus,  $E'$ , (b) loss modulus,  $E''$ , and (c) loss factor  $\tan \delta$  as a function of temperature for neat PP and PPCN [304]. Reproduced from Liu and Wu by permission of Elsevier Science Ltd, UK.

The dynamic mechanical properties of neat PP and PPCNs prepared with EM-MMT are shown in Fig. 73 [304]. These results clearly show that the incorporation of EM-MMT into the PP matrix results in a remarkable increase in stiffness and a decrease in  $\tan \delta$ . The  $G'$  curves show an enhanced rubbery plateau, indicating that the addition of EM-MMT induces a reinforcement effect; at very high temperatures this reinforcement effect strengthens. This behavior further indicates enhancement of the thermal–mechanical stability of these materials at high temperature.

Similar to previous systems, these PPCNs show two peaks in  $\tan \delta$  (see Fig. 73c). The dominant relaxation process at ca. 10 °C is the glass–rubber relaxation of the amorphous portion of PP. The weak peak appearing as a shoulder at about 100 °C is associated with the crystalline regions ( $\alpha$ -phase) of PP. Another interesting phenomenon is that the  $T_g$  values of PPCNs do not further decrease above an EM-MMT content of 3 wt%. However, the mechanism for this behavior is not yet understood [304].

The remarkable improvement in  $G'$ , related to the strong interaction between the matrix and OMLS, is clearly observed in N6/OMLS nanocomposites [426]. Fig. 74 represents the temperature dependence of  $G'$ ,  $G''$ , and  $\tan \delta$  of the N6 matrix and various nanocomposites (N6CNs). The details of the dynamic temperature ramp test for neat N6 and various N6CNs are summarized in Table 12. All N6CNs show a strong increase in modulus at all temperatures.

Increases in  $G'$  related to the dimension of the dispersed clay particles is further demonstrated in

PLACNs [374]. In order to understand the effect of compatibilizers on morphology and mechanical properties, the authors also prepared PLACNs with very small amount of oligo( $\epsilon$ -caprolactone) ( $o$ -PCL). The composition details and designations for various types of nanocomposites are presented in Table 8.

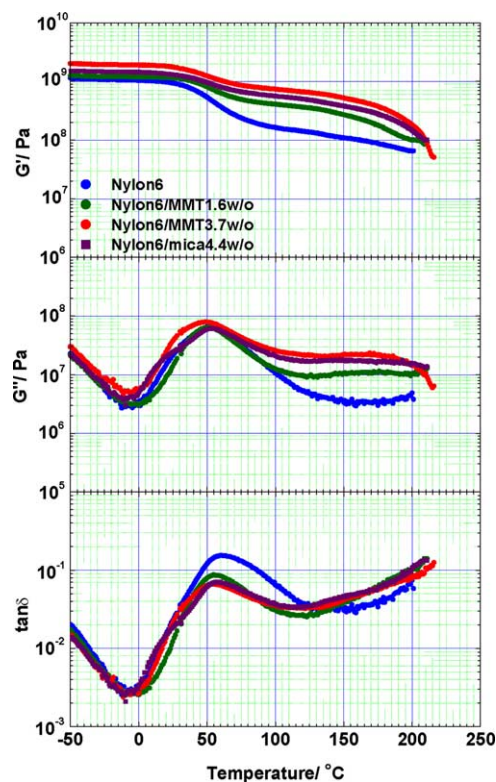


Fig. 74. Temperature dependence of  $G'$ ,  $G''$  and  $\tan \delta$  for N6 matrix and various N6CNs.

Table 12  
Summary of DMA test for N6 and various N6CNs under different temperature range

| Sample  | Term                            | 0 °C | 25 °C | 50 °C | 100 °C | 150 °C | 200 °C |
|---------|---------------------------------|------|-------|-------|--------|--------|--------|
| N6      | $\alpha \times 10^5$ (cm/cm °C) | 9.5  | 12    | 14    | 22     | 31     | 48     |
|         | $G'$ (GPa)                      | 1.04 | 0.94  | 0.52  | 0.16   | 0.11   | 0.065  |
| N6CN1.6 | $\alpha \times 10^5$ (cm/cm °C) | 8.9  | 9.7   | 11    | 16     | 22     | 60     |
|         | $G'$ (GPa)                      | 1.2  | 1.1   | 0.8   | 0.41   | 0.27   | 0.01   |
| N6CN3.7 | $\alpha \times 10^5$ (cm/cm °C) | 6.4  | 6.6   | 8.7   | 8.5    | 14     | 67     |
|         | $G'$ (GPa)                      | 1.9  | 1.8   | 1.2   | 0.74   | 0.52   | 0.18   |
| N6CN4.4 | $\alpha \times 10^5$ (cm/cm °C) | 7.1  | 7.7   | 9.8   | 11     | 15     | 42     |
|         | $G'$ (GPa)                      | 1.4  | 1.3   | 0.95  | 0.56   | 0.38   | 0.14   |

Parts a and b of Fig. 75 show the temperature dependence of  $G'$ ,  $G''$  and  $\tan \delta$  of the PLA matrices and the various PLACNs, respectively. For all PLACNs, the enhancement of  $G'$  can be seen over the investigated temperature range when compared to

the matrix, indicating that C18-MMT has a strong effect on the elastic properties of neat PLA. Below  $T_g$ , the enhancement of  $G'$  is clear for various intercalated PLACNs. On the other hand, all PLACNs show a greater increase in  $G'$  at high temperature compared to

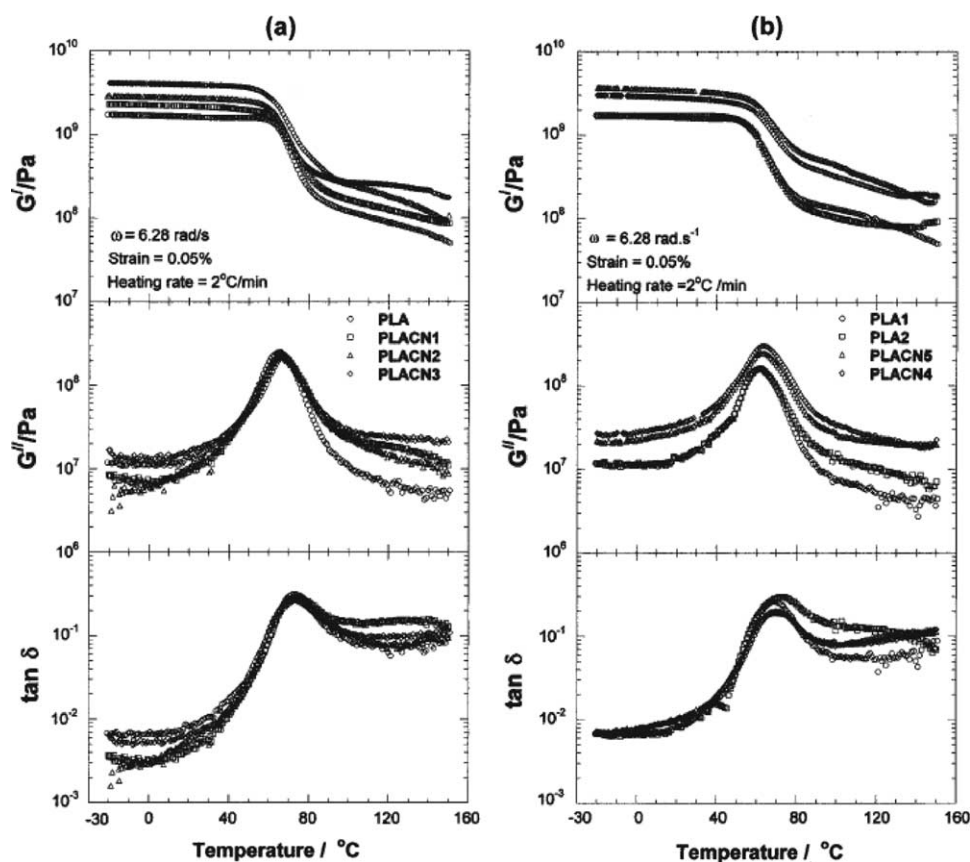


Fig. 75. Temperature dependence of  $G'$ ,  $G''$  and their ratio  $\tan \delta$  for PLACNs and the corresponding matrices: (a) without *o*-PCL and (b) with *o*-PCL [374]. Reproduced from Sinha Ray, Maiti, Okamoto, Yamada and Ueda by permission of American Chemical Society, USA.



that of the PLA matrices. This is due to both mechanical reinforcement by the clay particles and extended intercalation at high temperature [311]. Above  $T_g$ , when materials become soft, the reinforcement effect of the clay particles becomes prominent due to the restricted movement of the polymer chains. This is accompanied by the observed enhancement of  $G'$ .

At the other extreme, PLACN4 and PLACN5 samples exhibited strong enhancement of  $G'$  compared to that of the PLACN2 sample with comparable clay loading, and to PLA/*o*-PCL matrices containing up to 0.5 wt% *o*-PCL (see Table 9, Fig. 75b). The presence of small amounts of *o*-PCL did not lead to a large shift or broadening of the  $\tan \delta$  curves. However, a large increase in  $G'$  above  $T_g$  became clear, indicating that the large anisotropy of dispersed flocculated particles enhanced the loss component.

The  $G'$  values over different temperature ranges of various PLACNs and corresponding matrices without clay are summarized in Table 13. PLACNs with a very small amount of *o*-PCL (PLACN4 and PLACN5) exhibited a very large enhancement of the mechanical properties compared to that of PLACN with comparable clay loading (PLACN2). The essential factor governing the enhancement of mechanical properties in the nanocomposites is the aspect ratio of the dispersed clay particles [427]. From the TEM figures (see Fig. 62), it is clearly

seen that, in the presence of a very small amount of *o*-PCL, flocculation of the dispersed clay particles took place, again due to the strong edge–edge interaction of the clay particles. The 2D aspect ratios of the dispersed clay particles  $L_{\text{clay}}/d_{\text{clay}}$  estimated from TEM observation are 22 for PLACN4 and 12 for PLACN2 (see Table 9). This large aspect ratio leads to the observed enhancement of mechanical properties.

The hypothesis that an increase in  $G'$  depends directly on the aspect ratio of dispersed clay particles is also clearly observed in PBSCNs. The temperature dependence of  $G'$  for PBS and various PBSCNs are presented in Fig. 76a. The nature of the enhancement of  $G'$  in PBSCNs with temperature is somewhat different from the well-established theories, which explains the similar behavior observed in systems that are either intercalated (PP-MA/MMT) [303] or exfoliated (N6/MMT) [132]. In the later system,  $G'$  typically increases by as much as 40–50%, when compared to that of the matrix well below  $T_g$ , while above  $T_g$  there is a strong enhancement ( $>200\%$ ) in  $G'$ . This behavior is common for the above reported nanocomposites, and the reason has been shown to be the strong reinforcement effect of the clay particles above  $T_g$  (when materials become soft). However, in the case of PBSCNs, the order of enhancement in  $G'$  is almost the same below and above  $T_g$ , and this behavior may be due to the extremely low  $T_g$  ( $-29^\circ\text{C}$ ) of the PBS matrix.

Over the temperature range of  $-50$  to  $-10^\circ\text{C}$ , the increases in  $G'$  are 18% for PBSCN1, 31% for PBSCN2, 67% for PBSCN3 and 167% for PBSCN4 compared to that of neat PBS. Furthermore, at room temperature PBSCN3 and PBSCN4 show a higher increase in  $G'$ , 82 and 248%, respectively, compared to that of neat PBS, while those of PBSCN1 and PBSCN2 are 18.5 and 44% higher. At  $90^\circ\text{C}$ , only PBSCN4 exhibits a very strong enhancement of  $G'$  compared to that of the other three PBSCNs.

In contrast, PBSCNs prepared with qC<sub>16</sub>-sap exhibit a relatively weak enhancement of  $G'$  compared to that of PBSCNs prepared with C18-MMT [391] (see Fig. 76b). For PBSCN6, the increases in  $G'$  are 102.5% at  $-50^\circ\text{C}$ , 128.6% at  $25^\circ\text{C}$  and 100% at  $90^\circ\text{C}$ , compared to PBS. These values are much smaller compared to those of PBSCN4, although both species contain comparable clay content (inorganic

Table 13

$G'$  value of various PLACNs and corresponding matrices without clay at different temperature range [374]

| Samples | Storage modulus, $G'$ (GPa) |                    |                     |                     |
|---------|-----------------------------|--------------------|---------------------|---------------------|
|         | $-20^\circ\text{C}$         | $40^\circ\text{C}$ | $100^\circ\text{C}$ | $145^\circ\text{C}$ |
| PLACN1  | 2.32                        | 2.07               | 0.16                | 0.09                |
| PLACN2  | 2.90                        | 2.65               | 0.25                | 0.10                |
| PLACN3  | 4.14                        | 3.82               | 0.27                | 0.19                |
| PLACN4  | 3.71                        | 3.21               | 0.43                | 0.16                |
| PLACN5  | 3.04                        | 2.60               | 0.32                | 0.16                |
| PLACN6  | 2.08                        | 1.97               | 0.23                | 0.08                |
| PLACN7  | 1.86                        | 1.76               | 0.16                | 0.07                |
| PLA     | 1.74                        | 1.60               | 0.13                | 0.06                |
| PLA1    | 1.73                        | 1.60               | 0.13                | 0.06                |
| PLA2    | 1.68                        | 1.55               | 0.12                | 0.06                |
| PLA3    | 1.67                        | 1.62               | 0.12                | 0.06                |

Reproduced from Sinha Ray, Maiti, Okamoto, Yamada and Ueda by permission of American Chemical Society, USA.

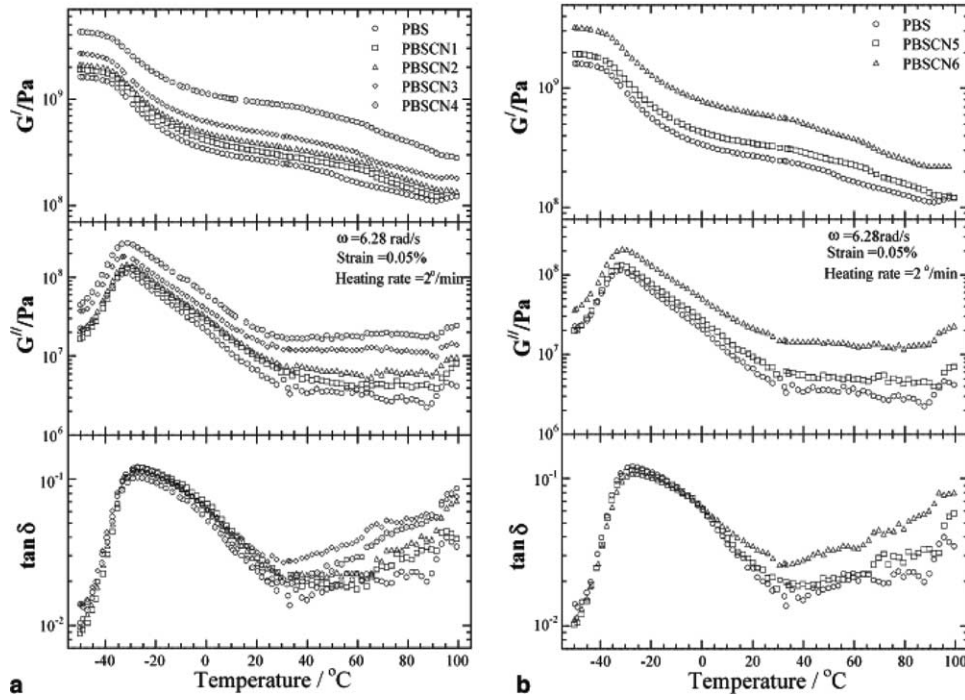


Fig. 76. Temperature dependence of  $G'$ ,  $G''$  and their ratio  $\tan \delta$  for (a) PBSCNs (prepared with C18-MMT) and neat PBS, (b) PBSCNs [391]. Reproduced from Sinha Ray, Okamoto and Okamoto by permission of American Chemical Society, USA.

part). Two factors may be suggested for the very large enhancement of the modulus in the case of PBSCN4, compared to that of PBSCN6; one factor is the very high aspect ratio of dispersed clay particles and another factor is the well-ordered intercalated structure in PBSCN4.

The clay content dependence of  $G'$  for various types of nanocomposites obtained well below  $T_g$ , are summarized in Fig. 77, showing the Einstein coefficient,  $k_E$ , which is derived by using Halpin and Tai's theoretical expression modified by Nielsen and represents the aspect ratio ( $L/D$ ) of dispersed clay particles without intercalation. Halpin-Tai's-Nielsen expression of the modulus of nanocomposites,  $G'_{\text{nanocomposite}}$  is given by [428].

$$\frac{G'_{\text{nanocomposite}}}{G'_{\text{matrix}}} = \frac{1 + XY\phi_{\text{clay}}}{1 - X\psi\phi_{\text{clay}}} \quad (1)$$

where

$$X = k_E - 1 \quad (2)$$

$$Y = \frac{(G'_{\text{clay}}/G'_{\text{matrix}}) - 1}{(G'_{\text{clay}}/G'_{\text{matrix}}) + X} \quad (3)$$

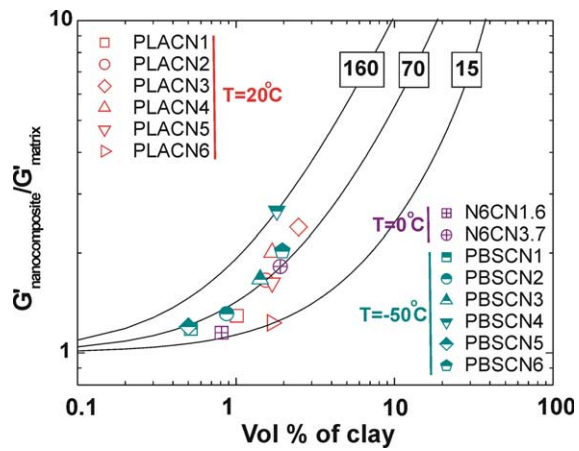


Fig. 77. Plots of  $G'_{\text{nanocomposite}}/G'_{\text{matrix}}$  vs. vol% of clay for various nanocomposites. The Einstein coefficient  $k_E$  is shown with the number in the box. The lines show the calculated results from Halpin and Tai's theory with various  $k_E$ .

$$\psi = 1 + \left[ \frac{1 - \phi_m}{\phi_m^2} \right] \phi_{\text{clay}} \quad (4)$$

Here,  $G'_{\text{matrix}}$  and  $G'_{\text{clay}}$  are the storage moduli of the matrix (here PLA, PBS, PP-MA and N6) and clay, respectively.  $X$  is a constant that depends on the type of nanocomposite structure, and is related to the aspect ratio, and  $\phi_{\text{clay}}$  and  $\phi_m$  are the volume fractions of clay reinforcement and the maximum packing volume fraction of clay (generally equal to 0.63), respectively. The assumption that the value of  $G'_{\text{clay}}$  is equal to 170 GPa [429], permits estimation of the composition dependence of  $G'_{\text{nanocomposite}}/G'_{\text{matrix}}$  using the equations above. Furthermore, the values of  $k_E$  were estimated by selecting an appropriate value from the best fit to the experimentally obtained  $G'_{\text{nanocomposite}}/G'_{\text{matrix}}$  vs.  $\phi_{\text{clay}}$  plots (see Fig. 77).

From Fig. 77, it is clearly observed that PBSCNs show a strong increase in  $G'$  compared to other nanocomposites having the same clay content in the matrix. PPCNs are well known as intercalated systems, N6CNs are well-established exfoliated nanocomposites, PLACNs are considered intercalated-and-flocculated nanocomposites, while PBSCNs are intercalated-and-extended flocculated nanocomposites [391,392]. Due to the strong interaction between hydroxylated edge–edge groups, the clay particles are sometimes flocculated in the polymer matrix. As a result of this flocculation, the length of the clay particles increases enormously, resulting in a corresponding increase in overall aspect ratio. For the preparation of high molecular weight PBS, diisocyanate end-groups are generally used as a chain extender [424]. These isocyanate end groups make urethane bonds with hydroxy-terminated LMW PBS. Each high molecular weight PBS chain contains two such bonds (see schematic illustration in Fig. 78). These urethane type bonds lead to the strong

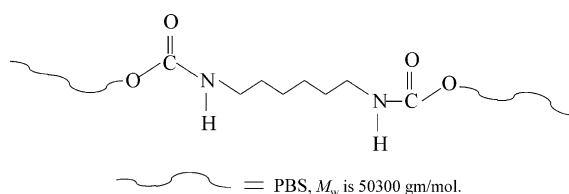


Fig. 78. Formation of urethane bonds in high molecular weight PBS [391]. Reproduced from Sinha Ray, Okamoto and Okamoto by permission of American Chemical Society, USA.

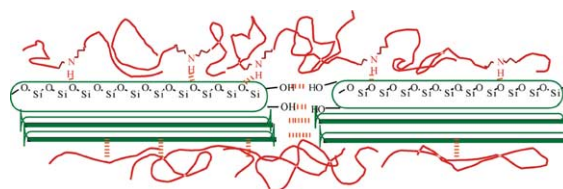


Fig. 79. Formation of hydrogen bonds between PBS and clay, which leads to the flocculation of the dispersed silicate layers [391]. Reproduced from Sinha Ray, Okamoto and Okamoto by permission of American Chemical Society, USA.

interaction with the silicate surface by forming hydrogen bonds, and hence strong flocculation (see Fig. 79). For this reason, the aspect ratio of dispersed clay particles is much higher in the case of PBSCNs compared to other nanocomposites, and hence the high enhancement of modulus.

#### 4.1.2. Tensile properties

The tensile modulus of a polymeric material has been shown to be remarkably improved when nanocomposites are formed with layered silicates. N6 nanocomposites prepared through the in situ intercalative ring opening polymerization of  $\epsilon$ -caprolactam, leading to the formation of exfoliated nanocomposites, exhibit a drastic increase in the tensile properties at rather low filler content. The main reason for the drastic improvement in tensile modulus in N6 nanocomposites is the strong interaction between matrix and silicate layers via formation of hydrogen bonds, as shown in Fig. 80.

In the case of nanocomposites, the extent of the improvement of the modulus depends directly upon

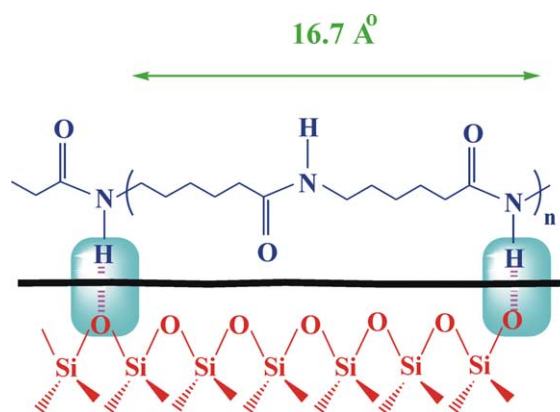


Fig. 80. Schematic illustration of formation of hydrogen bonds in N6/MMT nanocomposite.

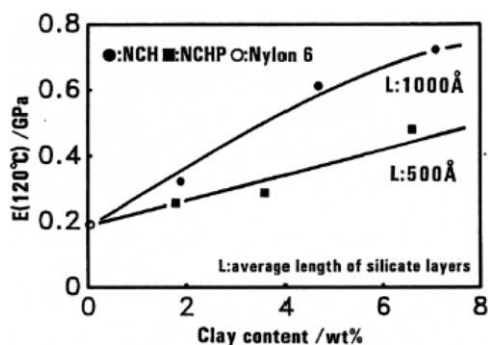


Fig. 81. Effect of clay content on tensile modulus in case of N6/OMLS nanocomposites prepared via melt extrusion [133]. Reproduced from Kojima, Usuki, Kawasumi, Okada, Kurauchi and Kamigaito by permission of Materials Research Society, USA.

the average length of the dispersed clay particles, and hence the aspect ratio. Fig. 81 represents the dependence of the tensile modulus  $E$  measured at 120 °C for exfoliated N6 nanocomposites with various clay content, obtained by the in situ intercalative polymerization of  $\epsilon$ -caprolactam in the presence of protonated aminododecanoic acid-modified MMT and saponite. Moreover, the difference in the extent of exfoliation, as observed for N6-based nanocomposites synthesized by the in situ intercalative polymerization of  $\epsilon$ -caprolactam using  $\text{Na}^+$ -MMT and various acids, strongly influenced the final modulus of the nanocomposites.

Table 14 summarizes the tensile modulus of 1potNCH together with neat N6 and NCH prepared via in situ intercalative ring-opening polymerization of  $\epsilon$ -caprolactam [135]. The excellent modulus in the case of 1potNCH is attributed to the uniformly dispersed silicate layers. Furthermore, 1potNCH has

improved mechanical properties when compared with NCH. The polymer matrix in the nanocomposites prepared by a one pot synthesis is the homopolymer of N6, whereas in the case of NCH prepared via intercalative ring-opening polymerization, the matrix is a copolymer of N6 and a small amount of N12. The presence of N12 may give rise to the lower modulus.

One can observe variations of the modulus of the nanocomposites based on the various kinds of acids used to catalyze the polymerization [135]. The WAXD peak intensity ( $I_m$ , inversely related to the exfoliation of clay particles) also depends on the nature of the acid used to catalyze the polymerization process. For an increase in the  $I_m$  values, a parallel decrease in the modulus is observed, indicating that exfoliated layers are the main factor responsible for the stiffness improvement. Intercalated particles, having a less important aspect ratio, play a minor role. These observations are further confirmed in Fig. 82, which presents the evolution of the tensile modulus at room temperature of N6 nanocomposites obtained by melt extrusion as a function of the filler content [142].

The effect of MMT content and N6 molecular weight on the tensile modulus of nanocomposites prepared using MMT modified with  $(\text{HE})_2\text{M}_1\text{R}_1$  is shown in Fig. 83. The addition of organoclay leads to a substantial improvement in stiffness for the composites based on each of the three N6, i.e. LMW, MMW and HMW. Interestingly, the stiffness increases with increasing matrix molecular weight at any given concentration even though the moduli of the neat N6 are all quite similar. Table 15 summarizes the moduli and other mechanical properties of the virgin

Table 14  
Mechanical properties of 1potNCH synthesized in presence of phosphoric acid [135]

| Mechanical properties  | Method used | N6   | NCH <sup>a</sup> (MMT = 4.7 wt%) | 1potNCH (MMT = 4.1 wt%) |
|------------------------|-------------|------|----------------------------------|-------------------------|
| Tensile modulus (GPa)  |             |      |                                  |                         |
| 23 °C                  | ASTM-D 638M | 1.11 | 1.87                             | 2.25                    |
| 120 °C                 | JIS-K 7113  | 0.19 | 0.61                             | 0.67                    |
| Tensile strength (MPa) |             |      |                                  |                         |
| 23 °C                  | ASTM-D 638M | 68.6 | 97.2                             | 102                     |
| 120 °C                 | JIS-K 7113  | 26.6 | 32.3                             | 34.7                    |
| HDT (°C) at 1.82 MPa   | ASTM-D 648  | 65   | 152                              | 160                     |

Reproduced from Kojima, Usuki, Kawasumi, Okada, Kurauchi and Kamigaito by permission of John Wiley and Sons, Inc.

<sup>a</sup> Prepared by in situ intercalative method.

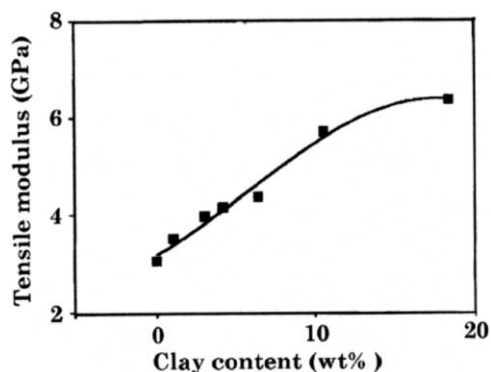


Fig. 82. Dependence of tensile modulus ( $E$ ) on clay content measured at 120 °C [141]. Reproduced from Alexander and Doubis by permission of Elsevier Science Ltd, UK.

materials and selected  $(HE)_2M_1R_1$  organoclay/N6 nanocomposites. The slightly larger modulus of 2.82 GPa for LMW may be the result of a higher degree of crystallinity, creating faster crystallization kinetics during the cooling of the specimen during injection molding.

Similar trends with respect to the level of organoclay content and molecular weight are evident in the yield strength results. The dependence of yield strength on MMT content and molecular weight is shown in Fig. 84. Yield strength increases with the content of MMT, however, there are notable differences in the level of strength improvement for pure polyamides. The HMW- and MMW-based nanocomposites show a steady increase in strength with content

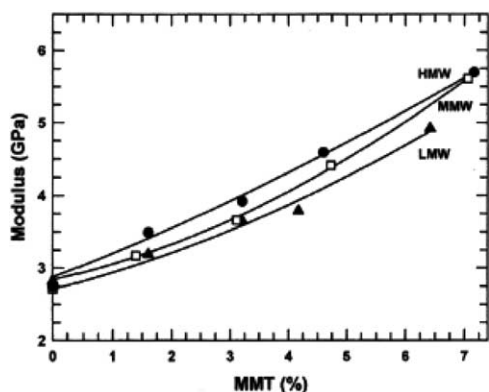


Fig. 83. Effect of MMT content on tensile modulus for LMW, MMW, and HMW based nanocomposites [149]. Reproduced from Fomes, Yoon, Keskkula and Paul by permission of Elsevier Science Ltd, UK.

of clay, while the LMW-based nanocomposites show a less pronounced effect. The differences in strength improvement with respect to molecular weight are very prominent at the highest clay content. The increase in strength relative to the virgin matrix for the HMW composite is nearly double to that of the LMW composite.

The relationship between MMT content and elongation at break for the different matrices is shown in Fig. 85 for two different rates of extension. Fig. 85a shows that the virgin polyamides are very ductile at a test rate of 0.51 cm/min. With increasing clay content the ductility gradually decreases, however, the HMW and MMW based composites attain reasonable levels of ductility at MMT concentrations as high as 3.5 wt%. The elongation at break for the LMW-based nanocomposites decreases rapidly at low MMT content (around 1 wt%). The larger reduction in the LMW-based systems may be due to the presence of stacked silicate layers, as seen in TEM photographs (see Fig. 46). In contrast, the higher testing rate of 5.1 cm/min yields similar trends, as shown in Fig. 85b, but the absolute level of the elongation at break is significantly lower. Interestingly, the strain at break for LMW composites is relatively independent of the rate of extension, similar to what has been observed in glass fiber reinforced composites. Even at the highest clay content, the HMW composite exhibits ductile fracture, whereas the LMW- and MMW-based nanocomposites fracture in a brittle manner at the highest clay content.

In the case of PPCNs, most studies report the tensile properties as a function of clay content. The results of an Instron study of a neat-PP/f-MMT composite compared to a PP/2C18-MMT ‘conventional’ composite are shown in Fig. 86. In PP/layered silicate nanocomposites, there is a sharp increase in tensile modulus for very small clay loading ( $\leq 3$  wt%), followed by a much slower increase beyond a clay loading of 4 wt%. This is behavior characteristic of PLS nanocomposites. With an increase in clay content, strength does not change markedly compared to the neat-PP value, and there is only a small decrease in the maximum strain at break. Conventional composites of PP with the same fillers do not exhibit as much of an improvement in their tensile modulus. On the other hand, as the PP/layered silicate interaction is improved, for example when

Table 15  
Mechanical properties of some N6/(HE)<sub>2</sub>M<sub>1</sub>R<sub>1</sub> nanocomposites [149]

| N6/(HE) <sub>2</sub> M <sub>1</sub> R <sub>1</sub> nanocomposites | Modulus (GPa) | Yield strength (MPa) | Strain <sup>a</sup> (%) | Elongation at break (%) crosshead speed |            | Izod impact strength (J/m) |
|---|---------------|----------------------|-------------------------|---|------------|----------------------------|
|   |               |                      |                         | 0.51 cm/min                             | 5.1 cm/min |                            |
| <i>LMW</i>  |               |                      |                         |   |            |                            |
| 0.0 wt% MMT   | 2.82          | 69.2                 | 4.0                     | 232                                     | 28         | 36.0                       |
| 3.2 wt% MMT   | 3.65          | 78.9                 | 3.5                     | 12                                      | 11         | 32.3                       |
| 6.4 wt% MMT   | 4.92          | 83.6                 | 2.2                     | 2.4                                     | 4.8        | 32.0                       |
| <i>MMW</i>  |               |                      |                         |   |            |                            |
| 0.0 wt% MMT   | 2.71          | 70.2                 | 4.0                     | 269                                     | 101        | 39.3                       |
| 3.1 wt% MMT   | 3.66          | 86.6                 | 3.5                     | 81                                      | 18         | 38.3                       |
| 7.1 wt% MMT   | 5.61          | 95.2                 | 2.4                     | 2.5                                     | 5          | 39.3                       |
| <i>HMW</i>  |               |                      |                         |   |            |                            |
| 0.0 wt% MMT   | 2.75          | 69.7                 | 4.0                     | 3.4                                     | 129        | 43.9                       |
| 3.2 wt% MMT   | 3.92          | 84.9                 | 3.3                     | 119                                     | 27         | 44.7                       |
| 7.2 wt% MMT   | 5.70          | 97.6                 | 2.6                     | 4.1                                     | 6.1        | 46.2                       |

Reproduced from Fornes, Yoon, Keskkula and Paul by permission of Elsevier Science Ltd, UK.

<sup>a</sup> Strain at yield point measured during modulus and yield strength testing using a crosshead speed of 0.51 cm/min.

MA functional groups are incorporated into the polymer, the stress is much more efficiently transferred from the polymer matrix to the inorganic filler, resulting in a higher increase in tensile properties. Parts a and b of Fig. 87 represent the dependence of the tensile modulus and strength on MMT content of various PPCNs prepared by melt extrusion of PP-MA and C18-MMT, respectively. The modulus of the PPCNs systematically increases with increasing clay content, as does the tensile strength up to 4 wt%, where it levels off.

If the interaction between nanocomposite components is not thermodynamically favorable, these properties will change during processing because the nanocomposite structure will change. Recent work by Reichert et al. [430] systematically found the dependencies on compatibilizer functionality and organic modification, and revealed that considerable tensile property enhancement could be achieved only when appropriate PP-MA compatibilizers were used to pretreat the OMLS in conjugation with specific organic modifications of the MMT. Similar materials under different processing conditions showed much smaller improvements in the practical material properties [430].

The tensile properties of various PPCNs prepared with EM-MMT, a new type of co-intercalated MMT,

are summarized in Fig. 88 [304]. The PPCN containing 1 wt% EM-MMT is abbreviated as PPCN1, while the PPCNs with 3, 5 and 7 wt% of EM-MMT are abbreviated as PPCN3, PPCN5, and PPCN7, respectively. The tensile strength of the PPCNs increase rapidly with increasing EM-MMT content from 0 to 5 wt%, but the trend is less pronounced when the clay content increases beyond 5 wt%. A similar trend is observed for the tensile modulus. In contrast, the notched Izod impact strength of the PPCNs is

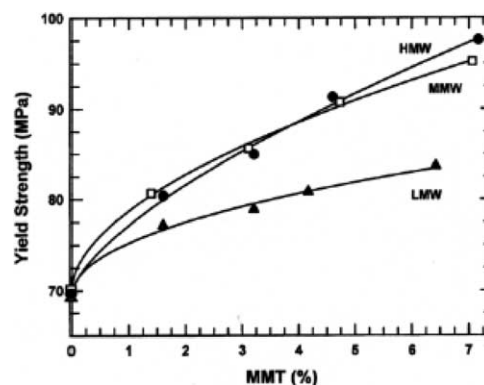


Fig. 84. Effect of MMT content on yield strength for LMW, MMW, and HMW based nanocomposites [149]. Reproduced from Fornes, Yoon, Keskkula and Paul by permission of Elsevier Science Ltd, UK.

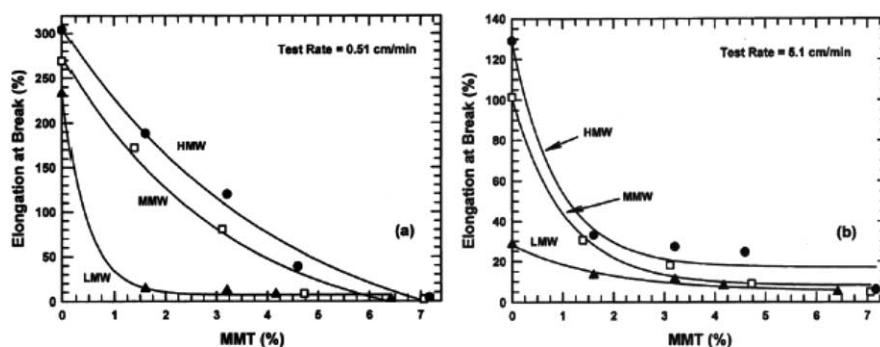


Fig. 85. Effect of MMT content on elongation at break for LMW, MMW, and HMW based nanocomposites at a crosshead speed of (a) 0.51 cm/min and (b) 5.1 cm/min [149]. Reproduced from Fornes, Yoon, Keskkula and Paul by permission of Elsevier Science Ltd, UK.

constant, within experimental error, in the EM-MMT content range between 0 and 7 wt%.

The evolution of the tensile modulus for the epoxy matrix with three different types of layered silicates is presented in Fig. 89 [228]. A C18-MMT, a C18A-magadiite, and a magadiite modified with methyl-octadecylammonium cation (C18A1M-magadiite) were used for nanocomposite preparation. This figure shows a significant increase in the modulus for the MMT-based nanocomposites with filler content of 4 wt%. According to the present authors, this behavior is due to the difference in layer charge between magadiite and MMT. Organomagadiites have a higher layer charge density, and subsequently higher alkylammonium content than organo-MMT. As the alkylammonium ions interact with the epoxy resin while polymerizing, dangling chains are formed, and more of these chains are formed in the presence of organomagadiites. These dangling chains are known to weaken the polymer matrix by reducing the degree of network cross-linking, then compromising the reinforcement effect of the silicate layer exfoliation.

For thermoset matrices, a significant enhancement in the tensile modulus is observed for an exfoliated structure when alkylammonium cations with different chain length modified MMTs were used for nanocomposite preparations, with the exception of the MMT modified with butylammonium, which only gives an intercalated structure with a low tensile modulus.

In a recent work, Mulhaupt et al. [234] reported the correlations between polymer morphology, silicate structure, stiffness, and toughness of thermoset

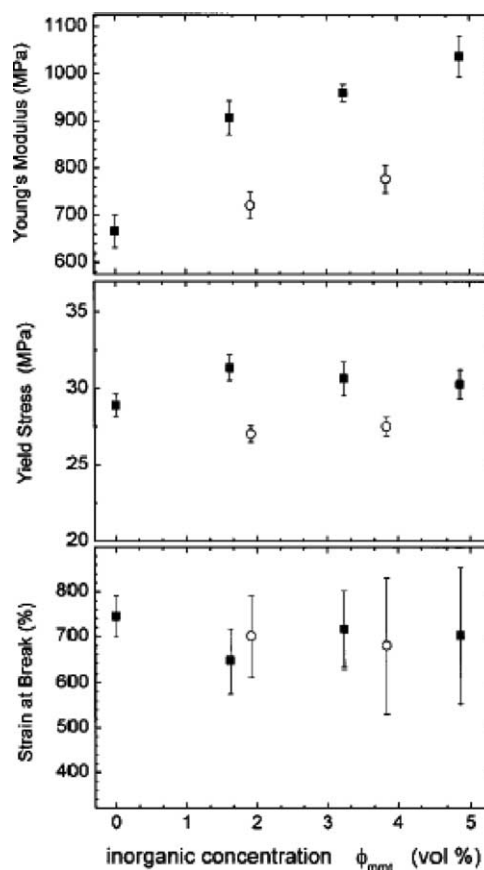


Fig. 86. Tensile characterization of the PP/f-MMT nanocomposites (■) by Instron. For comparison, conventionally filled PP/2C18-MMT 'macro' composites are also shown (○) [305]. Reproduced from Manias, Touny, Strawhecker, Lu and Chang by permission of American Chemical Society, USA.

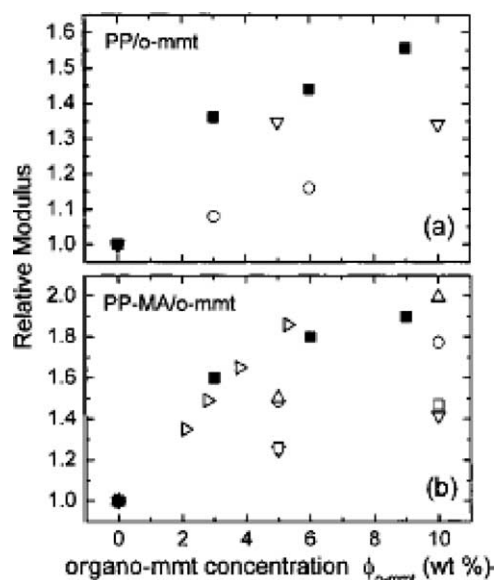


Fig. 87. Relative moduli of various PP-based nanocomposites, each normalized by modulus of the respective neat PP. (a) PP-based nanocomposites with: f-MMT (■), C18-MMT (△), and 2C18-MMT (○). (b) PP-g-MA/2C18-MMT nanocomposite (■) and PP hybrids with various PP-g-MA pretreated organically modified MMT: C18-MMT (right triangle open), C18-MMT (○, △), and C8-MMT (△, △) [305]. Reproduced from Manias, Touny, Strawhecker, Lu and Chang by permission of American Chemical Society, USA.

nanocomposites as a function of layered silicate type and content. They suggest that the main factor for the matrix stiffness improvement resides in the formation of supramolecular assemblies obtained by the presence of dispersed anisotropic laminated nanoparticles. They also describe a stiffening effect when the MMT is modified by a functionalized organic cation

(carboxylic acid or hydroxyl groups) that can strongly interact with the matrix during curing.

The tensile properties of APES/Cloisite 30B and APES/Cloisite 10A nanocomposites at various clay contents are presented in Table 16 [398]. In comparison to the APES, the tensile strength and modulus have been improved with a slight decrease in elongation at break. APES/Cloisite 30B nanocomposites exhibit a much higher tensile strength and modulus compared to the APES/Cloisite 10A nanocomposites. This is also attributed to the strong interaction between the APES matrix and Cloisite 30B. These results further confirm the importance of strong interaction between matrix and clay, which ultimately leads to better overall dispersion, as already observed by TEM analysis.

#### 4.1.3. Flexural properties

Nanocomposite researchers are generally interested in the tensile properties of final materials, but there are very few reports concerning the flexural properties of neat polymer and its nanocomposites with OMLS. Very recently, Sinha Ray et al. [386] reported the detailed measurement of flexural properties of neat PLA and various PLACNs. They conducted flexural property measurements with injection-molded samples according to the ASTM D-790 method. Table 17 summarizes the flexural modulus, flexural strength, and distortion at break of neat PLA and various PLACNs measured at 25 °C. There was a significant increase in flexural modulus for PLACN4 when compared to that of neat PLA, followed by a much slower increase with increasing OMLS content, and a maximum at 21% for PLACN7.

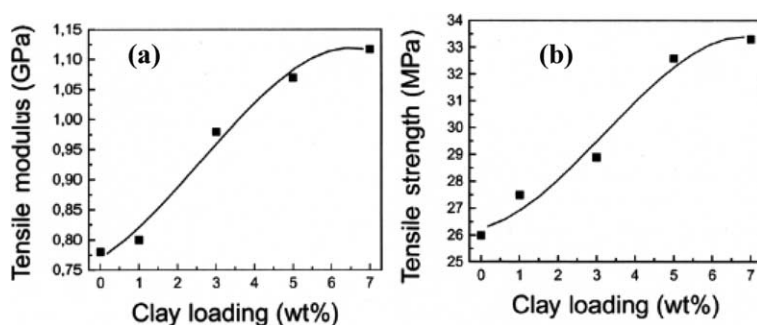


Fig. 88. Effect of clay loading on: (a) tensile modulus, and (b) tensile strength of PPCNs [304]. Reproduced from Liu and Wu by permission of Elsevier Science Ltd, UK.



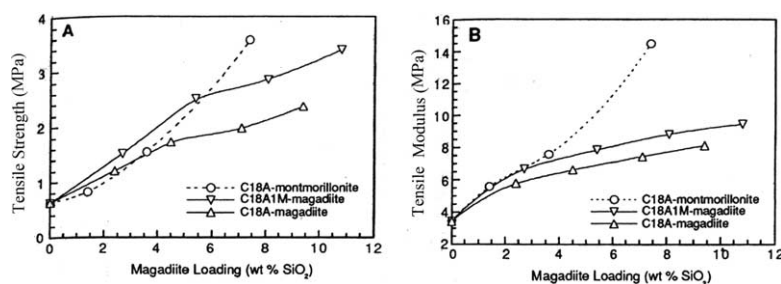


Fig. 89. A comparison of (A) the tensile strengths and (B) tensile moduli for epoxy nanocomposites prepared from C18A-MMT, C18A-magnitide, and C18A1M-magnitide. The silicate loading was determined by calcining the composites in air at 650 °C for 4 h at a heating rate of 2 °C/min [228]. Reproduced from Wang, Lan and Pinnavaia by permission of American Chemical Society, USA.

On the other hand, the flexural strength and distortion at break shows a remarkable increase with PLACN4, then gradually decreases with OMLS loading. According to the author, this behavior may be due to the high OMLS content, which leads to brittleness in the material.

#### 4.2. Heat distortion temperature

Heat distortion temperature (HDT) of a polymeric material is an index of heat resistance towards applied load. Most of the nanocomposite studies report HDT as a function of clay content, characterized by the procedure given in ASTM D-648. Kojima et al. [133] first showed that the HDT of pure N6 increases up to 90 °C after nanocomposite preparation with OMLS. In their further work [134] they reported the clay content dependence of HDT of N6/MMT nanocomposites. In N6/MMT nanocomposites, there is a marked increase in HDT from 65 °C for the neat N6 to 152 °C for 4.7 wt% nanocomposite. Beyond that

Table 16  
Tensile properties of APES/Closite 30B nanocomposites [398]

| Closite 30B content (wt%) | Modulus (kgf/cm <sup>2</sup> ) | Strength (kgf/cm <sup>2</sup> ) | Elongation at break (%) |
|---------------------------|--------------------------------|---------------------------------|-------------------------|
| 0                         | 106.7                          | 131.7                           | 12.45                   |
| 1                         | 112.3                          | 139.0                           | 12.25                   |
| 3                         | 114.4                          | 144.1                           | 11.95                   |
| 5                         | 118.2                          | 149.8                           | 11.40                   |
| 10                        | 129.5                          | 157.7                           | 10.90                   |
| 20                        | 144.4                          | 190.8                           | 11.30                   |
| 30                        | 173.8                          | 213.5                           | 12.25                   |

Reproduced from Lee, Park, Lim, Kang, Li, Cho and Ha by permission of Elsevier Science Ltd, UK.

wt% of MMT, the HDT of the nanocomposites level off. They also conducted HDT tests on various N6 nanocomposites prepared with different lengths of clay and found that the HDT also depends on the aspect ratio of dispersed clay particles [133]. Like all other mechanical properties, the HDT of 1potNCH is higher than that of NCH prepared by in situ intercalative polymerization [135].

Since the degree of crystallinity of N6 nanocomposites is independent of the amount and nature of clay, the HDT of N6 nanocomposites is due to the presence of strong hydrogen bonds between the matrix and silicate surface (see Fig. 80). Although N6 in nanocomposites results in a different crystal phase ( $\gamma$ -phase) than that found in pure N6, this different crystal phase is not responsible for the higher mechanical properties of N6 nanocomposites because the  $\gamma$ -phase is a very soft crystal phase. The increased mechanical properties of N6 nanocomposites with increasing clay content is due to the mechanical reinforcement effect.

The nano-dispersion of MMT in the PP matrix also promotes a higher HDT [305]. The HDT of PP and its nanocomposites based on f-MMT and

Table 17  
Comparison of materials properties between neat PLA and various PLACNs prepared with octadecyltrimethylammonium modified MMT [386]

| Materials properties    | PLA | PLACN4 | PLACN5 | PLACN7 |
|-------------------------|-----|--------|--------|--------|
| Bending modulus (GPa)   | 4.8 | 5.5    | 5.6    | 5.8    |
| Bending strength (MPa)  | 86  | 134    | 122    | 105    |
| Distortion at break (%) | 1.9 | 3.1    | 2.6    | 2      |

Reproduced from Sinha Ray, Yamada, Okamoto and Ueda by permission of Elsevier Science Ltd, UK.

Table 18  
HDT of PP/MMT nanocomposites and the respective unfilled PP [305]

| Organically modified mmt (wt%) | HDT (°C) |                      |
|--------------------------------|----------|----------------------|
|                                | PP/f-MMT | PP/alkyl-MMT         |
| 0                              | 109 ± 3  | 109 ± 3              |
| 3                              | 144 ± 5  | 130 ± 7 <sup>a</sup> |
| 6                              | 152 ± 5  | 141 ± 7 <sup>b</sup> |
| 9                              | 153 ± 5  |                      |

Reproduced from Manias, Touny, Strawhecker, Lu and Chang by permission of American Chemical Society, USA.

<sup>a</sup> C18-mmt filler, extruder processed.

<sup>b</sup> 2C18-MMT filler, twin-head mixer.

alkylammonium modified MMT are summarized in Table 18. Like previous systems, there is a significant increase in HDT, from 109 °C for the neat PP to 152 °C for a 6 wt% of clay, after which the HDT of the nanocomposites levels off. This improvement in HDT for neat PP after nanocomposite preparation originates from the greater mechanical stability of the nanocomposite as compared to neat PP, since there is no increase in melting point of neat PP after nanocomposite preparation.

The nanodispersion of octadecyltrimethylammonium modified MMT (qC18-MMT) in neat PLA also promotes a higher HDT. Sinha Ray et al. [386] examined the HDT of neat PLA and various PLACNs with different load conditions. As seen in Fig. 90a, there is a marked increase of HDT with an intermediate load of 0.98 MPa, from 76 °C for the neat PLA to 93 °C for PLACN4. This value gradually increases with increasing clay content, and in the case of PLACN7 with 7 wt% of OMLS, the value increases to 111 °C.

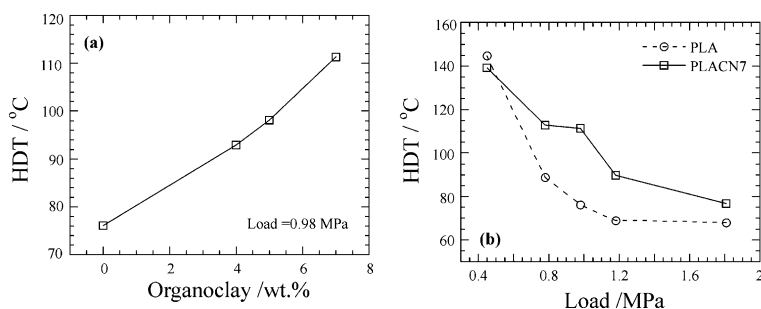


Fig. 90. (a) Organoclay (wt%) dependence of HDT of neat PLA and various PLACNs. (b) Load dependence of HDT of neat PLA and PLACN7 [386]. Reproduced from Sinha Ray, Yamada, Okamoto and Ueda by permission of Elsevier Science Ltd, UK.

On the other hand, an imposed load dependence on HDT is clearly observed in the case of PLACNs. Fig. 90b shows the typical load dependence in PLACN7. In the case of high load (1.81 MPa), it is very difficult to achieve high HDT enhancement without a strong interaction between the polymer matrix and OMLS, as observed N6 based nanocomposites. For PLACNs, the values of  $T_m$  do not change significantly as compared to that of neat PLA. Furthermore, in WAXD analyses up to  $2\theta = 70^\circ$ , no large shifting or formation of new peaks in the crystallized PLACNs was observed. This suggests that the improvement of HDT with intermediate load originates from the better mechanical stability, reinforcement by the dispersed clay particles, and higher degree of crystallinity and intercalation.

The increase of HDT due to clay dispersion is a very important property improvement for any polymeric material, not only from application or industrial point of view, but also because it is very difficult to achieve similar HDT enhancements by chemical modification or reinforcement by conventional filler.

#### 4.3. Thermal stability

The thermal stability of polymeric materials is usually studied by thermogravimetric analysis (TGA). The weight loss due to the formation of volatile products after degradation at high temperature is monitored as a function of temperature. When the heating occurs under an inert gas flow, a non-oxidative degradation occurs, while the use of air or oxygen allows oxidative degradation of the samples. Generally, the incorporation of clay into the polymer matrix was found to enhance thermal stability by acting as a

superior insulator and mass transport barrier to the volatile products generated during decomposition.

Blumstein [42] first reported the improved thermal stability of a PLS nanocomposite that combined PMMA and MMT clay. These PMMA nanocomposites were prepared by free radical polymerization of MMA intercalated in the clay. He showed that the PMMA that was intercalated ( $d$  spacing increase of 0.76 nm) between the galleries of MMT clay resisted the thermal degradation under conditions that would otherwise completely degrade pure PMMA. TGA data revealed that both linear and cross-linked PMMA intercalated into MMT layers have a 40–50 °C higher decomposition temperature. Blumstein argues that the stability of the PMMA nanocomposite is due not only to its different structure, but also to the restricted thermal motion of the PMMA in the gallery.

Recently, there have been many reports concerned with the improved thermal stability of nanocomposites prepared with various types of OMLS and polymer matrices [6,7,14,141]. Very recently, Zanetti et al. [331] conducted detailed TG analyses of nanocomposites based on EVA. The inorganic phase was fluorohectorite (FH) or MMT, both exchanged with octadecylammonium cation. They found that the deacylation of EVA in nanocomposites is accelerated, and may occur at temperatures lower than those for the pure polymer or corresponding microcomposite due to catalysis by the strongly acidic sites created by thermal decomposition of the silicate modifier. These sites are active when there is intimate contact between the polymer and the silicate. Slowing down the volatilization of the deacylated polymer in nitrogen may occur because of the labyrinth effect of the silicate layers in the polymer matrix [431,432].

In air, the nanocomposite exhibits a significant delay in weight loss that may derive from the barrier effect caused by diffusion of both the volatile thermo-oxidation products to the gas and oxygen from the gas phase to the polymer. According to Gilman et al. [433] this barrier effect increases during volatilization owing to the reassembly of the reticular of the silicate on the surface.

Fig. 91 represents the TGA analysis of a phosphonium-PS nanocomposite compared with virgin PS. It shows that the thermal stability of the nanocomposite is enhanced relative to that of virgin PS [98], and the typical the onset temperature of

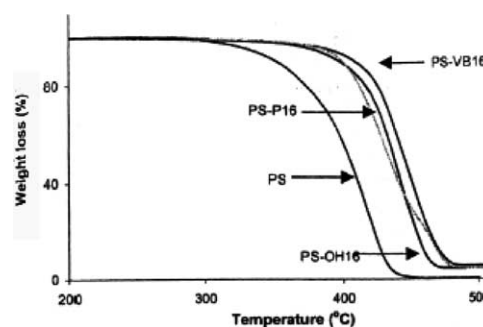


Fig. 91. TGA curves for polystyrene, PS and the nanocomposites [98]. Reproduced from Zhu, Morgan, Lamelas and Wilkei by permission of American Chemical Society, USA.

the degradation is about 50 °C higher for the nanocomposites. From Fig. 91 it is clearly observed that the degradation mechanism of phosphonium nanocomposites is somehow different from the others; there is a second step in the degradation. This second step accounts for about 30% of the degradation of the phosphonium-PS nanocomposite, and must be attributed to some interaction between the clay and the PS that serves to stabilize the nanocomposite. The most likely explanation is that the higher decomposition temperature of the phosphonium clay provides for the formation of char at a more opportune time to retain the PS. In the case of ammonium clays, char formation occurs earlier and can be broken up by the time the polymer degrades.

The variation of the temperature at which 10% degradation occurs for all three nanocomposites is shown as a function of the amount of clay in Fig. 92 [98]. Even with as little as 0.1 wt% of clay present in the nanocomposite, the onset temperature was significantly increased.

Fig. 93 [275] shows the TGA results for pure PSF and for nanocomposites containing 1 and 5 wt% of the OMLS. The approximate decomposition temperatures of these three materials were 494, 498 and 513 °C, respectively. There were significant increases in thermal stability resulting from the exfoliated clay platelets, which may be due to kinetic effects, with the platelets retarding diffusion of oxygen into the polymer matrix.

The thermal stability of the PCL-based composites has also been studied by TGA. Generally, the degradation of PCL fits a two-step mechanism [141,171]; first random chain scission through

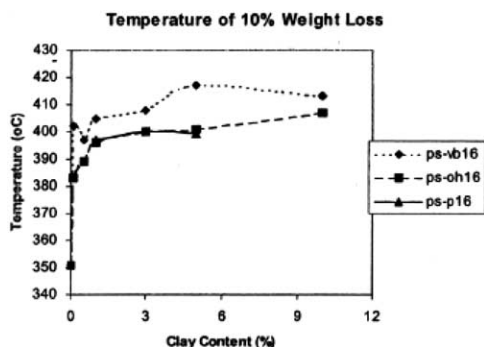


Fig. 92. Temperature of 10% mass loss for nanocomposites as a function of the fraction of clay [98]. Reproduced from Zhu, Morgan, Lamelas and Wilkei by permission of American Chemical Society, USA.

pyrolysis of the ester groups, with the release of  $\text{CO}_2$ ,  $\text{H}_2\text{O}$  and hexanoic acid, then in the second step,  $\epsilon$ -caprolactone (cyclic monomer) is formed as a result of an unzipping depolymerization process. The thermograms of nanocomposites prepared with Mont-Alk and pure PCL recovered after clay extraction are presented in Fig. 94 [171]. Both intercalated and exfoliated nanocomposites show higher thermal stability when compared to the pure PCL or to the corresponding microcomposites. The nanocomposites exhibit a 25 °C high in decomposition temperature at 50% weight loss. The shift of the degradation temperature may be ascribed to a decrease in oxygen and volatile degradation products permeability/diffusivity due to the homogeneous incorporation of clay sheets, to a barrier of these high-aspect ratio fillers, and char

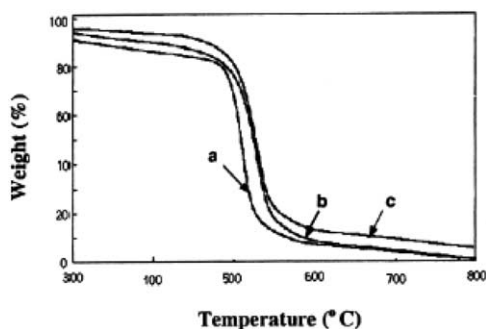


Fig. 93. TGA curves (relative weight loss as a function of temperature) for (a) pure polysulfone, (b) nanocomposite with 1 wt% clay, and (c) nanocomposite with 5 wt% clay [275]. Reproduced from Sur, Sun, Lyu and Mark by permission of Elsevier Science Ltd, UK.

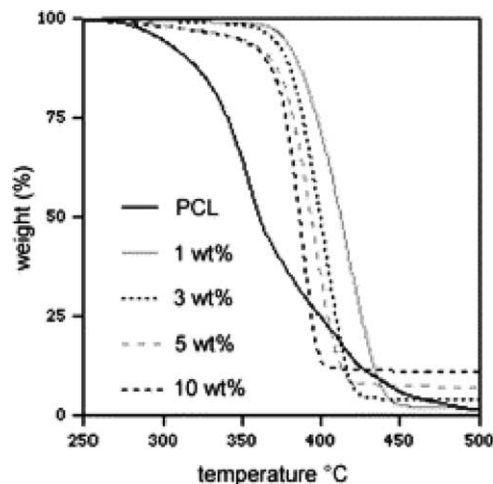


Fig. 94. Temperature dependence of the weight loss under an air flow for neat PCL and PCL nanocomposites containing 1, 3, 5, and 10 wt% (relative to inorganics) of MMT-Alk [171]. Reproduced from Lepoittevin, Devalckenaere, Pantoustier, Alexandre, Kubies, Calberg, Jerome and Dubois by permission of Elsevier Science Ltd, UK.

formation. The thermal stability of the nanocomposites systematically increases with increasing clay, up to a loading of 5 wt%.

Different behavior is observed in synthetic biodegradable aliphatic polyester BAP/OMLS nanocomposite systems, in which the thermal degradation temperature and thermal degradation rate systematically increases with increasing amounts of OMLS up to 15 wt% [401]. The TGA results for neat BAP and various nanocomposites are presented in Fig. 95.

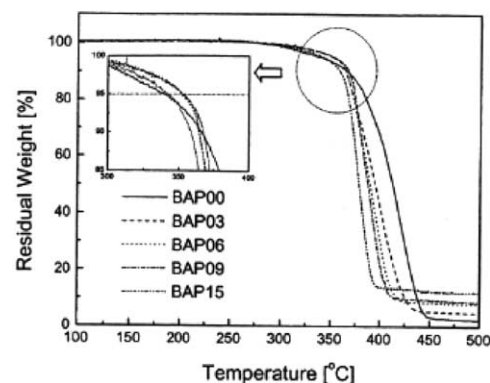


Fig. 95. TGA of BAP/organically modified MMT with different organoclay [401]. Reproduced from Lim, Hyun, Choi and Jhon by permission of American Chemical Society, USA.

Like PS-based nanocomposites, a small amount of clay also increased the residual weight of BAP/OMMT because of the restricted thermal motion of the polymer in the silicate layers. The residual weight of various materials at 450 °C increased in the order BAP < BAP03 < BAP06 < BAP09 < BAP15 (here number indicates wt% of clay). These improved thermal properties are also observed in other systems like SAN [126,434], the intercalated nanocomposite prepared by emulsion polymerization.

The role of clay in the nanocomposite structure may be the main reason for the difference in TGA results of these systems compared to the previously reported systems. The clay acts as a heat barrier, which enhances the overall thermal stability of the system, as well as assist in the formation of char after thermal decomposition. In the early stages of thermal decomposition, the clay would shift the decomposition to higher temperature. After that, this heat barrier effect would result in a reverse thermal stability. In other words, the stacked silicate layers could hold accumulated heat that could be used as a heat source to accelerate the decomposition process, in conjunction with the heat flow supplied by the outside heat source.

#### 4.4. Fire retardant properties

The Cone calorimeter is one of the most effective bench-scale methods for studying the fire retardant

properties of polymeric materials. Fire-relevant properties such as the heat release rate (HRR), heat peak HRR, smoke production, and CO<sub>2</sub> yield, are vital to the evaluation of the fire safety of materials.

In 1976 Unitika Ltd, Japan, first presented the potential flame retardant properties of N6/layered silicate nanocomposites [435]. Then in 1997 Gilman et al. reported detailed investigations on flame retardant properties of N6/layered silicate nanocomposite [13]. Subsequently, they chose various types of nanocomposite materials and found similar reductions in flammability [15–17]. Recently, Gilman reviewed the flame retardant properties of nanocomposites in detail [14]. Since the decreased flammability of nanocomposites is one of the most important properties, the results of some of the most recent studies on flame retardant properties of nanocomposites are reported in the following.

Table 19 represents the cone calorimeter data of three different kinds of polymer and their nanocomposites with MMT. As shown in Table 19, all of the MMT-based nanocomposites reported here exhibit reduced flammability. The peak HRR is reduced by 50–75% for N6, PS, and PP-g-MA nanocomposites [17]. According to the authors, the MMT must be nanodispersed for it to affect the flammability of the nanocomposites. However, the clay need not be completely delaminated. In general, the nanocomposites' flame retardant mechanism involves

Table 19  
Cone calorimeter data of various polymers and their nanocomposites with OMLS [17]

| Sample (structure)                                | % residue yield (±0.5) | Peak HRR (kW/m <sup>2</sup> ) (Δ%) | Mean HRR (kW/m <sup>2</sup> ) (Δ%) | Mean H <sub>c</sub> (MJ/kg) | Mean SEA (m <sup>2</sup> /kg) | Mean CO yield (kg/kg) |
|---|------------------------|------------------------------------|------------------------------------|-----------------------------|-------------------------------|-----------------------|
| N6  | 1                      | 1010                               | 603                                | 27                          | 197                           | 0.01                  |
| N6 nanocomposite 2% (delaminated)                 | 3                      | 686 (32)                           | 390 (35)                           | 27                          | 271                           | 0.01                  |
| N6 nanocomposite 5% (delaminated)                 | 6                      | 378 (63)                           | 304 (50)                           | 27                          | 296                           | 0.02                  |
| PS  | 0                      | 1120                               | 703                                | 29                          | 1460                          | 0.09                  |
| PS-silicate mix 3% (immiscible)                   | 3                      | 1080                               | 715                                | 29                          | 1840                          | 0.09                  |
| PS-nanocomposite 3% (intercalated/delaminated)    | 4                      | 567 (48)                           | 444 (38)                           | 27                          | 1730                          | 0.08                  |
| PSw/DBDPO/Sb <sub>2</sub> O <sub>3</sub> ) 30%    | 3                      | 491 (56)                           | 318 (54)                           | 11                          | 2580                          | 0.14                  |
| PpgMA   | 5                      | 1525                               | 536                                | 39                          | 704                           | 0.02                  |
| PpgMA-nanocomposite 2% (intercalated/delaminated) | 6                      | 450 (70)                           | 322 (40)                           | 44                          | 1028                          | 0.02                  |
| PpgMA-nanocomposite 4% (intercalated/delaminated) | 12                     | 381 (75)                           | 275 (49)                           | 44                          | 968                           | 0.02                  |

Heat flux, 35 kW/m<sup>2</sup>. H<sub>c</sub>, specific heat of combustion; SEA, specific extinction area. Peak HRR, mass loss rate, and SEA data, measured at 35 kW/m<sup>2</sup>, are reproducible to within ±10%. The carbon monoxide and heat of combustion data are reproducible to within ±15%. Reproduced from Gilman, Jackson, Morgan, Harris Jr, Manias, Giannelis, Wuthemow, Hilton and Phillips by permission of American Chemical Society, USA.

a high-performance carbonaceous-silicate char, which builds up on the surface during burning. This insulates the underlying material and slows the mass loss rate of decomposition products.

In a recent study, Zhu et al. [98] reported the fire retardant properties of PS/MMT nanocomposites, which were prepared using three different types of new organically modified MMT (see Fig. 25). They initially used phosphonium salt for the modification of clay, and then examined the differences between organo ammonium and phosphonium salt treatments of clay fillers in nanocomposites towards thermal stability. The peak HRR for PS and the three nanocomposites is also shown graphically in Fig. 96. As mentioned above, the suggested mechanism by which clay nanocomposites function involves the formation of a char that serves as a barrier to both mass and energy transport [17]. As the fraction of clay increases, the amount of char that can be formed increases, and the rate at which heat is released decreases. One of these nanocomposites, OH-16, is mostly intercalated. This yields a slight reduction in the rate of heat release compared with the other two systems, which contain a significant exfoliated fraction. This observation again supports the suggestion that an intercalated material is more effective than an exfoliated material in fire retardance [433].

In contrast, the decrease in the rate of heat release corresponds to (1) a decrease in mass loss rate and the amount of energy released by the time PS has ceased

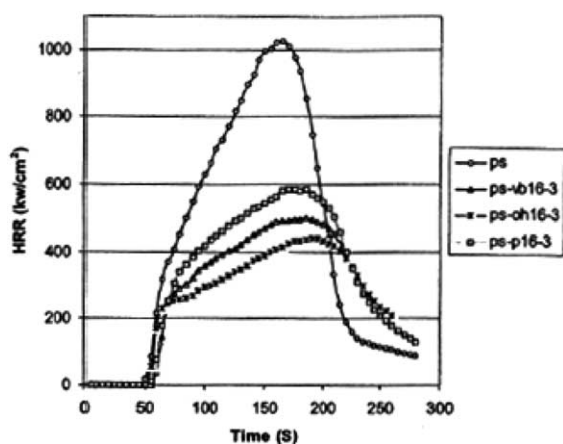


Fig. 96. Peak HRRs for PS and the three nanocomposites [98]. Reproduced from Zhu, Morgan, Lamelas and Wilkei by permission of American Chemical Society, USA.

burning, and (2) a modest increase in the time at which the peak heat release is reached. The production of a char barrier must serve to retain some of the PS, and thus both the energy released and the mass loss rate decrease. The amount of smoke evolved and specific extinction area also decrease with the formation of the nanocomposites. There is some variability in the smoke production. Although it is observed that the formation of the nanocomposites reduces smoke production, the presence of additional clay does not continue this smoke reduction.

#### 4.5. Gas barrier properties

Clays are believed to increase the barrier properties by creating a maze or 'tortuous path' (see Fig. 97) that retards the progress of the gas molecules through the matrix resin. The direct benefit of the formation of such a path is clearly observed in polyimide/clay nanocomposites by dramatically improved barrier properties, with a simultaneous decrease in the thermal expansion coefficient [11,255,257]. The polyimide/layered silicate nanocomposites with a small fraction of OMLS exhibited reduction in the permeability of small gases, e.g. O<sub>2</sub>, H<sub>2</sub>O, He, CO<sub>2</sub>, and ethylacetate vapors [11]. For example, at 2 wt% clay loading, the permeability coefficient of water vapor was decreased ten-fold with synthetic mica relative to pristine polyimide. By comparing nanocomposites made with layered silicates of various aspect ratios, the permeability was seen to decrease with increasing aspect ratio.

Oxygen gas permeability has been measured for near to exfoliated PLA/synthetic mica nanocomposites prepared by Sinha Ray et al. [383]. The relative permeability coefficient value, i.e.  $P_{\text{PLACN}}/P_{\text{PLA}}$  where  $P_{\text{PLACN}}$  and  $P_{\text{PLA}}$  are the nanocomposite and pure PLA permeability coefficient, respectively, is plotted as a function of the wt% of OMLS in Fig. 98. The data are analyzed with the Nielsen theoretical expression [436], allowing prediction of

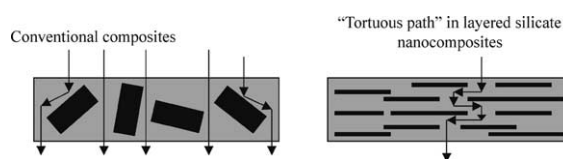


Fig. 97. Formation of tortuous path in PLS nanocomposites.

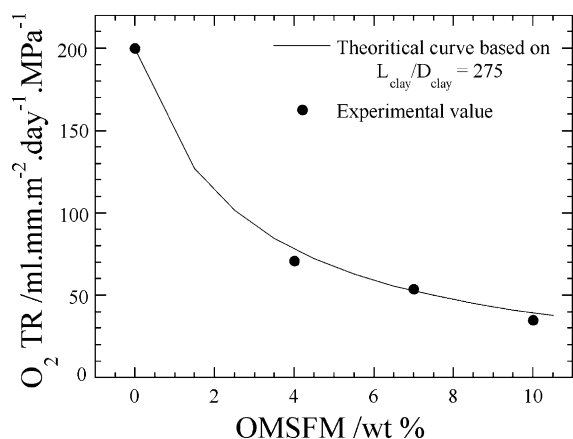


Fig. 98. Oxygen gas permeability of neat PLA and various PLACNs as a function of OMS content measured at 20 °C and 90% relative humidity. The filled circles represent the experimental data. Theoretical fits based on Nelson tortuosity model [383]. Reproduced from Sinha Ray, Yamada, Okamoto, Ogami and Ueda by permission of American Chemical Society, USA.

gas permeability as a function of the length and width of the filler particles, as well as their volume fraction in the PLA-matrix.

The H<sub>2</sub>O-vapor permeability for the PUU/OMLS nanocomposites is presented in Fig. 99 in terms of  $P_c/P_o$ , the ratio of the permeability coefficient of the nanocomposite ( $P_c$ ) to that of the neat PUU ( $P_o$ ) [8]. The nanocomposite formation results in a dramatic decrease in H<sub>2</sub>O-vapor transmission through the PUU sheet. The solid lines in Fig. 99 are based on

the tortuosity model for aspect ratios of 300 and 1000. The comparison between the experimental values and the theoretical model suggests a gradual change in the effective aspect ratio of the filler.

Although the enhancement in barrier properties in nanocomposites is well known, the dependence on factors such as the relative orientation and dispersion (intercalated, exfoliated or some intermediate) is not well understood. Very recently, Bharadwaj [9] addressed the modeling of barrier properties in PLS nanocomposites based completely upon the tortuosity arguments described by Nielsen [436]. The correlation between the sheet length, concentration, relative orientation, and state of aggregation is expected to provide guidance in the design of better barrier materials using the nanocomposite approach.

The presence of filler, spherical, plate, cylindrical, etc. introduces a tortuous path for a diffusing penetrant. The reduction of permeability arises from the longer diffusive path that the penetrants must travel in the presence of filler, as shown in the inset in Fig. 100. A sheet-like morphology is particularly efficient at maximizing the path length due to the large length-to-width ratio, when compared to other filler shapes such as spheres or cubes. The tortuosity factor  $\tau$  is defined as the ratio of the actual distance  $d'$  that a penetrant must travel to the shortest distance  $d$  that it would travel in the absence of barriers. It is expressed in terms of the length  $L$ , width  $W$ , and volume fraction

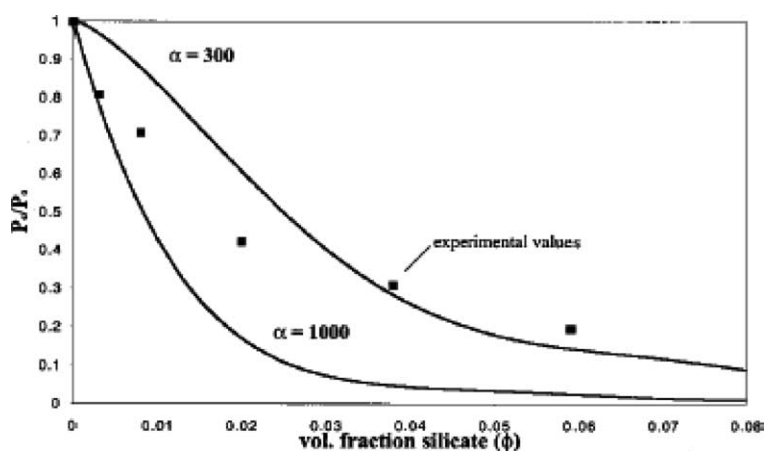


Fig. 99. Relative H<sub>2</sub>O vapor permeability for the PUU nanocomposites. The nanocomposite formation results in a dramatic decrease in H<sub>2</sub>O vapor transmission through the PUU membrane. The solid lines represent the theoretical value for aspect ratios = 300 and 1000 [8]. Reproduced from Xu, Manias, Snyder, Runt by permission of American Chemical Society, USA.

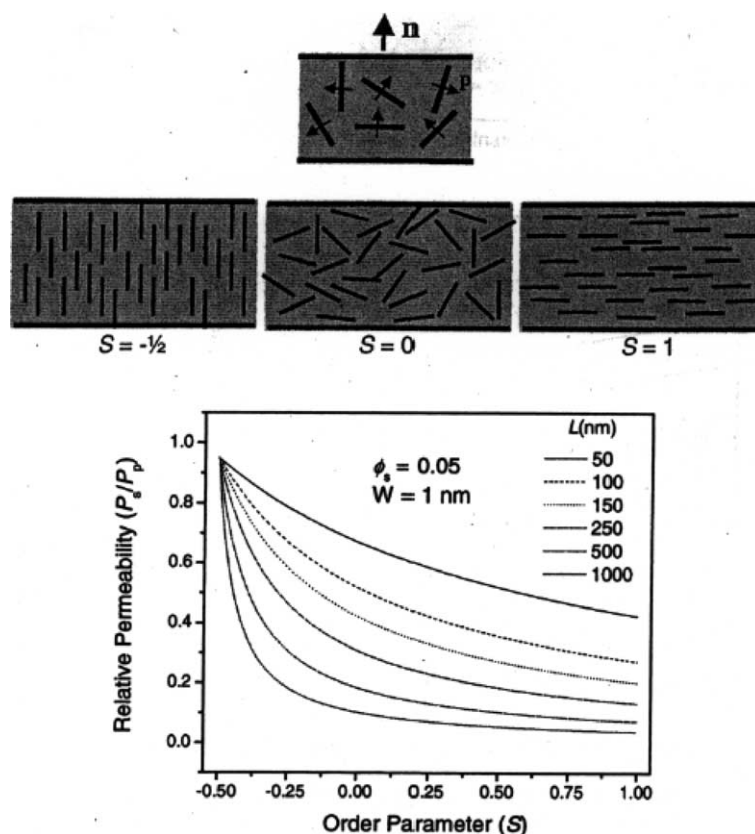


Fig. 100. Effect of sheet orientation on the relative permeability in exfoliated PLS nanocomposites at  $\phi_s = 0.05$  and  $W = 1$  nm. The illustrations show the definition of the direction of preferred orientation ( $n$ ) of the silicate sheet normals ( $p$ ) with respect to the film plane. Illustration for three values of the order parameter ( $S$ )— $1/2$ ,  $0$ , and  $1$  are also shown [9]. Reproduced from Bharadwaj by permission of American Chemical Society, USA.

of the sheets  $\phi_s$  as

$$\tau = \frac{d'}{d} = 1 + \frac{L}{2W} \phi_s \quad (5)$$

The effect of tortuosity on the permeability is expressed as

$$\frac{P_s}{P_p} = \frac{1 - \phi_s}{\tau} \quad (6)$$

where  $P_s$  and  $P_p$  represent the permeabilities of the nanocomposite and pure polymer, respectively. In the present case, the polygonal aluminosilicate sheets are approximated as disks with a mean diameter  $L$  ranging from 30 to 200 nm and a width of 1 nm.

Although the above equations were developed to model the diffusion of small molecules in conventional composites, they do extremely well in reproducing

experimental results for the relative permeability in PLS nanocomposites. The key assumption of this model is that the sheets are placed in an arrangement such that the direction of diffusion is normal to the direction of the sheets. Clearly, this arrangement results in the highest tortuosity, and any deviation from the arrangement where the sheet normal lies perpendicular to the film plane would in fact lead to deterioration of the barrier properties. A range of relative sheet orientations with respect to each other and to the plane of the film is shown in Fig. 101.

#### 4.6. Ionic conductivity

Solvent-free electrolytes are of much interest because of their charge-transport mechanism and their possible applications in electrochemical devices.



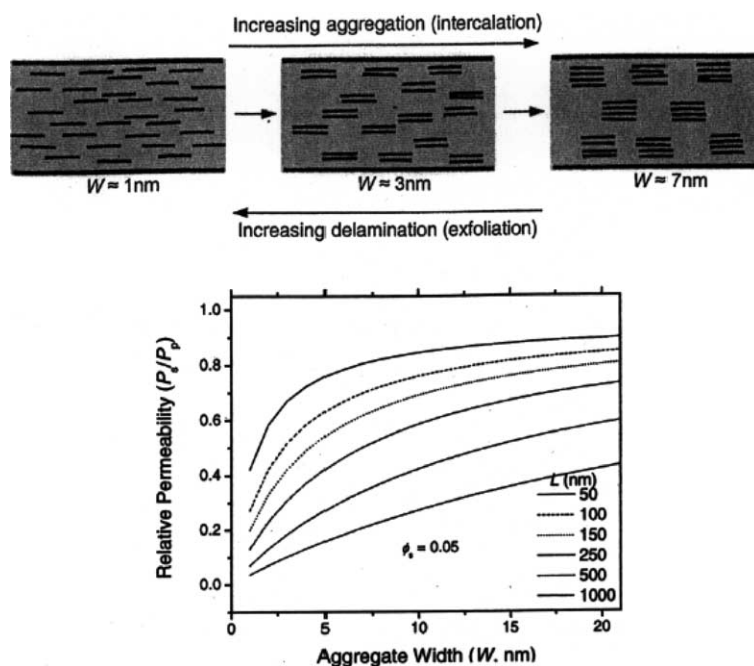


Fig. 101. Effect of incomplete exfoliation on the relative permeability. The illustrations show the effect of having one, two, and four sheet aggregates dispersed throughout the matrix. The plot shows the relative permeability as a function of the aggregate width at several different lengths of the sheets at  $\phi_s = 0.05$  [9]. Reproduced from Bharadwaj by permission of American Chemical Society, USA.

Vaia et al. [189] studied the preparation of PEO/layered silicate nanocomposites to fine tune the ionic conductivity of PEO. An intercalated nanocomposite prepared by melt intercalation of PEO (40 wt%) into  $\text{Li}^+$ -MMT (60 wt%) was shown to enhance the stability of the ionic conductance at lower temperatures when compared to a more conventional PEO/ $\text{LiBF}_4$  mixture. This improvement in conductivity is explained by the fact that PEO is not able to crystallize when intercalated, eliminating the presence of crystallites, which are non-conductive. The higher conductivity at room temperature, compared to conventional PEO/ $\text{LiBF}_4$  electrolytes with a single ionic conductor, makes these nanocomposites promising new electrolyte materials. The same type ionic conductivity behavior was observed in a poly[bis(methoxy-ethoxy) ethoxy phosphazene/ $\text{Na}^+$ -MMT nanocomposites prepared by Hutchison et al. [437].

#### 4.7. Optical transparency

Although layered silicates are microns in lateral size, they are just 1 nm thick. Thus, when single layers

are dispersed in a polymer matrix, the resulting nanocomposite is optically clear in visible light. Fig. 102 presents the UV/visible transmission spectra of pure PVA and PVA/ $\text{Na}^+$ -MMT nanocomposites with 4 and 10 wt% MMT. The spectra show that the visible region is not affected by the presence of the silicate layers, and retains the high transparency of PVA. For UV wavelengths, there is strong scattering and/or absorption, resulting in very low transmission of UV light. This behavior is not surprising, as the typical MMT lateral sizes are 50–1000 nm.

Like PVA, various other polymers also show optical transparency after nanocomposite preparation with OMLS [141,305].

#### 4.8. Biodegradability of biodegradable polymers-based nanocomposites

Another interesting and exciting aspect of nanocomposite technology is the significant improvement of biodegradability after nanocomposite preparation with OMLS. Tetto et al. [438] first reported results on the biodegradability of nanocomposites based on

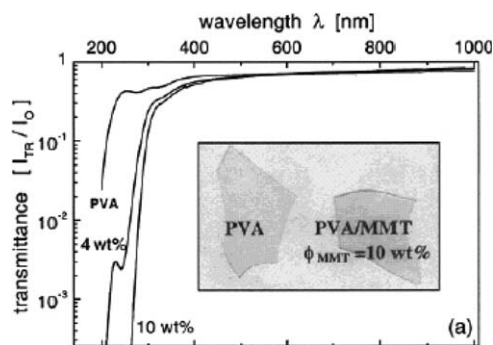


Fig. 102. UV–vis transmittance spectra of PVA and PVA/MMT nanocomposites containing 4 and 10 wt% MMT [111]. Reproduced from Strawhecker and Manias by permission of American Chemical Society, USA.

PCL, reporting that the PCL/OMLS nanocomposites showed improved biodegradability compared to pure PCL. The improved biodegradability of PCL after nanocomposites formation may be due to a catalytic role of the OMLS in the biodegradation mechanism, but it is not clear.

Recently, Lee et al. [398] reported the biodegradation of aliphatic polyester-based nanocomposites under compost. Parts a and b of Fig. 103 show the clay content dependence of the biodegradation of APES-based nanocomposites prepared with two different types of clays. They assumed that the retardation of biodegradation was due to the improvement of the barrier properties of the aliphatic APSE after nanocomposite preparation with clay. However, they do not provide permeability data.

Very recently, Sinha Ray et al. [18,386] reported the biodegradability of neat PLA and the corresponding nanocomposites prepared with octadecyltrimethylammonium-modified MMT (C18C<sup>3</sup>-MMT), along

with a detailed mechanism of the degradation. The compost used was prepared from food waste, and tests were carried out at a temperature of  $(58 \pm 2)^\circ\text{C}$ . Fig. 104a shows the recovered samples of neat PLA and PLACN4 (C18C<sup>3</sup>-MMT = 4 wt%) from compost. The decrease in  $M_w$  and residual weight percentage of the initial test samples are also reported in Fig. 104b. Obviously, the biodegradability of neat PLA is significantly enhanced after nanocomposite preparation with C18C<sup>3</sup>-MMT. Within one month, both the extent of  $M_w$  and the extent of weight loss are at the same level for both neat PLA and PLACN4. However, after one month, a sharp change occurs in the weight loss of PLACN4, and within 2 months it is completely degraded by compost.

The presence of terminal hydroxylated edge groups in the silicate layers may be one of the factors responsible for this behavior. In the case of PLACN4, the stacked ( $\sim 4$  layers) and intercalated silicate layers are homogeneously dispersed in the PLA matrix (from TEM image), and these hydroxy groups start heterogeneous hydrolysis of the PLA matrix after absorbing water from the compost. This process takes some time to start. For this reason, the weight loss and degree of hydrolysis for PLA and PLACN4 are almost the same up to 1 month (see Fig. 104b). However, after 1 month there is a sharp weight loss in the case of PLACN4 compared to that of PLA. That means that 1 month is the critical timescale to start heterogeneous hydrolysis, and due to this type of hydrolysis, the matrix decomposes into very small fragments and eventually disappears with the compost. This assumption was confirmed by conducting the same experimental procedure with PLACN prepared with dimethyldioctadecylammonium salt modified synthetic mica, which

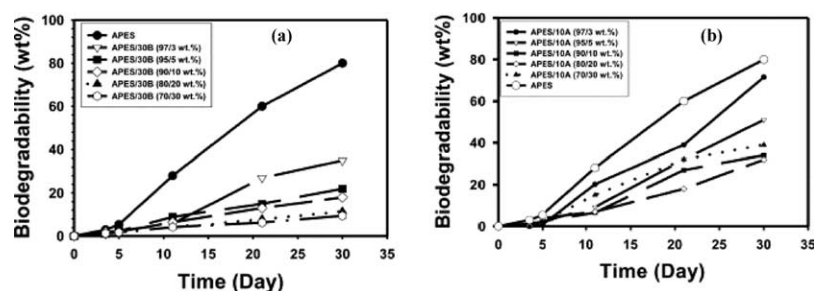


Fig. 103. Biodegradability of APES nanocomposites with: (a) Closite 30B and (b) Closite 10A [398]. Reproduced from Lee, Park, Lim, Kang, Li, Cho and Ha by permission of Elsevier Science Ltd, UK.

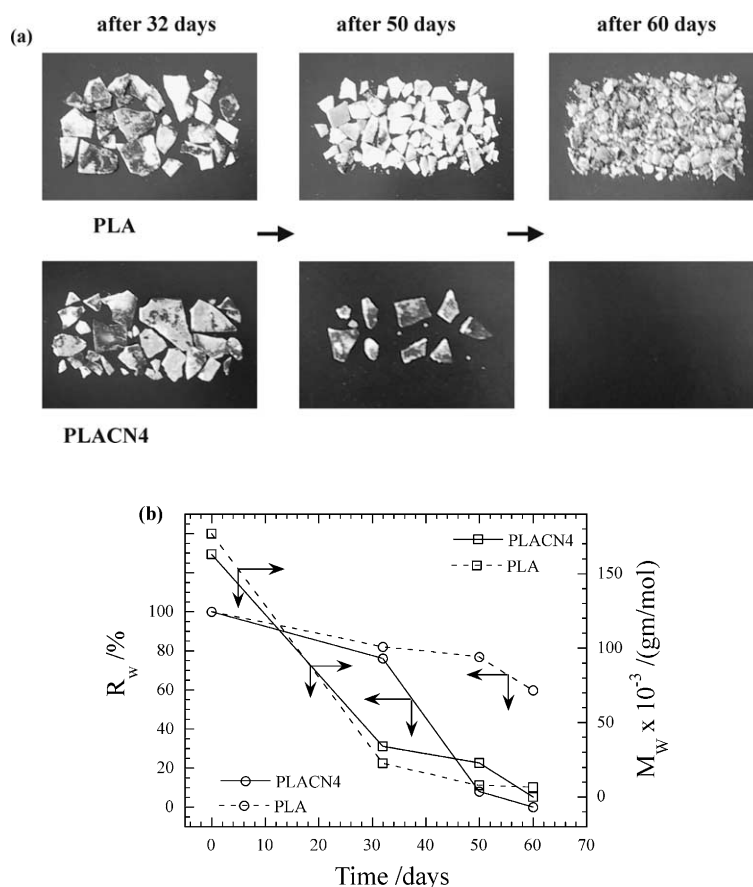


Fig. 104. (a) Real picture of biodegradability of neat PLA and PLACN4 recovered from compost with time. Initial shape of the crystallized samples was  $3 \times 10 \times 0.1 \text{ cm}^3$ . (b) Time dependence of residual weight,  $R_w$  and of matrix,  $M_w$  of PLA and PLACN4 under compost at  $(58 \pm 2)^\circ\text{C}$  [386]. Reproduced from Sinha Ray, Yamada, Okamoto and Ueda by permission of Elsevier Science Ltd, UK.

has no terminal hydroxylated edge group. The same degradation tendency was found with PLA [439].

A respirometric test has also been used to study the degradation of the PLA matrix in a compost environment at  $(58 \pm 2)^\circ\text{C}$  [377,383]. For this test compost was made from bean-curd refuse, food waste, and cattle feces. Unlike the weight loss, which reflects the structural changes in the test sample,  $\text{CO}_2$  evolution provides an indicator of the ultimate biodegradability of PLA in PLACN4 (prepared with  $(N(\text{coco alkyl})N,N\text{-bis}(2\text{-hydroxyethyl})-N\text{-methylammonium}$  modified synthetic mica), via mineralization, of the samples. Fig. 105 shows the time dependence of the degree of biodegradation of neat PLA and PLACN4, indicating that the biodegradability of PLA in PLACN4 is enhanced significantly. The presence of MEE clay

may cause a different mode of attack on the PLA component due to the presence of hydroxy groups. Details regarding the mechanism of biodegradability can be found in relevant literature [377,383].

#### 4.9. Other properties

PLS nanocomposites also show improvement in most general polymeric properties. For example, in addition to the decreased permeability of liquids and gases, nanocomposites also show significant improvement in solvent uptake. Scratch resistance is another property that is strongly enhanced by the incorporation of layered silicates [305].

The potential to use PANI-based nanocomposites as electrorheologically sensitive fluids [342], or to use

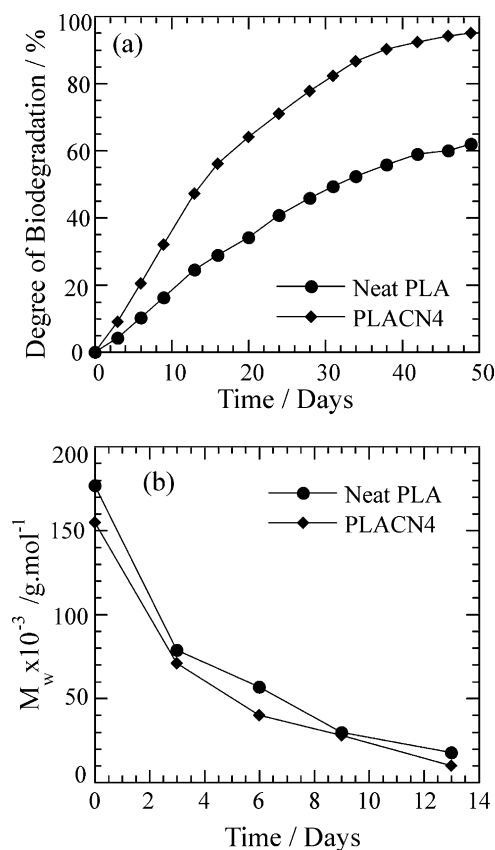


Fig. 105. Degree of biodegradation (i.e.  $\text{CO}_2$  evolution), and (b) time-dependent change of matrix  $M_w$  of neat PLA and PLACN4 (MEE clay = 4 wt%) under compost at  $(58 \pm 2)^\circ\text{C}$  [383]. Reproduced from Sinha Ray, Yamada, Ogami, Okamoto and Ueda by permission of American Chemical Society, USA.

the combination of dispersed layered silicates in a liquid crystal medium is also an attractive application. This could result in a stable electro-optical device that is capable of exhibiting a bistable and reversible electro-optical effect between an opaque and transparent state [5].

Finally, nanocomposites have been used in highly technical areas such as in the improvement of ablative properties in aeronautics [5,365].

## 5. Crystallization behavior and morphology of nanocomposites

Crystallization is one of the most effective processes used to control the extent of intercalation

of polymer chains into silicate galleries, and hence to control the mechanical and various other properties of the nanocomposites. Okamoto et al. [311,312] first studied the crystallization behavior and morphology of neat PP-MA and three different nanocomposites (PPCNs) in detail. They found that clay particles act as a nucleating agent for the crystallization of the matrix PA-MA, but that the linear growth rate and overall crystallization rate is not influenced significantly by the presence of clay. WAXD analyses reveal that the intergallery spacing increases with crystallization temperature  $T_c$  for any amount of clay content in nanocomposites. Furthermore, at constant  $T_c$  the extent of intercalation increases with decreasing clay content. The microstructure of the nanocomposites, observed directly by TEM, showed that the clay particles are well dispersed at low  $T_c$ , and that segregation of silicate layers occurs at high  $T_c$ . With the increase of  $T_c$ , there is a corresponding increase in  $G'$ . This enhancement is a maximum (30%) for nanocomposites with a low content of clay (~4 wt%), decreasing to only 13% with further clay addition. Thus, by controlling intercalation through crystallization at a suitable temperature, one can control the fine structure, morphology, and mechanical properties of crystalline polymer/clay nanocomposites. Maiti and Okamoto [440] also studied the crystallization behavior of pure N6 and various MMT nanocomposites. In contrast to PP, the crystallization rate of pure N6 is much faster in the presence of clay particles, and the mechanism is completely different from that of PP in PPCNs. N6 crystallizes exclusively in the  $\gamma$ -form in the N6CN structures because of the epitaxial crystallization. This is clearly observed from the TEM images (see Fig. 106, Sandwiched structure) of the crystallized sample. The  $G'$  of the N6CN is always higher than that of the pure N6, irrespective of crystallization temperatures. A much higher increase in storage modulus for pure N6 with increasing crystallization temperature is explained by the higher amount of the thermally stable  $\alpha$ -form at higher temperatures.

The nucleation and growth processes of N6 in N6CN are presented in Fig. 107, following direct observation by TEM. A unique mechanism can explain the higher crystallization rate along with

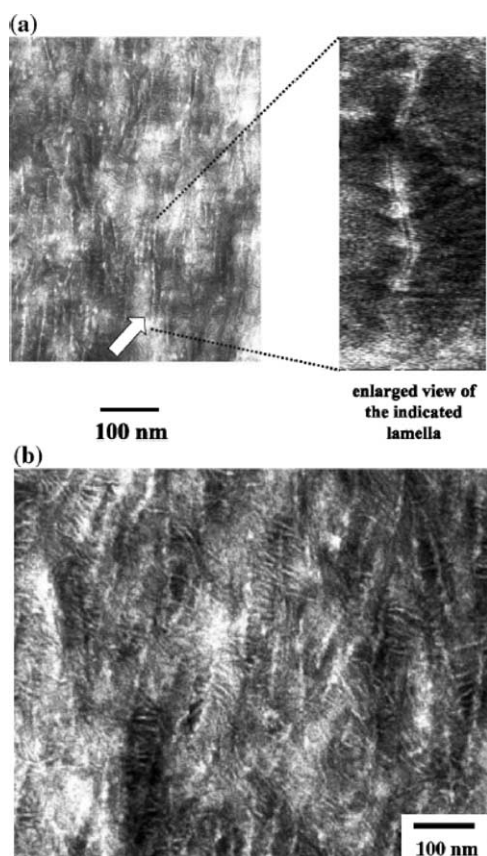


Fig. 106. Typical TEM images of N6CN3.7 crystallized at (a) 170 and 210 °C. The enlarge part shown (a) is from the indicated lamella in the original image. The black strip inside the white part is clay. Figure (b) shows the typical shish-kebab type of structure [440]. Reproduced from Maiti and Okamoto by permission of Wiley-VCH, Germany.

the morphology and developed internal structure of N6CNs. This sandwiched structure, with each silicate layer strongly covered by polymer crystals, makes the system very rigid. As a result, the HDT increases up to 80 °C, but the surrounding excess amorphous regions can easily retain the original polymeric properties, such as the impact strength. This structure ultimately leads to an improved PLS nanocomposites. Recently, Lincoln et al. [144] studied the secondary structure and elevated temperature crystallite morphology of N6CN, and the time-resolved shear behavior of end-tethered N6CNs, followed by non-isothermal crystallization [145].

## 6. Rheology

### 6.1. Melt rheology and structure–property relationship

PLS nanocomposites show improved material properties such as a higher modulus, higher thermal stability, decreased flammability and barrier properties, increased biodegradability of biodegradable polymers and various other properties in comparison with the virgin polymers or conventional composites. In order to understand the processibility of these materials, i.e. the final stage of any polymeric material, one must understand the detailed rheological behavior of these materials in the molten state. Understanding the rheological properties of nanocomposite melts is not only important in gaining a fundamental knowledge of the processibility, but is also helpful in understanding the structure–property relationships in these materials.

#### 6.1.1. Dynamic oscillatory shear measurements

Dynamic oscillatory shear measurements of polymeric materials are generally performed by applying a time dependent strain  $\gamma(t) = \gamma_0 \sin(\omega t)$ , and measuring the resultant shear stress  $\sigma(t) = \gamma_0 [G' \sin(\omega t) + G'' \cos(\omega t)]$ , where  $G'$  and  $G''$  are the storage and loss moduli, respectively.

Generally, the rheology of polymer melts depends strongly on the temperature at which the measurement is carried out. It is well known that for thermorheologically simple materials, bilogarithmic plots of the isotherms of the storage modulus  $G'(\omega)$ , loss modulus  $G''(\omega)$  and complex viscosity ( $|\eta^*(\omega)|$ ) can be superimposed by horizontal shifts  $\log(a_T)$ , along the  $\log(\omega)$  axis, and vertical shifts given by  $\log(b_T)$  such that:

$$b_T G'(a_T \omega, T) = G'(\omega, T_{\text{ref}})$$

$$b_T G''(a_T \omega, T) = G''(\omega, T_{\text{ref}})$$

$$(b_T/a_T) |\eta^*(a_T \omega, T_{\text{ref}})| = |\eta^*(\omega, T_{\text{ref}})|$$

where  $T_{\text{ref}}$  is the reference temperature. All isotherms measured for pure polymer and for various nanocomposites can be superimposed in this way.

In the case of polymer samples, it is expected at the temperatures and frequencies at which the rheological measurements were carried should

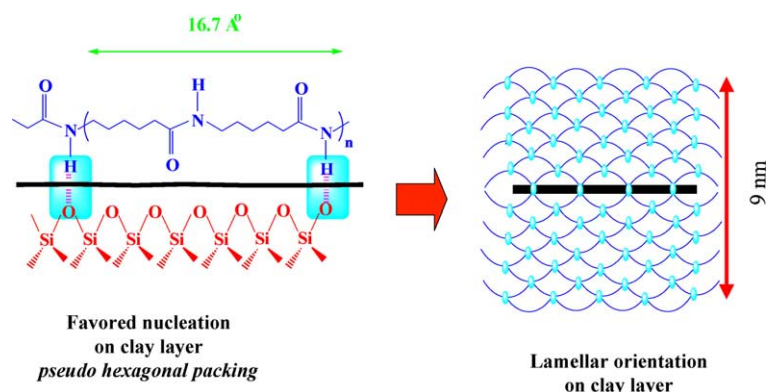


Fig. 107. Schematic view of the nucleation and growth mechanism in nylon-6 nanocomposite [440]. Reproduced from Maiti and Okamoto by permission of Wiley-VCH, Germany.

exhibit characteristic homopolymer-like terminal flow behavior, expressed by the power-laws  $G' \propto \omega^2$  and  $G'' \propto \omega$ .

The rheological properties of in situ polymerized nanocomposites with end-tethered polymer chains were first described by Krisnamoorti and Giannelis [165]. The flow behavior of PCL and N6-based nanocomposites differed significantly from that of the corresponding neat matrices, whereas the thermorheological properties of the nanocomposites were entirely determined by the behavior of the matrices [165]. The slopes of  $\log G'(\omega)$  and  $G''(\omega)$  vs.  $\log a_T \omega$  are much smaller than 2 and 1, respectively. Values of 2 and 1 are expected for non-crosslinked polymer melts, but large deviations occur, especially in the presence of a very small amount of layered silicate loading, which may be due to the formation of a network structure in the molten state. However, nanocomposites based on the in situ polymerization technique exhibit a fairly broad molar mass distribution in the polymer matrix, which hides the relevant structural information and impedes the interpretation of the results.

The linear dynamic mechanical properties of several nanocomposites have been examined for a wide range of polymer matrices including N6 with various matrix molecular weights [149], polystyrene [93], polystyrene–polyisoprene (PS–PI) block copolymers [128,129], PCL [171], PP [297,298,316] PLA [374,386], and PBS [389–394].

Recently, Fornes et al. [149] have conducted dynamic and steady shear capillary experiments

over a large range of frequencies and shear rates of pure N6 with different molecular weights, and their nanocomposites with OMLS. Fig. 108 shows bilogarithmic plots of the complex viscosity,  $|\eta^*|$  vs.  $\omega$  at 240 °C for pure N6 and  $(HE)_2M_1R_1$  nanocomposites based on (a) HMW, (b) MMW, and (c) LMW, obtained using the parallel plate oscillating rheometer. Fig. 108 also shows a bilogarithmic plot of the steady-state shear viscosity  $\eta$  vs. shear rate  $\dot{\gamma}$ , obtained using a capillary rheometer. Inspection of these figures reveals a significant difference between the nanocomposites, particularly at low frequencies. The HMW-based nanocomposites show very strong non-Newtonian behavior, and this is more pronounced at low frequencies. On the other hand, the magnitude of the non-Newtonian behavior gradually decreases with decreasing molecular weight of the matrix, and with LMW it behaves like pure polymer. This trend is more clearly observed in the plot of  $G'$  vs.  $\omega$ , due to the extreme sensitivity of  $G'$  towards dispersed morphology in the molten state, as presented in Fig. 109. The difference in the terminal zone behavior may be due to different extents of exfoliation of the clay particles in the three types of matrices.

At the other extreme, the steady shear capillary rheology shows a trend with respect to the matrix molecular weight. The HMW- and MMW-based nanocomposites exhibit lower viscosities compared to that of their corresponding matrices, whereas the viscosities of LMW-based nanocomposites are higher than the pure matrix. This behavior is also due the higher degree of exfoliation in the case of

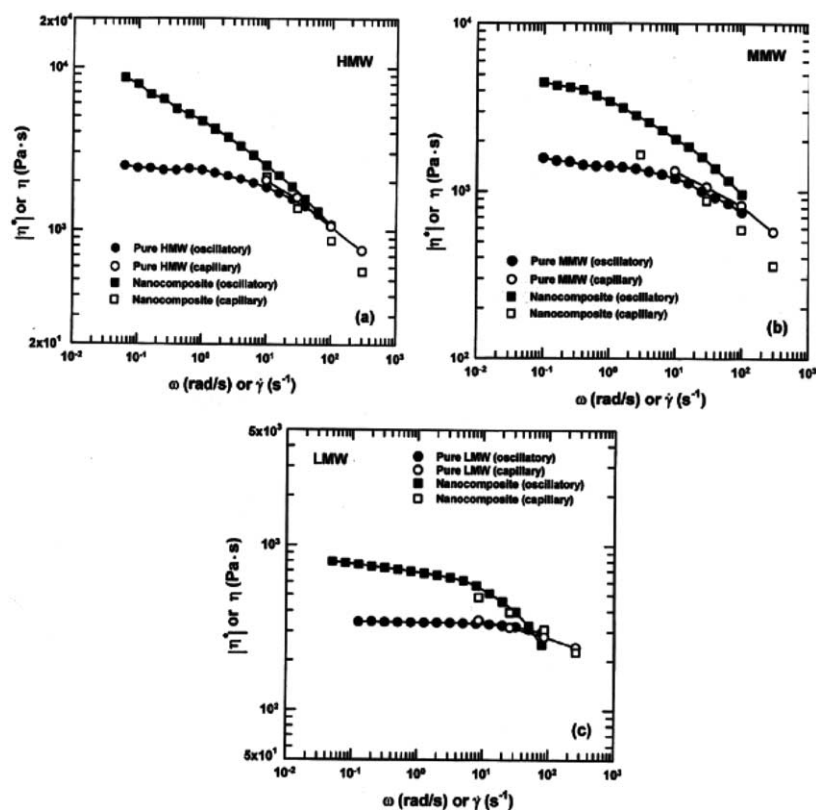


Fig. 108. Complex viscosity vs. frequency from a dynamic parallel plate rheometer (solid points) and steady shear viscosity vs. shear rate from a capillary rheometer (open points) at 240 °C for (a) pure HMW N6 and its nanocomposite with (HE)<sub>2</sub>M<sub>1</sub>R<sub>1</sub> organoclay, (b) pure MMW N6 and its nanocomposite with (HE)<sub>2</sub>M<sub>1</sub>R<sub>1</sub> organoclay, and (c) pure LMW N6 and its nanocomposite with (HE)<sub>2</sub>M<sub>1</sub>R<sub>1</sub> organoclay. The content of MMT in each nanocomposite = 3 wt% [149]. Reproduced from Fornes, Yoon, Keskkula and Paul by permission of Elsevier Science Ltd, UK.

HMW- and MMW-based nanocomposites compared to the LMW-based nanocomposite.

Finally they considered the differences in the melt viscosity among the three systems. Over the range of frequencies and shear rates tested, the melt viscosity of the three systems follows the order HMW > MMW > LMW, and hence the resulting shear stresses exerted by the pure polymers also follow same order. Therefore, during melt mixing the level of stress exerted on the OMLS by the LMW polyamide is significantly lower than those developed in the presence of HMW or MMW polyamides. As a result, the breakup of clay particles is much easier in the case of HMW polyamides, and clay particle dispersion is ultimately improved. In Fig. 110 shows schematic suggestions of various roles that shear stress may play during the melt compounding of nanocomposites. The role of polymer molecular weight is believed to stem

from an increase in the melt viscosity, facilitating the degradation of the taller stacks into shorter ones. The final step in exfoliation involves peeling away the platelets of the stacks one by one, and this takes time and requires the strong matrix-OMLS interaction to cause spontaneous wetting.

Parts a and b of Fig. 111 show the time dependent evolution of the storage and loss moduli for PPCH8 (PP = 91 wt%, MMT = 9 wt%) and PPCH9 (PP = 82 wt%, MA = 9 wt% and MMT = 9 wt%) samples, subjected to small strain oscillatory shear tests every 10 min during their total annealing time of 3 h at 200 °C. At high frequencies the elastic moduli of PPCH8 and PPCH9 are comparable at similar annealing times, and both decrease with annealing due to possible degradation of the PP-matrix. At low frequencies the elastic modulus of PPCH9 is qualitatively different than that of PPCH8.

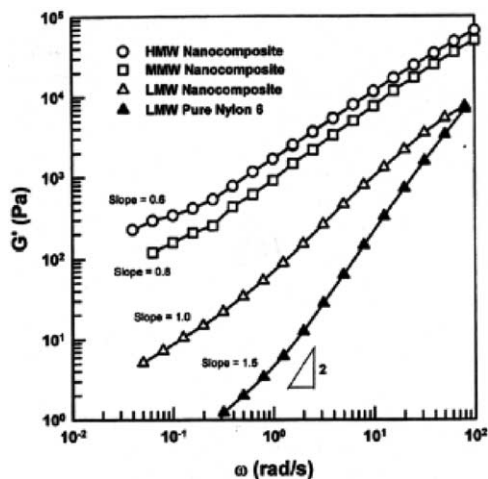


Fig. 109. Influence of frequency on  $G'$  for pure LMW N6 and various N6 based nanocomposites [149]. Reproduced from Fornes, Yoon, Keskula and Paul by permission of Elsevier Science Ltd, UK.

The low-frequency elastic modulus of as-extruded PPCH9 is always higher than that of PPCH8, indicating that most of the micro-structural development in PPCH9 has already occurred during

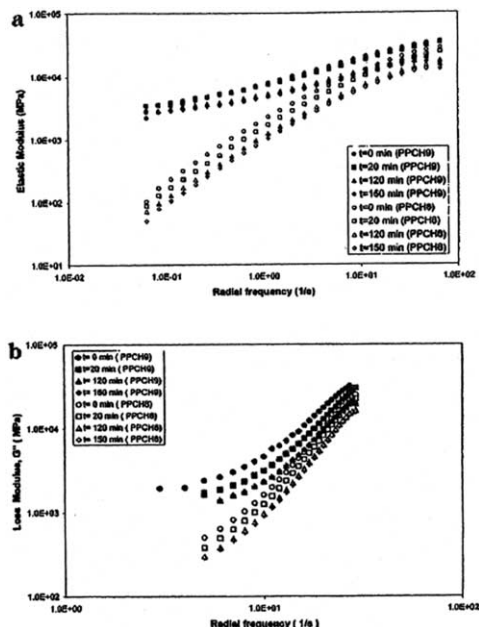


Fig. 111. (a) Storage modulus of PPCH8 (unfilled symbols) and PPCH9 (filled symbols) samples as a function of annealing time at 200 °C. (b) Loss modulus of PPCH8 (unfilled symbols) and PPCH9 (filled symbols) samples [297]. Reproduced from Galgali, Ramesh and Lele by permission of American Chemical Society, USA.

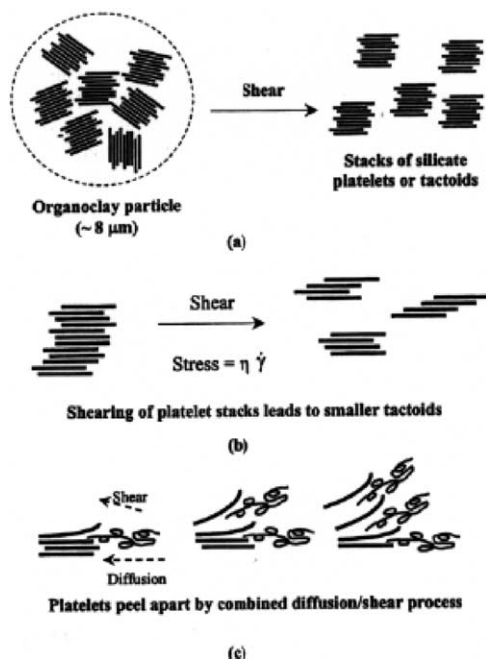


Fig. 110. Stepwise mechanism of clay platelets exfoliation during melt compounding: (a) OMLS breakup, (b) intercalated OMLS tactoid breakup, and (c) platelet exfoliation [149]. Reproduced from Fornes, Yoon, Keskula and Paul by permission of Elsevier Science Ltd, UK.

the extrusion process, while only subtle micro-structural changes occurred during annealing. Furthermore, the elastic modulus of PPCH8 at low frequency decreases with annealing time, but that of PPCH9 remains more or less unchanged. Thus at high frequency, the response of the PPCH9 hybrid is dominated by the matrix, while at lower frequencies its solid-like response is strongly influenced by the presence of clay. On the other hand, the low frequency response of PPCH8 is not dominated by the presence of clay, which highlights the important role played by PP-MA in the formation of the hybrids.

The above results show that the solid-like rheological behavior of nanocomposites at lower frequencies is completely independent on the fine structure of the nanocomposites, i.e. whether it is end-tethered or stacked intercalated, but it depends primarily upon the amount of clay loading in the nanocomposites. Galgali et al. [297] have also shown that the typical rheological response in nanocomposites arises from frictional interactions between the silicate layers and not due to the immobilization of confined polymer



chains between the silicate layers. They have also shown a dramatic decrease in the creep compliance for the PPCH prepared with MA modified PP and 6 wt% MMT. In contrast, for PPCH prepared with MA modified PP and 9 wt% of MMT, they show a dramatic three-order of magnitude drop in the zero shear viscosity beyond the apparent yield stress, suggesting that the solid-like behavior in the quiescent state is a result of the percolated structure of the layered-silicate.

Hoffmann et al. [93] recently conducted rheological measurements of nanocomposites of polystyrene (PS100) with synthetic mica (ME100) modified with amine-terminated polystyrene (AT-PS8) and 2-phenylethylamine (PEA), respectively, in order to verify the presence of a particle network formation via interparticle interaction and self-assembly. Fig. 112 represents  $G'(\omega)$  vs.  $a_T\omega$  for PS100 and its corresponding nanocomposites prepared with AT-PS8 modified ME100 (C-PS) and PEA modified ME100 (C-PEA). The rheological responses of PS100 and C-PEA are same, whereas the rheological response of C-PS is completely different. At the lowest frequencies, which correspond to the marked region III,  $G'(\omega)$  strongly increases, and the slope approaches to zero. Such behavior is an indication of network formation involving the assembly of individual plates composed of silicate layers. In the regime of intermediate frequencies (region II, see Fig. 112) the  $G'(\omega)$  value is lower in comparison to that of PS100. This might be due to dilution of the amine-terminated PS being

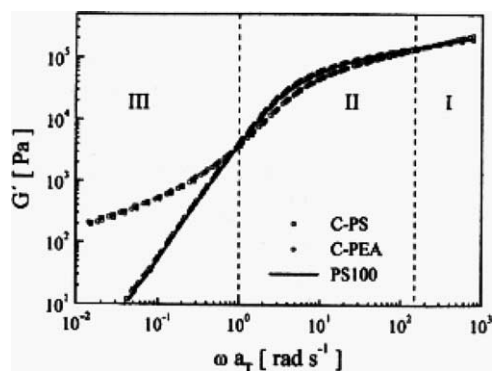


Fig. 112.  $G'$  vs. reduced frequency for PS100 matrix (black line), C-PS ( $\square$ ), and C-PEA ( $\circ$ ). Silicate loading: 5 wt% [93]. Reproduced from Hoffman, Dietrich, Thomann, Friedrich and Mulhaupt by permission of Wiley-VCH, Germany.

below the entanglement molecular weight. On the other hand, in high frequency region (region I, Fig. 112) the rheological behavior is the same for all systems.

Ren et al. [128] measured the viscoelastic behavior of a series of nanocomposites of disordered PS–PI block copolymers and MMT. Dynamic moduli and stress relaxation measurements indicate solid-like behavior for nanocomposites with more than 6.7 wt% MMT, at least on a time scale of 100 s. They suggest that this solid-like behavior is due to the physical jamming or percolation of the randomly distributed silicate layers, at a surprisingly low volume fraction, due to their anisotropic nature. The fact that the alignment of the silicate layers by large shear stresses results in a liquid-like relaxation supports the percolation argument.

A solid-like rheological response is also observed for PCL-based nanocomposites with OMLS content of 3 wt% or more [171].  $G'(\omega)$  and  $G''(\omega)$  in the terminal region are substantially higher for all of the nanocomposites compared with neat PCL or PCL-based micro-composites.

Parts a and b of Fig. 113 show the frequency dependence of  $G'(\omega)$ ,  $G''(\omega)$  and complex viscosity  $|\eta^*|$  for various PLACNs and the corresponding matrices. As expected, the moduli of the nanocomposites increase with increasing clay loading at all frequencies. At high frequencies, the qualitative behavior of  $G'(\omega)$  and  $G''(\omega)$  is essentially the same. However, at low frequencies,  $G'(\omega)$  and  $G''(\omega)$  increase monotonically with increasing clay content. On the other hand, for  $a_T\omega < 5$  rad/s, the viscoelastic response (particularly,  $G'(\omega)$ ) for all nanocomposites displays significantly diminished frequency dependence as compared to the matrices. In fact, for all PLACNs,  $G'(\omega)$  becomes nearly independent of frequency at low  $a_T\omega$  and exceeds  $G''(\omega)$ , characteristic of materials exhibiting pseudo-solid like behavior.

As seen in TEM observations (see Fig. 62),  $\xi_{\text{clay}} < L_{\text{clay}}$  for PLACNs, suggesting the formation of a spatially linked structure of the dispersed clay particles in the PLA-matrix (see Table 9). According to this structure, the individual silicate layers are incapable of free rotation, and hence the relaxation of the structure by imposing small  $\omega$  are almost completely prevented. This type of prevented

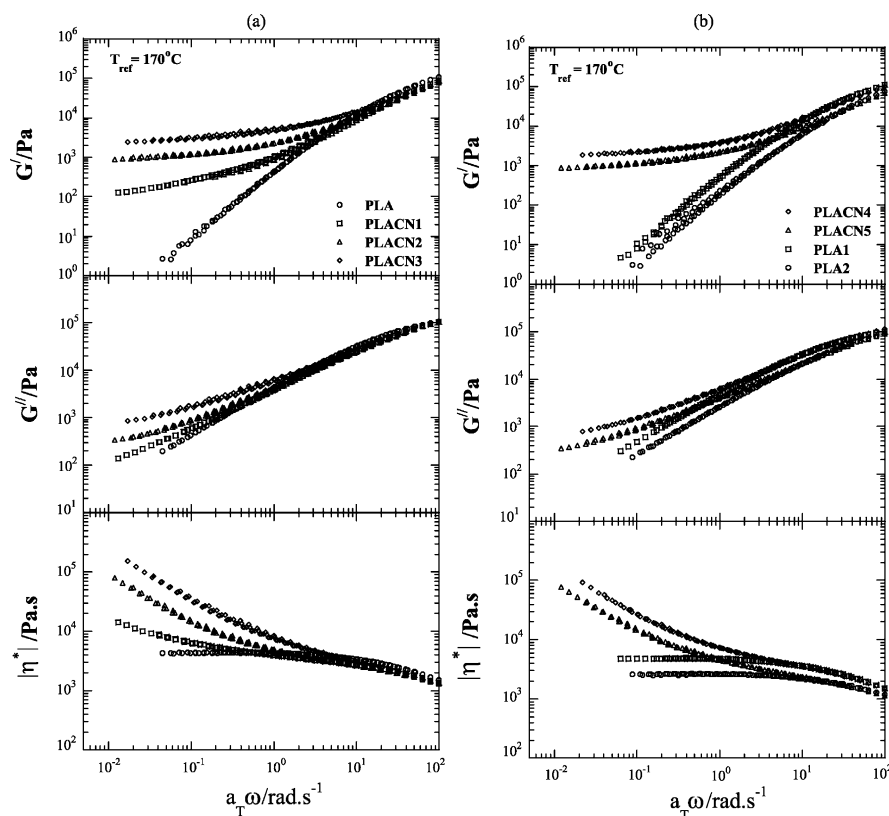


Fig. 113. Reduced frequency dependence of storage modulus, ( $G'(\omega)$ ), loss modulus, ( $G''(\omega)$ ), and complex viscosity, ( $|\eta^*|$ ) of PLACNs and PLA matrices: (a) without *o*-PCL and (b) with *o*-PCL [374]. Reproduced from Sinha Ray, Maiti, Okamoto, Yamada and Ueda by permission of American Chemical Society, USA.

relaxation due to the geometric constraints of the stacked silicate layers leads to the presence of the pseudo-solid like behavior observed in PLACNs. This behavior corresponds to the shear-thinning tendency, which appears strongly in the viscosity curves ( $\omega < 5$  rad/s) ( $|\eta^*|$  vs.  $a_T \omega$ ) of the PLACNs.

### 6.1.2. Steady shear measurements

The steady shear rheological behavior of neat PBS and various PBSCNs are shown in Fig. 114. The steady state shear viscosity of PBSCNs is enhanced considerably at all shear rates with respect to time, and at a fixed shear rate it increases monotonically with increasing silicate loading. On the other hand, all intercalated PBSCNs exhibit strong rheopexy behavior, which becomes prominent at low shear rates, while neat PBS exhibits a time independent viscosity at all shear rates studied. With increasing shear rates,

the shear viscosity attains a plateau after a certain time, however the time required to attain this plateau decreases with increasing shear rate. One possible explanation for this behavior may involve planar alignment of the clay particles towards the flow direction under shear. For very slow ( $0.001 \text{ s}^{-1}$ ) shear rate, clay particles take a longer time to attain complete planar alignment along the flow direction, and the measurement time (1000 s) is too short to attain such alignment, hence strong rheopexy behavior is observed. By contrast, under little high shear rates ( $0.005$  or  $0.01 \text{ s}^{-1}$ ) this measurement time is long enough to attain such alignment, and hence the nanocomposites show a time independent shear viscosity.

Fig. 115 shows the shear rate dependence of the viscosity for neat PBS and the corresponding nanocomposites measured at  $120^\circ\text{C}$ . While

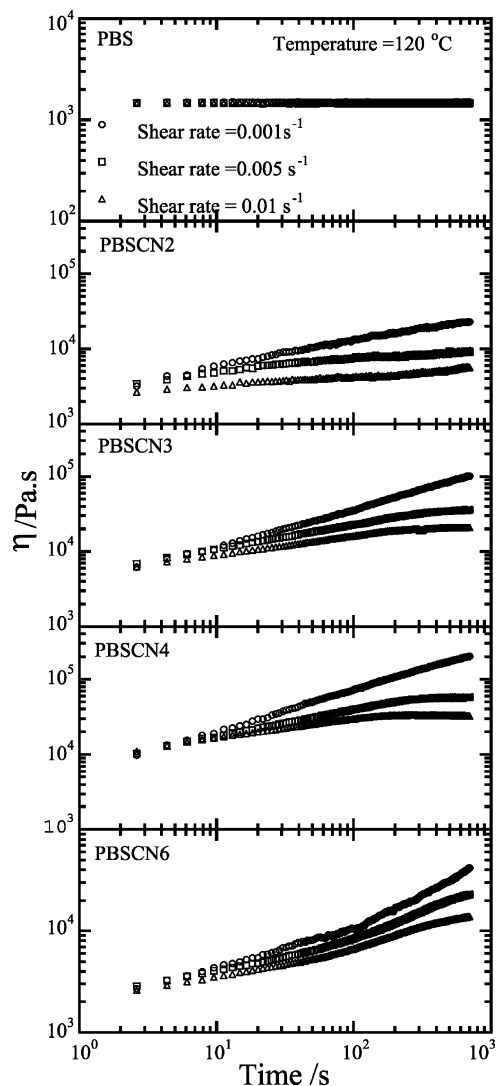


Fig. 114. Shear viscosity as a function of time [391]. Reproduced from Sinha Ray, Okamoto and Okamoto by permission of American Chemical Society, USA.

the neat PBS exhibits nearly Newtonian behavior at all shear rates, nanocomposites exhibited non-Newtonian behavior. At very low shear rates, the shear viscosity of the nanocomposites initially exhibits shear-thickening behavior, and corresponding to the rheopexy behavior observed at very low shear rates (see Fig. 114). Subsequently, all nanocomposites show very strong shear thinning behavior at all shear rates, analogous to the results obtained in the case of dynamic oscillatory shear

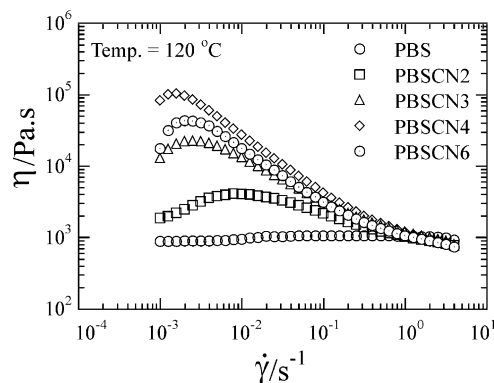


Fig. 115. Shear viscosity as a function of shear rates [391]. Reproduced from Sinha Ray, Okamoto and Okamoto by permission of American Chemical Society, USA.

measurements [391]. Additionally, at very high shear rates the viscosities of the nanocomposites are comparable to that of pure PBS. These observations suggest that the silicate layers are strongly oriented towards the flow direction at high shear rates, and that the shear thinning behavior observed at high shear rates is dominated by that of pure polymer.

Polymer/OMLS nanocomposites [441–443] always exhibit significant deviations from the Cox–Merz relation [444], while all neat polymers obey the empirical relation, which requires that for  $\dot{\gamma} = \omega$ , the viscoelastic data obeys the relationship  $\eta(\dot{\gamma}) = |\eta^*(\omega)|$ . Two possible reasons may be offered for the deviation from the Cox–Merz relation in case of nanocomposites. First, this rule is only applicable for homogenous systems like homo-polymer melts, but nanocomposites are heterogeneous systems. Second, the structure formation is different when nanocomposites are subjected to dynamic oscillatory shear vs. steady shear measurements.

### 6.1.3. Elongation flow rheology

Okamoto et al. [307] first conducted elongation tests of PPCN4 in the molten state at constant Hencky strain rate,  $\dot{\epsilon}_0$  using elongation flow optorheometry [445]. Fig. 116 shows double-logarithmic plots of the transient elongation viscosity  $\eta_E(\dot{\epsilon}_0; t)$  vs. time  $t$ , observed for PPCN4 (4 wt% of MMT) at 150 °C with different  $\dot{\epsilon}_0$  values ranging from 0.001 to 1.0 s<sup>-1</sup>. The solid line on the curve represents  $3\eta_0(\dot{\gamma}; t)$ , the three-fold shear viscosity of PPCN4, measured with

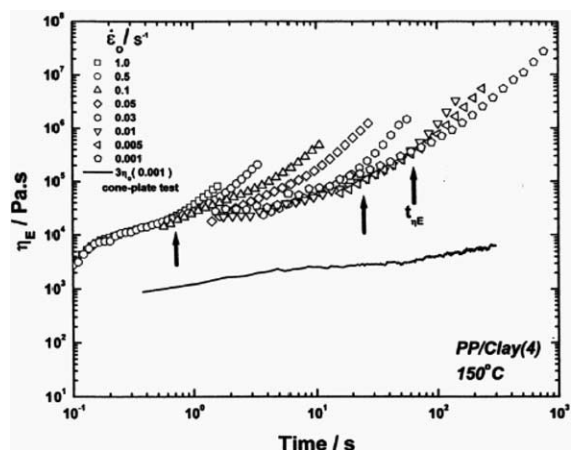


Fig. 116. Time dependence of elongation viscosity for PP/clay (4) (PPCN4) melt at 150 °C. The upward arrows indicate up-rising time for different strain rate. The solid line shows three times the shear viscosity, taken at a low shear rate of  $0.001 \text{ s}^{-1}$  on a cone plate [307]. Reproduced from Okamoto, Nam, Maiti, Kotaka, Hasegawa and Usuki by permission of American Chemical Society, USA.

a constant  $\dot{\gamma}$  of  $0.001 \text{ s}^{-1}$  at 150 °C. A very strong *strain-induced hardening* behavior for PPCN4 may be seen in Fig. 116. At short times,  $\eta_E(\dot{\epsilon}_0; t)$  gradually increases with time, but is independent of  $\dot{\epsilon}_0$ ; this is generally called the linear region of the  $\eta_E(\dot{\epsilon}_0; t)$  curve. After a certain time  $t_{\eta_E}$ , generally called the up-rising time (marked with the upward arrows), there is a rapid upward deviation of  $\eta_E(\dot{\epsilon}_0; t)$  from the curves of the linear region.

On the other hand, the shear viscosity curve shows two distinctive features: first, the extended Trouton rule is not valid in this case and second, the shear viscosity of PPCN4 increases continuously with time within the experimental time span. This time-dependent thickening behavior, as mentioned before, is called rheopexy. These differences in the time-dependent responses reflect differences in the shear flow-induced vs. elongation-induced internal structure formation in the case of PPCN4 in the molten state. The same experiments conducted with a PP-MA matrix without clay did not exhibit any strain-induced hardening or rheopexy behavior in the molten state.

Fig. 117 represents typical TEM photographs of the center portions of the recovered samples after elongation. The  $x$ - and  $y$ -axes of the elongated specimen correspond to directions parallel and perpendicular to the stretching direction, respectively.

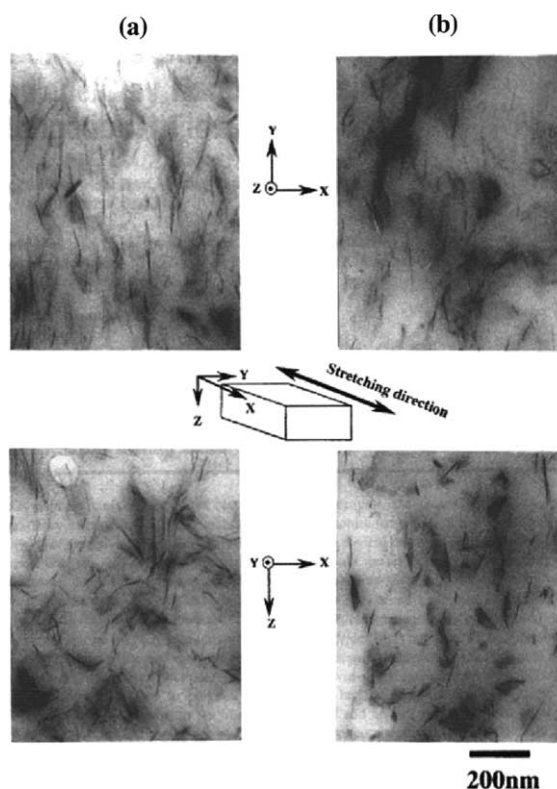


Fig. 117. TEM micrographs showing PPCN4 elongated at 150 °C with (a)  $\dot{\epsilon}_0 = 1.0 \text{ s}^{-1}$  up to  $\epsilon_0 = 1.3$  ( $\lambda = 3.7$ ) and (b)  $\dot{\epsilon}_0 = 0.001 \text{ s}^{-1}$  up to  $\epsilon_0 = 0.5$  ( $\lambda = 1.7$ ), respectively. Upper pictures are in the  $x$ - $y$  plane, and lower are in  $x$ - $z$  plane along the stretching direction [307]. Reproduced from Okamoto, Nam, Maiti, Kotaka, Hasegawa and Usuki by permission of American Chemical Society, USA.

A converging flow is applied to the thickness direction ( $y$ - and  $z$ -axes) with stretching if the assumption of an affine deformation without volume change is valid. Interestingly, for the specimen elongated with a high strain rate, there is perpendicular alignment of the silicate layers (edges) along the stretching direction ( $x$ -axis) in the  $x$ - $y$  plane. For the  $x$ - $z$  plane, the silicate layers (edges) disperse into the PP-MA matrix along the  $z$ -axis direction rather than randomly, but these faces cannot be seen in this plane. On the basis of experimental results and two-directional TEM observations, the authors concluded that the formation of a 'house-of-cards' like structure was observed under slow elongational flow. Details regarding the data collection and explanations are presented in Ref. [307].

## 6.2. Electrorheology

Electrorheological fluids (ERFs), sometimes referred to as ‘smart fluids’, are suspensions comprising polarizable particles dispersed in an insulating media [446]. A mismatch in the conductivity or dielectric constant between the dispersed particles and the continuous medium phase induces polarization upon application of an electric field. The induced particle dipoles in the presence of an electric field tend to attract neighboring particles and cause the particles to form fibril-like structures, which are aligned in the electric field direction [447].

Among various materials [448–450], semiconducting polymers are one of the most important novel intrinsic ER systems, since they have the advantage of a wide range of working temperatures, reduced abrasion, low cost, and a relatively low current density. As a result, the development of a high-performance ER fluid, followed by conducting polymer optimization and tuning, has been the subject of considerable interest for practical applications as a new electromechanic material. Unfortunately, the yield stress and modulus of ER fluids is lower than those of magnetorheological fluids. Thus the performance of conducting polymer-based ER fluids is still insufficient for the successful development of specific applications devices.

Kim et al. [342] first introduced nanocomposites as ERFs using PANI/clay nanocomposites with an intercalated structure. Although PANI/clay intercalated nanocomposites are new for the application of ER materials, the yield stresses of the system were less than 100 Pa at 1.2 kV/mm (20 wt% suspensions). This value is lower than the yield stress of a pure PANI particle system [450]. In other words, no synergistic effect of clay on yield stress was shown.

Recently, Park et al. [451] have observed a remarkable enhancement of the yield stress for electrorheological fluids in PANI-based nanocomposites of clay. In their study [452], they fabricated three kinds of ERFs containing different contents of PANI/clay nanocomposites and pure PANI particles, in order to systematically investigate the effect of nanocomposite particles on the enhancement of yield stress. They observed that there is an optimum ratio between the nanocomposite and the pure PANI particles to produce a minimum yield stress. Details

regarding data collection and explanations can be found in Ref. [452].

## 7. Processing of nanocomposites

### 7.1. Foam processing

For several decades, polymeric foams have been widely used as packing materials because they are lightweight, have a high strength/weight ratio, have superior insulating properties, and high energy absorbing performance. Linear polyolefins such as neat PP have some limitations in foam processing because such polymers do not demonstrate a high strain-induced hardening, which is the primary requirement to withstand the stretching force experienced during the latter stages of bubble growth. The branching of polymer chains, grafting with another copolymer, or blending of branched and linear polymers are the common methods used to improve the extensional viscosity of a polyolefin in order to make it suitable for foam formation. PPCNs have already been shown to exhibit a high modulus and, under uniaxial elongation, a tendency toward strong strain-induced hardening [307]. On the basis of these results, Okamoto et al. [308,313] first conducted foam processing of PPCNs with the expectation that they would provide advanced foams with many desirable properties. They used a physical foaming method, i.e. batch process, in order to conduct foam processing. This process consists of four stages: (a) saturation of CO<sub>2</sub> in the sample at the desired temperature, (b) cell nucleation when the release of CO<sub>2</sub> pressure starts (forming supersaturated CO<sub>2</sub>), (c) cell growth to an equilibrium size during the release of CO<sub>2</sub>, and (4) stabilization of the cell *via* a cooling process of the foamed sample. An illustration of the autoclave setup used in their study shown in Fig. 118. Fig. 119 shows the SEM images of the fracture surface of PP-MA and various PPCN foams at various temperatures. The SEM images exhibit closed-cell structures with cells having 12 or 14-hedron shapes, with the exception of PPCN4 and PPCN7.5 foams prepared at 130.6 °C. The formed cells show their faces mostly as pentagons or hexagons, which express the most energetically stable state of polygon cells. The distribution function of cell sizes calculated from the SEM images is shown

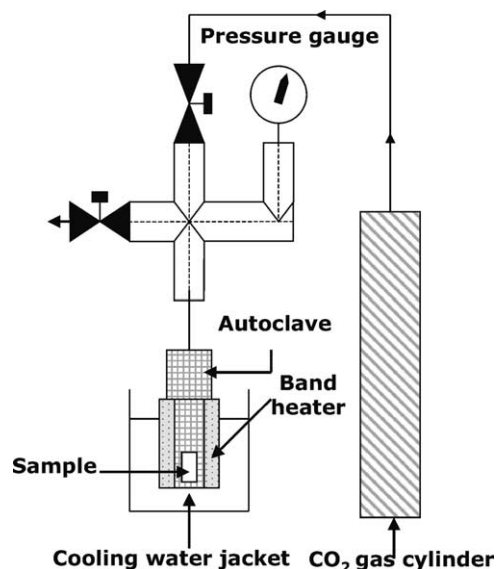


Fig. 118. Schematic representation of autoclave setup [313]. Reproduced from Nam, Maiti, Okamoto, Kotaka, Nakayama, Takada, Ohshima, Usuki, Hasegawa and Okamoto by permission of Society of Plastics Engineers.

in Fig. 120. From the distribution curve it is clearly seen that the PPCN7.5 sample exhibited a bimodal distribution of cell sizes, whereas the other samples followed a Gaussian distribution. Another observation

from Fig. 120 is that the width of the distribution peaks, representing the polydispersity of the cell size, became narrower with the addition of clay into the matrix (PPCN2 and PPCN4). This behavior may be due to the heterogenous clay acting as sites for cell nucleation, and their uniform dispersion in the matrix, which, if present, led to homogeneity in cell size. On the other hand, the cell size of the prepared foams gradually decreases with increasing clay content in the PPCNs. This behavior is due to the intrinsically high viscosity of the materials with increasing clay loading. In contrast, the cell density of the foams behaved in the opposite way. The characteristic parameters of pre- and post-formed samples are summarized in Table 20.

Fig. 121 shows the TEM images of (a) the structure of the nano-cell wall and (b) the junction of the three cell walls in the PPCN4 foam conducted at 134.7 °C. Interestingly, in Fig. 121a, the clay particles in the cell wall align along the interface between the solid and gas phase. In other words, the clay particles arrange along the boundaries of the cells. It also shows the perpendicular alignment of the clay particles to the stretching or elongating direction, which is the main cause of the strain-induced hardening behavior in the uniaxial elongation viscosity [307]. During foam processing, a similar structure formation occurred

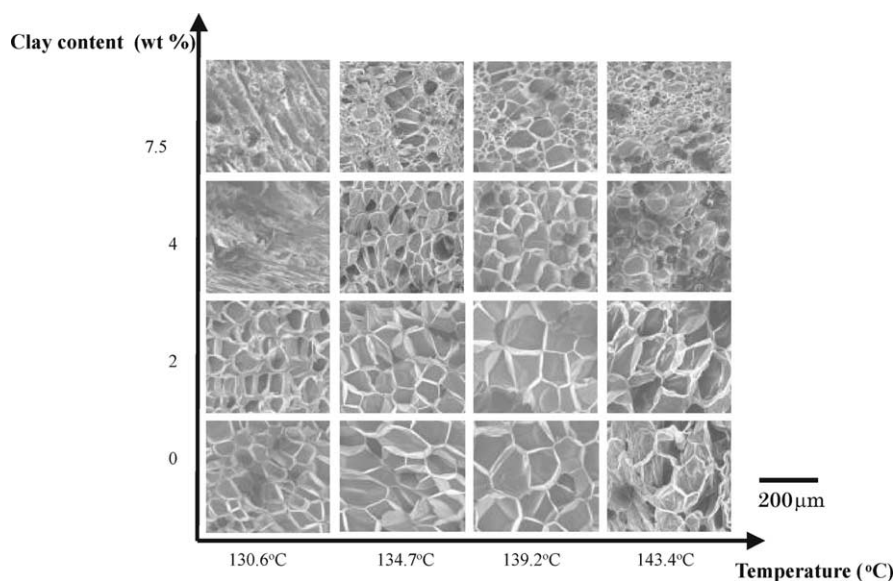


Fig. 119. SEM images for PP-MA and various PPCNs foamed at different temperatures.

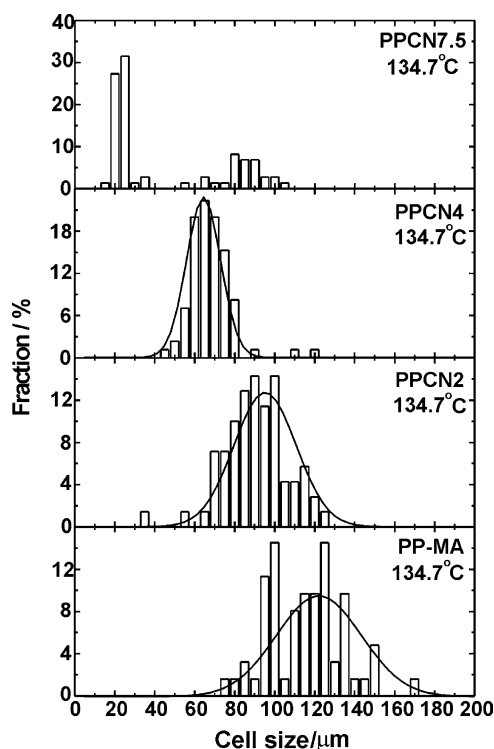


Fig. 120. Typical example for cell size distribution of foamed PP-MA and various PPCNs in experiment at 134.7 °C. Average values  $d$  in  $\mu\text{m}$  and variances  $\sigma_d^2$  in  $\mu\text{m}^2$  in the Gaussian fit through the data are 122.1 and 12.1 for PP-MA foam, 95.1 and 9.8 for PPCN2 foam, 64.4 and 3.1 for PPCN4 foam [313]. Reproduced from Nam, Maiti, Okamoto, Kotaka, Nakayama, Takada, Ohshima, Usuki, Hasegawa and Okamoto by permission of Society of Plastic Engineering.

with a different mechanism. Owing to the biaxial flow of the material during foam processing, the clay particles either turned their faces, or assumed a fixed face orientation and aligned along the flow direction, i.e. along the cell boundary. This type of alignment behavior in clay particles may help cells withstand the stretching force that might otherwise break the thin cell wall, helping to improve the strength of the foam towards. The authors suggest that the clay particles seem to act as a secondary layer to protect the cells from being destroyed by external forces.

The clay particles can also be randomly dispersed in the central part of the junction (see Fig. 121b, marked with arrow). Such behavior of clay particles presumably reflects the effect of the stagnation flow

region of the material under the growth of three contacting cells.

Recently, some literatures are also available [453, 454] related to the reactive extrusion foaming of various nanocomposites.

### 7.2. Shear processing

In order to obtain a material with improved material properties, Okamoto et al. [455] conducted shear-processing of N6/clay nanocomposites (N6CS) in relation to the rheological properties. They found that the mechanical properties of N6CN are significantly improved after shear processing of the material in the molten state. The details regarding the experimental procedure are presented in the relevant literature [455].

## 8. Conclusions: status and prospects of polymer/layered silicate nanocomposites

Several examples of polymer nanocomposites with layered silicates have been presented herein. Nanocomposite preparation with layered silicates has been discussed for a number of polymers, with particular emphasis was placed on biodegradable polymers. The resulting PLS nanocomposites possess several advantages:

- They generally exhibit improved mechanical properties compared to conventional composites, because reinforcement in the PLS nanocomposites occurs in 2D rather than 1D, and no special processing is required to laminate the composites.
- They exhibit a remarkable increase in thermal stability, as well as self-extinguishing characteristics for flammability, such that the flammability of pristine polymers are significantly reduced after nanocomposite formation with layered silicate.
- They show a several-fold reduction in the permeability of small gases, e.g. O<sub>2</sub>, H<sub>2</sub>O, He, CO<sub>2</sub>, and the organic vapor ethyl acetate, because of the formation of a 'tortuous path' in the presence of clay in the nanocomposite.

Table 20

Characteristic parameters of pre- and post-foamed PP-MA and various PPCNs [313]

| Sample       | $T_f$ (°C) | $\rho$ (g ml <sup>-1</sup> ) | $d$ (μm) | $N_c$ ( $\times 10^7$ cells ml <sup>-1</sup> ) | $\delta$ (μm) |
|--------------|------------|------------------------------|----------|--|---------------|
| PP-MA        |            | 0.854                        |          |  |               |
| PP-MA foam   | 130.6      | 0.219                        | 74.4     | 1.8  | 11.88         |
| PP-MA foam   | 134.7      | 0.114                        | 122.1    | 0.48   | 9.07          |
| PP-MA foam   | 139.2      | 0.058                        | 155.3    | 0.25   | 5.56          |
| PP-MA foam   | 143.4      | 0.058                        | 137.3    | 0.35   | 6.46          |
| PPCN2        |            | 0.881                        |          |  |               |
| PPCN2 foam   | 130.6      | 0.213                        | 72.5     | 1.99   | 10.76         |
| PPCN2 foam   | 134.7      | 0.113                        | 95.1     | 1.01   | 6.76          |
| PPCN2 foam   | 139.2      | 0.058                        | 133.3    | 0.39   | 4.62          |
| PPCN2 foam   | 143.4      | 0.113                        | 150.3    | 0.26   | 10.68         |
| PPCN4        |            | 0.900                        |          |  |               |
| PPCN4 foam   | 130.6      | 0.423                        |          |  |               |
| PPCN4 foam   | 134.7      | 0.196                        | 64.4     | 2.92   | 8.41          |
| PPCN4 foam   | 139.2      | 0.193                        | 93.4     | 0.96   | 11.98         |
| PPCN4 foam   | 143.4      | 0.341                        | 56.1     | 3.52   | 15.08         |
| PPCN7.5      |            | 0.921                        |          |  |               |
| PPCN7.5 foam | 130.6      | 0.473                        |          |  |               |
| PPCN7.5 foam | 134.7      | 0.190                        | 35.1     | 18.35  | 4.30          |
| PPCN7.5 foam | 139.2      | 0.131                        | 33.9     | 22.00  | 2.70          |
| PPCN7.5 foam | 143.4      | 0.266                        | 27.5     | 34.2   | 5.11          |

Reproduced from Nam, Maiti, Okamoto, Kotaka, Nakayama, Takada, Ohshima, Usuki, Hasegawa and Okamoto by permission of Society of Plastics Engineers.

- (d) The degradation rate of biodegradable polymers is significantly enhanced in the presence of OMLSs.
- (e) They may be utilized as unique model systems to study the states and dynamics of polymer chains in confined environments, which are fundamental

to many industrially important fields, including tribology, adhesion, fabrication, and catalysis [6,456].

These improved properties are generally attained at lower silicate content ( $\leq 5$  wt%) compared to that

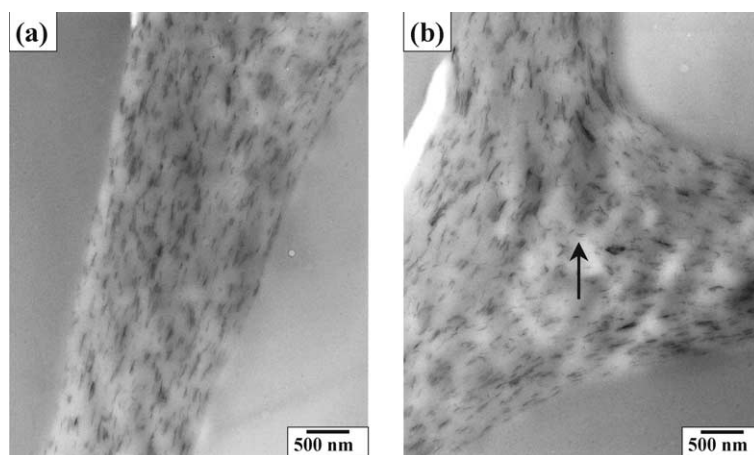


Fig. 121. TEM micrographs from PPCN4 foamed at 134.7 °C: (a) mono-cell wall; (b) junction of three contacting cells [313]. Reproduced from Nam, Maiti, Okamoto, Kotaka, Nakayama, Takada, Ohshima, Usuki, Hasegawa and Okamoto by permission of Society of Plastic Engineering.



of conventionally filled systems. For these reasons, PLS nanocomposites are far lighter in weight than conventional composites, and make them competitive with other materials for specific applications. Furthermore, the unique combination of their key properties and potentially low production costs paves the way to a wide range of applications. Recently, some PLS nanocomposites became commercially available, and were applied to the automotive [293,457] and food packaging industries. Biodegradable polymer based nanocomposites appear to have a very bright future for a wide range of applications as high performance biodegradable materials [458–460].

Although a significant amount of work has already been done on various aspects of PLS nanocomposites, much research still remains in order to understand the complex structure–property relationships in various nanocomposites. It is necessary to conduct detailed rheological measurements of various nanocomposites in the molten state in order to further our knowledge of processing conditions for these materials.

Finally, the fact that PLS nanocomposites show concurrent improvement in various material properties at very low filler content, together with the ease of preparation through simple processes such as melt intercalation, melt extrusion or injection molding, opens a new dimension for plastics and composites.

## Acknowledgements

Financial support from the *Japan Society for the Promotion of Science* to Dr S. Sinha Ray is greatly acknowledged. We express our appreciation to the reviewer for his constructive and meticulous assessment of the manuscript. Grateful appreciation is also extended to the editors for their continuous help during the writing of this article.

## References

- [1] Okada A, Kawasumi M, Usuki A, Kojima Y, Kurauchi T, Kamigaito O. Synthesis and properties of nylon-6/clay hybrids. In: Schaefer DW, Mark JE, editors. Polymer based molecular composites. MRS Symposium Proceedings, Pittsburgh, vol. 171; 1990. p. 45–50.
- [2] Giannelis EP. Polymer layered silicate nanocomposites. *Adv Mater* 1996;8:29–35.
- [3] Giannelis EP, Krishnamoorti R, Manias E. Polymer-silicate nanocomposites: model systems for confined polymers and polymer brushes. *Adv Polym Sci* 1999;138:107–47.
- [4] LeBaron PC, Wang Z, Pinnavaia TJ. Polymer-layered silicate nanocomposites: an overview. *Appl Clay Sci* 1999;15:11–29.
- [5] Vaia RA, Price G, Ruth PN, Nguyen HT, Lichtenhan J. Polymer/layered silicate nanocomposites as high performance ablative materials. *Appl Clay Sci* 1999;15:67–92.
- [6] Biswas M, Sinha Ray S. Recent progress in synthesis and evaluation of polymer–montmorillonite nanocomposites. *Adv Polym Sci* 2001;155:167–221.
- [7] Giannelis EP. Polymer-layered silicate nanocomposites: synthesis, properties and applications. *Appl Organomet Chem* 1998;12:675–80.
- [8] Xu R, Manias E, Snyder AJ, Runt J. New biomedical poly(urethane urea)-layered silicate nanocomposites. *Macromolecules* 2001;34:337–9.
- [9] Bharadwaj RK. Modeling the barrier properties of polymer-layered silicate nanocomposites. *Macromolecules* 2001;34:1989–92.
- [10] Messersmith PB, Giannelis EP. Synthesis and barrier properties of poly( $\epsilon$ -caprolactone)-layered silicate nanocomposites. *J Polym Sci, Part A: Polym Chem* 1995;33:1047–57.
- [11] Yano K, Usuki A, Okada A, Kurauchi T, Kamigaito O. Synthesis and properties of polyimide–clay hybrid. *J Polym Sci, Part A: Polym Chem* 1993;31:2493–8.
- [12] Kojima Y, Usuki A, Kawasumi M, Fukushima Y, Okada A, Kurauchi T, Kamigaito O. Mechanical properties of nylon 6–clay hybrid. *J Mater Res* 1993;8:1179–84.
- [13] Gilman JW, Kashiwagi T, Lichtenhan JD. Flammability studies of polymer-layered silicate nanocomposites. *SAMPE J* 1997;33:40–5.
- [14] Gilman JW. Flammability and thermal stability studies of polymer-layered silicate (clay) nanocomposites. *Appl Clay Sci* 1999;15:31–49.
- [15] Dabrowski F, Bras M Le, Bourbigot S, Gilman JW, Kashiwagi T. PA-6 montmorillonite nanocomposite in intumescent fire retarded EVA. Proceedings of the Eurofillers'99, Lyon-Villeurbanne, France; 6–9 September 1999.
- [16] Bourbigot S, LeBras M, Dabrowski F, Gilman JW, Kashiwagi T. PA-6 clay nanocomposite hybrid as char forming agent in intumescent formulations. *Fire Mater* 2000;24:201–8.
- [17] Gilman JW, Jackson CL, Morgan AB, Harris Jr R, Manias E, Giannelis EP, Wuthenow M, Hilton D, Phillips SH. Flammability properties of polymer-layered silicate nanocomposites. Propylene and polystyrene nanocomposites. *Chem Mater* 2000;12:1866–73.
- [18] Sinha Ray S, Yamada K, Okamoto M, Ueda K. New polylactide/layered silicate nanocomposite: a novel biodegradable material. *Nano Lett* 2002;2:1093–6.
- [19] Dabrowski F, Bourbigot S, Delbel R, Bras ML. Kinetic molding of the thermal degradation of polyamide-6 nanocomposite. *Eur Polym J* 2000;36:273–84.

- [20] Vaia RA, Jandt KD, Kramer EJ, Giannelis EP. Kinetics of polymer melts intercalation. *Macromolecules* 1995;28:8080–5.
- [21] Vaia RA, Giannelis EP. Lattice of polymer melt intercalation in organically-modified layered silicates. *Macromolecules* 1997;30:7990–9.
- [22] Vaia RA, Giannelis EP. Polymer melts intercalation in organically-modified layered silicates: model predictions and experiment. *Macromolecules* 1997;30:8000–9.
- [23] Lee JY, Baljon ARC, Loring RF, Panagiopoulos AZ. Simulation of polymer melt intercalation in layered nanocomposites. *J Chem Phys* 1998;109:10321–30.
- [24] Balazs AC, Singh C, Zhulina E. Modeling the interactions between the polymers and clay surfaces through self-consistent field theory. *Macromolecules* 1998;31:8370–81.
- [25] Balazs AC, Singh C, Zhulina E, Lyatskaya Y. Modeling the phase behavior of polymer–clay composites. *Acc Chem Res* 1999;32:651–7.
- [26] Fredrickson GH, Bicerano J. Barrier properties of oriented disk composites. *J Chem Phys* 1999;110:2181–8.
- [27] Ginzburg VV, Balazs AC. Calculating phase diagram of polymer-platelet mixtures using density functional theory: implication for polymer/clay composites. *Macromolecules* 1999;32:5681–8.
- [28] Baljon ARC, Lee JY, Loring RF. Molecular view of polymer flows into a strongly attractive slit. *J Chem Phys* 2000;111:9068–72.
- [29] Ginzburg VV, Singh C, Balazs AC. Theoretical phase diagram of polymer/clay composites: the role of grafted organic modifier. *Macromolecules* 2000;33:1089–99.
- [30] Kuznetsov D, Balazs AC. Scaling theory for end-functionalized polymers confined between two surfaces: predictions for fabricating polymer nanocomposites. *J Chem Phys* 2000;112:4365–75.
- [31] Lee JY, Baljon ACR, Sogah DY, Loring RF. Molecular dynamics study of intercalation of diblock copolymer into layered silicates. *J Chem Phys* 2000;112:9112–9.
- [32] Singh C, Balazs AC. Effect of polymer architecture on the miscibility of polymer/clay mixtures. *Polym Int* 2000;49:469–71.
- [33] Manias E, Chen E, Krishnamoorti R, Genzer J, Kramer EJ, Giannelis EP. Intercalation kinetics of long polymers in 2 nm confinements. *Macromolecules* 2000;33:7955–66.
- [34] Ginzburg VV, Balazs AC. Calculating phase diagrams for nanocomposites: the effect of adding end-functionalized chains to polymer/clay mixture. *Adv Mater* 2000;12:1805–9.
- [35] Hackett E, Manias E, Giannelis EP. Molecular dynamics simulations of organically modified layered silicates. *J Chem Phys* 1998;108:7410–5.
- [36] Hackett E, Manias E, Giannelis EP. Computer simulation studies of PEO/layered silicate nanocomposites. *Chem Mater* 2000;12:2161–7.
- [37] Anastasiadis SH, Karatasos K, Vlachos G, Manias E, Giannelis EP. Nanoscopic-confinement effects on local dynamics. *Phys Rev Lett* 2000;84:915–8.
- [38] Zax DB, Yang DK, Santos RA, Hegmann H, Giannelis EP, Manias E. Dynamical heterogeneity in nanoconfined poly(styrene) chains. *J Chem Phys* 2000;112:2945–51.
- [39] Manias E, Kuppa V. Molecular simulations of ultra-confined polymers. Polystyrene intercalated in layered-silicates. In: Vaia RA, Krishnamoorti R, editors. *Polymer nanocomposites*. ACS symposium series, vol. 804, Oxford: Oxford University Press; 2002. p. 193–207.
- [40] Kuppa V, Manias E. Computer simulation of PEO/layered-silicate nanocomposites: 2. Lithium dynamics in PEO/Li<sup>+</sup> montmorillonite intercalates. *Chem Mater* 2002;14:2171–5.
- [41] Manias E, Kuppa V. Relaxation of polymers in 2-nm slit-pores: confinement induced segmental dynamics and suppression of the glass transition. *Colloids Surf., A* 2001;187–188:509–21.
- [42] Blumstein A. Polymerization of adsorbed monolayers: II. Thermal degradation of the inserted polymers. *J Polym Sci A* 1965;3:2665–73.
- [43] Theng BKG. *Formation and properties of clay–polymer complexes*. Amsterdam: Elsevier; 1979.
- [44] Vaia RA, Ishii H, Giannelis EP. Synthesis and properties of two-dimensional nanostructures by direct intercalation of polymer melts in layered silicates. *Chem Mater* 1993;5:1694–6.
- [45] Brindly SW, Brown G, editors. *Crystal structure of clay minerals and their X-ray diffraction*. London: Mineralogical Society; 1980.
- [46] Aranda P, Ruiz-Hitzky E. Poly(ethylene oxide)-silicate intercalation materials. *Chem Mater* 1992;4:1395–403.
- [47] Greenland DJ. Adsorption of poly(vinyl alcohols) by montmorillonite. *J Colloid Sci* 1963;18:647–64.
- [48] Krishnamoorti, Vaia RA, Giannelis EP. Structure and dynamics of polymer-layered silicate nanocomposites. *Chem Mater* 1996;8:1728–34.
- [49] Lagaly G. Interaction of alkylamines with different types of layered compounds. *Solid State Ionics* 1986;22:43–51.
- [50] Vaia RA, Teukolsky RK, Giannelis EP. Interlayer structure and molecular environment of alkylammonium layered silicates. *Chem Mater* 1994;6:1017–22.
- [51] Blumstein A, Malhotra SL, Watterson AC. Polymerization of monolayers. V. Tacticity of the insertion poly(methyl methacrylate). *J Polym Sci, Part A-2: Polym Phys* 1970;8:1599–615.
- [52] Lee DC, Jang LW. Preparation and characterization of PMMA–clay composite by emulsion polymerization. *J Appl Polym Sci* 1996;61:1117–22.
- [53] Chen G, Chen X, Lin Z, Ye W, Yao K. Preparation and properties of PMMA/clay nanocomposite. *J Mater Sci Lett* 1999;18:1761–3.
- [54] Chen G, Yao K, Zhao J. Montmorillonite clay/poly(methyl methacrylate) hybrid resin and its barrier property to the plasticizer within poly(vinyl chloride) composite. *J Appl Polym Sci* 1999;73:425–30.
- [55] Tabtiang A, Lumlong S, Venables RA. Influence of preparation method upon structure and relaxation characteristics PMMA/clay composites. *Eur Polym J* 2000;36:2559–68.

- [56] Tabtiang A, Lumlong S, Venables RA. The effects of shear and thermal history upon the microstructure of solution polymerized poly(methyl methacrylate)/clay composites. *Polym Plast Technol Engng* 2000;39:293–303.
- [57] Okamoto M, Morita S, Taguchi H, Kim YH, Kotaka T, Tateyama H. Synthesis and structure of smectic clay/poly(methyl methacrylate) and clay polystyrene nanocomposites via in situ intercalative polymerization. *Polymer* 2000;41:3887–90.
- [58] Bandyopadhyay S, Giannelis EP. Thermal and thermomechanical properties of PMMA nanocomposites. *Polym Mater Sci Engng* 2000;82:208–9.
- [59] Huang X, Brittain WJ. Synthesis and characterization of PMMA nanocomposites by suspension and emulsion polymerization. *Macromolecules* 2001;34:3255–60.
- [60] Zeng C, Lee LJ. Poly(methyl methacrylate) and polystyrene/clay nanocomposites prepared by in-situ polymerization. *Macromolecules* 2001;34:4098–103.
- [61] Salahuddin N, Shehata M. Poly(methyl methacrylate)–montmorillonite composites: preparation, characterization and properties. *Polymer* 2001;42:8379–85.
- [62] Bottcher H, Hallensleben ML, Nu S, Wurm H, Bauer J, Behrens P. Organic/inorganic hybrids by ‘living’/controlled ATRP grafting from layered silicates. *J Mater Chem* 2002; 12:1351–4.
- [63] Zerda AS, Caskey TC, Lesser AJ. Highly concentrated, intercalated silicate nanocomposites: synthesis and characterization. *Macromolecules* 2003;36:1603–8.
- [64] Su S, Wilkie CA. Exfoliated poly(methyl methacrylate) and polystyrene nanocomposites occur when the clay cation contains a vinyl monomer. *J Polym Sci, Part B: Polym Phys* 2003;41:1124–35.
- [65] Forte C, Geppi M, Giamberini S, Ruggeri G, Veracini CA, Mendez B. Structure determination of clay/methylmethacrylate copolymer interlayer complexes by means of  $^{13}\text{C}$  solid state nmr. *Polymer* 1998;39:2651–6.
- [66] Dietsche F, Thomann Y, Thomann R, Mulhaupt R. Translucent acrylic nanocomposites containing anisotropic laminated nanoparticles derived from intercalated layered silicates. *J Appl Polym Sci* 2000;75: 396–405.
- [67] Okamoto M, Morita S, Kotaka T. Dispersed structure and ionic conductivity of smectic clay/polymer nanocomposites. *Polymer* 2001;42:2685–8.
- [68] Okamoto M, Morita S, Kim YH, Kotaka T, Tateyama H. Dispersed structure change of smectic clay/poly(methyl methacrylate) nanocomposites by copolymerization with polar comonomers. *Polymer* 2001;42:1201–6.
- [69] Seckin T, Onal Y, Aksoy I, Yakinci ME. Synthesis and characterization of novel polyacrylate–clay sol–gel materials. *J Mater Sci* 1996;31:3123–7.
- [70] Dietsche F, Mulhaupt R. Thermal properties and flammability of acrylic nanocomposites based upon organophilic layered silicates. *Polym Bull* 1999;43:395–402.
- [71] Chen Z, Huang C, Liu S, Zhang Y, Gong K. Synthesis, characterization and properties of clay–polyacrylate hybrid materials. *J Appl Polym Sci* 2000;75:796–801.
- [72] Billingham J, Breen C, Yarwood J. Adsorption of polyamine, polyacrylic acid and poly(ethylene glycol) on montmorillonite: an in situ study using ATR-FTIR. *Vib Spectrosc* 1997;14: 19–34.
- [73] Lin J, Wu J, Yang Z, Pu M. Synthesis and properties of poly(acrylic acid)/mica superabsorbent nanocomposite. *Macromol Rapid Commun* 2001;22:422–4.
- [74] Blumstein R, Blumstein A, Parikh KK. Synthesis and properties of polyacrylonitrile/clay nanocomposite. *Appl Polym Symp* 1994;25:81–9.
- [75] Sugahara Y, Satakawa S, Kuroda K, Kato C. Evidence for the formation of interlayer polyacrylonitrile in kaolinite. *Clays Clay Miner* 1988;36:343–8.
- [76] Bergaya F, Kooli F. Intercalated polyacrylonitrile/clay nanocomposite. *Clay Miner* 1991;26:33–40.
- [77] Choi YS, Wang KH, Xu M, Chung IJ. Synthesis of exfoliated polyacrylonitrile/Na-MMT nanocomposites via emulsion polymerization. *Chem Mater* 2002;14:2936–9.
- [78] Kato C, Kuroda K, Takahara H. Preparation and electrical properties of quaternary ammonium montmorillonite–polystyrene complexes. *Clays Clay Miner* 1981;29:294–8.
- [79] Akelah A. Polystyrene/clay nanocomposites. In: Prasad PN, Mark JE, Ting FJ, editors. *Polymers and other advanced materials. Emerging technologies and business opportunities*. New York: Plenum Press; 1995. p. 625–30.
- [80] Vaia RA, Jant KD, Kramer EJ, Giannelis EP. Microstructural evaluation of melt-intercalated polymer-organically modified layered silicate nanocomposites. *Chem Mater* 1996;8: 2628–35.
- [81] Park CI, Park OO, Lim JG, Kim HJ. The fabrication of syndiotactic polystyrene/organophilic clay nanocomposites and their properties. *Polymer* 2001;42:7465–75.
- [82] Akelah A, Moet M. Polymer–clay nanocomposites: free-radical grafting of polystyrene on to organophilic montmorillonite interlayers. *J Mater Sci* 1996;31:3589–96.
- [83] Sikka M, Cerini LN, Ghosh SS, Winey KI. Melt intercalation of polystyrene in layered silicates. *J Polym Sci, Part B: Polym Phys* 1996;34:1443–9.
- [84] Laus M, Camerani M, Lelli M, Sparnacci K, Sandrolini F, Francescangeli OF. Hybrid nanocomposites based on polystyrene and a reactive organophilic clay. *J Mater Sci* 1998;33:2883–8.
- [85] Doh JG, Cho I. Synthesis and properties of polystyrene–organoammonium montmorillonite hybrid. *Polym Bull* 1998; 41:511–8.
- [86] Porter TL, Hagerman ME, Reynolds BP, Eastman ME. Inorganic/organic host–guest materials: surface and inter-clay reactions of styrene with copper(II)-exchanged hectorite. *J Polym Sci, Part B: Polym Phys* 1998;36:673–9.
- [87] Hasegawa N, Okamoto H, Kawasumi M, Usuki A. Preparation and mechanical properties of polystyrene/clay hybrid. *J Appl Polym Sci* 1999;74:3359–64.
- [88] Noh MW, Lee DC. Synthesis and characterization of PS–clay nanocomposite by emulsion polymerization. *Polym Bull* 1999;42:619–26.
- [89] Weimer MW, Chen H, Giannelis EP, Sogah DY. Direct synthesis of dispersed nanocomposites by in situ living free

- radical polymerization using a silicate-anchored initiator. *J Am Chem Soc* 1999;121:1615–6.
- [90] Fu X, Qutubuddin S. Polymer–clay nanocomposites: exfoliation of organophilic montmorillonite nanolayers in polystyrene. *Polymer* 2001;42:807–13.
- [91] Chen G, Liu S, Zhang S, Qi Z. Self-assembly in a polystyrene/montmorillonite nanocomposite. *Macromol Rapid Commun* 2000;21:746–9.
- [92] Lim YT, Park OO. Rheological evidence for the microstructure of intercalated polymer/layered silicate nanocomposite. *Macromol Rapid Commun* 2000;21:231–5.
- [93] Hoffman B, Dietrich C, Thomann R, Friedrich C, Mulhaupt R. Morphology and rheology of polystyrene nanocomposites based upon organoclay. *Macromol Rapid Commun* 2000;21:57–61.
- [94] Zilg C, Thomann R, Baumert M, Finter J, Mulhaupt R. Organic/inorganic hybrid materials and nanocomposites based upon layered silicate modified with cyclic imidines. *Macromol Rapid Commun* 2000;21:1214–9.
- [95] Wu HD, Tseng CR, Chang FC. Chain conformation and crystallization behavior of the syndiotactic polystyrene nanocomposites studied using Fourier transform infrared analysis. *Macromolecules* 2001;34:2992–9.
- [96] Xiao P, Xiao M, Gong K. Preparation of exfoliated graphite/polystyrene composite by polymerization-filling technique. *Polymer* 2001;42:4813–6.
- [97] Tseng C-R, Wu J-Y, Lee H-Y, Chang F-C. Preparation and crystallization behavior of syndiotactic polystyrene–clay nanocomposites. *Polymer* 2001;42:10063–70.
- [98] Zhu J, Morgan AB, Lamelas FJ, Wilkie CA. Fire properties of polystyrene–clay nanocomposites. *Chem Mater* 2001;13:3774–80.
- [99] Zeng QH, Wang DZ, Yu AB, Lu GQ. Synthesis of polymer–montmorillonite nanocomposites by in situ intercalative polymerization. *Nanotechnology* 2002;13:549–53.
- [100] Beyer FL, Tan NCB, Dasgupta A, Galvin ME. Polymer-layered silicate nanocomposites from model surfactants. *Chem Mater* 2002;14:2983–8.
- [101] Gilman JW, Awad WH, Davis RD, Shields J, Harris Jr RH, Davis C, Morgan AB, Sutto TE, Callahan J, Trulove PC, DeLong HC. Polymer/layered silicate nanocomposites from thermally stable trialkylimidazolium-treated montmorillonite. *Chem Mater* 2002;14:3776–85.
- [102] Argoti SD, Reeder S, Zhao H, Shipp DA. Polystyrene nanocomposites using atom transfer radical polymerization. *Polym Prepr (USA)* 2002;43:267–8.
- [103] Gelfer MY, Hyun HS, Liu L, Hsiao BS, Chu B, Rafailovich M, Si M, Zaitsev V. Effect of organoclays on morphology and thermal and rheological properties of polystyrene and poly(methyl methacrylate) blends. *J Polym Sci, Part B: Polym Phys* 2003;41:44–54.
- [104] Friedlander HZ, Frink CR. Organized polymerization. III. Monomers intercalated in montmorillonite. *J Polym Sci, Part B* 1964;2:475–9.
- [105] Churochkina NA, Starodoubtsev SG, Khokhlov AR. Swelling and collapse of the gel composites based on natural and slightly charged poly(acrylamide) gels containing Na<sup>+</sup>-montmorillonite. *Polym Gels Networks* 1998;6:205–15.
- [106] Gao D, Heimann RB, Williams MC, Wardhaugh LT, Muhammad M. Rheological properties of poly(acrylamide)–bentonite composite hydrogels. *J Mater Sci* 1999;34:1543.
- [107] Xia X, Yih J, D'Souza NA, Hu Z. Swelling and mechanical behavior of poly(*N*-isopropylacrylamide)/Na<sup>+</sup> montmorillonite layered silicates composite gels. *Polymer* 2003;44:3389–93.
- [108] Wheeler A. Poly(vinyl alcohol)/clay nanocomposites. *US Pat* 1958; 2,847,391.
- [109] Ogata N, Kawakage S, Ogihara T. Poly(vinyl alcohol)–clay and poly(ethylene oxide)–clay blend prepared using water as solvent. *J Appl Polym Sci* 1997;66:573–81.
- [110] Matsuyama H, Young JF. Intercalation of polymers in calcium silicate hydrate: a new synthetic approach to biocomposites. *Chem Mater* 1999;11:16–19.
- [111] Strawhecker KE, Manias E. Structure and properties of poly(vinyl alcohol)/Na<sup>+</sup>-montmorillonite nanocomposites. *Chem Mater* 2000;12:2943–9.
- [112] Wang Y, Wang Y, Yan D. Properties of poly(vinyl alcohol)/montmorillonite nanocomposite fiber. *Polym Prepr (USA)* 2003;44:1102–3.
- [113] Francis CW. Adsorption of polyvinylpyrrolidone on reference clay minerals. *Soil Sci* 1973;115:40–54.
- [114] Carrado KA, Xu L. In-situ synthesis of polymer–clay nanocomposites from silicate gel. *Chem Mater* 1998;10:1440–5.
- [115] Gultek A, Seckin T, Onal Y, Icduygu G. Preparation and phenol captivating properties of polyvinylpyrrolidone–montmorillonite hybrid materials. *J Appl Polym Sci* 2001;81:512–9.
- [116] Levy R, Francis CW. Interlayer adsorption of polyvinylpyrrolidone on montmorillonite. *J Colloid Interface Sci* 1975;50:442–50.
- [117] Koo CM, Ham HT, Choi MH, Kim SO, Chung JJ. Characteristic of poly(vinyl pyrrolidone)-layered silicate nanocomposites prepared by attrition ball milling. *Polymer* 2003;44:681–9.
- [118] Komori Y, Sugahara Y, Kuroda K. Direct intercalation of poly(vinylpyrrolidinone) into kaolinite by a refined guest displacement method. *Chem Mater* 1999;11:3–6.
- [119] Nisha A, Rajeswari MK, Dhamodharan R. Intercalative redox polymerization and characterization of poly(*n*-vinyl-2-pyrrolidinone) in the gallery of vermiculite: a novel inorganic–organic hybrid material. *J Appl Polym Sci* 2000;76:1825–30.
- [120] Fournaris KG, Karakassides MA, Petridis D, Yiannakopoulou K. Clay–polyvinylpyridine nanocomposites. *Chem Mater* 1999;11:2372–81.
- [121] Parfitt RL, Greenland DJ. The adsorption of poly(ethylene glycols) on clay minerals. *Clay Miner* 1970;8:305–15.
- [122] Zhao X, Urano K, Ogasawara S. Adsorption of poly(ethylene vinyl alcohol) from aqueous solution on montmorillonite clays. *Colloid Polym Sci* 1989;267:899–906.

- [123] Priya L, Jog JP. Intercalated poly(vinylidene fluoride)/clay nanocomposites: structure and properties. *J Polym Sci, Part B: Polym Phys* 2003;41:31–8.
- [124] Oriakhi CO, Zhang X, Lerner MM. Synthesis and luminescence properties of a poly(*p*-phenylenevinylene)/montmorillonite layered nanocomposite. *Appl Clay Sci* 1999;15:109–18.
- [125] Hsu SLC, Chang KC. Synthesis and properties of poly-benzoxazole–clay nanocomposites. *Polymer* 2002;43:4097–101.
- [126] Kim SW, Jo WH, Lee MS, Ko MB, Jho JY. Preparation of clay-dispersed poly(styrene-*co*-acrylonitrile) nanocomposites using poly( $\epsilon$ -caprolactone) as a compatibilizer. *Polymer* 2001;42:9837–42.
- [127] Artzi N, Nir Y, Nakris M, Seigmann A. Melt blending of ethylene–vinyl alcohol copolymer/clay nanocomposites: effect of the clay type and processing conditions. *J Polym Sci, Part B: Polym Phys* 2002;40:1741–53.
- [128] Ren J, Silva AS, Krishnamoorti R. Linear viscoelasticity of disordered polystyrene–polyisoprene block copolymer based layered-silicate nanocomposites. *Macromolecules* 2000;33:3739–46.
- [129] Mitchell CA, Krishnamoorti R. Rheological properties of diblock copolymer/layered-silicate nanocomposites. *J Polym Sci, Part B: Polym Phys* 2002;40:1434–43.
- [130] Mark JE. Ceramic reinforced polymers and polymer-modified ceramics. *Polym Engng Sci* 1996;36:2905–20.
- [131] Usuki A, Kawasumi M, Kojima Y, Okada A, Kurauchi T, Kamigaito O. Swelling behavior of montmorillonite cation exchanged for  $\omega$ -amine acid by  $\epsilon$ -caprolactam. *J Mater Res* 1993;8:1174–8.
- [132] Usuki A, Kojima Y, Kawasumi M, Okada A, Fukushima Y, Kurauchi T, Kamigaito O. Synthesis of nylon-6–clay hybrid. *J Mater Res* 1993;8:1179–83.
- [133] Kojima Y, Usuki A, Kawasumi M, Okada A, Fukushima Y, Kurauchi T, Kamigaito O. Mechanical properties of nylon 6–clay hybrid. *J Mater Res* 1993;8:1185–9.
- [134] Kojima Y, Usuki A, Kawasumi M, Okada A, Kurauchi T, Kamigaito O. Synthesis of nylon-6 hybrid by montmorillonite intercalated with  $\epsilon$ -caprolactam. *J Polym Sci, Part A: Polym Chem* 1993;31:983–6.
- [135] Kojima Y, Usuki A, Kawasumi M, Okada A, Kurauchi T, Kamigaito O. One-pot synthesis of nylon 6–clay hybrid. *J Polym Sci, Part A: Polym Chem* 1993;31:1755–8.
- [136] Kojima Y, Usuki A, Kawasumi M, Okada A, Kurauchi T, Kamigaito O. Sorption of water in nylon 6–clay hybrid. *J Appl Polym Sci* 1993;49:1259–64.
- [137] Okada A, Usuki A. The chemistry of polymer–clay hybrids. *Mater Sci Engng* 1995;C3:109–15.
- [138] Kojima Y, Usuki A, Kawasumi M, Okada A, Kurauchi T, Kamigaito O, Kaji K. Fine structure of nylon 6–clay hybrid. *J Polym Sci, Part B: Polym Phys* 1994;32:625–30.
- [139] Kojima Y, Usuki A, Kawasumi M, Okada A, Kurauchi T, Kamigaito O, Kaji K. Novel preferred orientation in injection-molded nylon 6–clay nanocomposites. *J Polym Sci, Part B: Polym Phys* 1995;33:1039–45.
- [140] Usuki A, Koiwai A, Kojima Y, Kawasumi M, Okada A, Kurauchi T, Kamigaito O. Nylon 6/clay nanocomposites. *J Appl Polym Sci* 1995;55:119–23.
- [141] Alexandre M, Dubois P. Polymer-layered silicate nanocomposites: preparation, properties and uses of a new class of materials. *Mater Sci Engng R* 2000;28:1–63.
- [142] Liu LM, Qi ZN, Zhu XG. Studies on nylon 6/clay nanocomposites by melt-intercalation process. *J Appl Polym Sci* 1999;71:1133–8.
- [143] Wu SH, Wang FY, Ma C-CM, Chang WC, Kuo CT, Kuan HC, Chen WJ. Mechanical, thermal and morphological properties of glass fiber and carbon fiber reinforced polyamide-6 and polyamide-6/clay nanocomposites. *Mater Lett* 2001;49:327–33.
- [144] Lincoln DM, Vaia RA, Wang ZG, Hsiao BS. Secondary structure and elevated temperature crystallite morphology of nylon-6/layered silicate nanocomposites. *Polymer* 2001;42:1621–31.
- [145] Medellin-Rodriguez FJ, Burger C, Hsiao BS, Chu B, Vaia RA, Phillips S. Time-resolved shear behavior of end-tethered nylon 6–clay nanocomposites followed by non-isothermal crystallization. *Polymer* 2001;42:9015–23.
- [146] Dennis HR, Hunter DL, Chang D, Kim S, White JL, Cho JW, Paul DR. Effect of melt processing conditions on the extent of exfoliation in organoclay-based nanocomposites. *Polymer* 2001;42:9513–22.
- [147] VanderHart DL, Asano A, Gilman JW. Solid-state NMR. Solid-state NMR investigation of paramagnetic nylon-6 clay nanocomposites. 1. Crystallinity, morphology, and the direct influence of  $\text{Fe}^{3+}$  on nuclear spins. *Chem Mater* 2001;13:3781–95.
- [148] Shelley JS, Mather PT, DeVries KL. Reinforcement and environmental degradation of nylon 6/clay nanocomposites. *Polymer* 2001;42:5849–58.
- [149] Fornes TD, Yoon PJ, Keskkula H, Paul DR. Nylon 6 nanocomposites: the effect of matrix molecular weight. *Polymer* 2001;42:9929–40.
- [150] Liu X, Wu Q. Phase transition in nylon 6/clay nanocomposites on annealing. *Polymer* 2002;43:1933–6.
- [151] Fornes TD, Yoon PJ, Hunter DL, Keskkula H, Paul DR. Effect of organoclay structure on nylon-6 nanocomposite morphology and properties. *Polymer* 2002;43:5915–33.
- [152] Kamal MR, Borse NK, Garcia-Rejon A. The effect of pressure and clay on the crystallization behavior and kinetics of polyamide-6 in nanocomposites. *Polym Engng Sci* 2002;42:1883–96.
- [153] Bureau MN, Denault J, Cole KC, Enright GD. The role of crystallinity and reinforcement in the mechanical behavior of polyamide-6/clay nanocomposites. *Polym Engng Sci* 2002;42:1897–907.
- [154] Uribe-Arocha P, Mehler C, Puskas JE, Altstadt V. Effect of sample thickness on the mechanical properties of molded polyamide-6 and polyamide-6 clay nanocomposites. *Polymer* 2003;44:2441–6.
- [155] Hasegawa N, Okamoto H, Kato M, Usuki A, Sato N. Nylon 6–montmorillonite nanocomposites prepared by

- compounding nylon 6 with Na-montmorillonite slurry. *Polymer* 2003;44:2933–7.
- [156] Ding Y, Jones DJ, Maireles-Torres P, Roziere J. Two-dimensional nanocomposites: alternating inorganic–organic polymer layers in zirconium phosphate. *Chem Mater* 1995;7:562–71.
- [157] Reichert P, Kressler J, Thomann R, Mulhaupt R, Stoppelmann G. Nanocomposites based on a synthetic layer silicate and polyamide-12. *Acta Polym* 1998;49:116–23.
- [158] Hoffman B, Kressler J, Stoppelmann G, Friedrich C, Kim GM. Rheology of nanocomposites based on layered silicate and polyamide-12. *Colloid Polym Sci* 2000;278:629–36.
- [159] Giza E, Ito H, Kikutani T, Okui N. Structural control of polyamide 6/clay nanocomposites fibers in-line drawing process. *J Polym Engng* 2000;20:403–25.
- [160] Kim GM, Lee DH, Hoffmann B, Kresler J, Stoppelmann G. Influence of nanofillers on the deformation process in layered silicate/polyamide-12 nanocomposites. *Polymer* 2001;42:1095–100.
- [161] Nair SV, Goettler LA, Lysek BA. Toughness of nanoscale and multiscale polyamide-6,6 composites. *Polym Engng Sci* 2002;42:1872–82.
- [162] Liu X, Wu Q, Zhang Q, Mo Z. Phase transition in polyamide-66/montmorillonite nanocomposites on annealing. *J Polym Sci, Part B: Polym Phys* 2003;44:6367.
- [163] Messersmith PB, Giannelis EP. Polymer-layered silicate nanocomposites: in-situ intercalative polymerization of  $\epsilon$ -caprolactone in layered silicates. *Chem Mater* 1993;5:1064–6.
- [164] Jimenez G, Ogata N, Kawai H, Ogihara T. Structure and thermal/mechanical properties of poly( $\epsilon$ -caprolactone)–clay blend. *J Appl Polym Sci* 1997;64:2211–20.
- [165] Krishnamoorti R, Giannelis EP. Rheology of end-tethered polymer layered silicate nanocomposites. *Macromolecules* 1997;30:4097–102.
- [166] Utracki LA. Flow behavior of nanocomposites with polycaprolacton matrix. PPS Meeting Proceedings, Taipei, Taiwan; Nov. 4–8, 2002.
- [167] Pantoustier N, Alexandre M, Degee P, Calberg C, Jerome R, Henrist C, Cloots R, Rulmont A, Dubois P. Poly( $\epsilon$ -caprolactone) layered silicate nanocomposites: effect of clay surface modifiers on the melt intercalation process. *e-Polymer* 2001;9:1–9.
- [168] Shima R, Utracki LA, Garcia-Rejon A. Pressure–volume–temperature relations of a poly- $\epsilon$ -caprolactam and its nanocomposite. *Compos Interfaces* 2001;8:345–53.
- [169] Pantoustier N, Lepoittevin B, Alexandre M, Kubies D, Calberg C, Jerome R, Dubois P. Biodegradable polyester layered silicate nanocomposites based on poly( $\epsilon$ -caprolactone). *Polym Engng Sci* 2002;42:1928–37.
- [170] Lepoittevin B, Pantoustier N, Devalckenaere M, Alexandre M, Kubies D, Calderg C, Jerome R, Dubois P. Poly( $\epsilon$ -caprolactone)/clay nanocomposites by in-situ intercalative polymerization catalyzed by dibutyltindimethoxide. *Macromolecules* 2002;35:8385–90.
- [171] Lepoittevin B, Devalckenaere M, Pantoustier N, Alexandre M, Kubies D, Calberg C, Jerome R, Dubois P. Poly( $\epsilon$ -caprolactone)/clay nanocomposites prepared by melt intercalation: mechanical, thermal and rheological properties. *Polymer* 2002;43:4017–23.
- [172] Gorrasi G, Tortora M, Vittoria V, Pollet E, Lepoittevin B, Alexandre M, Dubois P. Vapor barrier properties of polycaprolactone montmorillonite nanocomposites: effect of clay dispersion. *Polymer* 2003;44:2271–9.
- [173] Utracki LA, Simha R, Garcia-Rejon A. Pressure–volume–temperature dependence of poly- $\epsilon$ -caprolactam/clay nanocomposites. *Macromolecules* 2003;36:2114–21.
- [174] Lepoittevin B, Pantoustier N, Devalckenaere M, Alexandre M, Calberg C, Jerome R, Henrist C, Rulmont A, Dubois P. Polymer/layered silicate nanocomposites by combined intercalative polymerization and melt intercalation: a master batch process. *Polymer* 2003;44:2033–40.
- [175] Wu TM, Cheng J-C, Yan M-C. Crystallization and thermoelectric behavior of conductive-filler-filled poly( $\epsilon$ -caprolactone)/poly(vinyl butyral)/montmorillonite nanocomposites. *Polymer* 2003;44:2553–62.
- [176] Ke YC, Long C, Qi Z. Crystallization, properties, and crystal and nanoscale morphology of PET–clay nanocomposites. *J Appl Polym Sci* 1999;71:1139–46.
- [177] Sekelik DJ, Stepanov Enazarenko S, Schiraldi D, Hiltner A, Baer E. Oxygen barrier properties of crystallized and talc-filled poly(ethylene terephthalate). *J Polym Sci, Part B: Polym Phys* 1999;37:847–57.
- [178] Matayabas Jr JC, Turner SR, Sublett BJ, Connell GW, Barbee RB. Nanocomposite technology for enhancing the gas barrier of polyethylene terephthalate. *PCT Int Appl Wo* 98/29499; July 9, 1998.
- [179] Takekoshi T, Khouri FF, Campbell JR, Jordan TC, Dai KH. PET nanocomposites prepared by in situ incorporation of varying amounts of four different organoclays. *US Pat* 5,530,052 (General Electric Co.); June 25, 1996.
- [180] Tsai TY. Polyethylene terephthalate–clay nanocomposites. In: Pinnavaia TJ, Beall GW, editors. *Polymer–clay nanocomposites*. England: Wiley; 2000. p. 173–89.
- [181] Davis CH, Mathias LJ, Gilman JW, Schiraldi DA, Shields JR, Trulove P, Sutto TE, Delong HC. Effects of melt-processing conditions on the quality of poly(ethylene terephthalate) montmorillonite clay nanocomposites. *J Polym Sci, Part B: Polym Phys* 2002;40:2661–6.
- [182] Imai Y, Nishimura S, Abe E, Tateyama H, Abiko A, Yamaguchi A, Aoyama T, Taguchi H. High-modulus poly(ethylene terephthalate)/expandable fluorine mica nanocomposites with a novel reactive compatibilizer. *Chem Mater* 2002;14:477–9.
- [183] Liu Z, Yan D, Chen K. Preparation of poly(trimethylene terephthalate)/montmorillonite nanocomposite by melt intercalation. *Polym Prepr (USA)* 2003;44:1138–9.
- [184] Duan Q, Yan D. Poly(trimethylene terephthalate)–montmorillonite nanocomposite made by in situ polymerization. *Polym Prepr (USA)* 2003;44:1140–1.
- [185] Chisholm BJ, Moore RB, Barber G, Khouri F, Hempstead A, Larsen M, Olson E, Kelley J, Balch G, Caraher J. Nanocomposites derived from sulfonated poly(butylene terephthalate). *Macromolecules* 2002;35:5508–16.

- [186] Huang X, Lewis S, Brittain WJ, Vaia RA. Synthesis of polycarbonate-layered silicate nanocomposites via cyclic oligomers. *Macromolecules* 2000;33:2000–4.
- [187] Mitsunaga M, Ito Y, Sinha Ray S, Okamoto M, Hironaka K. Polycarbonate/clay nanocomposites: nanostructure control and foam processing. *Macromol Mater Engng* 2003;288:543–8.
- [188] Wu J, Lerner MM. Structural, thermal, and electrical characterization of layered nanocomposites derived from sodium-montmorillonite and polyethers. *Chem Mater* 1993;5:835–8.
- [189] Vaia RA, Vasudevan S, Krawiec W, Scanlon LG, Giannelis EP. New polymer electrolyte nanocomposites: melt intercalation of poly(ethylene oxide) in mica-type silicates. *Adv Mater* 1995;7:154–6.
- [190] Wong S, Vasudevan S, Vaia RA, Giannelis EP, Zax D. Dynamics in a confined polymer electrolyte: a  $^7\text{Li}$  and  $^2\text{H}$  NMR study. *J Am Chem Soc* 1995;117:7568–9.
- [191] Vaia RA, Sauer BB, Tse OK, Giannelis EP. Relaxations of confined chains in polymer nanocomposites: glass transition properties of poly(ethylene oxide) intercalated in montmorillonite. *J Polym Sci, Part B: Polym Phys* 1997;35:59–67.
- [192] Aranda P, Galvan JC, Ruiz-Hitzky E. Isotropic PEO–clay nanocomposites prepared by microwave-assisted blending intercalation. In: Laine RM, Sanchez C, Brinker JF, Giannelis EP, editors. *Organic/inorganic hybrid materials. MRS Symposium Proceedings, Warrendale, PA, vol. 519; 1998. p. 375–80.*
- [193] Hatharasinghe HLM, Smalley MV, Swenson J, Williams CD, Heenan RK, King SM. Neutron scattering study of vermiculite–PEO mixtures. *J Phys Chem B* 1998;102:6804–8.
- [194] Hernan L, Morales J, Santos J. Synthesis and characterization of poly(ethylene oxide) nanocomposites of misfit layer chalcogenides. *J Solid State Chem* 1998;141:327–9.
- [195] Harris DJ, Bonagamba TJ, Schmidt-Rhor K. Conformation of poly(ethylene oxide) intercalated in clay and  $\text{MoS}_2$  studied by two dimensional double-quantum NMR. *Macromolecules* 1999;32:6718–24.
- [196] Chen W, Xu Q, Yuan RZ. Modification of poly(ethylene oxide) with polymethylmethacrylate in polymer-layered silicate nanocomposites. *J Mater Sci Lett* 1999;18:711–3.
- [197] Bujdak J, Hackett E, Giannelis EP. Effect of layer charge on the intercalation of poly(ethylene oxide) in layered silicates: implications on nanocomposite polymer electrolytes. *Chem Mater* 2000;12:2168–74.
- [198] Schmidt G, Nakatani AI, Butler PD, Karim A, Han CC. Shear orientation of viscoelastic polymer–clay solutions probed by flow birefringence and SANS. *Macromolecules* 2000;33:7219–22.
- [199] Xiao Y, Hu KA, Yu QC, Wu RJ. Preparation of polyethylene oxide/ $\text{Li}_x\text{V}_{2-\delta}\text{O}_{4-\delta}$  nanocomposites. *J Appl Polym Sci* 2001;80:2162–6.
- [200] Choi HJ, Kim SG, Hyun YH, Jhon MS. Preparation and rheological characteristics of solvent-cast poly(ethylene oxide)/montmorillonite nanocomposites. *Macromol Rapid Commun* 2001;22:320–5.
- [201] Hyun YH, Lim ST, Choi HJ, Jhon MS. Rheology of poly(ethylene oxide)/organoclay nanocomposites. *Macromolecules* 2001;34:8084–93.
- [202] Liao B, Song M, Liang H, Pang Y. Polymer-layered silicate nanocomposites. 1. A study of poly(ethylene oxide)/ $\text{Na}^+$ -montmorillonite nanocomposites as polyelectrolytes and polyethylene-*block*-poly(ethylene glycol) copolymer/ $\text{Na}^+$ -montmorillonite nanocomposites as fillers for reinforcement of polyethylene. *Polymer* 2001;42:10007–11.
- [203] Chen HW, Chang FC. The novel polymer electrolyte nanocomposite composed of poly(ethylene oxide), lithium triflate and mineral clay. *Polymer* 2001;42:9763–9.
- [204] Chen HW, Chiu CY, Wu HD, Shen IW, Chang FC. Solid-state electrolyte nanocomposites based on poly(ethylene oxide), poly(oxypropylene) diamine, mineral clay and lithium perchlorate. *Polymer* 2002;43:5011–6.
- [205] Shen Z, Simon GP, Cheng YB. Comparison of solution intercalation and melt intercalation of polymer–clay nanocomposites. *Polymer* 2002;43:4251–60.
- [206] Lim SK, Kim JW, Chin I, Kwon YK, Choi HJ. Preparation and interaction characteristics of organically modified montmorillonite nanocomposite with miscible polymer blend of poly(ethylene oxide) and poly(methyl methacrylate). *Chem Mater* 2002;14:1989–94.
- [207] Strawhecker KE, Manias E. Crystallization behavior of poly(ethylene oxide) in the presence of  $\text{Na}^+$ -montmorillonite fillers. *Chem Mater* 2003;15:844–9.
- [208] Chaiko DJ. New poly(ethylene oxide)–clay composites. *Chem Mater* 2003;15:1105–10.
- [209] Fischer HR, Gielgens LH, Koster TPM. Ethylene oxide copolymers/clay nanocomposites. In: Laine RM, Sanchez C, Brinker JF, Giannelis EP, editors. *Organic/inorganic hybrid materials. MRS Symposium Proceedings, Warrendale, vol. 519; 1998. p. 517–20.*
- [210] Fischer HR, Gielgens LH, Koster TPM. Nanocomposites from polymers and layered minerals. *Acta Polym* 1999;50:122–6.
- [211] Wei L, Rocci-Lane M, Brazis P, Kannevorf CR, Kim YI, Lee W, Choy JH, Kanatzidis MG.  $\alpha\text{-RuCl}_3$ /polymer nanocomposites: the first group of intercalative nanocomposites with transition metal halides. *J Am Chem Soc* 2000;122:6629–40.
- [212] Burnside SD, Giannelis EP. Synthesis and properties of new poly(dimethylsiloxane) nanocomposites. *Chem Mater* 1995;7:1597–600.
- [213] Wang SJ, Long C, Wang X, Li Q, Qi Z. Synthesis and properties of silicone rubber organomontmorillonite hybrid nanocomposites. *J Appl Polym Sci* 1998;69:1557–61.
- [214] Takeuchi H, Cohen C. Reinforcement of poly(dimethylsiloxane) elastomers by chain-end anchoring to clay particles. *Macromolecules* 1999;32:6792–9.
- [215] Burnside SD, Giannelis EP. Nanostructure and properties of polysiloxane-layered silicate nanocomposites. *J Polym Sci, Part B: Polym Phys* 2000;38:1595–604.
- [216] Bokobza L, Nugay N. Orientational effect of mica in fumed silica reinforced composites. *J Appl Polym Sci* 2001;81:215–22.

- [217] Osman MA, Atallah A, Muller M, Suter UW. Reinforcement of poly(dimethylsiloxane) networks by mica flakes. *Polymer* 2001;42:6545–56.
- [218] Nugay N, Kusefoglu S, Erman B. Swelling and static-dynamic mechanical behavior of mica-reinforced linear and star-branched polybutadiene composites. *J Appl Polym Sci* 1997;66:1943–52.
- [219] Akelah A, El-Borai MA, El-Aal MFA, Rehab A, Abou-Zeid MS. New catalytic systems based on intercalated polymer-montmorillonite supports. *Macromol Chem Phys* 1999;200:955–63.
- [220] Zhang L, Wang Y, Wang Y, Sui Y, Yu D. Morphology and mechanical properties of clay/styrene-butadiene rubber nanocomposites. *J Appl Polym Sci* 2000;78:1873–8.
- [221] Wang Y, Zhang L, Tang C, Yu D. Preparation and characterization of rubber-clay nanocomposites. *J Appl Polym Sci* 2000;78:1879–83.
- [222] Manna AK, Tripathy DK, De PP, De SK, Chatterjee MK, Pfeiffer DG. Bonding between epoxidized natural rubber and clay in presence of silane coupling agent. *J Appl Polym Sci* 1999;72:1895–903.
- [223] Vu YT, Mark JE, Pham LH, Engelhardt M. Clay nanolayer reinforcement of *cis*-1,4-polyisoprene and epoxidized natural rubber. *J Appl Polym Sci* 2001;82:1391–403.
- [224] Messersmith PB, Giannelis EP. Synthesis and characterization of layered silicate-epoxy nanocomposites. *Chem Mater* 1994;6:1719–25.
- [225] Lan T, Pinnavaia TJ. Clay-reinforced epoxy nanocomposites. *Chem Mater* 1994;6:2216–9.
- [226] Wang MS, Pinnavaia TJ. Clay-polymer nanocomposites formed from acidic derivatives of montmorillonite and an epoxy resin. *Chem Mater* 1994;6:468–74.
- [227] Lan T, Kaviratna PD, Pinnavaia TJ. Mechanism of clay tactoid exfoliation in epoxy-clay nanocomposites. *Chem Mater* 1995;7:2144–50.
- [228] Wang Z, Lan T, Pinnavaia TJ. Hybrid organic-inorganic nanocomposites formed from an epoxy polymer and a layered silicic acid (Magadiite). *Chem Mater* 1996;8:2200–4.
- [229] Shi H, Lan T, Pinnavaia TJ. Interfacial effects on the reinforcement properties of polymer-organoclay nanocomposites. *Chem Mater* 1996;8:1584–7.
- [230] Pinnavaia TJ, Lan T, Wang Z, Shi H, Kaviratna PD. Mechanism of clay tactoid exfoliation in epoxy-clay nanocomposites. In: Chow GM, Gonsalves KE, editors. *Nanotechnology. Molecularly designated materials*. ACS Symposium Series, Washington, vol. 622; 1996. p. 250–4.
- [231] Wang Z, Pinnavaia TJ. Hybrid organic-inorganic nanocomposites: exfoliation of magadiite nanolayers in an elastomeric epoxy polymer. *Chem Mater* 1998;10:1820–6.
- [232] Wang Z, Massam J, Pinnavaia TJ. Epoxy-clay nanocomposites. In: Pinnavaia TJ, Beall GW, editors. *Polymer-clay nanocomposites*. New York: Wiley; 2000. p. 127–49.
- [233] Lee DC, Jang JW. Characterization of epoxy-clay hybrid composite prepared by emulsion polymerization. *J Appl Polym Sci* 1998;68:1997–2005.
- [234] Zilg C, Mulhaupt R, Finter J. Morphology and toughness/stiffness balance of nanocomposites based upon anhydride-cured epoxy resins and layered silicates. *Macromol Chem Phys* 1999;200:661–70.
- [235] Kornmann X, Lindberg H, Berglund LA. Synthesis of epoxy-clay nanocomposites: influence of the nature of the clay on structure. *Polymer* 2001;42:1303–10.
- [236] Jiankun L, Yucai K, Zongneng Q, Xiao-Su Y. Study on intercalation and exfoliation behavior of organoclays in epoxy resin. *J Polym Sci, Part B: Polym Phys* 2001;39:115–20.
- [237] Chin IJ, Albrecht T, Kim HC, Wang J. On exfoliation of montmorillonite in epoxy. *Polymer* 2001;42:5947–52.
- [238] Kornmann X, Lindberg H, Berglund LA. Synthesis of epoxy-clay nanocomposites. influence of the nature of the curing agent on structure. *Polymer* 2001;42:4493–9.
- [239] Zerda AS, Lesser AJ. Intercalated clay nanocomposites: morphology, mechanics, and fracture behavior. *J Polym Sci Part B: Polym Phys* 2001;39:1137–46.
- [240] Chin IJ, Albrecht TT, Kim HC, Russell TP, Wang J. On exfoliation of montmorillonite in epoxy. *Polymer* 2001;42:5947–52.
- [241] Kornmann X, Thomann R, Mulhaupt R, Finter J, Berglund LA. High performance epoxy-layered silicate nanocomposites. *Polym Engng Sci* 2002;42:1815–26.
- [242] Feng W, Ait-Kadi A, Rield B. Polymerization compounding: epoxy-montmorillonite nanocomposites. *Polym Engng Sci* 2002;42:1827–35.
- [243] Becker O, Varley R, Simon G. Morphology, thermal relaxations and mechanical properties of layered silicate nanocomposites based upon high-functionality epoxy resins. *Polymer* 2002;43:4365–73.
- [244] Chen JS, Poliks MD, Ober CK, Zhang Y, Wiesner U, Giannelis EP. Study of the interlayer expansion mechanism and thermal-mechanical properties of surface-initiated epoxy nanocomposites. *Polymer* 2002;43:4895–904.
- [245] Kong D, Park CH. Real time exfoliation behavior of clay layers in epoxy-clay nanocomposites. *Chem Mater* 2003;15:419–24.
- [246] Park JH, Jana CH. The relationship between nano- and micro-structures and mechanical properties in PMMA-epoxy-nanoclay composites. *Polymer* 2003;44:2091–100.
- [247] Park JH, Jana CH. Mechanism of exfoliation of nanoclay particles in epoxy-clay nanocomposites. *Macromolecules* 2003;36:2758–68.
- [248] Choi MH, Chung IJ, Lee JD. Morphology and curing behaviors of phenolic resin-layered silicate nanocomposites prepared by melt intercalation. *Chem Mater* 2000;12:2977–83.
- [249] Wang H, Zhao T, Zhi L, Yan Y, Yu Y. Synthesis of novolac/layered silicate nanocomposites by reaction exfoliation using acid-modified montmorillonite. *Macromol Rapid Commun* 2002;23:44–8.
- [250] Wang Z, Pinnavaia TJ. Nanolayer reinforcement of elastomeric polyurethane. *Chem Mater* 1998;10:3769–71.



- [251] Chen TK, Tien YI, Wei KH. Synthesis and characterization of novel segmented polyurethane/clay nanocomposite via poly( $\epsilon$ -caprolactone)/clay. *J Polym Sci, Part A: Polym Chem* 1999;37:2225–33.
- [252] Tien YI, Wei KH. Hydrogen bonding and mechanical properties in segmented montmorillonite/polyurethane nanocomposites of different hard segment ratios. *Polymer* 2001;42:3213–21.
- [253] Yao KJ, Song M, Hourston DJ, Luo DZ. Polymer/layered clay nanocomposites: 2. Polyurethane nanocomposites. *Polymer* 2002;43:1017–20.
- [254] Xu R, Manias E, Snyder AJ, Runt J. Low permeability biomedical polyurethane nanocomposites. *J Biomed Mater Res* 2003;64A:114–9.
- [255] Yano K, Usuki A, Okada A, Kurauchi T, Kamigaito O. Synthesis and properties of polyimide–clay hybrid. *Polym Prepr (Jpn)* 1991;32(1):65–7.
- [256] Lan T, Kaviratna PD, Pinnavaia TJ. On the nature of polyimide–clay hybrid composites. *Chem Mater* 1994;6:573–5.
- [257] Yano K, Usuki A, Okada A. Synthesis and properties of polyimide–clay hybrid films. *J Polym Sci, Part A: Polym Chem* 1997;35:2289–94.
- [258] Zhu Z-K, Yang Y, Yin J, Wang XY, Ke YC, Qi ZN. Preparation and properties of organosoluble montmorillonite/polyimide hybrid materials. *J Appl Polym Sci* 1999;73:2063.
- [259] Yang Y, Zhu ZK, Yin J, Wang XY, Qi ZE. Preparation and properties of hybrids of organo-soluble polyimide and montmorillonite with various chemical surface modification methods. *Polymer* 1999;40:4407–14.
- [260] Tyan HL, Wei KH, Hsieh TE. Mechanical properties of clay–polyimide (BTDA-ODA) nanocomposites via ODA-modified organoclay. *J Polym Sci, Part B: Polym Phys* 2000;38:2873.
- [261] Yano K, Usuki A, Okada A. Polyimide/montmorillonite hybrid. *Polym Prepr (201 ACS)* 1991;32:65–6.
- [262] Gu A, Chang FC. A novel preparation of polyimide/clay hybrid films with low coefficient of thermal expansion. *J Appl Polym Sci* 2001;79:289–94.
- [263] Gu A, Kuo SW, Chang FC. Syntheses and properties of PI/clay hybrids. *J Appl Polym Sci* 2001;79:1902–10.
- [264] Hsiao SH, Liou GS, Chang LM. Synthesis and properties of organosoluble polyimide/clay hybrids. *J Appl Polym Sci* 2001;80:2067–72.
- [265] Tyan HL, Leu CM, Wei KH. Effect of reactivity of organics-modified montmorillonite on the thermal and mechanical properties of montmorillonite/polyimide nanocomposites. *Chem Mater* 2001;13:222–6.
- [266] Huang JC, Zhu ZK, Ma XD, Qian XF, Yin J. Preparation and properties of montmorillonite/organo-soluble polyimide hybrid materials prepared by a one-step approach. *J Mater Sci* 2001;36:871.
- [267] Agag T, Koga T, Takeichi T. Studies on thermal and mechanical properties of polyimide–clay nanocomposites. *Polymer* 2001;42:3399–408.
- [268] Morgan AB, Gilman JW, Jackson CL. Characterization of the dispersion of clay in a polyetherimide nanocomposite. *Macromolecules* 2001;34:2735–8.
- [269] Leu CM, Wu ZW, Wei KH. Synthesis and properties of covalently bonded layered silicates/polyimide (BTDA-ODA) nanocomposites. *Chem Mater* 2002;14:3016–21.
- [270] Magaraphan R, Lilayuthaler W, Sirivat A, Schwank JW. Preparation, structure, properties and thermal behavior of rigid-rod polyimide/montmorillonite nanocomposites. *Compos Sci Technol* 2001;61:1253–64.
- [271] Delozier DM, Orwoll RA, Cahoon JF, Ladislav JS, Smith Jr JG, Connell JW. Polyimide nanocomposites prepared from high-temperature reduced charge organoclays. *Polymer* 2003;44:2231–41.
- [272] Liang Z-M, Yin J, Xu H-J. Polyimide/montmorillonite nanocomposites based on thermally stable, rigid-rod aromatic amine modifiers. *Polymer* 2003;44:1391–9.
- [273] Tyan HL, Liu YC, Wei KH. Enhancement of imidization of poly(amic acid) through poly(amic acid)/organoclay nanocomposites. *Polymer* 1999;40:4877–86.
- [274] Kim J, Ahmed R, Lee SJ. Synthesis and linear viscoelastic behavior of poly(amic acid)–organoclay hybrid. *J Appl Polym Sci* 2001;80:592–603.
- [275] Sur GS, Sun HL, Lyu SG, Mark JE. Synthesis, structure, mechanical properties, and thermal stability of some polysulfone/organoclay nanocomposites. *Polymer* 2001;42:9783–9.
- [276] Lee J, Takekoshi T, Giannelis EP. Fire retardant polyetherimide nanocomposites. *Mater Res Soc Symp Proc* 1997;457:513–8.
- [277] Huang JC, Zhu ZK, Qian XF, Sun YY. Poly(etherimide)/montmorillonite nanocomposites prepared by melt intercalation: morphology, solvent resistance properties and thermal properties. *Polymer* 2001;42:873–7.
- [278] Vora RH, Pallathadka PK, Goh SH, Chung T-S, Lim YX, Bang TK. Preparation and characterization of 4,4'-bis(4-aminophenoxy)diphenyl sulphone based fluoropoly(etherimide)/organo-modified clay. *Macromol Mater Engng* 2003;288:337–56.
- [279] Kurokawa Y, Yasuda H, Oya A. Preparation of nanocomposites of polypropylene and smectite. *J Mater Sci Lett* 1996;15:1481–7.
- [280] Furuichi N, Kurokawa Y, Fujita K, Oya A, Yasuda H, Kiso M. Preparation and properties of polypropylene reinforced by smectite. *J Mater Sci* 1996;31:4307–10.
- [281] Tudor J, Willington L, O'Hare D, Royan B. Intercalation of catalytically active metal complexes in phyllosilicates and their application as propene polymerization catalyst. *Chem Commun* 1996;2031–2.
- [282] Kurokawa Y, Yasuda H, Kashiwagi M, Oya A. Structure and properties of a montmorillonite/polypropylene nanocomposite. *J Mater Sci Lett* 1997;16:1670–2.
- [283] Nyden MR, Gilman JW. Molecular dynamics simulations of the thermal degradation of nano-confined polypropylene. *Comput Theor Polym Sci* 1997;7:191–8.
- [284] Kato M, Usuki A, Okada A. Synthesis of polypropylene oligomer–clay intercalation compounds. *J Appl Polym Sci* 1997;66:1781–5.

- [285] Usuki A, Kato M, Okada A, Kurauchi T. Synthesis of polypropylene-clay hybrid. *J Appl Polym Sci* 1997;63: 137-8.
- [286] Kawasumi M, Hasegawa N, Kato M, Usuki A, Okada A. Preparation and mechanical properties of polypropylene-clay hybrids. *Macromolecules* 1997;30: 6333-8.
- [287] Hasegawa N, Kawasumi M, Kato M, Usuki A, Okada A. Preparation and mechanical properties of polypropylene-clay hybrids using a maleic anhydride-modified polypropylene oligomer. *J Appl Polym Sci* 1998;67: 87-92.
- [288] Oya A. Polypropylene-clay nanocomposites. In: Pinnavaia TJ, Beall GW, editors. *Polymer-clay nanocomposites*. London: Wiley; 2000. p. 151-72.
- [289] Hasegawa N, Okamoto H, Kato M, Usuki A. Preparation and mechanical properties of polypropylene-clay hybrids based on modified polypropylene and organophilic clay. *J Appl Polym Sci* 2000;78:1918-22.
- [290] Oya A, Kurokawa Y, Yasuda H. Factors controlling mechanical properties of clay mineral/polypropylene nanocomposites. *J Mater Sci* 2000;35:1045-50.
- [291] Lee JW, Lim YT, Park OO. Thermal characteristics of organoclay and their effects upon the formation of polypropylene/organoclay nanocomposites. *Polym Bull* 2000;45: 191-8.
- [292] Zhang Q, Fu Q, Jiang L, Lei Y. Preparation and properties of polypropylene/montmorillonite layered nanocomposites. *Polym Int* 2000;49:1561-4.
- [293] Garces JM, Moll DJ, Bicerano J, Fibiger R, McLeod DG. Polymeric nanocomposites for automotive applications. *Adv Mater* 2000;12:1835-9.
- [294] Hasegawa N, Okamoto H, Kawasumi M, Kato M, Tsukigase A, Usuki A. Polyolefin-clay hybrids based on modified polyolefins and organoclay. *Macromol Mater Engng* 2000; 280/281:76-9.
- [295] Hambir S, Bulakh N, Kodgire P, Kalgaonkar R, Jog JP. PP/clay nanocomposites: a study of crystallization and dynamic mechanical behavior. *J Polym Sci, Part B: Polym Phys* 2001; 39:446-50.
- [296] Zanetti M, Camino G, Reichert P, Mulhaupt R. Thermal behaviour of poly(propylene) layered silicate nanocomposites. *Macromol Rapid Commun* 2001;22:176-80.
- [297] Galgali G, Ramesh C, Lele A. A rheological study on the kinetics of hybrid formation in propylene nanocomposites. *Macromolecules* 2001;34:852-8.
- [298] Solomon MJ, Almusallam AS, Seefeldt KF, Somwangthanaroj A, Varadan P. Rheology of polypropylene/clay hybrid materials. *Macromolecules* 2001;34:1864-72.
- [299] Gloaguen JM, Lefebvre JM. Plastic deformation behavior of thermoplastic/clay nanocomposites. *Polymer* 2001;42: 5841-7.
- [300] Garcia-Martinez JM, Laguna O, Areso S, Collar EP. Polypropylene/mica composites modified by succinic anhydride-grafted atactic polypropylene: a thermal and mechanical study under dynamic conditions. *J Appl Polym Sci* 2001; 81:625-36.
- [301] Schmidt D, Shah D, Giannelis EP. New advances in polymer/layered silicate nanocomposites. *Curr Opin Solid State Mater Sci* 2002;6:205-12.
- [302] Reichert P, Hoffman B, Bock T, Thomann R, Mulhaupt R, Friedrich C. Morphological stability of polypropylene nanocomposites. *Macromol Rapid Commun* 2001;22:519-23.
- [303] Nam PH, Maiti P, Okamoto M, Kotaka T, Hasegawa N, Usuki A. A hierarchical structure and properties of intercalated polypropylene/clay nanocomposites. *Polymer* 2001;42:9633-40.
- [304] Liu X, Wu Q. PP/clay nanocomposites prepared by grafting-melt intercalation. *Polymer* 2001;42:10013-9.
- [305] Nam PH, Maiti P, Okamoto M, Kotaka T. Foam processing and cellular structure of polypropylene/clay nanocomposites. *Proceeding Nanocomposites*, June 25-27, 2001, Chicago, Illinois, USA: ECM Publication; 2001.
- [306] Manias E. A direct-blending approach for polypropylene/clay nanocomposites enhances properties. *Mater Res Soc Bull* 2001;26:862-3.
- [307] Okamoto M, Nam PH, Maiti P, Kotaka T, Hasegawa N, Usuki A. A house-of-cards structure in polypropylene/clay nanocomposites under elongational flow. *Nano Lett* 2001;1: 295-8.
- [308] Okamoto M, Nam PH, Maiti M, Kotaka T, Nakayama T, Takada M, Ohshima M, Usuki A, Hasegawa N, Okamoto H. Biaxial flow-induced alignment of silicate layers in polypropylene/clay nanocomposite foam. *Nano Lett* 2001;1: 503-5.
- [309] Hambir S, Bulakh N, Kodgire P, Kalgaonkar R, Jog JP. PP/clay nanocomposites: a study of crystallization and dynamic mechanical behavior. *J Polym Sci, Part B: Polym Phys* 2001; 39:446-50.
- [310] Sun T, Garces JM. High-performance polypropylene-clay nanocomposites by in-situ polymerization with metallocene/clay catalysts. *Adv Mater* 2002;14:128-30.
- [311] Maiti P, Nam PH, Okamoto M, Kotaka T, Hasegawa N, Usuki A. Influence of crystallization on intercalation, morphology, and mechanical properties of propylene/clay nanocomposites. *Macromolecules* 2002;35:2042-9.
- [312] Maiti P, Nam PH, Okamoto M, Kotaka T, Hasegawa N, Usuki A. The effect of crystallization on the structure and morphology of polypropylene/clay nanocomposites. *Polym Engng Sci* 2002;42:1864-71.
- [313] Nam PH, Maiti P, Okamoto M, Kotaka T, Nakayama T, Takada M, Ohshima M, Usuki A, Hasegawa N, Okamoto H. Foam processing and cellular structure of polypropylene/clay nanocomposites. *Polym Engng Sci* 2002;42:1907-18.
- [314] Hambir S, Bulakh N, Jog JP. Propylene/clay nanocomposites: effect of compatibilizer on the thermal, crystallization and dynamic mechanical behavior. *Polym Engng Sci* 2002; 42:1800-7.
- [315] Kaempfer D, Thomann R, Mulhaupt R. Melt compounding of syndiotactic polypropylene nanocomposites containing organophilic layered silicates and in situ formed core/shell nanoparticles. *Polymer* 2002;43:2909-16.
- [316] Lele A, Mackley M, Galgali G, Ramesh C. In situ rheo-X-ray investigation of flow-induced orientation in layered

- silicate-syndiotactic polypropylene nanocomposite melt. *J Rheol* 2002;46:1091–110.
- [317] Zhang Q, Wang Y, Fu Q. Shear-induced change of exfoliation and orientation in polypropylene/montmorillonite nanocomposites. *J Polym Sci, Part B: Polym Phys* 2003; 41:1–10.
- [318] Somwangthanaroj A, Lee EC, Solomon MJ. Early stage quiescent and flow-induced crystallization of intercalated polypropylene nanocomposites by time-resolved light scattering. *Macromolecules* 2003;36:2333–42.
- [319] Morgan AB, Harris JD. Effects of organoclay soxhlet extraction on mechanical properties, flammability properties and organoclay dispersion of polypropylene nanocomposites. *Polymer* 2003;44:2113–320.
- [320] Jeon HG, Jung HT, Lee SW, Hudson SD. Morphology of polymer silicate nanocomposites. High density polyethylene and a nitrile. *Polym Bull* 1998;41:107–13.
- [321] Heinemann J, Reichert P, Thomason R, Mulhaupt R. Polyolefin nanocomposites formed by melt compounding and transition metal catalyzed ethane homo- and copolymerization in the presence of layered silicates. *Macromol Rapid Commun* 1999;20:423–30.
- [322] Privalko VP, Calleja FJB, Sukhorukov DI, Privalko EG, Walter R, Friedrich K. Composition-dependent properties of polyethylene/Kaolin composites. Part II. Thermoelastic behavior of blow-molded samples. *J Mater Sci* 1999;34: 497–508.
- [323] Bergman JS, Chen H, Giannelis EP, Thomas MG, Coates GW. Synthesis and characterization of polyolefin-silicate nanocomposites: a catalyst intercalation and in situ polymerization approach. *J Chem Soc Chem Commun* 1999;21: 2179–80.
- [324] Rong J, Jing J, Li H, Sheng M. A polyethylene nanocomposite prepared via in-situ polymerization. *Macromol Rapid Commun* 2001;22:329–34.
- [325] Wang KH, Choi MH, Koo CM, Choi YS, Chung IJ. Synthesis and characterization of maleated polyethylene/clay nanocomposites. *Polymer* 2001;42:9819–26.
- [326] Alexandre M, Dubois P, Sun T, Graces JM, Jerome R. Polyethylene-layered silicate nanocomposites prepared by the polymerization-filling technique: synthesis and mechanical properties. *Polymer* 2002;43:2123–32.
- [327] Gopakumar TG, Lee JA, Kontopoulou M, Parent JS. Influence of clay exfoliation on the physical properties of montmorillonite/polyethylene composites. *Polymer* 2002;43: 5483–91.
- [328] Jin Y-H, Park H-J, Im S-S, Kwak S-Y, Kwak S. Polyethylene/clay nanocomposite by in situ exfoliation of montmorillonite during Ziegler–Natta polymerization of ethylene. *Macromol Rapid Commun* 2002;23:135–40.
- [329] Bafna A, Beaucage G, Mirabella F, Mehta S. 3D hierarchical orientation in polymer–clay nanocomposite films. *Polymer* 2003;44:1103–15.
- [330] Osman MA, Seyfang G, Suter UW. Two-dimensional melting of alkane monolayers ionically bonded to mica. *J Phys Chem B* 2000;104:4433–9.
- [331] Zanetti M, Camino G, Thomann R, Mulhaupt R. Synthesis and thermal behavior of layered silicate-EVA nanocomposites. *Polymer* 2001;42:4501–7.
- [332] Usuki A, Tugigase A, Kato M. Preparation and properties of EPMD–clay hybrids. *Polymer* 2002;43:2185–9.
- [333] Wanjale SD, Jog JP. Poly(1-butene)/clay nanocomposites: preparation and properties. *J Polym Sci, Part B: Polym Phys* 2003;41:1014–21.
- [334] Nazzal AI, Street GB. Pyrrole-styrene graft copolymers. *J Chem Soc Chem Commun* 1985;375–6.
- [335] Sun Y, Ruckenstein E. Polypyrrole-bearing conductive composite prepared by an inverted emulsion pathway involving nonionic surfactants. *Synth Met* 1995;72:261–7.
- [336] Wang L, Brazis P, Rocci M, Kannewurf CR, Kanatzidis MG. A new redox host for intercalative polymerization: insertion of polyaniline into  $\alpha$ -RuCl<sub>3</sub>. *Chem Mater* 1998;10: 3298–300.
- [337] Sinha Ray S, Biswas M. Preparation and evaluation of composites from montmorillonite and some heterocyclic polymers: 3. A water dispersible nanocomposite from pyrrole–montmorillonite polymerization system. *Mater Res Bull* 1999;35:1187–94.
- [338] Kim BH, Jung JH, Joo J, Kim JW, Choi HJ. Nanocomposite of polyaniline and Na<sup>+</sup>-montmorillonite (MMT) clay. *Nanocomposites 2001, Proceedings*. Chicago, Illinois, USA: ECM Publication.
- [339] Kim JW, Liu F, Choi HJ, Hong SH, Joo J. Intercalated polypyrrole/Na<sup>+</sup>-montmorillonite nanocomposite via an inverted emulsion pathway method. *Polymer* 2003;44: 289–93.
- [340] Biswas M, Sinha Ray S. Preparation and evaluation of composites from montmorillonite and some heterocyclic polymers. 1: poly(*N*-vinylcarbazole)–montmorillonite system. *Polymer* 1998;39:6423–8.
- [341] Sinha Ray S, Biswas M. Preparation and evaluation of composites from montmorillonite and some heterocyclic polymers, II. Nanocomposite from *N*-vinylcarbazole and ferric chloride impregnated montmorillonite polymerization system. *J Appl Polym Sci* 1999;73:2971–6.
- [342] Kim JW, Kim SG, Choi HJ, Jhon MS. Synthesis and electrorheological properties of polyaniline–Na<sup>+</sup>-montmorillonite suspensions. *Macromol Rapid Commun* 1999;20: 450–2.
- [343] Biswas M, Sinha Ray S. Water-dispersible nanocomposites of polyaniline and montmorillonite. *J Appl Polym Sci* 2000; 77:2948–56.
- [344] Dai L, Wang Q, Wan M. Direct observation of conformational transitions for polyaniline chains intercalated in clay particles upon secondary doping. *J Mater Sci Lett* 2000; 19:1645–7.
- [345] Lee D, Lee SH, Char K, Kim J. Expansion distribution of basal spacing of the silicate layers in polyaniline/Na<sup>+</sup>-montmorillonite nanocomposites monitored with X-ray diffraction. *Macromol Rapid Commun* 2000;21:1136–9.
- [346] Wu Q, Xue Z, Qi Z, Wang F. Synthesis and characterization of PAN/clay nanocomposite with extended chain conformation of polyaniline. *Polymer* 2000;41:2029–32.

- [347] Uemura S, Yoshie M, Kobayashi N, Nakahira T. Photopolymerization of aniline dimer by photocatalytic reaction of ruthenium trisbipyridyl in the interlayer of hectorite clay. *Polym J* 2000;32:987–90.
- [348] Kim BH, Jung JH, Joo J, Kim JW, Choi HJ. Charge transport and structure of nanocomposites of polyaniline and inorganic clay. *J Korean Phys Soc* 2000;36:366–70.
- [349] Yeh JM, Liou SJ, Lai CY, Wu PC, Tsai TY. Enhancement of corrosion protection effect in polyaniline via the formation of polyaniline–clay nanocomposite materials. *Chem Mater* 2001;13:1131–6.
- [350] Feng B, Su Y, Song J, Kong K. Electropolymerization of polyaniline/montmorillonite nanocomposite. *J Mater Sci Lett* 2001;20:293–4.
- [351] Kim JW, Kim SG, Choi HJ, Suh MS, Shin MJ, Jhon MS. Synthesis and electrorheological characterization of polyaniline and Na<sup>+</sup>-montmorillonite clay nanocomposite. *Int J Mod Phys* 2001;15:657–64.
- [352] Kim BH, Jung JH, Kim JW, Choi HJ, Joo J. Physical characterization of polyaniline–Na<sup>+</sup>-montmorillonite nanocomposite intercalated by emulsion polymerization. *Synth Met* 2001;117:115–8.
- [353] Choi HJ, Kim JW, Joo J, Kim BH. Synthesis and electrorheology of emulsion intercalated PANI–clay nanocomposite. *Synth Met* 2001;121:1325–6.
- [354] Cho MS, Choi HJ, Kim KY, Ahn WS. Synthesis and characterization of polyaniline/mesoporous SBA-15 nanocomposite. *Macromol Rapid Commun* 2002;23:713–6.
- [355] Kim BH, Jung JH, Hong SH, Joo J, Epstein AJ, Mizoguchi K, Kim JW, Choi HJ. Nanocomposite of polyaniline and Na<sup>+</sup>-montmorillonite clay. *Macromolecules* 2002;35:1419–23.
- [356] Nascimento GMdo, Constantino VRL, Temperini MLA. Spectroscopic characterization of a new type of conducting polymer–clay nanocomposite. *Macromolecules* 2002;35:7535–7.
- [357] Winkler B, Dai L, Mau AW-H. Organic–inorganic hybrid light-emitting composites: poly(*p*-phenylene vinylene) intercalated clay nanoparticles. *J Mater Sci Lett* 1999;18:1539–41.
- [358] Ke S, Ying M, Ya-an C, Zhao-Hui C, Xue-hai J, Jian-niah Y. Inclusion of poly(tetramethyl-*p*-phenyl-enediamine dihydrochloride) into MoO<sub>3</sub>: a cooperative formation route to construct a polymer/MoO<sub>3</sub> layered structure. *Chem Mater* 2001;13:250–2.
- [359] Skotheim TA, Elsenbaumer RL, Reynolds JR, editors. *Hand book of conducting polymers*, 2nd ed. NY: Marcel Dekker [chapter 25].
- [360] Pennwell RC, Ganguly BN, Smith TW. Poly(*N*-vinyl carbazole): a selective review of its polymerization, structure, properties, and electrical characteristics. *J Polym Sci, Macromol Rev* 1973;13:63160.
- [361] Biswas M, Das SK. Recent progress in carbazole based polymers. *Polymer* 1982;23:1713–26.
- [362] Biswas M, Sinha Ray S. A poly(*N*-vinylcarbazole) based nanocomposite form montmorillonite. In: Srinivasan KSV, editor. *Macromolecules new frontiers*. Proceedings of the IUPAC International Symposium on Advances in Polymer Science and Technology, MACRO'98, vol. II, New Delhi: Allied Publishers Ltd; 1998. p. 710–3.
- [363] Biswas M, Mitra P. Synthesis and thermal stability, dielectric, and conductivity characteristics of some aromatic anhydride-modified carbazole polymers. *J Appl Polym Sci* 1991;42:1989–95.
- [364] Lagaly G. Characterization of clays by organic compounds. *Clay Miner* 1981;16:1–21.
- [365] Kawasumi M, Hasegawa N, Usuki A, Okada A. Nematic liquid crystal/clay mineral composites. *Mater Sci Engng C* 1998;6:135–43.
- [366] Vaia RA, Giannelis EP. Liquid crystal polymer nanocomposites: direct intercalation of thermotropic liquid crystalline polymers into layered silicates. *Polymer* 2001;42:1281–5.
- [367] Zhou W, Mark JE, Unroe MR, Arnold FE. Some clay nanocomposites based on a high temperature, high performance polymer. *J Macromol Sci Pure Appl Chem* 2001;A38:1–9.
- [368] Chang JH, Seo BS, Hwang DH. An exfoliation of organoclay in thermotropic liquid crystalline polyester nanocomposites. *Polymer* 2002;43:2969–74.
- [369] Plummer CJG, Garamszegi L, Leterrier Y, Rodlert M, Manson J-AE. Hyperbranched polymer-layered silicate nanocomposites. *Chem Mater* 2002;14:486–8.
- [370] Ganguli S, Dean D, Jordan K, Price G, Vaia R. Mechanical properties of intercalated cyanate ester-layered silicate nanocomposites. *Polymer* 2003;44:1315–9.
- [371] Young SK, Mauritz KA. Nafion<sup>®</sup>/(organically modified silicate) nanocomposites via polymer in situ sol–gel reactions: mechanical tensile properties. *J Polym Sci, Part B: Polym Phys* 2002;40:2237–47.
- [372] Wright ME, Schorman DA, Feher FJ, Jin R-Z. Synthesis and thermal curing of aryl-ethyl-terminated coPOSS imide oligomers: new inorganic/organic hybrid resins. *Chem Mater* 2003;15:264–8.
- [373] Ogata N, Jimenez G, Kawai H, Ogihara T. Structure and thermal/mechanical properties of poly(L-lactide)–clay blend. *J Polym Sci Part B: Polym Phys* 1997;35:389–96.
- [374] Sinha Ray S, Maiti P, Okamoto M, Yamada K, Ueda K. New polylactide/layered silicate nanocomposites. 1. Preparation, characterization and properties. *Macromolecules* 2002;35:3104–10.
- [375] Sinha Ray S, Okamoto K, Yamada K, Okamoto M. Novel porous ceramic material via burning of polylactide/layered silicate nanocomposite. *Nano Lett* 2002;2:423–6.
- [376] Sinha Ray S, Okamoto M, Yamada K, Ueda K. New polylactide/layered silicate nanocomposites. Roll of organoclay on morphology, materials properties and biodegradability. *Polym Prepr Jpn* 2002;155–6.
- [377] Sinha Ray S, Yamada K, Ogami A, Okamoto M, Ueda K. New polylactide layered silicate nanocomposite. Nanoscale control of multiple properties. *Macromol Rapid Commun* 2002;23:493–7.
- [378] Sinha Ray S, Okamoto M, Yamada K, Ueda K. New polylactide/layered silicate nanocomposites: concurrent improvement of materials properties and biodegradability.

- Nanocomposites 2002 Proceedings, San Diego, USA: ECM Publication; 2002.
- [379] Sinha Ray S, Okamoto M, Yamada K, Ueda K. New and novel biodegradable polylactide/layered silicate nanocomposites: preparation, characterization and melt rheology. PPS2002 Proceedings, Taipei; 2002.
- [380] Sinha Ray S, Okamoto M, Yamada K, Ueda K. New biodegradable polylactide/layered silicate nanocomposites: preparation, characterization and materials properties. ICCE-9 Proceedings, San Diego, USA; 2002. p. 659–60.
- [381] Maiti P, Yamada K, Okamoto M, Ueda K, Okamoto K. New polylactide/layered silicate nanocomposites. Role of organoclay. *Chem Mater* 2002;14:4654–61.
- [382] Pluta M, Caleski A, Alexandre M, Paul M-A, Dubois P. Polylactide/montmorillonite nanocomposites and microcomposites prepared by melt blending: structure and some physical properties. *J Appl Polym Sci* 2002;1497–506.
- [383] Sinha Ray S, Yamada K, Okamoto M, Ogami A, Ueda K. New polylactide/layered silicate nanocomposites. 3. High performance biodegradable materials. *Chem Mater* 2003;15:1456–65.
- [384] Paul M-A, Alexandre M, Degee P, Henrist C, Rulmont A, Dubois P. New nanocomposite materials based on plasticized poly(L-lactide) and organo-modified montmorillonites: thermal and morphological study. *Polymer* 2003;44:443–50.
- [385] Chang J-H, Uk-An Y, Sur GS. Poly(lactic acid) nanocomposites with various organoclays. I. Thermomechanical properties, morphology, and gas permeability. *J Polym Sci, Part B: Polym Phys* 2003;41:94–103.
- [386] Sinha Ray S, Yamada K, Okamoto M, Ueda K. New polylactide/layered silicate nanocomposites. 2. Concurrent improvements of material properties, biodegradability and melt rheology. *Polymer* 2003;44:857–66.
- [387] Isobe Y, Ino T, Kageyama Y, Nakano M, Usuki A. Improvement of heat resistance for bioplastics. SAE World Congress, Detroit, Michigan; March 3–6, 2003.
- [388] Sinha Ray S, Yamada K, Okamoto M, Ueda K. Biodegradable polylactide/montmorillonite nanocomposites. *J Nanosci Nanotechnol*. In press.
- [389] Sinha Ray S, Okamoto K, Okamoto M. New poly(butylene succinate)/layered silicate nanocomposites. Preparation, characterization and mechanical properties. *Nanocomposites 2002 Proceedings, ECM; 2002*.
- [390] Sinha Ray S, Okamoto K, Maiti P, Okamoto M. New poly(butylene succinate)/layered silicate nanocomposites. 1. Preparation, characterization, and mechanical properties. *J Nanosci Nanotechnol* 2002;2:171–6.
- [391] Sinha Ray S, Okamoto K, Okamoto M. Structure–property relationship in biodegradable poly(butylene succinate)/layered silicate nanocomposites. *Macromolecules* 2003;36:2355–67.
- [392] Okamoto K, Sinha Ray S, Okamoto M. New poly(butylene succinate)/layered silicate nanocomposites. 2. Effect of organically modified layered silicates on morphology, materials properties, melt rheology, and biodegradability. *J Polym Sci, Part B*. In press.
- [393] Sinha Ray S, Okamoto K, Okamoto M. Biodegradable poly(butylene succinate)/layered silicate nanocomposites prepared by melt intercalation. *J Mater Chem*. Submitted for publication.
- [394] Kornmann X, Berglund LA, Sterete J, Giannelis EP. Nanocomposites based on montmorillonite and unsaturated polyester. *Polym Engng Sci* 1998;38:1351–8.
- [395] Choi HJ, Kim JH, Kim J. Mechanical spectroscopy studies on biodegradable synthetic and biosynthetic aliphatic polyesters. *Macromol Symp* 1997;119:149–55.
- [396] Park SH, Choi HJ, Lim ST, Shin TK, Jhon MS. Viscoelasticity of biodegradable polymer blends of poly(3-hydroxybutyrate) and poly(ethylene oxide). *Polymer* 2001;42:5737–42.
- [397] Maiti P, Batt CA, Giannelis EP. Renewable plastics: synthesis and properties of PHB nanocomposites. *Polym Mater Sci Engng* 2003;88:58–9.
- [398] Lee SR, Park HM, Lim HL, Kang T, Li X, Cho WJ, Ha CS. Microstructure, tensile properties, and biodegradability of aliphatic polyester/clay nanocomposites. *Polymer* 2002;43:2495–500.
- [399] Lepoittevin B, Pantoustier N, Alexander M, Calberg C, Jerome R, Dubois P. Polyester layered silicate nanohybrids by controlled grafting polymerization. *J Mater Chem* 2002;12:3528–32.
- [400] Bharadwaj RK, Mehrabi AR, Hamilton C, Murga MF, Chavira A, Thompson AK. Structure–property relationships in cross-linked polyester–clay nanocomposites. *Polymer* 2002;43:3699–705.
- [401] Lim ST, Hyun YH, Choi HJ, Jhon MS. Synthetic biodegradable aliphatic polyester/montmorillonite nanocomposites. *Chem Mater* 2002;14:1839–44.
- [402] Morgan AB, Gilman JW. Characterization of poly-layered silicate (clay) nanocomposites by transmission electron microscopy and X-ray diffraction: a comparative study. *J Appl Polym Sci* 2003;87:1329–38.
- [403] Mathias LJ, Davis RD, Jarrett WL. Observation of  $\alpha$ - and  $\gamma$ -crystal forms and amorphous regions of nylon 6-clay nanocomposites using solid-state  $^{15}\text{N}$  nuclear magnetic resonance. *Macromolecules* 1999;32:7958–60.
- [404] Roe R. Methods of X-ray and neutron scattering in polymer science. New York: Oxford University Press; 2000. p. 199.
- [405] Bafna A, Beaucage G, Mirabella F, Skillas G, Sukumaran S. Optical properties and orientation in polyethylene blown films. *J Polym Sci, Part B: Polym Phys* 2001;39:2923–36.
- [406] Bafna A, Beaucage G, Mirabella F, Mehata S. Shear induced orientation and associated property enhancement in polymer/clay nanocomposites. *Proceedings Nanocomposites, Sept. 23–25, 2002, San Diego, CA, USA: ECM Publication; 2002*.
- [407] Alexander L. X-ray diffraction methods in polymer science. Florida: R.E. Krieger Publications; 1985. p. 245.
- [408] VanderHart DL, Asano A, Gilman JW. NMR measurements related to clay dispersion quality and organic-modifier stability in nylon 6/clay nanocomposites. *Macromolecules* 2001;34:3819–22.
- [409] Bensimon Y, Deroide B, Zanchetta JV. Comparison between the electron paramagnetic resonance spectra

- obtained in X- and W-bands on a fired clay: a preliminary study. *J Phys Chem Solid* 1999;60:813–8.
- [410] Yang DK, Zax DB.  $\text{Li}^+$  dynamics in a polymer nanocomposite: an analysis of dynamic line shapes in nuclear magnetic resonance. *J Chem Phys* 1991;110:5325–36.
- [411] Blumberg WE. Nuclear spin–lattice relaxation caused by paramagnetic impurities. *Phys Rev* 1960;119:79–84.
- [412] Abragam A, editor. The principles of nuclear magnetism. New York: Oxford University Press; 1961. [chapter V].
- [413] VanderHart DL, Asano A, Gilman JW. Solid-state NMR investigation of paramagnetic nylon 6 clay nanocomposites. 2. Measurement of clay dispersion, crystal stratification, and stability of organic modifiers. *Chem Mater* 2001;13:3796–809.
- [414] Sahoo SK, Kim DW, Kumar J, Blumstein A, Cholli AL. Nanocomposites from in-situ polymerization substituted polyacetylene within lamellar surface of the montmorillonite: a solid-state NMR study. *Macromolecules* 2003;36:2777–84.
- [415] Hou SS, Bonagamba TJ, Beyer FL, Madison PH, Schmidt-Rohr K. Clay intercalation of poly(styrene-ethylene oxide) block copolymers studied by two-dimensional solid-state NMR. *Macromolecules* 2003;36:2769–76.
- [416] Loo LS, Gleason KK. Fourier transforms infrared investigation of the deformation behavior of montmorillonite in nylon 6/nanoclay nanocomposite. *Macromolecules* 2003;36:2587–90.
- [417] Rausell-Colom JA, Serratos JM. Reactions of clays with organic substances. In: Newman ACD, editor. Chemistry of clays and clay minerals. ; 1987. p. 371.
- [418] Manias E, Touny A, Wu L, Lu B, Strawhecker K, Gilman JW, Chung TC. Polypropylene/silicate nanocomposites, synthetic routes and materials properties. *Polym Mater Sci Engng* 2000;82:282–3.
- [419] Chung TC, Lu HL, Jankivul W. A novel synthesis of PP-*b*-PMMA copolymers via metallocene catalysis and borane chemistry. *Polymer* 1997;38:1495–502.
- [420] Lu HL, Hong S, Chung TC. Synthesis of new polyolefin elastomers. Poly(ethylene-*ter*-propylene-*ter*-*p*-methylstyrene) and Poly(ethylene-*ter*-1-octene-*ter*-*p*-methylstyrene), using metallocene catalysts with constrained ligand geometry. *Macromolecules* 1998;31:2028–34.
- [421] Lu HL, Hong S, Chung TC. Synthesis of polypropylene-*co*-*p*-methylstyrene copolymers by metallocene and Ziegler–Natta catalysts. *J Polym Sci, Part A: Polym Chem* 1999;37:2795–802.
- [422] Lu B, Chung TC. Synthesis of maleic anhydride grafted polyethylene and polypropylene, with controlled molecular structures. *J Polym Sci, Part A: Polym Chem* 2000;38:1337–43.
- [423] Manias E. Origins of materials properties enhancement in polymer/clay nanocomposites. Nanocomposites 2001 Proceedings, Chicago, IL: ECM Publication; 2001.
- [424] Yasuda T, Takiyama, E. Polyester injection-molded articles. US Patent 5391644; 1995.
- [425] McCrum NG, Read BE, Williams G. Anelastic and dielectric effects in polymeric solids. London: Wiley; 1967.
- [426] Okamoto M, Nam PH, Hasegawa N, Usuki A. Uniaxial flow-induced alignment of silicate layers in polypropylene/clay nanocomposites. *Macromol Mater Engng*. Submitted for publication.
- [427] Nielsen LE. Mechanical properties of polymer and composites, vol. 2. New York: Marcel Dekker; 1981.
- [428] Halpin JC, Kardos JL. The Halpin–Tsai equations: a review. *Polym Engng Sci* 1976;16:344–52.
- [429] Somoza AM, Tarazona P. Density functional application for hard-body liquid crystal. *J Chem Phys* 1989;91:517–27.
- [430] Reichert P, Nitz H, Klinke S, Brandsch R, Thomann R, Mulhaupt R. Poly(propylene)/organoclay nanocomposite formation: influence of compatibilizer functionality and organoclay modification. *Macromol Mater Engng* 2000;275:8–17.
- [431] Mc Neill LS. Comprehensive polymer science, vol. 6. Oxford: Pergamon Press; 1989.
- [432] Camino G, Sgobbi R, Colombier S, Scelza C. Investigation of flame retardancy in EVA. *Fire Mater* 2000;24:85–90.
- [433] Gilman JW, Ksahiwagi T, Giannelis EP, Manias E, Lomakin S, Lichtenhan JD, Jones P. Flammability properties of polymer-layered silicate nanocomposites. In: Al-Malaika S, Golovoy A, Wilkie CA, editors. Chemistry and technology of polymer additives. Oxford: Blackwell Science; 1999. [chapter 14].
- [434] Yoon JT, Jo WH, Lee MS, Ko MB. Effects of comonomers and shear on the melt intercalation of styrenics/clay nanocomposites. *Polymer* 2001;42:329–36.
- [435] Fujiwara S, Sakamoto T. Flammability properties of Nylon-6/mica nanocomposites. Kokai patent application, no. SHO511976-109998; 1976.
- [436] Nielsen L. Platelet particles enhance barrier of polymers by forming tortuous path. *J Macromol Sci Chem* 1967;A1(5):929–42.
- [437] Hutchison JC, Bissessur R, Shiver DF. Conductivity anisotropy of polyphosphazene–montmorillonite composite electrolytes. *Chem Mater* 1996;8:1597–9.
- [438] Tetto JA, Steeves DM, Welsh EA, Powell BE. Biodegradable poly( $\epsilon$ -caprolactone)/clay nanocomposites. ANTEC'99. p. 1628–32.
- [439] Sinha Ray S, Yamada K, Okamoto M, Ueda K. Control of biodegradability of polylactide via nanocomposite technology. *Macromol Mater Engng* 2003;288:203–8.
- [440] Maiti P, Okamoto M. Crystallization controlled by silicate surfaces in nylon 6–clay nanocomposites. *Macromol Mater Engng* 2003;288:440–5.
- [441] Krishnamoorti R, Giannelis EP. Strain hardening in model polymer brushes under shear. *Langmuir* 2001;17:1448–52.
- [442] Krishnamoorti R, Ren J, Silva AS. Shear response of layered silicate nanocomposites. *J Chem Phys* 2001;115:4968–73.
- [443] Krishnamoorti R, Yurekli K. Rheology of polymer/layered silicate nanocomposites. *Curr Opin Colloid Interface Sci* 2001;6:464–70.
- [444] Cox WP, Merz EH. Correlation of dynamic and steady flow viscosities. *J Polym Sci* 1958;28:619–22.
- [445] Kotaka T, Kojima A, Okamoto M. Elongational flow opto-rheometry for polymer melts—1. Construction of an

- elongational flow opto-rheometer and some preliminary results. *Rheol Acta* 1997;36:646–57.
- [446] Block H, Kelly JP. Electro-rheology. *J Phys D* 1988;21:1661–77.
- [447] Chin BD, Park OO. Rheology and microstructures of electrorheological fluids containing both dispersed particles and liquid drops in a continuous phase. *J Rheol* 2000;44:397–412.
- [448] Halsey TC. Electrorheological fluids. *Science* 1992;258:761–6.
- [449] Trau M, Sankaran S, Saville DA, Aksay IA. Electric field-induced patterns formation in colloidal dispersion. *Nature* 1995;374:437–9.
- [450] Kim JW, Noh MH, Choi HJ, Lee DC, Jhon MS. Synthesis and electrorheological characteristics of SAN–clay composite suspensions. *Polymer* 2000;41:1229–31.
- [451] Park JH, Lim YT, Park OO. New approach to enhance the yield stress of electro-rheological fluids by polyaniline-coated layered silicate nanocomposites. *Macromol Rapid Commun* 2001;22:616–9.
- [452] Lim YT, Park JH, Park OO. Improved electrorheological effect in polyaniline nanocomposite suspensions. *J Colloid Interface Sci* 2002;245:198–203.
- [453] Svoboda P, Zeng C, Wang H, Lee LJ. Structure and mechanical properties of polypropylene and polystyrene organoclay nanocomposites. *Nanocomposites 2001 Proceedings*, San Diego, CA, USA: ECM; 2002.
- [454] Abiko T, Kawato H, Kanai T, Oda T, Saito H. Foaming polypropylene-nanocomposites with supercritical fluid. *Proceedings Nanocomposites*, September 23–25, 2002, San Diego, CA, USA: ECM Publication; 2002.
- [455] Okamoto M, Nam PH, Maiti P, Usuki A. Nylon-6/clay nanocomposites: designing through processing operation. *Macromol Mater Engng*. Submitted for publication.
- [456] Tanaka Y, Kakiuchi H. Study of epoxy compounds. Part I. curing reactions of epoxy resin and acid anhydride with amine and alcohol as catalyst. *J Appl Polym Sci* 1963;7:1063–81.
- [457] Leaversuch R. Nanocomposites. *Plastic technology*, On-line article; October 2001. [www.plastictechnology.com](http://www.plastictechnology.com)
- [458] Mohanty AK, Drazal LT, Misra M. Nano reinforcements of bio-based polymers—the hope and the reality. *Polym Mater Sci Engng* 2003;88:60–1.
- [459] Leaversuch R. Biodegradable polyesters: packaging goes green. *Plastic Technology*. On-line article, September 2002: [www.plastictechnology.com/articles/200209fa3.html](http://www.plastictechnology.com/articles/200209fa3.html)
- [460] Sinha Ray S, Okamoto M. Biodegradable polylactide/layered silicate nanocomposites: opening a new dimension for plastics and composites. *Macromol Rapid Commun* 2003; 24:814–40.